The Complexity of Semaphorin and Plexin Signalling in the Healthy and Diseased Brain

Suzanne Lemstra

About the cover:

Inspired by Matt Might, the illustrated guide to a Ph.D.

Imagine the knowledge of the world as a circle. As you reach the edge of the circle, you find the information written in research papers. During a PhD you focus on this boundary of knowledge and you push at it for many years until it gives way. For the last years I have focussed on the boundaries regarding axonal guidance molecules resulting in novel insights. This thesis is "my dent" at the world's knowledge pushed out by a growth cone.

Colophon

The research described in this thesis was performed at the Department of Translational Neuroscience, Brain Center Rudolf Magnus, University Medical Center Utrecht, The Netherlands.

Publications of this thesis was financially supported by the Brain Center Rudolf Magnus.

Cover and Lay-out: Suzanne Lemstra
Printing: Proefschrift-All In One | www.proefschrift-aio.nl
ISBN: 978-90-393-7230-2

The Complexity of Semaphorin and Plexin Signalling in the Healthy and Diseased Brain

De Complexiteit van Semaphorine en Plexine Signalering in de Gezonde en Zieke Hersenen
(met een samenvatting in het Nederlands)

Proefschrift

ter verkrijging van de graad van doctor aan de
Universiteit Utrecht
op gezag van de
rector magnificus, prof. dr. H.R.B.M. Kummeling,
ingevolge het besluit van het college voor promoties in het openbaar te verdedigen
op

donderdag 19 december 2019 des ochtends te 10.30 uur

door

Suzanne Lemstra

geboren op 8 november 1989
te Hoogeveen

Promotoren:
Prof. dr. R. Jeroen Pasterkamp
Dr. Geert M. J. Ramakers

Contents

Chapter 1

General Introduction

Semaphorins and Plexins are key regulators of brain development

During development of the brain, cells are specifically instructed to migrate, differentiate, synapse and integrate into neuronal networks. During further maturation of neuronal networks excessive axons and synapses are pruned. In adulthood, axonal and synaptic plasticity and adult neurogenesis occur to ensure proper brain functioning [1]. Correct brain development and neuronal network integration is crucial and small disturbances in these processes can lead to neurological disorders [2]. Various proteins govern pre- and postnatal neural circuit development through complex signalling mechanisms, many of which occur simultaneously.

In order for neurons to connect to each other, axons must often travel long distances. Neurons use a hand-shaped structure, the growth cone, located at the tip of their axons to sample the environment for guidance cues (Fig. 1a). When the growth cone encounters guidance cues that are attractive, downstream signalling pathways will guide the axon towards the positive signal. On the other hand, when repulsive cues are encountered, the actin network of the growth cone will disassemble, collapse, and the axon will move in an opposite direction. When the axon reaches its target tissue, it will form a synapse on the target cell (Fig. 1b). One group of axonal guidance cues with important roles during brain development and maintenance are the Semaphorins [3–5].

The Semaphorin family consists of 30 proteins, which fall into 8 classes. Sema1a-b, Sema2a-b and Sema5c are found in invertebrates; Sema3A-H, Sema4A-G, Sema5A-B, Sema6A-E and Sema7A are expressed in vertebrates; and SemaVA and SemaVB form a viral subclass [3,6]. Semaphorin proteins are characterized by their Semaphorin, PSI (Plexin/Semaphorin/integrin) and Ig-like extracellular domains [7–10]. These domains are responsible for binding (co-) receptor and other signalling molecules. Canonical receptors for Semaphorins are members of the Plexin family. The nine Plexins are categorized in 4 classes (PlexinA-D) [11]. Plexin proteins contain Sema, PSI and Ig-like/Plexin/transcription factor (IPT) extracellular domains [9,12–14]. Other receptors for Semaphorins have been described. For example, β1-containing integrins can interact with Sema7A, SemaVA and SemaVB [15], and CD72 and T-cell immunoglobulin and mucin domain 2 (TIM2) are established receptors for class 4 Semaphorins [16,17]. Plexin intracellular domains are characterized by GTPase-activating proteins (GAP) and Rho GTPase-binding domains [12,13]. Unfortunately, crystal structures of the intracellular domain of Semaphorins are lacking, limiting our understanding of this region. Nevertheless, crystal structures of Semaphorins and Plexins have provided invaluable information about their downstream signalling cascades and molecular regulation.

In this thesis we studied the role of vertebrate Semaphorins during brain development. Vertebrate Semaphorins can be transmembrane proteins (Sema4-6) or associated with the membrane via a glycosylphosphatidylinositol (GPI)-link (Sema7a). Class 3 Semaphorins function as secreted guidance molecules [18–20]. In addition, proteolytic cleavage has been shown for Sema4D, Sema5B and Sema7A [21–24] converting these proteins into secreted guidance cues. Semaphorin-Plexin signalling can result in both attractive or repulsive guidance effects and regulate numerous aspects of neuronal circuit development and plasticity ranging from proliferation and spatial localization of (stem) cells and neurites during early development to synapse formation and maintenance in adulthood [25–28]. Given their important role in neuronal circuit development and the fact that defects in Semaphorins have been linked to brain disease, a further understanding of the molecular mechanisms that underlie vertebrate Semaphorin-Plexin signalling may deepen our

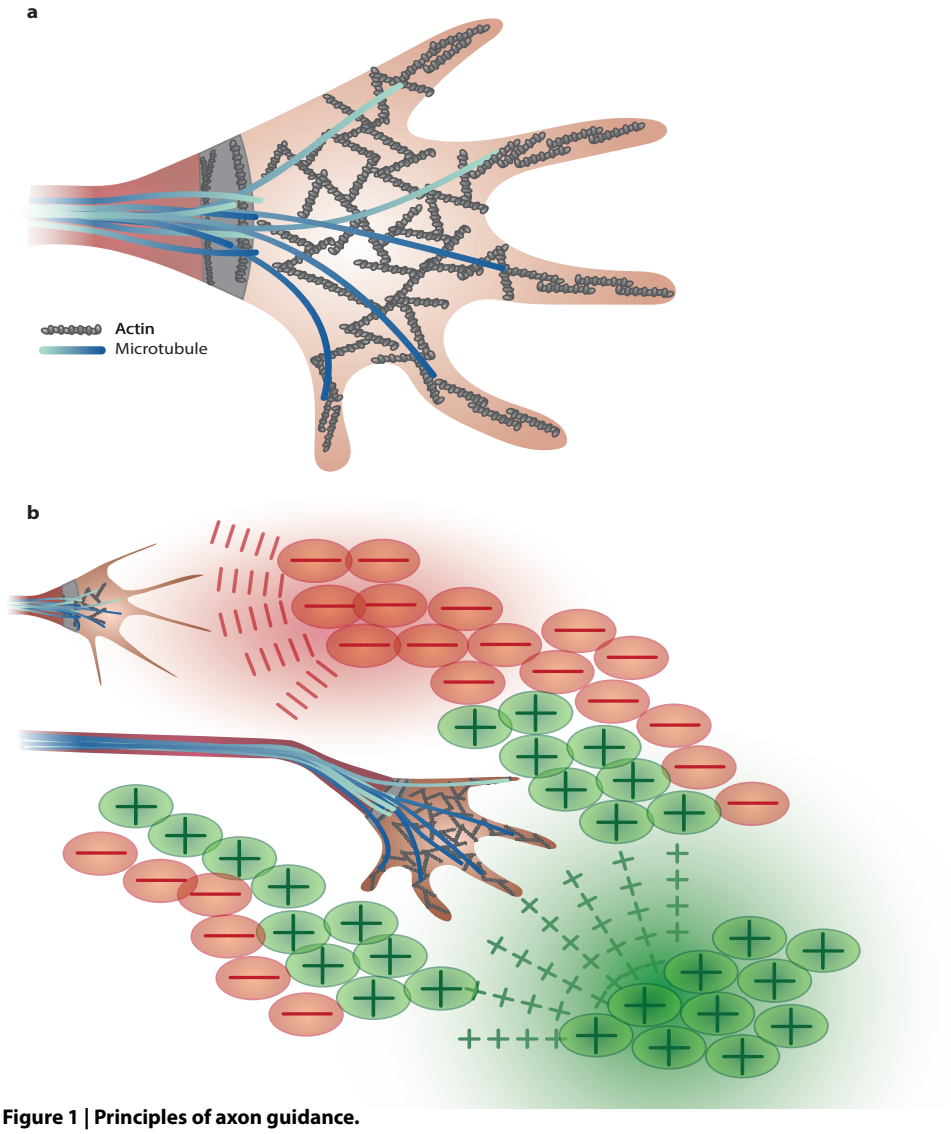

Figure 1 | Principles of axon guidance.
(**a**) The tip of the axon consists of the growth cone. This is a highly motile structure that detects and reacts to cues in the environment. The growth cone contains actin filaments that are lined as a meshwork in the growth cone to form lamellipodia. In the outward extending protrusions, the filopodia, actin filaments are bundles together. The microtubule network ensures that proteins are delivered and can be removed from the growth cone.
(**b**) A neuron samples the environment with its growth cone. Attractive and repulsive cues induce extension or collapse of the actin network. Shown are two growth cones. The top growth cone arrives in an area that contains repulsive cues. As a result, F-actin is destabilized and the growth cone collapses. The bottom growth cone is positioned past the repulsive environment and is surrounded by attractive cues. The actin structures will extend further to guide the axon towards its target tissue.

understanding of brain disease and eventually lead to new therapeutic strategies.
To further understand the development of the brain, it is important to characterize poorly characterized guidance cues and study their intracellular signalling mechanisms. Not all proteins in the Semaphorin and Plexin families are well characterized. In **Chapter 2** we study a poorly characterized Semaphorin, Sema4F. A detailed spatiotemporal mRNA expression profile of *Sema4F* is provided in this chapter. Furthermore, the first *Sema4F* (knock-out) KO mouse is generated to investigate the *in vivo* function of Sema4F during development and in adulthood.

Transcriptional regulation of Semaphorins and Plexins

Differential expression of guidance cues contributes to the organization and development of neuronal connections. The expression of Semaphorins and Plexins is highly regulated to control their spatial and temporal expression and effects via transcription factors. For example, SoxC transcription factors (Sox4, Sox11 and Sox12) upregulate PlexinA1 and Ng-CAM related Cell Adhesion Molecule (Nr-CAM) by binding to their promoters between E17.5 and P0. PlexinA1 and Nr-CAM function as receptors for Sema6D, which facilitates contralateral retinal ganglion axon midline crossing. On the other hand, Notch-Hes5 signalling is required to maintain progenitor states of retinal ganglion cells. SoxC transcription factors repress Notch-Hes5 signalling to promote retinal ganglion cell differentiation and contralateral crossing at the optic chiasm via PlexinA1 and Nr-CAM [29–31]. In addition, other strategies, such as local translation, endocytosis, protein degradation, phosphorylation and protein binding are used to control the expression and function of Semaphorins and Plexins [32–36]. An increasing number of transcription factors that control the expression of Semaphorins and Plexins are being identified. In **Chapter 4** the transcription factors upstream of *PlexinC1* in mesodiencephalic dopamine circuit formation are studied. PlexinC1 expression is repressed by Lmx1a/b and regulates mesodiencephalic dopamine axon guidance.

Diversification of Semaphorin-Plexin signalling

Transmembrane Semaphorins and Plexins are repeatedly used throughout neural circuit development. Through specialised modes of action for Semaphorin-Plexin signalling, a limited number of guidance cues is sufficient to regulate a disproportionally large number of cellular events. Several of these so-called diversification mechanisms have been identified and are described below, including *trans* or *cis* interactions, bifunctional signalling, bidirectional signalling and heteromultimeric receptor complex formation.

Semaphorin-Plexin signalling can be controlled through ***trans*** or ***cis*** **interactions**. Canonical signalling pathways require Semaphorins and Plexins on separate cells where a *trans* interaction results in a cellular event. During *cis* interactions, the receptor and ligand are both present on the same cell and this interaction often results in signalling inhibition. For example, mossy fibers from the dentate gyrus (DG) synapse in the stratum lucidum of the (Cornu Ammonis) CA region in the hippocampus during development. Sema6A expressing pyramidal cells in the CA region repel growing mossy fibers that express PlexinA4. The target area, stratum lucidum, expresses PlexinA2 in addition to Sema6A. Cis interaction between Sema6A and PlexinA2 reduces the repulsive effect of Sema6A on PlexinA4^{+} mossy fibers, enabling the mossy fibers to synapse within a specific lamina [37]. This indicates that *cis* interactions between Semaphorins and Plexins control the possibility

of *trans* interactions, thereby attenuating the effects of Semaphorins. Thus, *trans* and *cis* interactions regulate Semaphorin-Plexin downstream signalling events.

Bifunctional signalling occurs when a single protein can have different, sometimes opposing, biological effects. For Semaphorins and Plexins bifunctional signalling is classically used to describe proteins that can exert repulsive (i.e. negative or inhibitory) and attractive (i.e. positive or promoting) effects. The ability for bifunctional signalling of Semaphorins can be dependent on receptors. For instance, in this thesis it is shown that Sema7A can have two distinct effects on the same cell (**Chapter 3**). When bound to PlexinC1, it controls the proliferation of adult born granule cells in the hippocampus. While in the dendrites of new-born granule cells, Sema7A-β1-integrin promotes dendritic integration [38]. Bifunctional Semaphorin-Plexin signalling can also depend on the availability of other intrinsic and extrinsic molecules. This is exemplified in Sema4D-PlexinB1 signalling. In the hypothalamus, gonadotropin-releasing hormone expression neurons (GnRH neurons) are attracted towards Sema4D via PlexinB1 through Met tyrosine kinase activity [39]. In contrast, in hippocampal neurons Sema4D-PlexinB1 signalling causes growth cone collapse through a phosphatase and tensin homolog (PTEN)-dependent decrease in Ras-related protein (R-Ras) activity [40]. Bifunctional signalling is a common feature of Semaphorins.

Bidirectional signalling describes the ability of Semaphorins to act both as ligands (forward signalling) and receptors (reverse signalling) [41,42]. Forward signalling is described for all Semaphorins, while reverse signalling is currently only clearly established for Sema4A, Sema4D, Sema6A, Sema6B and Sema6D [43–49]. The intracellular amino acid sequence of Semaphorins belonging to a particular subclass is highly conserved, suggesting that reverse signalling capacities occur more generally for class 4-6 Semaphorins [9,50,51]. Forward signalling of Sema4A induces growth cone collapse in cultured hippocampal neurons [52] and cell collapse in COS-7 cells via PlexinB receptors [11]. Reverse signalling of PlexinB1-Sema4A promotes dendritic cell migration *in vitro* through downstream signalling of Scrib [47]. These seemingly opposite effects are also described for Sema6A. Decreased migration of cultured cerebellar explants is found when grown on Sema6A-expressing 3T3 cells. However, when reverse signalling through Sema6A is induced by PlexinA2-expressing 3T3 cells, migration of cerebellar granular cells is increased compared to control [43]. Semaphorins and Plexins can expand their signalling capacities by functioning both as a ligands and receptors. Major questions about these mechanisms remain. For instance, what is the *in vivo* significance of bidirectional signalling and how is it regulated? In **Chapter 5** reverse signalling downstream of Sema6A is studied by identifying novel Sema6A-interacting proteins via mass spectrometry.

Another regulatory mechanism that controls Semaphorin-Plexin signalling is the formation of **heteromultimeric receptor complexes**. Crystal structures show a preference of Semaphorins to function as homodimers. In contrast, Plexins do not show this preference and often appear monomeric [9,14,53,54]. Literature shows that Plexins not only bind co-receptor proteins such as neuropilins, but can also structurally interact with other Plexins [55,56]. The most recent example was shown in gliobastoma cell lines where PlexinD1-PlexinA4 heterodimers allow Sema3C-induced collapse [57]. How monomer and dimer configurations are used to control Semaphorin-Plexin signalling is unclear. It is likely that heterodimers of Plexins, and perhaps Semaphorins, could fulfil specialised functions during brain development.

Within one system, multiple modes of Semaphorin-Plexin signalling, as described above, may be used. For example, commissural axons cross at the floorplate in chick embryos. Dorsal spinal cord axons express PlexinA2 that binds Sema3A in *trans* causing

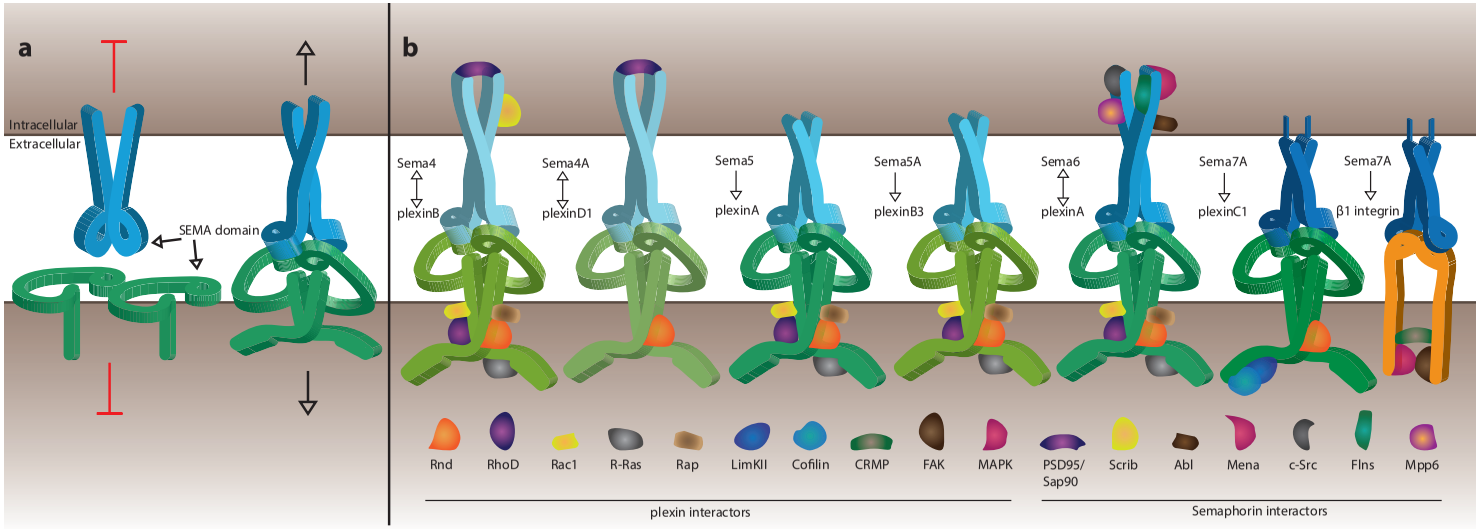

Figure 2 | Schematic overview of mammalian membrane-associated Semaphorins, Plexins and downstream interactors.
(**a**) Mammalian membrane-associated Semaphorins (blue) are found as non-active dimers in the membrane. Their canonical receptors, Plexins (green), are found in dimers and monomers in the membrane. When Plexins form dimers, a head-to-stalk conformation is constructed resulting in auto-inhibition. When Semaphorins (Sema) and Plexins interact in heterodimers a conformational change causes the Plexin Sema domain to connect with the Sema domain of the Semaphorin. Now signalling can occur downstream of Plexins and Semaphorins. Only trans-interactions between Semaphorins and Plexins are depicted here. However, *cis* interaction can also occur, often resulting in a reduction in *trans* interactions between Semaphorins and Plexins. (**b**) A schematic overview of the downstream interactors established for membrane-associated Semaphorins and Plexins. Sema4s generally interact with PlexinBs. PlexinB downstream interactors include GTPase-activating proteins (GAP) and RhoGTPases. Reverse signalling is also established for Sema4s via postsynaptic density protein 95 (PSD95) or Scrib. Apart from PlexinBs, Sema4A interacts with PlexinD1. For Sema5A, only forward signalling is currently established. The canonical receptors for Sema5A are PlexinAs that can transduce signalling events through RhoGTPases and RasGTPases. PlexinB3 also interacts with Sema5A. Forward and reverse signalling is established for Sema6s that interact with PlexinAs. Downstream of PlexinAs RhoGTPases and RasGTPases are activated. Downstream of Sema6s various pathways are described including the Evl/Mena/VASP pathway, Abelson (Abl) signalling, c-Src, Filamins and membrane palmitoylated protein 6 (Mpp6). Sema7A is linked to the membrane and can interact with PlexinC1 or β1-integrin. PlexinC1 can signal via RhoGTPases or Lim domain Kinase II, resulting in Cofilin phosphorylation. Sema7A-β1-integrin signalling results in the activation of Focal Adhesion (FA)- mitogen activated protein kinase (MAPK) pathway leading to actin remodelling. The arrows indicate forward and / or reverse signalling.

axon repulsion at the floorplate. However, as axons approach the floorplate, dorsal axons co-express Sema6B that interacts in *cis* with axonal PlexinA2, making axons unresponsive to Sema3A. Following floorplate crossing, PlexinA2 is expressed at the floorplate binding axonal Sema6A binding in trans. As a consequence, axonal PlexinA2 becomes available to interact in *trans* with Sema3A at the floorplate resulting in axonal repulsion once more. [44,58,59]. The diversification mechanisms that regulate Semaphorin-Plexin signalling are just beginning to be understood and more insight is needed into downstream receptor and intracellular signalling mechanisms involved.

Downstream signalling of Semaphorins and Plexins

Upon Semaphorin-Plexin interaction, conformational changes lead to activation of downstream signalling mechanisms (Fig. 2a). Crystal structures of extracellular parts of Semaphorins and Plexins have shown that intermolecular binding occurs via the Sema binding domain of both proteins [8–10,54]. Prior to binding, Plexins are located at the membrane in a ring-like conformation in a head-to-stalk cis-interaction with another Plexin molecule via their PSI domains (Plexin, Sema, integrin domain), causing auto-inhibition [14]. Upon binding to Semaphorin, the conformation of Plexin changes and intracellular modules, including the Rho binding domain (RBD) and GTPase activating protein (GAP) domains, come into close vicinity and lead to downstream signalling (forward signalling). Semaphorins can also activate downstream signalling via reverse signalling mechanisms. In this section, well-established interactors downstream of Semaphorins and Plexins are described (Fig. 2b).

Intracellular interactors of Plexins

There are several well-described signalling mechanisms downstream of Plexins that regulate the (dis)assembly of the cytoskeleton to control the morphology of the growth cone (Fig. 2b). The first described interactor was collapsin response mediator protein (CRMP) that is activated downstream of integrins and PlexinAs (-neuropilin) resulting in actin disassembly of growth cones *in vitro* [60–62]. Other signalling proteins are members of the Rho family that bind to the RBD and PDZ domains of Plexins to control cytoskeletal dynamics. RhoGTPases regulate their activity via specific Guanine nucleotide Exchange Factors (GEFs) and GAPs. For instance, Rnd GTPase proteins act downstream of all Plexin classes [63–65]. However, only weak binding is shown for PlexinC1 and PlexinD1 [66]. RhoD has been found downstream of class A and B Plexins [65], while Rac1 functions solely downstream of class B Plexins. Downstream signalling of Plexins also involves Ras GTP-binding protein (Rap). Rap is recruited to the GAP domain upon Plexin activation to permit growth cone collapse [66–68]. Noteworthy, Rap is not recruited when Plexins are auto-inhibited suggesting that dimerization (with or without Plexin's extracellular domain) is crucial for downstream signalling activation [14,67]. To achieve actin remodelling, additional proteins are involved in these signalling cascades downstream of Plexins. For instance, roles for cyclic adenosine monophosphate (AMP) and guanosine monophosphate (GMP) are described in *Drosophila* downstream of PlexA [69] and are considered important for (in)vertebrate neuronal connectivity [70–72]. Also, actin-remodelling proteins themselves are often part of the signalling cascade. For example, Cofilin, a well-known modulator of F-actin, is found downstream of PlexinC1 [73]. Conclusive, extensive signalling cascades function downstream of Plexins to accomplish actin remodelling.

Intracellular interactors of transmembrane Semaphorins

Reverse signalling is currently firmly established for Sema4A, Sema4D, Sema6A, Sema6B, and Sema6D in vertebrates [43–49]. The transmembrane class 5 Semaphorins have large intracellular domains, implying that reverse signalling could also occur downstream of these Semaphorins. Class 4 and 6 Semaphorins have distinct downstream signalling cascades. However, most downstream interactors remain unidentified. Co-immunoprecipitations approaches could provide information regarding downstream signalling cascade of transmembrane Semaphorins. In the following paragraphs, the known downstream interactors for Sema4 and Sema6 are described.

For Sema4s only one reverse signalling cascade is identified. Sema4A stimulates the migration of cultured cancer and dendritic cells via the Scrib/rac/ Cell division control protein 42 homolog (Cdc42) pathway [47]. PlexinB1-Sema4A signalling removes Scrib from its complex, the Rac/Cdc42 exhange factor βPIX, thereby decreasing the activity of Rac1 and Cdc42 and impairing migration [47]. Another possible reverse signalling mechanism downstream of Sema4 could involve the intracellular PDZ-binding motif. Sema4B, Sema4C, Sema4F and Sema4G can bind to postsynaptic density protein 95 (PSD-95/SAP90) [74–76]. Semaphorins may interact with PSD-95/SAP90 for cell localization. For example, co-transfection of Sema4F or Sema4B with PSD-95/SAP90 in cell lines shows translocation and clustering of the complex [74,76]. In hippocampal cultures, Sema4B-PSD-95/SAP90 interaction is important for synaptic localization [76]. Whether the PDZ-binding motif of Sema4s is solely used for cellular localization remains to be determined. Potentially, specific downstream signalling cascades can be induced via PSD-95/SAP90 given the many functions and interactors of this complex [77–79]. Thus other, unidentified, reverse signalling cascades may be initiated via the PDZ-binding motif and may involve PSD-95/SAP90 or other proteins containing PDZ-binding motifs for class 4 Semaphorins.

The signalling cascade downstream of Sema6A and Sema6D involves the Ena/ VASP-like protein (Evl)/ Murine Ena (Mena)/ Vasodilator stimulated phosphoprotein (VASP) pathway, which is activated via the zyxin-like carboxy-terminal domain [41]. Upon activation, the Sema6 cytoplasmic domain interacts with Abelson (Abl) and Mena, shown by immunoprecipitation (IP) of overexpressed Sema6A or Sema6D in COS-7 and HEK cells, respectively [43,45,49]. The tyrosine kinase Abl (*Drosophila* homologous to Enable) is an Evl/Mena/VASP pathway modulator [43,80]. Abl can phosphorylate Mena to promote cell migration and actin remodelling [45,81,82], possibly via lamellipodin [83]. The Sema6A-Abl-Mena complex binds β–actin to control actin dynamics [84] for instance to decrease axonal length in cultured cerebellar neurons [43]. Interestingly, the signalling cascade downstream of Sema6A seems to depend upon its activation mode. A recent study showed that Sema6A reverse signalling is activated by ligand binding (PlexinA2 or PlexinA4) or by multimerisation of Sema6A [43]. When Sema6A is activated via PlexinA2, Abl is recruited and phosphorylated. Multimerisation of Sema6A, i.e. activation of Sema6A independent of a ligand, does not activate Abl *in vitro*. Interestingly, recruitment of Mena is found independent of PlexinA2 binding [43]. This implies that the interactor of Sema6A (possibly PlexinA2, PlexinA4 or Sema6A) regulates the reverse signalling cascade downstream of Sema6A involving the Evl/Mena/VASP pathway.

A slightly different mode of action is established for Sema6B. The intracellular Src homology 3 (SH3) binding domain of Sema6B interacts with the proto-oncogene tyrosine protein kinase Src (c-Src) when overexpressed in COS-7 cells [46]. C-Src interacts with the Evl/Mena/VASP pathway, possibly via Mena to influence actin polymerisation [80,85,86]. Phosphorylation of EVL controls its actin remodelling activity where phosphorylated EVL

displayed reduced actin nucleation compared to dephosphorylated EVL [80]. This suggests that interactors downstream of Sema6B could influence the phosphorylation of the Evl/Mena/VASP pathway to control actin-remodelling.

Identifying all the downstream interactors of Semaphorins and Plexins is crucial to understand their signalling mechanism and functions during brain development and maintenance. A growing number of intracellular interactors downstream of Semaphorins and Plexins are being identified. A recent study confirmed binding between Sema6A-D and Filamins (Flns) A-C and membrane palmitoylated protein 6 (Mpp6) in HEK293T cells. The *Drosophila* orthologous of these proteins, Cheerio and Varicose, potentially induce the repulsive action of Pebble and Sema1a [87]. Interestingly, the PDZ binding motif is necessary for Varicose but not for Cheerio binding [87], suggesting distinct binding sites on Sema1a. In this thesis, we performed mass spectrometry following immunoprecipitation of full length Sema6A to find new intracellular components of the reverse signalling cascade of Sema6A (**Chapter 3**).

Semaphorins and Plexins control brain development and maintenance *in vivo*

Membrane-associated Semaphorins and Plexins have specialised tasks during the development and maintenance of the brain. Semaphorins and Plexins can induce specific downstream signalling cascades to induce their biological effects. However, many studies focussing on Semaphorin-Plexin signalling are carried out *in vitro*. The functions and downstream signalling cascades of Semaphorins and Plexins are incompletely determined *in vivo*. The following paragraphs illustrate the *in vivo* roles of Semaphorins and Plexins during prenatal development of the hippocampus and cortex, as well as postnatal roles during adult neurogenesis. Per region, the *in vivo* effects of Semaphorin-Plexin signalling are described for neurogenesis, axon projections and circuit formation.

Hippocampal development controlled by Semaphorins and Plexins

The hippocampus is an important structure for memory formation and spatial orientation. Secreted factors instruct the medial telencephalon to form the hippocampus at E8.5. Morphogens and transcription factors such as Fibroblast Growth Factors (FGFs), wingless-type MMTV integration site (Wnt), and Empty Spiracles Homeobox 2 (EMX2) ensure the first steps of the formation of the substructures of the hippocampus, such as the dentate gyrus. CA 1-3, (pre, para) subiculum and the entorhinal cortex. Neurogenesis in the ventricular zone provides progenitors that migrate via radial glia cells towards Cajal-Retzius cells located at the marginal zone. The hippocampus is formed in an inside-out manner, where the earliest born neurons locate in the CA3 region at E11.5. Progenitors proliferate and differentiate into multipolar neurons. Neurons attach to radial glia processes, become bipolar and initiate migration towards the pial surface. At E17, two streams of tangentially migrating interneurons, at the marginal and intermediate zones, move into the hippocampus. The DG is formed by tangentially migrating progenitors via the sub-pial stream at E18. The suprapyramidal blade of the DG is formed at E19, followed by the infrapyramidal blade at P5 (See for a more detailed overview: [88–91]). In *PlexinA2* KO mice, granular cells of the DG are mislocalized. The blades are not separated at P1 and display odd shaped turns at P30. This phenotype is not present in a mouse line lacking the GAP function downstream of

PlexinA2, suggesting that PlexinA2 acts as a ligand. Interestingly, a similar phenotype was found in *Sema5A* KO mice [37,92,93], suggesting an important role for signalling via Sema5A-PlexinA2 in cell migration in the dentate gyrus.

Mossy fiber projections from granule cells in the dentate gyrus innervate the stratum lucidum of the pyramidal layer. These projections are regulated via Sema6A/B and PlexinA2/4 interactions. In short, Sema6A in pyramidal cells in the CA region repel outgrowing PlexinA4$^+$ mossy fiber projections. In the stratum lucidum, Sema6A/PlexinA2 *cis* binding inhibits the repulsive action of Sema6A on PlexinA4$^+$ projections, enabling mossy fiber synapse formation on pyramidal cells [37,94]. In accordance, aberrant mossy fiber projections are found in *PlexinA2* and *PlexinA4* KO mice. Interestingly, this is not the case for hypomorphic *Sema6A* KO mice [95–97]. Surprisingly, *Sema6B* KO mice do show disturbed mossy fiber projections, and even more pronounced mossy fiber defects are detected in *Sema6A;Sema6B* double KO mice. Together, this suggests that regulation of mossy fiber projections is more complex than initially described, implicating both Sema6A and Sema6B in this process [98].

In the hippocampus, granule cells in the dentate gyrus receive information from pyramidal cells in layer II/III of the entorhinal cortex and extend this information to pyramidal cells in the CA3 region. In their turn, CA3 axons synapse on CA1 pyramidal cells to provide feedback to layer V of the entorhinal cortex. The assembly and elimination of synapses in the hippocampus is under tight control. Several studies have shown roles for Sema4B, Sema4D and Sema5B in glutamatergic and GABAergic synapse development. In vitro, Sema4B is required for both inhibitory and excitatory synapse formation [99,100], whereas Sema4D regulates inhibitory synapse development [100–103]. Proteolytically cleaved Sema5B is involved in synapse elimination. Overexpression of Sema5B reduces synapse number in hippocampal cultures [21,104]. Future *in vivo* studies are needed to provide more insight into the role of Semaphorin-Plexin signalling in synapse development in the hippocampus.

The hippocampus is an important hub, processing information from and to the entorhinal cortex [89,105,106]. Its development is complex and requires Semaphorins, Plexins and many other (guidance) cues. Many Semaphorins and Plexins are expressed in the hippocampus (**Chapter 2**, **5** and **6**). However, their precise function and signalling cascades in the hippocampus remain incompletely understood. Future research into the precise roles of these guidance cues will provide more detailed information on the development of the hippocampus.

Cortical development controlled by Semaphorins and Plexins

Cortical prenatal neurogenesis occurs in the mouse from E12 till E18. The precise processes by which the layers of the cortex are formed are described in recent reviews [107–112]. In short, asymmetric proliferation of progenitors at the ventricular zone leads to the generation of neurons. The initial formation of the cortex is similar to the formation of the hippocampus. In the multipolar accumulation zone newborn neurons will extend multiple processes dynamically before they acquire a bipolar morphology. Via the fibers of radial glial cells, neurons will migrate laterally into more superficial positions. The processes of the neurons will attach to the surface and move their nucleus towards the marginal zone containing Cajal-Retzius cells, which are located on top of the cortical plate. The neurons will detach and form a cortical layer together with neurons born around the same time, forming the six layers of the cortex in an inside-out manner under the control of Reelin.

The six layers of the cortex contain distinct neurons based on morphology and projections. Corticogenesis and the laminar organisation of the cortex are strictly controlled

by various signalling mechanisms. Semaphorins and Plexins are known to influence corticogenesis, migration and laminar organization of cortical neurons [95–97,113–117]. In 2010, Hirschberg et al., showed that Sema4D-PlexinB2 signalling regulates cell specification, differentiation and migration during corticogenesis. Mice lacking *PlexinB2* show reduced numbers of mature ($NeuN^+$) neurons and abnormal patterning and density of radial glia ($GFAP^+$) and progenitor cells ($Nestin^+$) at E18 [114,115]. In addition, decreased numbers of Cajal-Retzius cells ($Reelin^+$, $Calretinin^+$) are positioned at the marginal zone in these mice [114]. In *ex vivo* cortex organotypic slice and explants cultures, addition of Sema4D enhanced cell proliferation as measured by BrdU uptake and promoted the migration of progenitors at E14.5 in a PlexinB2-dependent manner [114]. The laminar organisation of the cortex depends on various guidance cues. Deletion of Sema6A in mice results in the formation of clusters in layer II of the cortex, suggesting a role for Sema6A in lamination of the neocortex [97]. Although PlexinA2 and PlexinA4, receptors for Sema6A, are both present in the cortex, how Sema6A, its receptors and signalling mechanism regulate cortical lamination is unclear. In **Chapter 5** we show that this process is dependent on reverse signalling downstream of Sema6A.

The cortex is a highly integrated structure. Astrocytes and oligodendrocytes are postnatally produced in the subventricular zone and migrate into the cortical layers. Interneurons will integrate into the cortical layers, via radial migration from the medial ganglionic eminence or via tangential migration in case of neurons originating from the caudal ganglionic eminence. Furthermore, projections are formed between layers together with incoming axons from the contralateral hemisphere, thalamus and other brain regions [107–112]. Semaphorins and Plexins are important for the integration of afferent projections into the cortex. Deletion of *Sema6A* or *PlexinA2/A4* resulted in aberrant routing of early thalamocortical axons [95,118,119]. Although part of the misrouted axons do eventually find their target region, the structure and volume of the visual cortex is decreased [95], showing that Sema6A-PlexinA2/A4 signalling is required for the correct development of thalamocortical projections. In addition, Sema7A is required for thalamocortical integration in the barrel cortex [116,120,121]. Absence of Sema7A, in spiny stellate cells and GABAergic interneurons, functionally impairs thalamocortical synaptic response by disrupting barrel cytoarchitecture and by reducing the asymmetrical orientation of spiny stellate cell dendrites [120]. Together, these data show that members of the Semaphorin and Plexin families are involved in circuit development of the cortex.

Semaphorins and Plexins play a significant role during cortical development. Many *in vitro* studies show that Semaphorins and Plexins can modulate the growth cone morphology of cortical neurons [122–128]. However, the precise *in vivo* role of Semaphorins and Plexins is more complicated and encompasses many signalling cascades. Future research should identify other Semaphorin-Plexin signalling cascades important for cortical development as well as determine the precise downstream signalling mechanisms involved (**Chapter 2** and **5**).

Regulation of adult neurogenesis by Semaphorins and Plexins

Two brain regions, i.e. the cortex and hippocampus, contain neural progenitors that remain active throughout life. In the subventricular zone of the cortex, stem cells divide to produce new progenitor cells. These cells migrate via the rostral migratory stream (RMS) towards the olfactory bulb and integrate into a pre-existing network. A similar mechanism is at play in the subgranular zone of the hippocampal DG. Adult stem cells generate new-born neural progenitor cells that integrate into the granular layer of the DG. Intrinsic and

external factors influence the proliferation, migration and integration of these progenitors and adult-born neurons [129–134].

Several protein families, such as Notch, Wnts and bone morphogenetic proteins (BMPs) have been identified to regulate one or multiple steps of adult neurogenesis. The Semaphorin and Plexin families also show specific expression in the subventricular or subgranular zones. However, data that link Semaphorin or Plexins to adult neurogenesis is limited. Sema4A, 4C, 4D, 4F and 4G are expressed in the adult olfactory bulb [135–138] or in the subventricular zone [139]. Their receptors, PlexinB1 and PlexinB2 are found in the subgranular or subventricular zones, respectively [115,135,139–142]. PlexinB2 mutant mice showed decreased proliferation and migration in the subventricular zone 135. Furthermore, Sema4C expression in the subgranular zone is upregulated following ischemia-induced neurogenesis [139]. This indicates a role for Sema4-PlexinB signalling in the proliferation and migration during adult neurogenesis.

During the dendritic integration of adult-born neurons, Sema5A negatively regulates synaptogenesis via PlexinA2. P33 hippocampus of *Sema5A* and *PlexinA2* KO mice shows increased synapse formation in adult-born granule cells. Transfection of Sema5A into DG cultures attenuates this effect [93]. Consequently, disturbances in social behaviour and memory formation are found in Sema5A and *PlexinA2* KO mice [92,93]. This supports a role for Sema5A-PlexinA2 interactions in *cis* during the integration of adult-born neurons. Together, these data show a role for Semaphorin-Plexin signalling during adult neurogenesis. The function of Sema7A and its receptors, PlexinC1 and β1-integrin, in adult neurogenesis is studied in **Chapter 3**.

Semaphorin-Plexin signalling disturbances can lead to brain disease

Membrane-associated Semaphorins and Plexins have pleiotropic effects during brain development and function. Perturbation of these cues leads to various brain diseases (for more information see van Battum et al. 2015). Genomics analyses can provide novel and important information regarding genetic influences in (disease) phenotypes. For instance, genome-wide copy number variation links *Sema5A* to Autism Spectrum Disorder (ASD) [93,143–145]. Genome-wide association studies performed within families with ASD or unrelated patients identify *SEMA4D, SEMA6A, SEMA7A, PLXNC1* and *PLXNA4* [143,146,147]. In addition, Semaphorins and Plexins have been linked to neurodegenerative diseases such as ALS, Parkinson's disease and Alzheimer's disease [147–152]. Closer in-depth analysis of the consequences of genetic variations within Semaphorin and Plexin family members will provide information about their function in humans and may provide a translational approach towards treatment. In **Chapter 6** whole exome sequencing reveals variation in the humans *PLXNB3* gene in patients with neurodevelopmental disorders. In this chapter the functional consequences of these SNPs are studied *in silico* and *in vitro* in relation to the patient's phenotype.

Thesis aim and outline

A myriad of proteins and signalling mechanisms function during brain development. The specific roles of transmembrane Semaphorins and their Plexin receptors are explored in this thesis. Perturbation of Semaphorin-Plexin signalling can lead to neurological disorders. To better understand these pathological conditions a complete fundamental understanding of the complex signalling routes that lead to correct formation of neuronal connections is crucial.

It is important to identify all regulators of brain development. Some of the Plexins and Semaphorins remain poorly characterized, making it impossible to understand their contribution to the development of the brain. **Chapter 2** focuses on Sema4F, a thus far poorly characterized Semaphorin. In this chapter, the *Sema4F* expression profile is validated over time and a *Sema4F* KO mouse model is presented to study *in vivo* functions of Sema4F. Other Semaphorins are better characterized but lack understanding of their precise mechanism-of-action within certain brain regions. In **Chapter 3**, we explore the role of Sema7A and its receptors during adult neurogenesis in the dentate gyrus. We show that Sema7A induces different effects on the same cell via distinct receptors using *in vitro* and *in vivo* approaches. In **Chapter 4**, the regulation of axonal guidance cues is investigated. We show that PlexinC1 expression is under the control of transcription factors Lmx1a and Lmx1b during dopaminergic circuit development. Reverse signalling is studied in **Chapter 5** by identifying new Sema6A-interacting proteins via mass spectrometry. The final experimental chapter provides insights into the importance of Semaphorin-Plexin signalling in human brain disease. In **Chapter 6**, *PLXNB3* variants are found in patients with neurodevelopmental disorders. The functional consequences of these variants are studied *in silico* and *in vitro* in relation to brain development.

In conclusion, this thesis aims to comprehend multiple aspects of Semaphorin-Plexin signalling in the healthy (**Chapter 2-5**) and diseased brain (**Chapter 6**). The results show that Semaphorin-Plexin signalling is necessary for proper brain development via complex and diverse signalling mechanisms. These findings are linked to the fundamental understanding of Semaphorin-Plexin signalling and therefore contribute to the understanding of brain development in health and disease.

1

References

1. Sanes, J. R. & Yamagata, M. Many paths to synaptic specificity. *Annu Rev Cell Dev Biol* 25, 161–195 (2009).
2. van Battum, E. Y., Brignani, S. & Pasterkamp, R. J. Axon guidance proteins in neurological disease. *Lancet Neurol* 14, 532–546 (2015).
3. Pasterkamp, R. J. Getting neural circuits into shape with semaphorins. *Nat Rev Neurosci* 13, 605–18 (2012).
4. Russell, S. A. & Bashaw, G. J. Axon guidance pathways and the control of gene expression. *Dev Dyn* 247, 571–580 (2018).
5. Stoeckli, E. Where does axon guidance lead us? *F1000Research* 6, 1–8 (2017).
6. Alto, L. T. & Terman, J. R. Semaphorins and their Signaling Mechanisms. *Methods Mol Biol* 1493, 1–25 (2017).
7. Antipenko, A. *et al.* Structure of the Semaphorin-3A receptor binding module. *Neuron* 39, 589–598 (2003).
8. Love, C. A. *et al.* The ligand-binding face of the semaphorins revealed by the high-resolution crystal structure of SEMA4D. *Nat Struct Biol* 10, 843–846 (2003).
9. Janssen, B. J. C. *et al.* Structural basis of semaphorin–plexin signalling. *Nature* 467, 1118–1122 (2010).
10. Liu, H. *et al.* Structural basis of semaphorin-plexin recognition and viral mimicry from sema7A and A39R complexes with PlexinC1. Cell 142, 749–761 (2010).
11. Yukawa, K. *et al.* Sema4A induces cell morphological changes through B-type plexin-mediated signaling. *Int J Mol Med* 25, 225–230 (2010).
12. He, H., Yang, T., Terman, J. R. & Zhang, X. Crystal structure of the plexin A3 intracellular region reveals an autoinhibited conformation through active site sequestration. *Proc Natl Acad Sci* U S A 106, 15610–5 (2009).
13. Tong, Y. *et al.* Structure and function of the intracellular region of the plexin-B1 transmembrane receptor. *J Biol Chem* 284, 35962–35972 (2009).
14. Kong, Y. *et al.* Structural Basis for Plexin Activation and Regulation. *Neuron* 91, 548–560 (2016).
15. Oinuma, I., Katoh, H. & Negishi, M. Semaphorin 4D/Plexin-B1-mediated R-Ras GAP activity inhibits cell migration by regulating β1 integrin activity. *J Cell Biol* 173, 601–613 (2006).
16. Kuklina, E. M., Nekrasova, I. V., Baidina, T. V. & Danchenko, I. Y. The role of the sema4D/CD72-dependent signal in the regulation of B-cell activity in multiple sclerosis. *Dokl Biol Sci* 458, 316–318 (2014).
17. Leitner, D. F., Todorich, B., Zhang, X. & Connor, J. R. Semaphorin4A Is Cytotoxic to Oligodendrocytes and Is Elevated in Microglia and Multiple Sclerosis. *ASN Neuro* 7, (2015).
18. Esselens, C. *et al.* The cleavage of semaphorin 3C induced by ADAMTS1 promotes cell migration. *J Biol Chem* 285, 2463–2473 (2010).
19. Bribián, A. *et al.* Sema3E/PlexinD1 regulates the migration of hem-derived Cajal-Retzius cells in developing cerebral cortex. *Nat Commun* 5, 4265 (2014).
20. Messersmith, E. K. *et al.* Sernaphorin III can function as a selective chemorepellent to pattern sensory projections in the spinal cord. *Neuron* 14, 949–959 (1995).
21. Browne, K., Wang, W., Liu, R. Q., Piva, M. & O'Connor, T. P. Transmembrane semaphorin5B is proteolytically processed into a repulsive neural guidance cue. *J Neurochem* 123, 135–146 (2012).
22. Elhabazi, A., Delaire, S., Bensussan, A., Boumsell, L. & Bismuth, G. Biological Activity of Soluble CD100. I. The Extracellular Region of CD100 Is Released from the Surface of T Lymphocytes by Regulated Proteolysis. *J Immunol* 166, 4341–4347 (2001).
23. Angelisová, P., Drbal, K., Cerný, J., Hilgert, I. & Horejsí, V. Characterization of the human leukocyte GPI-anchored glycoprotein CDw108 and its relation to other similar molecules. *Immunobiology* 200, 234–245 (1999).
24. Sadanandam, A. *et al.* Secreted semaphorin 5A suppressed pancreatic tumour burden but increased metastasis and endothelial cell proliferation. *Br J Cancer* 107, 501–507 (2012).
25. De Wit, J. & Verhaagen, J. Role of semaphorins in the adult nervous system. *Prog Neurobiol* 71, 249–267 (2003).
26. Brignani, S. & Pasterkamp, R. J.Neuronal Subset-Specific Migration and Axonal Wiring Mechanisms in the Developing Midbrain Dopamine System. *Front Neuroanat* 11, 55 (2017).
27. Battistini, C. & Tamagnone, L. Transmembrane semaphorins, forward and reverse signaling: have a look both ways. *Cell Mol Life Sci* 73, 1609–22 (2016).
28. Jongbloets, B. C. & Pasterkamp, R. J. Semaphorin signalling during development. *Development* 141, 3292–3297 (2014).

29. Kuwajima, T., Soares, C. A., Sitko, A. A., Lefebvre, V. & Mason, C. SoxC Transcription Factors Promote Contralateral Retinal Ganglion Cell Differentiation and Axon Guidance in the Mouse Visual System. *Neuron* 93, 1110–1125 (2017).
30. Kuwajima, T. *et al.* Optic Chiasm Presentation of Semaphorin6D in the Context of Plexin-A1 and Nr-CAM Promotes Retinal Axon Midline Crossing. *Neuron* 74, 676–690 (2012).
31. Huang, H. Y. *et al.* SOX4 Transcriptionally Regulates Multiple SEMA3/Plexin Family Members and Promotes Tumor Growth in Pancreatic Cancer. *PLoS One* 7, e48637 (2012).
32. Kong, Y. *et al.* Structural Basis for Plexin Activation and Regulation. *Neuron* 91, 548–560 (2016).
33. Yang, T. & Terman, J. R. Characterizing PKA-mediated phosphorylation of Plexin using purified proteins. *Methods Mol Biol* 1493, 147–159 (2017).
34. Lin, A. C. & Holt, C. E. Local translation and directional steering in axons. *EMBO J* 26, 3729–36 (2007).
35. Van Erp, S. *et al.* Lrig2 Negatively Regulates Ectodomain Shedding of Axon Guidance Receptors by ADAM Proteases Article Lrig2 Negatively Regulates Ectodomain Shedding of Axon Guidance Receptors by ADAM Proteases. *Dev Cell* 35, 537–552 (2015).
36. Derijck, A. a H. a, Van Erp, S. & Pasterkamp, R. J. Semaphorin signaling: molecular switches at the midline. *Trends Cell Biol* 20, 568–76 (2010).
37. Suto, F. *et al.* Interactions between Plexin-A2, Plexin-A4, and Semaphorin 6A Control Lamina-Restricted Projection of Hippocampal Mossy Fibers. *Neuron* 53, 535–547 (2007).
38. Jongbloets, B. C. *et al.* Stage-specific functions of Semaphorin7A during adult hippocampal neurogenesis rely on distinct receptors. *Nat Commun* 8, 14666 (2017).
39. Giacobini, P. *et al.* Semaphorin 4D regulates gonadotropin hormone – releasing hormone-1 neuronal migration through PlexinB1 – Met complex. *J Cell Biol* 183, 555–566 (2008).
40. Oinuma, I., Ito, Y., Katoh, H. & Negishi, M. Semaphorin 4D/Plexin-B1 stimulates PTEN activity through R-Ras GTPase-activating protein activity, inducing growth cone collapse in hippocampal neurons. *J Biol Chem* 285, 28200–28209 (2010).
41. Klostermann, A., Lutz, B., Gertler, F. & Behl, C. The orthologous human and murine semaphorin 6A-1 proteins (SEMA6A-1/Sema6A-1) bind to the enabled/vasodilator-stimulated phosphoprotein-like protein (EVL) via a novel carboxyl-terminal zyxin-like domain. *J Biol Chem* 275, 39647–39653 (2000).
42. Godenschwege, T. A., Hu, H., Shan-Crofts, X., Goodman, C. S. & Murphey, R. K. Bi-directional signaling by Semaphorin 1a during central synapse formation in Drosophila. *Nat Neurosci* 5, 1294–1301 (2002).
43. Perez-Branguli, F. *et al.* Reverse signaling by Semaphorin-6A regulates cellular aggregation and neuronal morphology. *PLoS One* 11, e0158686 (2016).
44. Andermatt, I. *et al.* Semaphorin 6B acts as a receptor in post-crossing commissural axon guidance. *Development* 141, 3709–20 (2014).
45. Toyofuku, T. *et al.* Guidance of myocardial patterning in cardiac development by Sema6D reverse signalling. *Nat Cell Biol* 6, 1204–1211 (2004).
46. Eckhardt, F., Behar, O. & Calautti, E. A Novel Transmembrane Semaphorin Can Bind c-src. *Mol Cell Neurosci* 419, 409–419 (1997).
47. Sun, T. *et al.* A reverse signaling pathway downstream of Sema4A controls cell migration via Scrib. *J Cell Biol* 216, 199–215 (2017).
48. Granziero, L. *et al.* CD100/plexin-B1 interactions sustain proliferation and survival of normal and leukemic CD5+ B lymphocytes. *Blood* 101, 1962–1969 (2003).
49. Kang, S. *et al.* Semaphorin 6D reverse signaling controls macrophage Lipid Metabolism and Anti-Inflammatory Polarization. *Nat Immunol* 19, 561–570 (2018).
50. Laht, P., Pill, K., Haller, E. & Veske, A. Plexin-B3 interacts with EB-family proteins through a conserved motif. *Biochim Biophys Acta* 1820, 888–893 (2012).
51. Lange, C. *et al.* New eukaryotic semaphorins with close homology to semaphorins of DNA viruses. *Genomics* 51, 340–350 (1998).
52. Yukawa, K. *et al.* Semaphorin 4A induces growth cone collapse of hippocampal neurons in a Rho / Rho-kinase-dependent manner. *Int J Mol Med* 16, 115–118 (2005).
53. Jones, E. Y. Understanding cell signalling systems : paving the way for new therapies. *Philos Trans R Soc A* 373, (2015).
54. Nogi, T. *et al.* Structural basis for semaphorin signalling through the plexin receptor. *Nature* 467, 1123–1127 (2010).
55. Ayoob, J. C., Terman, J. R. & Kolodkin, A. L. Drosophila Plexin B is a Sema-2a receptor required for axon guidance. *Development* 2135, 2125–2135 (2006).
56. Usui, H., Taniguchi, M., Yokomizo, T. & Shimizu, T. Plexin-A1 and plexin-B1 specifically interact at their

cytoplasmic domains. *Biochem Biophys Res Commun* 300, 927–931 (2003).
57. Smolkin, T. *et al.* complexes of Plexin-A4/Plexin-D1 convey Semaphorin-3C signals to induce cytoskeletal collapse in the absence of neuropilins. *J Cell Sci* 131, (2018).
58. Nawabi, H. *et al.* A midline switch of receptor processing regulates commissural axon guidance in vertebrates. *Genes Dev* 24, 396–410 (2010).
59. Parra, L. M. & Zou, Y. Sonic hedgehog induces response of commissural axons to Semaphorin repulsion during midline crossing. *Nat Neurosci* 13, 29–35 (2010).
60. Schmidt, E. F. & Strittmatter, S. M. Semaphorins: Receptor and Intracellular Signaling Mechanisms. *Adv Exp Med Biol* 600, 1–11 (2007).
61. Tan, B. T. *et al.* The Olig family affects central nervous system development and disease. *Neural Regen Res* 9, 329–336 (2014).
62. Zhou, Y., Gunput, R.-A. F. & Pasterkamp, R. J. Semaphorin signaling: progress made and promises ahead. *Trends Biochem Sci* 33, 161–70 (2008).
63. Zhang, L. & Buck, M. Molecular Dynamics Simulations Reveal Isoform Specific Contact Dynamics Between the Plexin Rho GTPase Binding Domain (RBD) and Small Rho GTPases Rac1 and Rnd1. *J Phys Chem* 121, 1485–1498 (2017).
64. Nasarre, P., Gemmill, R. M. & Drabkin, H. A. The emerging role of class-3 semaphorins and their neuropilin receptors in oncology. *Onco Targets Ther* 7, 1663–1687 (2014).
65. Rehman, M. & Tamagnone, L. Semaphorins in cancer : Biological mechanisms and therapeutic approaches. *Semin Cell Dev Biol* 24, 179–189 (2013).
66. Wang, H. *et al.* Structural basis of Rnd1 binding to plexin Rho GTPase binding domains (RBDs). *J Biol Chem* 286, 26093–26106 (2011).
67. Wang, Y. *et al.* Plexins Are GTPase-Activating Proteins for Rap and Are Activated by Induced Dimerization. *Sci Signal* 5, ra6 (2012).
68. Wang, Y., Pascoe, H. G., Brautigam, C. A., He, H. & Zhang, X. Structural basis for activation and non-canonical catalysis of the Rap GTPase activating protein domain of plexin. *Elife* 2, e01279 (2013).
69. Chak, K. & Kolodkin, A. L. Function of the Drosophila receptor guanylyl cyclase Gyc76C in PlexA-mediated motor axon guidance. *Development* 141, 136–47 (2014).
70. Nicol, X. & Gaspar, P. Routes to cAMP: shaping neuronal connectivity with distinct adenylate cyclases. *Eur J Neurosci* 39, 1742–51 (2014).
71. Sutherland, D. J. & Goodhill, G. J. The interdependent roles of Ca2+ and cAMP in axon guidance. *Dev Neurobiol* 75, 402–410 (2013).
72. Zhang, W. *et al.* IP3-dependent intracellular Ca2+ release is required for cAMP-induced c-fos expression in hippocampal neurons. *Biochem Biophys Res Commun* 425, 450–5 (2012).
73. Scott, G. a, McClelland, L. a, Fricke, A. F. & Fender, A. Plexin C1, a receptor for semaphorin 7a, inactivates cofilin and is a potential tumor suppressor for melanoma progression. *J Invest Dermatol* 129, 954–963 (2009).
74. Schultze, W. *et al.* Semaphorin4F interacts with the synapse-associated protein SAP90/PSD-95. *J Neurochem* 78, 482–489 (2001).
75. Inagaki, S. *et al.* Sema4C, a Transmembrane Semaphorin, Interacts with a Post-synaptic Density Protein, PSD-95. *J Biol Chem* 276, 9174–9181 (2001).
76. Burkhardt, C. *et al.* Semaphorin 4B interacts with the post-synaptic density protein PSD-95/SAP90 and is recruited to synapses through a C-terminal PDZ-binding motif. *FEBS Lett* 579, 3821–3828 (2005).
77. Funke, L., Dakoji, S. & Bredt, D. Membrane-Associated Guanylate Kinases Regulate Adhesion and Plasticity at Cell Junctions. *Annu Rev Biochem* 74, 219–45 (2005).
78. Sheng, M. & Hoogenraad, C. C. The Postsynaptic Architecture of Excitatory Synapses : A More Quantitative View. *Annu Rev Biochem* 76, 823–47 (2007).
79. Zheng, S. *et al.* PSD-95 is post-transcriptionally repressed during early neural development by PTBP1 and PTBP2. *Nat Publ Gr* 15, 381–388 (2012).
80. Lambrechts, A. *et al.* cAMP-dependent Protein Kinase Phosphorylation of EVL , a Mena / VASP Relative , Regulates Its Interaction with Actin and SH3 Domains. *J Biol Chem* 275, 36143–36151 (2001).
81. Colicelli, J. ABL Tyrosine Kinases: Evolution of Function, Regulation, and Specificity. *Sci Signal* 3, re6 (2010).
82. Woodring, P. J., Hunter, T. & Wang, J. Y. J. Regulation of F-actin-dependent processes by the Abl family of tyrosine kinases. *J Cell Sci* 116, 2613–2626 (2003).
83. Michael, M., Vehlow, A. & Navarro, C. c-Abl , Lamellipodin , and Ena / VASP Proteins Cooperate in Dorsal Ruffling of Fibroblasts and Axonal Morphogenesis. *Curr Biol* 20, 783–791 (2010).

84. Prislei, S. *et al.* From plasma membrane to cytoskeleton: a novel function for semaphorin 6A. *Mol Cancer Ther* 7, 233–41 (2008).
85. Peng, Y., Murray, E. L., Sarkar, M., Liu, X. & Schoenberg, D. R. The cytoskeleton-associated Ena / VASP proteins are unanticipated partners of the PMR1 mRNA endonuclease. *RNA* 15, 576–587 (2009).
86. Ahern-djamali, S. M. *et al.* Mutations in Drosophila Enabled and Rescue by Human Vasodilator-stimulated Phosphoprotein (VASP) Indicate Important Functional Roles for Ena / VASP Homology Domain 1 (EVH1) and EVH2 Domains. *Mol Biol Cell* 9, 2157–2171 (1998).
87. Jeong, S. *et al.* Varicose and cheerio collaborate with pebble to mediate semaphorin-1a reverse signaling in Drosophila. *Proc Natl Acad Sci* 114, E8254–E8263 (2017).
88. Khalaf-Nazzal, R. & Francis, F. Hippocampal development – Old and new findings. *Neuroscience* 248, 225–242 (2013).
89. Pelkey, K. A. *et al.* Hippocampal GABAergic Inhibitory Interneurons. *Physiol Rev* 97, 1619–1747 (2017).
90. Barry, G. *et al.* Specific Glial Populations Regulate Hippocampal Morphogenesis. *J Neurosci* 28, 12328–12340 (2008).
91. Gómez, R. L. & Edgin, J. O. The extended trajectory of hippocampal development: Implications for early memory development and disorder. *Dev Cogn Neurosci* 18, 57–69 (2016).
92. Zhao, X. *et al.* PlexinA2 Forward Signaling through Rap1 GTPases Regulates Dentate Gyrus development and Schizophrenia-like Behaviors. *Cell Rep* 22, 456–470 (2018).
93. Duan, Y. *et al.* Semaphorin 5A inhibits synaptogenesis in early postnatal- and adult-born hippocampal dentate granule cells. *Elife* 3, (2014).
94. Haklai-Topper, L., Mlechkovich, G., Savariego, D., Gokhman, I. & Yaron, A. Cis interaction between Semaphorin6A and Plexin-A4 modulates the repulsive response to Sema6A. *EMBO J* 29, 2635–2645 (2010).
95. Little, G. E. *et al.* Specificity and plasticity of thalamocortical connections in Sema6A mutant mice. *PLoS Biol* 7, 0756–0770 (2009).
96. Rünker, A. E., Little, G. E., Suto, F., Fujisawa, H. & Mitchell, K. J. Semaphorin-6A controls guidance of corticospinal tract axons at multiple choice points. *Neural Dev* 3, 34 (2008).
97. Rünker, A. E. *et al.* Mutation of Semaphorin-6A disrupts limbic and cortical connectivity and models neurodevelopmental psychopathology. *PLoS One* 6, e26488 (2011).
98. Tawarayama, H., Yoshida, Y., Suto, F., Mitchell, K. J. & Fujisawa, H. Roles of Semaphorin-6B and Plexin-A2 in Lamina-Restricted Projection of Hippocampal Mossy Fibers. *J Neurosci* 30, 7049–7060 (2010).
99. McDermott, J. E., Goldblatt, D. & Paradis, S. Class 4 Semaphorins and Plexin-B receptors regulate GABAergic and glutamatergic synapse development in the mammalian hippocampus. *Mol Cell Neurosci* 93, 5–66 (2018).
100. Paradis, S. *et al.* An RNAi-based Approach Identifies New Molecules Required for Glutamatergic and GABAergic Synapse development. *Neuron* 53, 217–232 (2007).
101. Kuzirian, M. S., Moore, A. R., Staudenmaier, E. K., Friedel, R. H. & Paradis, S. The class 4 semaphorin Sema4D promotes the rapid assembly of GABAergic synapses in rodent hippocampus. *J Neurosci* 33, 8961–73 (2013).
102. Acker, D. W. M., Wong, I., Kang, M. & Paradis, S. Semaphorin 4D promotes inhibitory synapse formation and suppresses seizures *in vivo. Epilepsia* 59, 1257–1268 (2018).
103. Raissi, A. J., Staudenmaier, E. K., David, S., Hu, L. & Paradis, S. Sema4D localizes to synapses and regulates GABAergic synapse development as a membrane-bound molecule in the mammalian hippocampus. *Mol Cell Neurosci* 57, 23–32 (2013).
104. Connor, T. P. O. *et al.* Semaphorin 5B mediates synapse elimination in hippocampal neurons. *Neural Dev* 19, 1–19 (2009).
105. Neves, G., Cooke, S. F. & Bliss, T. V. P. Synaptic plasticity, memory and the hippocampus - a neural network aproach to causality. *Nat Rev Neurosci* 9, 65–75 (2008).
106. Kempermann, G., Song, H. & Gage, F. H. Neurogenesis in the adult hippocampus. *Cold spring Harb Perspect Biol* 7, a018812 (2015).
107. López-bendito, G. & Molnár, Z. Thalamocortical development: How are we going to get there? *Nat Rev* 4, 276–289 (2003).
108. Greig, L. C., Woodworth, M., Galazo, M., Padmanabhan, H. & Macklis, J. Molecular logic of neocortical projection neuron specification, development and diversity. *Nat Rev Neurosci* 14, 755–69 (2013).
109. Butt, S. J. B., Stacey, J. A., Teramoto, Y. & Vagnoni, C. A role for GABAergic interneuron diversity in circuit development and plasticity of the neonatal cerebral cortex. *Curr Opin Neurobiol* 43, 149–155 (2017).
110. Barber, M. & Pierani, A. Tangential migration of glutamatergic neurons and cortical patterning during

development : Lessons from Cajal-Retzius Cells. *Dev Neurobiol* 76, 847–81 (2015).
111. Tomassy, G. S., Lodato, S., Trayes-gibson, Z. & Arlotta, P.Development and regeneration of projection neuron subtypes of the cerebral cortex. *sci prog* 93 (Pt 2), 151–69 (2010).
112. Hirota, Y. & Nakajima, K. Control of neuronal Migration and Aggregation by Reelin Signaling in the Developing Cerebral Cortex. Front cell *Dev Biol* 5, 40 (2017).
113. Azzarelli, R. *et al.* An antagonistic interaction between PlexinB2 and Rnd3 controls RhoA activity and cortical neuron migration. *Nat Commun* 5, 3405 (2014).
114. Hirschberg, a *et al.* Gene deletion mutants reveal a role for semaphorin receptors of the plexin-B family in mechanisms underlying corticogenesis. *Mol Cell* Biol 30, 764–780 (2010).
115. Daviaud, N., Chen, K., Huang, Y., Friedel, R. H. & Zou, H. Impaired cortical neurogenesis in Plexin-B1 and -B2 double deletion mutant. *Dev Neurobiol* 76, 882–99 (2015).
116. Vitalis, T. *et al.* RORα Coordinates Thalamic and Cortical Maturation to Instruct Barrel Cortex development. *Cereb Cortex* 28, 3994–4007 (2017).
117. Graus-Porta, D. *et al.* β1-Class Integrins Regulate the development of Laminae and Folia in the Cerebral and Cerebellar Cortex. *Neuron* 31, 367–379 (2001).
118. Lakhina, V., Falnikar, A., Bhatnagar, L. & Tole, S. Early thalamocortical tract guidance and topographic sorting of thalamic projections requires LIM-homeodomain gene Lhx2. *Dev Biol* 306, 703–713 (2007).
119. Mitsogiannis, M. D., Little, G. E. & Mitchell, K. J. Semaphorin-Plexin signaling influences early ventral telencephalic development and thalamocortical axon guidance. *Neural Dev* 12, 6 (2017).
120. Carcea, I. *et al.* Maturation of cortical circuits requires Semaphorin 7A. *Proc Natl Acad Sci* U S A 111, 13978–83 (2014).
121. Fukunishi, A. *et al.* The action of Semaphorin7A on thalamocortical axon branching. *J Neurochem* 118, 1008–1015 (2011).
122. Worzfeld, T., Puschel, A. W., Offermanns, S. & Kuner, R. Plexin-B family members demonstrate non-redundant expression patterns in the developing mouse nervous system : an anatomical basis for morphogenetic effects of Sema4D during development. *Eur J Neurosci* 19, 2622–2632 (2004).
123. Tasaka, G., Negishi, M. & Oinuma, I. Semaphorin 4D / Plexin-B1-Mediated M-Ras GAP Activity Regulates Actin-Based Dendrite Remodeling through Lamellipodin. *J Neurosci* 32, 8293–8305 (2012).
124. To, K. C. W., Church, J. & Connor, T. P. O. Combined activation of calpain and calcineurin during ligand-induced growth cone collapse. *Mol Cell Neurosci* 36, 425–434 (2007).
125. Burgaya, F. *et al.* Semaphorin 6C leads to GSK-3-dependent growth cone collapse and redistributes after entorhino-hippocampal axotomy. *Mol Cell Neurosci* 33, 321–34 (2006).
126. Qu, X. *et al.* Identification, Characterization, and Functional Study of the Two Novel Human Members of the Semaphorin Gene Family. *J Biol Chem* 277, 35574–35585 (2002).
127. Pasterkamp, R. J., Peschon, J. J., Spriggs, M. K. & Kolodkin, A. L. Semaphorin 7A promotes axon outgrowth through integrins and MAPKs. *Nature* 242, 398–405 (2003).
128. Moresco, E. M. Y., Donaldson, S., Williamson, A. & Koleske, A. J. Integrin-Mediated Dendrite Branch Maintenance Requires Abelson (Abl) Family Kinases. *J Neurosci* 25, 6105–6118 (2005).
129. Lledo, P.-M., Alonso, M. & Grubb, M. S. Adult neurogenesis and functional plasticity in neuronal circuits. *Nat Rev Neurosci* 7, 179–193 (2006).
130. Okano, H. & Sawamoto, K. Neural stem cells: involvement in adult neurogenesis and CNS repair. *Philos Trans R Soc B Biol Sci* 363, 2111–2122 (2008).
131. Toda, T., Parylak, S. L., Linker, S. B. & Gage, F. H. The role of adult hippocampal neurogenesis in brain health and disease. *Mol Psych*iatry 24, 67–87 (2019).
132. Peng, L. & Bonaguidi, M. A. Function and Dysfunction of Adult Hippocampal Neurogenesis in Regeneration and Disease. *Am J Pathol* 188, 23–28 (2018).
133. Smith, L. K., White, C. W. & Villeda, S. A. The systemic environment: at the interface of aging and adult neurogenesis. *Cell Tissue Res* 371, 105–113 (2018).
134. Malvaut, S. & Saghatelyan, A. The Role of Adult-Born neurons in the Constantly Changing Olfactory Bulb Network. *Neural Plast* 2016, 1614329 (2016).
135. Saha, B., Ypsilanti, A. R., Boutin, C., Cremer, H. & Chédotal, A. Plexin-B2 regulates the proliferation and migration of neuroblasts in the postnatal and adult subventricular zone. *J Neurosci* 32, 16892–905 (2012).
136. Oinuma, I. Molecular Dissection of the Semaphorin 4D Receptor Plexin-B1-Stimulated R-Ras GTPase-Activating Protein Activity and Neurite Remodeling in Hippocampal neurons. *J Neurosci* 24, 11473–11480 (2004).
137. Perälä, N., Sariola, H. & Immonen, T. More than nervous: The emerging roles of plexins. *Differentiation*

83, 77–91 (2012).
138. Maier, V. *et al.* Semaphorin 4C and 4G are ligands of Plexin-B2 required in cerebellar development. *Mol Cell Neurosci* 46, 419–431 (2011).
139. Wu, H. *et al.* Sema4C expression in neural stem/progenitor cells and in adult neurogenesis induced by cerebral ischemia. *J Mol Neurosci* 39, 27–29 (2009).
140. Moreau-Fauvarque, C. *et al.* The transmembrane semaphorin Sema4D/CD100, an inhibitor of axonal growth, is expressed on oligodendrocytes and upregulated after CNS lesion. *J Neurosci* 23, 9229–9239 (2003).
141. Perälä, N. M., Immonen, T. & Sariola, H. The expression of plexins during mouse embryogenesis. *Gene Expr Patterns* 5, 355–362 (2005).
142. Deng, S. *et al.* Plexin-B2, but not Plexin-B1, critically modulates neuronal migration and patterning of the developing nervous system *in vivo*. *J Neurosci* 27, 6333–6347 (2007).
143. Sbacchi, S., Acquadro, F., Calò, I., Calì, F. & Romano, V. Functional annotation of genes overlapping copy number variants in autistic patients: focus on axon pathfinding. *Curr Genomics* 11, 136–145 (2010).
144. O'Connor, T. P. *et al.* Semaphorin 5B mediates synapse elimination in hippocampal neurons. *Neural Dev* 4, 18 (2009).
145. Melin, M. *et al.* Constitutional downregulation of SEMA5A expression in autism. *Neuropsychobiology* 54, 64–69 (2006).
146. Suda, S. *et al.* Decreased expression of axon-guidance receptors in the anterior cingulate cortex in autism. *Mol Autism* 2, 14 (2011).
147. Hussman, J. P. *et al.* A noise-reduction GWAS analysis implicates altered regulation of neurite outgrowth and guidance in autism. *Mol Autism* 2, 1 (2011).
148. Xie, T. *et al.* A genome-wide association study combining pathway analysis for typical sporadic amyotrophic lateral sclerosis in Chinese Han populations. *Neurobiol Aging* 35, 1778.e9-1778.e23 (2014).
149. Antonell, A. *et al.* A preliminary study of the whole-genome expression profile of sporadic and monogenic early-onset Alzheimer's disease. *Neurobiol Aging* 34, 1772–1778 (2013).
150. Lesnick, T. G. *et al.* A genomic pathway approach to a complex disease: Axon guidance and Parkinson disease. *PLoS Genet* 3, 0984–0995 (2007).
151. Srinivasan, B. S. *et al.* Whole genome survey of coding SNPs reveals a reproducible pathway determinant of Parkinson disease. *Hum Mutat* 30, 228–238 (2009).
152. Bossers, K. *et al.* Analysis of gene expression in Parkinson's disease: Possible involvement of neurotrophic support and axon guidance in dopaminergic cell death. *Brain Pathol* 19, 91–107 (2009).

Chapter 2

Analysis of Sema4F knockout mice does not reveal major neural defects

Suzanne Lemstra[1], Wouter A.G. Beenker[1], Youri Adolfs[1], Geert M.J. Ramakers[1], R. Jeroen Pasterkamp[1]

[1.] Department of Translational Neuroscience, UMC Utrecht Brain Center, University Medical Center Utrecht, Utrecht University, Utrecht 3584 CG, the Netherlands

Abstract

The Semaphorin family of axon guidance proteins is important for the correct wiring of the brain during development and its maturation at postnatal and adult stages. Semaphorin 4F (Sema4F) is a transmembrane protein that is expressed throughout development and adulthood, and is known to be involved in axon guidance and oligodendrocyte precursor migration and differentiation. However, Sema4F has not been characterized in detail and its precise function *in vivo* remains unknown. Here we provide a detailed expression pattern analysis of *Sema4F* from E16.5 until adulthood showing highest expression between P0 and P14. The cerebellum, cortex, hippocampus and olfactory bulb show high expression of *Sema4F*. Furthermore, we describe the generation and validation of the first *Sema4F* knockout mouse. Preliminary characterization of this mouse does not reveal gross abnormalities in axon tracts or ganglia at E16.5, with the exception of the stellate ganglion. Expression of *Sema4F* is detected postnatally in the cerebellum. However, no differences were found at P14 or adulthood. Also, the number of oligodendrocytes was similar in knockout mice and littermate controls at adult stages. This is the first *Sema4F* knockout mouse described and it provides a powerful *in vivo* tool to determine Sema4F function in future studies.

Introduction

The Semaphorin family is well known for its role in axon guidance and is crucial for many aspects of proper brain development [1–3]. Semaphorins are guidance molecules that can act as repulsive or attractant cues, depending on the brain region, molecular interactors and downstream signalling routes [4–7]. In addition to axon guidance, many other roles for Semaphorins have been described, e.g. in proliferation, myelination, differentiation, and plasticity [8–13]. Deregulation of members of the Semaphorin family is thought to underlie diverse brain development defects [3]. Therefore, understanding the function and signalling mechanisms of individual Semaphorins is essential.

Class 4 Semaphorins are transmembrane proteins and consists of seven proteins: Sema4A to Sema4G. The canonical receptors for class 4 Semaphorins are members of the Plexin B class, which are abundantly expressed in, but not restricted to, the brain [14–17]. Sema4-PlexinB signalling in the brain is involved in many (non) neuronal processes, such as cortical neuron migration [18,19], dendritic and axonal complexity and guidance [20–24], cerebellar development [25], formation and regulation of GABAergic synapses [26,27], microglia activation [28], oligodendrocyte differentiation [9,28] and astrogliosis [29]. In addition, Sema4s can interact with PlexinD1, neuropilins, Tim2 and CD72 receptors in the brain and other organs [30]. Sema4A, via PlexinD1, can enhance lung fibrosis [31] and suppresses angiogenesis *in vivo* [32]. Sema4A binds to CD72 and TIM2 to influence the immune system by affecting oligodendrocytes, T-cell priming and regulation, and B-cell activity [33–40]. Thus, Sema4s can be important for various aspects of brain development. However, only Sema4A and Sema4D have been studied extensively and other family members remain incompletely characterized.

Sema4F was first identified by Encinas et al (1999) and shown to be a repulsive guidance molecule for retinal ganglion cells. The 4008 base pair *Sema4F* gene, located on mouse chromosome 6 (equivalent human chromosome 2), can be translated into a protein of 776 amino acids. Sema4F contains a Sema domain, Ig-like domain, transmembrane domain and cytosolic region terminating with a PDZ binding motif [41]. *Sema4F* expression is detected during embryonic development, gradually increasing at postnatal and adult stages. High mRNA and protein expression is found in the lung and the brain, especially in the cerebellum, hippocampus and olfactory bulb (OB) of adult rats [9,41]. Axon repulsion of cultured retinal ganglion axons by Sema4F is the only reported neuronal function for Sema4F to date [41]. Sema4F is expressed in cultured hippocampal neurons (and synapses) where it binds PSD-95/SAP90 via its PDZ binding-motif, as shown by immunoprecipitation from COS-7 cells [42]. In addition to neuronal expression and effects, Sema4F promotes oligodendrocyte migration and differentiation. Addition of exogenous Sema4F to cultured retinal explants of rats enhanced the migration of oligodendroglial precursors (OPCs). In addition, cultured OPCs show enhanced differentiation and myelin production under the influence of exogenous Sema4F *in vitro*. In accordance, addition of an antibody to decrease endogenous Sema4F delayed the production of myelin [9]. Furthermore, Parrinello and colleagues showed that downregulation of Sema4F disrupts Schwann cell – axonal contact possibly pushing Schwann cells into a differentiated active state. These observations indicate a role for Sema4F in the peripheral nervous system (PNS). Together, these data suggest that Sema4F could act as a repellent for axons, while promoting migration and differentiation of oligodendrocytes/Schwann cells. The Sema4F signalling cascades and receptors mediating these effects remain largely unknown. Furthermore, whether these effects are important *in vivo* remain to be established.

To provide insight into the *in vivo* role of Sema4F, the expression of this transmembrane Semaphorin was analysed in detail. Next, we generated and analysed the first *Sema4F* knockout mouse. Although this analysis did not reveal obvious defects in the nervous system it represents an excellent tool for further dissecting the role of Sema4F in future studies.

Methods

Animals. Animal experiments were in accordance to and approved by the CCD (central committee for animal research, the Netherlands), the University Medical Center Utrecht, the Dutch law (Wet op de Dierproeven 1996) and European regulation (Guideline 86/609/EEC). *Sema4F* KO mice were generated in collaboration with KOMP (knock out mouse project) and Innoser (Lelystad, The Netherlands) as part of the IMPact (innovative mouse platform) project. Embryonic stem cells were electroporated with a vector replacing >90% of the *Sema4F* gene with a cassette containing a *neomycin* selection gene and a *LacZ* reporter gene via homologous recombination. Embryonic stem cells were injected into blastocytes of C57BL/6NTac mice to generate a chimeric strain. F1 from the chimeric mouse were tested using PCR for the removal of *Sema4F* and the presence of the cassette. Offspring were backcrossed at least five times into a C57BL/6J background (mice were obtained from Charles River). *Sema4F* KO mice did not exhibit difficulties in breeding. For experiments, heterozygous *Sema4F* breeding was used. The following primers were used for genotyping: *Sema4F* exon 1 fw 5' GGAACGTTTCCATCCTTCTG '3, *Sema4F* exon 1 fw 5' GGCCTTAGATGGCTGTCACTG '3 and *Sema4F LacZ* rv 5' GTCTGTCCTAGCTTCCTCACTG '3 at 52 °C annealing temperature. Mice were kept according to CCD guidelines on wood-chip bedding with tissue paper for nest building. Mice pups were raised by their mother and weaned at 4-5 weeks of age. A 12h light cycle was kept with a temperature of 22 ± 1 °C. Animals had ad libitum access to food (211 RMG—TH diet, Hope Farms) and water.

***In situ* hybridisation and imaging.** C57Bl/6J animals were killed via decapitation (E16.5 to P0) or cervical dislocation (P14 to adult). Brains were cut fresh frozen on a cryostat in 18 µm sections, mounted on Superfrost slides (Merzel, Germany) and stored at -80°C. Probes for *Sema4F* (NM_011350.4) were generated via PCR (Veriti, Applied Biosystems) with 5' TTATGCTTGCGAGTGTCAGA '3 and 5' GCCATAGCAGAGGGCTACAG '3 primers creating a specific mRNA probe of 642 bp that was labelled with digoxigenin (coding region 2039-2702 bp) and used for *in situ* hybridisation as described previously [43]. In short, slides were hybridized overnight at 68 °C with 400 ng/ml RNA in 150 µl hybridisation mixture (50% deionized formamide, 5x standard saline citrate, 1x Denhardst solution, 0.25 mg/ml sonificated salmon sperm DNA and 0.5 mg/ml tRNA baker's yeast). Slides were washed with standard saline citrate solutions and incubated with anti-digoxigenin antibody (1:2,500, 1093274 Boehringer Mannheim) and developed using BCIP/NBT (Boehringer Mannheim) overnight. Next, sections were dehydrated and embedded using Entallan (Merck). Slides were imaged using a CMOS camera (Hamamatsu Orca-Flash 4.0 V2) and analysed using imaging-processing program FIJI (v1.0) and NDP view (v2.6.13) giving a resolution up to 40x.

Immunochemistry and imaging. For free-floating immunohistochemistry, brains were collected via an overdose of pentobarbital before transcardial perfusion using 4% PFA for P14 and P90. Brains were sectioned at 50 µm and incubated for >1hour at room

temperature in PBS containing 5% normal donkey serum and 0.1% Triton X-100 (blocking buffer). Primary antibodies were incubated overnight at 4°C in blocking buffer followed by PBS washes. Secondary antibodies were incubated in blocking buffer for 2 hours at room temperature at a 1:750 dilution. Sections were washed in PBS followed by 4',6-diamidino-2-phenylindole (DAPI, Sigma) staining prior to mounting on Superfrost slides (Merzel, Germany) with Prolong gold anti-fade reagent (Invitrogen). Sections were imaged using an Axioscope epifluorescent microscope (Zeiss) and analysed and tiled using FIJI (v1.0). Primary antibodies used were: mouse-anti-Calbindin (1:1000, Sigma, C9848), rabbit-anti-Olig2 (1:1000, Merck, AB9610). Secondary antibodies used were: donkey-anti-mouse (1:750, Life Technologies, A31570), donkey-anti-rabbit (1:750, abcam, ab150074).

3-Dimensional Imaging of Solvent-Cleared Organ (3DISCO) was performed as described previously [44]. In brief, E16.5 embryo's were killed and immersed in 4% PFA for 6 hours. Dehydration (PBS to 100% methanol), bleaching (10% H_2O_2 in methanol) and rehydration was executed (100% methanol to PBS), changing solutions every hour. Whole embryos were incubated in blocking solution (PBS-GT, 0.5% Triton X-100, 0.01% Thimerosal) on a horizontal shaker at room temperature for 24 hours. Primary antibody (rabbit-anti-Tyrosine hydroxylase, 1:1000, Milipore, AB152) was incubated on a horizontal shaker at 37 °C for 7 days followed by 6 washing steps of 30 minutes in PBS-GT. Secondary antibodies (anti-rabbit 647, 1:750) were incubated on a horizontal shaker at 37 °C for 1-3 days. For clearing, embryos were sequentially incubated in 50%, 80%, 100% (2 times) solutions of tetrahydrofurane (THF, Sigma, 87371) in steps of 1 hour. Tissue lipids were dissolved using 100% dichloromethane (DMC, Sigma, 270997) for 20 minutes. Tissue was cleared using 100% dibenzyl ether (DBE, Sigma, 108014) overnight and kept in DBE for storage. All steps were at room temperature. Tissue was imaged as previously described [44] by a light-sheet microscope (LSM 2, LaVision Biotech) using ImspectorPro software (LaVision BioTec). Samples were placed in a DBE container during scanning. A 680 nm laser scanned while switching sides. The step size per image was 3,5 µm. Images were analysed using Imaris 8 software (Bitplane). Stack images were converted to Imaris files, reduced to 8 bits followed by 3D reconstruction using volume rendering. To create an overlay of *Sema4F* WT and KO stellate ganglia, images were added into one file using Imaris 8 software (Bitplane). Magnifications of the 3D embryos were used for depicting differences between genotype (fig. 7) and brightness was adjusted using FIJI (v1.0).

For Xgal staining, brains were collected as for regular immunohistochemistry. Brain sections of 40 µm were stained with Xgal staining solution (40 mg/ml Xgal, 5mM $K_3Fe(CN)_6$, 5 mM $K_4Fe(CN)_6$)°H_2O, 2 mM $MgCl_2$ in PBS) for 3 hours at room temperature. Sections were mounted in DABCO (Sigma-Alterich) onto Superfrost slides (Merzel, Germany). Slides were imaged using a brightfield microscope (Zeiss) and analysed with FIJI (v1.0).

Stereology and statistics. Olig2 and Calbindin positive cells were counted as described previously (Jongbloets, Lemstra et al., 2017). In short, images of the whole brain or cerebellum were analysed using FIJI software for Olig2 or Calbindin positive staining, respectively. Cells were counted using systematic random sampling with a grid (25 mm^2) from sections of 50 µm. Every one in five squares was counted for quantification. For quantification, average number of cells was corrected for number of squares and was used to determine differences between genotype. Statistical analysis was performed in GraphPad Prism version 5.00 (GraphPad Software) using an unpaired two-tailed *t* test.

Results

Sema4F mRNA expression is strongest in early postnatal brains

Sema4F mRNA is broadly expressed in the brain between E14 and adulthood [9,41]. To determine the detailed pattern of expression of *Sema4F*, we performed *in situ* hybridization from E16 until adult stages (P90) (Table 1). Overall, low *Sema4F* expression was observed at E16.5. At early postnatal stages expression levels increased and highest expression was detected at P0 and P14. Strong *Sema4F* expression was found in the cortex, hippocampus, olfactory bulb, amygdala and cerebellum, but also in the striatal neuroepithelium, geniculate complex, ganglionic eminence and periaqueductal grey area. In the adult, many regions still showed *Sema4F* expression although expression was generally lower as compared to postnatal stages (see figure 1 for an overview of *Sema4F* expression). There are, however, exceptions to these general observations. For instance, moderate expression was observed in the superior colliculus and in the midbrain trigeminal nucleus at E16.5, while low expression was detected at postnatal ages. In contrast, the granular layer of the olfactory bulb and the cerebellum showed highest *Sema4F* expression at adult stages (table 1).

Strong Sema4F expression in hippocampus, cerebellum and cortex

Areas that displayed prominent *Sema4F* expression were analysed in more detail. At E16.5 it is difficult to distinguish specific regions within the hippocampus. However, moderate expression of *Sema4F* was already detected at E16.5 in the hippocampus (fig. 2a, e). The dentate gyrus (DG) and CA regions of the hippocampus are established at P0. Robust expression of *Sema4F* is observed in the DG and CA regions while moderate levels are observed in the alveus (fig. 2b, f). Around P14, hippocampal expression of *Sema4F* is strongest with prominent expression in the CA regions and DG. Interestingly, the subgranular zone of the DG displayed particularly strong labelling (fig. 2c, g). Similar expression patterns were found at adult stages (fig. 2d, h).

The hindbrain showed clear and age-dependent expression (table 1). At E16.5, low-to-moderate expression was observed throughout the cerebellum, pons and inferior colliculus (fig. 3a). In the brainstem, specific expression in the hypoglossal nucleus, facial nucleus and ambiguous nucleus was found (table 1). Labelling of these regions was even more pronounced at P0 (fig. 3b). The cerebellum displayed low *Sema4F* staining, while the inferior colliculus was moderately labelled. In addition, expression was visible in the hypoglossal nucleus, facial nucleus olivary nucleus and the paragigantocellular reticular nucleus in the brainstem (table 1). Expression increased postnatally and appeared strong in the external granule cell layer and granule cell layer of the cerebellum but also the inferior colliculus (fig. 3c). In the cerebellum, expression of *Sema4F* was found in Purkinje cells (fig. 3e). At adult stages, *Sema4F* expression was generally decreased. However, the granule cell layer and Purkinje cells of the cerebellum and the olivary nucleus still showed strong expression (fig. 3f). Other regions of the adult cerebellum, brainstem and inferior colliculus showed similar or lower expression as compared to P14 (fig. 3d).

Next we examined *Sema4F* expression in the cortex. At E16.5, weak expression of *Sema4F* was observed in the cortex, subventricular zone and bed nucleus of the anterior commissure (fig. 4a; data not shown, suppl. fig. 1a-d). These levels increased around birth, when moderate to high expression was found in the tenia tecta, indusium griseum and bed nucleus of anterior commissure. The deeper cortical layers showed low-moderate expression of *Sema4F* (fig. 4b). Around P14, cortical expression increased and moderate

Table 1 | Summary of *in situ* hybridization data for *Sema4F*.

Brain region		E16.5	P0	P14	Adult
Telencephalon					
Olfactory bulb	Mitral layer	-	+++	++	+++
	Glomerular layer	++	++	++	+++
	Granular layer	-	+	+	+++
	Anterior olfactory nucleus	-	-	++	++
	Acessory olfactory bulb	+	+	-	-
	Rostral migratory stream			+++	++
Cortex	Cortical plate	+	+	-	-
	Cortical subplate	+	+	-	-
	Bed nucleus of anterior commissure	+	++	+	+
	Taenia tecta		+	++	++
	Upper layers (II/III)		+	++	++
	Deeper layers (V/VI)		+	++	++
	Ventricular + subventricular zone		+	+++	++
	Piriform area molecular layer		-	+++	+++
Hippocampus		++			
	Dendate gyrus		+++	+++	+++
	CA3		+++	+++	+++
	CA2		++	++	++
	CA1		++	++	++
	Alveus		+	-	-
	Hilus / polymorph layer		-	+	+
	Induseum griseum		+	+	+
Amygdala		+			
	Medial amygdalar nucleus		++	+	++
	Lateral amygdalar nucleus		+++	++	++
	Basomedial amygdalar nucleus		+++	++	++
	Cortical amygdalar area		++	++	++
Basal forebrain	Caudoputamen	-	+	+	+
	Nucleus accumbens / globus pallidus	-	+	+	+
	Ventral pallidum	-	+	+	+
	Preoptic nucleus	+	+	-	-

Brain region		E16.5	P0	P14	Adult
	Ganglionic eminence	+	+	-	-
	Septal nucleus / Diagnonal band	-	+	+	+
Diencephalon					
Hypothalamus		+			
	Periventricular hypothalamic nucleus		+	+	+
	Anterior hypothalamic nucleus		++	+	+
	Medial zone		-	++	+
	Ventromedial hypothalamic nucleus		++	+	+
	Dorsomedial nucleus		++	+	+
Thalamus		++			
	Central medial nucleus		++	+	+
	Ventral lateral nucleus		++	+	++
	Lateral dorsal nucleus		++	+	+
	Mediodorsal nucleus		++	+	+
	Paraventricular nucleus		-	+	+
	Geniculate complex	+	+	+++	++
Epithalamus	Medial habenula		++	++	++
Mesencephalon					
	Superior colliculus	++	+	+	+
	Inferior colliculus	+	++	++	-
	Periaqueductal gray	+	+	+	+
	Nucleus raphe magnus	-	+	+	+
	Tegmental nucleus	-	+	+	+
	Pontine reticular nucleus	+	+	+	+
	Midbrain trigeminal nucleus	+++	+++	+	+
Hindbrain					
Cerebellum		+	+		
	External granular layer		+	+++	+
	Granular layer		+	+++	+++
	Purkinje layer		+	+	+
	Molecular layer		+	+	+

Brain region		E16.5	P0	P14	Adult
Brainstem	Hypoglossal nucleus	++	++	++	+
	Olivary nucleus	-	+	+	+
	Facial nerve	-	+	+	+
	Nucleus ambiguus	+	+	+	+
	Reticular nucleus	+	+	+	+
	Vestibular nuclei	+	+	+	+
	Spinal nucleus of trigeminal	+	+	+	+
	Cochlear nuclei	-	-	+	+
	Nucleus prepositus	+	+	+	+

Shown is the relative expression of *Sema4F* mRNA as detected by ***in situ*** hybridisation at four developmental stages of the mouse (referenced from Allen Mouse Brain Atlas). Expression levels vary from no expression (-) to high expression (+++). An empty box indicates that the area was not examined, for example because the region is not present or discernable at specific stages. At these stages the overall region was examined. $n = 3$ mice.

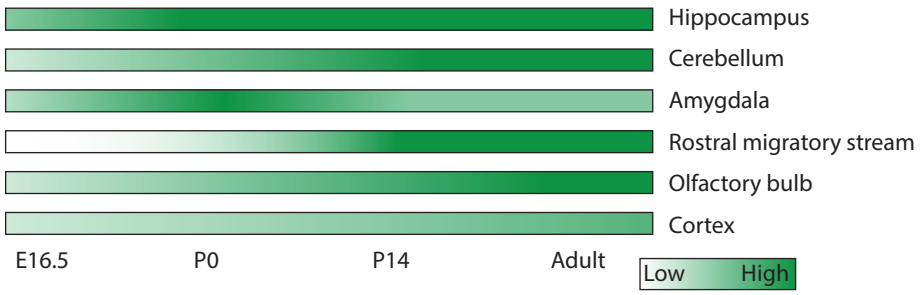

Figure 1 | Schematic representation of regions showing high *Sema4F* expression.
A schematic representation of *Sema4F* mRNA expression for six areas that show abundant expression in *in situ* hybridisation experiments. Relative expression of *Sema4F* is displayed ranging from no expression (in white) to high expression (in green) in four different temporal stages. More detailed expression data can be found in Table 1.

expression was found in upper and deeper layers, except for layer IV. Other cortical regions, such as the piriform cortex, showed strong expression (fig. 4c, table 1). Expression patterns at adult stages were similar to those found at P14. However, *Sema4F* expression decreased in the adult subventricular zone (fig. 4d, table 1).

In addition to the regions described above, a few other brain areas displayed strong *Sema4F* expression. At E16.5, the glomerular layer of the olfactory bulb showed moderate staining for *Sema4F* together with weak expression of the accessory bulb. At later ages, other regions such as the granular and mitral layer showed *Sema4F* expression (table 1.). Interestingly, also at adult stages the olfactory bulb showed strong expression of *Sema4F*. The olfactory bulb is one of two regions that receive newly generated cells from the subventricular zone at adult stages. Newborn cells from the subventricular zone move through the rostral migratory stream (RMS) towards and into the olfactory bulb 45. Strikingly, at P14 and P90 strong *Sema4F* expression was observed in the RMS and subventricular zone (svz) (fig. 5b-f). Also, strong expression of *Sema4F* is visible in the taenia tecta (fig. 5f). Weak

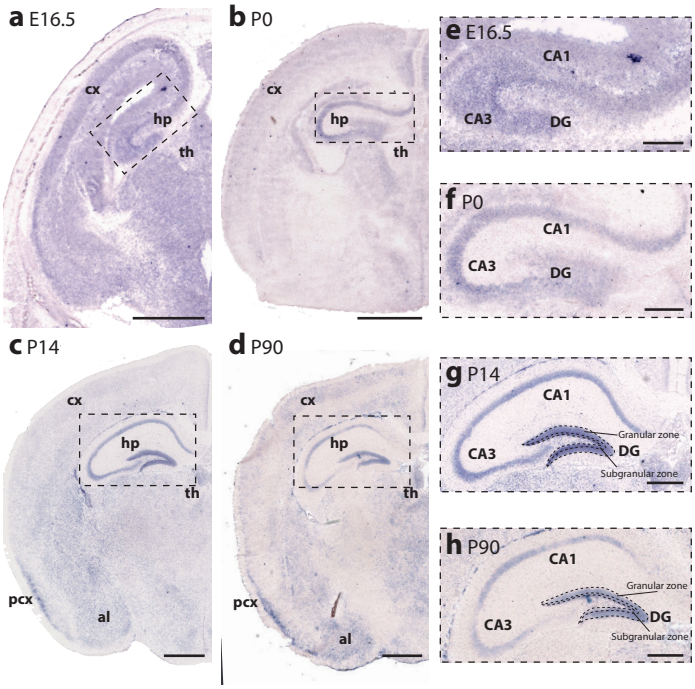

Figure 2 | *Sema4F* mRNA expression in the hippocampus.
In situ hybridization for *Sema4F* in coronal sections of the mouse brain at E16.5 (a), P0 (b), P14 (c) and P90 (d). Boxed areas show higher magnifications of the hippocampus (e-h). *n* = 3 mice. Scale bars (a-d) 1mm, (e-f) 250µm, (g-h) 500µm. Cx: cortex, hp: hippocampus, th: thalamus, pcx: piriform area, al: amygdala, DG: dentate gyrus.

expression is found in the inferior colliculus and periaqueductal grey (fig. 5g). Furthermore, robust expression was found in the in trigeminal nucleus of the periaquadectal grey area at E16.5, P0 and P90 (fig. 5g, table 1). Another distinctive area of *Sema4F* expression was the geniculate complex distal to the thalamus as well as the hippocampal formation (fig. 5h). In addition, hypothalamic areas such as the periventricular nucleus and the ventro- and dorsal-medial hypothalamic nucleus showed *Sema4F* expression (fig. 5i). In the P90 brainstem the spinal trigeminal nucleus and reticular nucleus show clear expression of *Sema4F*.

Labelling of *Sema4F* indicates a wide expression pattern throughout the developing and adult brain, insinuating a role for Sema4F in brain development and maturation.

Sema4F KO mice do not display gross neural defects

To study the *in vivo* role of *Sema4F*, we generated a *Sema4F* knockout (KO) mouse. A cassette containing *LacZ* and Neomycin genes was used to replace the *Sema4F* gene, as confirmed by PCR (fig. 6a-c). Next, *in situ* hybridisation showed complete ablation of *Sema4F* in the hippocampus of the *Sema4F* KO. In contrast, adult wild-type (WT) hippocampus showed prominent *Sema4F* expression (fig. 6d). Unfortunately, unavailability of specific anti-Sema4F antibodies prevented us from confirming absence of Sema4F at the protein level in *Sema4F* KO mice.

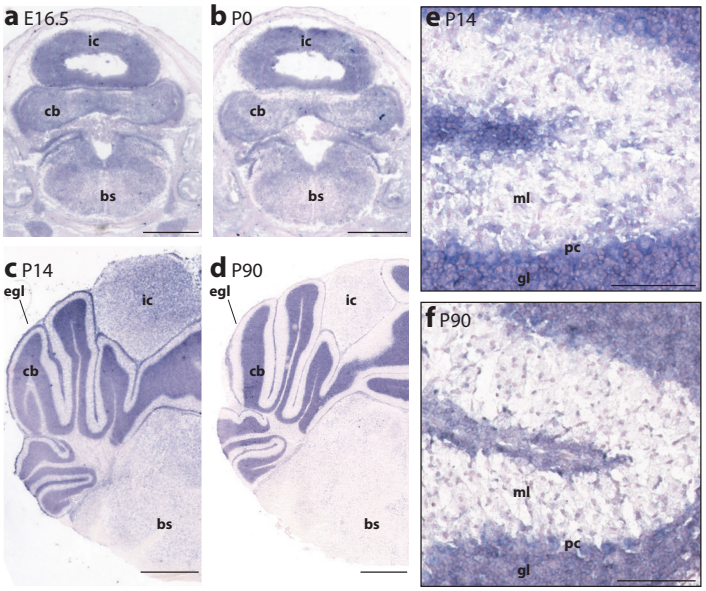

Figure 3 | *Sema4F* mRNA expression in the cerebellum. *In situ* hybridization for *Sema4F* in coronal sections of the mouse brain at E16.5 (a), P0 (b), P14 (c) and P90 (d). (e-f) Higher magnification of *Sema4F* expression in the cerebellum at P14 and P90. *n* = 3 mice. Scale bars (a-d) 1 mm, (e) 100µm, (f) 250µm. cb: cerebellum, bs: brainstem, pc: Purkinje cells, gl: granular layer, egl: external granular layer, ic: inferior colliculus, ml: molecular layer.

According to our ISH data (Fig. 1-4), *Sema4F* is expressed at embryonic stages. Sema4F has been shown to induce growth cone collapse in retinal ganglion explants from E6 chick embryos [41]. Also Sema4F was reported to be involved in axon-Schwann cell interactions [46]. To establish whether Sema4F has a functional role during axon development at embryonic stages, we studied the E16.5 peripheral nervous system using 3DISCO [44]. Tyrosine hydroxylase (Th) is an important enzyme for noradrenalin synthesis and is therefore expressed by sympathetic neurons. Using Th immunostaining in combination with 3DISCO one can visualize differences in sympathetic peripheral projections at the level of the whole embryo [44,47–49]. However, no obvious differences were found in the PNS of *Sema4F* KO mice as compared to WT littermates. At cervical to lumbar levels, ganglia were formed and innervated the forelimb, hindlimb, thorax, tail and other parts of the body (fig. 7a-d, a-b sagittal view, c-d dorsal view) [50,51]. Interestingly, the stellate ganglion (region within the dashed box in fig. 6a, b) seemed abnormal in the *Sema4F* KO. Normally, axons from thoracic level 1-4 innervate the bronchi, oesophagus, lungs, upper extremities and, via the stellate ganglion, the heart. The stellate ganglion is located in the upper thorax where large bundles of sympathetic axons descend dorsally to innervate the right sinus horn and right atrium. Other stellate ganglion projections extend laterally to reach the left ventricle and right atrium and ventricle, respectively [48,52]. In WT mice, stellate projections descending dorsally and laterally were established (fig. 7e, arrows indicate the tracts that run towards the spinal cord, dorsal-sagittal view). However, in the *Sema4F* KO, lateral projections appeared absent or only partially branched (fig. 7f, stars indicate where the tracts should be, dorsal-sagittal view). Overall, the projections of the stellate ganglion seemed more extensive in the WT compared to the *Sema4F* KO.

As the expression of *Sema4F* increases towards P14 and remains high at adult stages, *Sema4F* KO mice were analysed at P14 and P90 (fig. 8). First brain development was examined using the *LacZ* enzyme in *Sema4F* KO mice. Beta-Gal staining in WT mice did not reveal specific signals, but clear beta-gal-positive cells were present in KO mice. However, no gross defects in beta-gal-positive neurons were found in P90 *Sema4F* KO mice (fig. 8a).

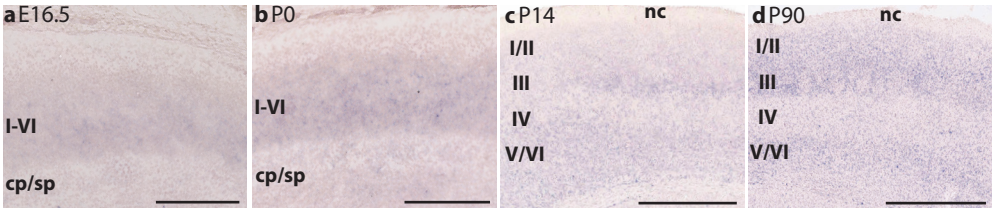

Figure 4 | *Sema4F* mRNA expression in the cortex.
In situ hybridization for *Sema4F* in coronal sections of the mouse cortex at E16.5 (a), P0 (b), P14 (c) and P90 (d). *n* = 3 mice. Scale bars: (a-b) 250µm, (c-d) 1mm. Pyramidal layer 1-6: I-VI, nc: neocortex, cp: cortical plate, sp: subplate.

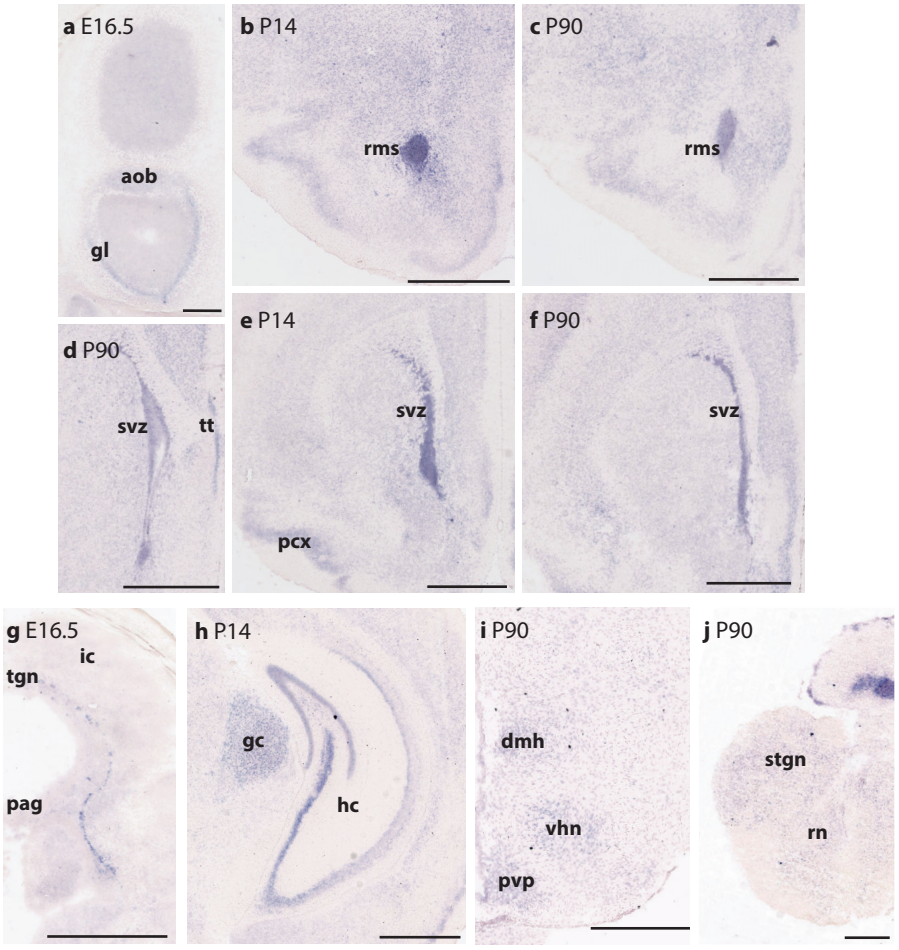

Figure 5 | High mRNA expression of *Sema4F*F in specific areas at E16.5, P0, P14 and P90.
Overview of distinct *Sema4F* mRNA expression patterns using *in situ* hybridisation (a-j). *n* = 3 mice. Scale bars: (a) 250 µm, (b-h) 1 mm, (i-j) 500 µm. gl: glomerular layer, aob: accessory olfactory bulb, svz: subventricular zone, rms: rostral migratory stream, tt: taenia tecta, pcx: piriform area, tgn: midbrain trigeminal nucleus, ic: inferior colliculus, pag: periaqueductal grey, hc: hippocampus, gc: geniculate complex, dmh: mediodorsal hypothalamus, vhn: ventrolateral hypothalamic nucleus, pvp: paraventricular nucleus, stgn: spinal trigeminal nucleus, rn: reticular nucleus.

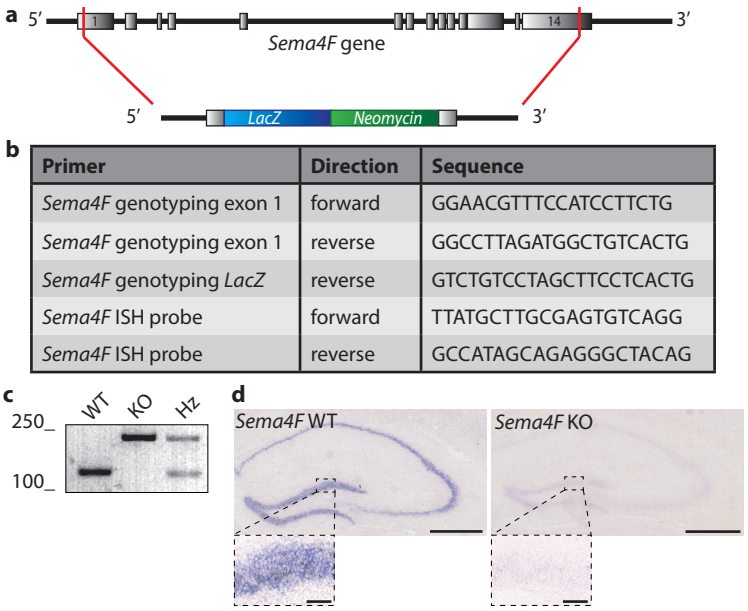

Primer	Direction	Sequence
Sema4F genotyping exon 1	forward	GGAACGTTTCCATCCTTCTG
Sema4F genotyping exon 1	reverse	GGCCTTAGATGGCTGTCACTG
Sema4F genotyping *LacZ*	reverse	GTCTGTCCTAGCTTCCTCACTG
Sema4F ISH probe	forward	TTATGCTTGCGAGTGTCAGG
Sema4F ISH probe	reverse	GCCATAGCAGAGGGCTACAG

Figure 6 | Generation and validation of a *Sema4F* knockout mouse model.
Schematic overview of the *Sema4F* KO mouse model. A cassette containing *LacZ* and Neomycin genes was electroporated in embryonic stem cells to replace *Sema4F* from exon 1 to 14 via homologous recombination in collaboration with KOMP (knock out mouse project) and Innoser (Lelystad, The Netherlands). After *neomycin* selection, embryonic stem cells were injected into blastocytes of C57BL/6NTac mice to create chimeric animals. Offspring from these mice were used for heterozygous breeding to create *Sema4F* KO mice (a). Table of genotyping and ISH primers used for *Sema4F* KO mouse validation (b). PCR was used to determine genotypes and to validate the *Sema4F* gene replacement at the DNA level (c). *In situ* hybridization for *Sema4F* in the dentate gyrus and CA regions of *Sema4F* WT and KO mice (d). n = 3 mice. Scale bars: (d) 500 µm and 50 µm in enlargement.

Robust expression of *Sema4F* was found in Purkinje cells and in the granule cell layer of the cerebellum at P14 and P90. The overall architecture of the cerebellum was intact in *Sema4F* KO mice (data not shown). Immunohistochemistry for Calbindin, a marker for Purkinje cells, was used to count cells per area (fig. 8b). Approximately 4 cells per 25*103 µm^2 were found, which is in line with previous reports [53–55]. This number was similar between WT and KO mice at P14 (unpaired *t* test: $p = 0{,}16$) and P90 (unpaired *t* test: $p = 0{,}90$) (fig. 8c).

Sema4F is also expressed in oligodendrocytes and influences their development and myelin production [9,46]. Therefore, immunohistochemistry for Olig2 was used to determine changes in the cortex of *Sema4F* KO mouse compared to WT. Approximately 6 cells per 25*103 µm^2 were found, which is similar to reported oligodendrocyte density in the mouse cortex [56]. However, no differences in the number of Olig2-positive cells were detected between WT and KO mice at P90 (fig. 8d; unpaired *t* test: $p = 0{,}73$) (Fig. 7e).

Together this study shows a first screen of the *Sema4F* KO mouse and reveals that *Sema4F* may be required for the development of the stellate ganglion in the periphery nervous system. In the postnatal central nervous system, the overall structure of the brain was not affected by *Sema4F* ablation.

Discussion

Sema4F is widely expressed throughout the brain and is therefore likely to contribute to many aspects of brain development and maturation. Despite its prominent expression, the function of this Semaphorin and its downstream signalling cascade remain unclear. Here we report robust expression of *Sema4F* from embryonic stages until adulthood with high expression in the cerebellum, cortex, hippocampus, olfactory bulb and RMS. Further, we present the first *Sema4F* KO mouse. Preliminary analysis of the *Sema4F* KO did not reveal obvious defects in nervous system development. However, more detailed analysis is needed to dissect the role of Sema4F *in vivo*.

Expression and function of Sema4F in the CNS and PNS

In this study, we provide a detailed overview of *Sema4F* expression in the hippocampus, cerebellum, cortex and olfactory bulb. Our data is in accordance with Armendariz et al., (2012). In our study we have replicated their main findings while, in addition, we provide a more detailed overview of selected expression patterns. For example, in our study the expression pattern in the amygdala, hypothalamus, thalamus and spinal cord is examined in detail. Hippocampal expression of *Sema4F* is supported by literature showing expression of Sema4F in hippocampal cells *in vitro* and *in vivo* [9,41,42]. For cerebellar expression, contrasting findings have been reported. Our *Sema4F* expression data are in line with those from Armendariz et al., 2012. However, Maier et al., 2011 did not observe expression in the cerebellum. Maier et al., followed different steps prior to fixation and hybridization containing methanol series and permeabilization steps. Perhaps the differences in *Sema4F* expression may be explained by differences in probe efficiency, protocols and tissue treatments. Nonetheless, our *Sema4F* expression data is in line with the other *Sema4F* screens available [9,41].

Expression of *Sema4F* in the cerebellum, hippocampus and other regions was weak at embryonic stages but stronger at early postnatal stages, suggesting a role for Sema4F in later developmental processes such as axon guidance. Other class 4 Semaphorins have been reported to influence the development of the cerebellum. For instance, Sema4D has a repulsive effect on cerebellar granule cells in stripe assays [57,58]. Furthermore, a dual role for Sema4C and Sema4G is apparent during cerebellar development. Both are necessary for granule cell migration *in vitro* and deficiency in Sema4C alone or Sema4C together with Sema4G leads to perturbed cerebellar development [25]. Together, these data suggest that Sema4s influence the development of the cerebellum. However, little is known about potential axon guidance effects of Sema4F. Therefore, we determined whether the cerebellum was affected by *Sema4F* deletion. At P14 and P90, we did not find alterations in the overall morphology of the cerebellum. From our preliminary data, it seems that Sema4F may be redundant for cerebellar development. Nonetheless, future studies should investigate in detail cerebellar development in relation to Sema4F.

Strong *Sema4F* expression was found in the trigeminal nucleus, dorsal root ganglia and Schwann cells (table 1, Encinas et al., 1999; Parrinello et al., 2008). In addition, treatment of retinal ganglion cells with Sema4F caused increased collapsed growth cones when compared to controls [41] showing a repulsive function for Sema4F. On the other hand, Schwann cell–peripheral axon contact requires Sema4F suggesting attractive properties of Sema4F [46]. Together, these data suggest a role for Sema4F in the PNS. To establish whether Sema4F influences PNS development, embryos were stained for Th at E16.5 and visualized using 3DISCO. No gross differences between genotypes were detected in this preliminary

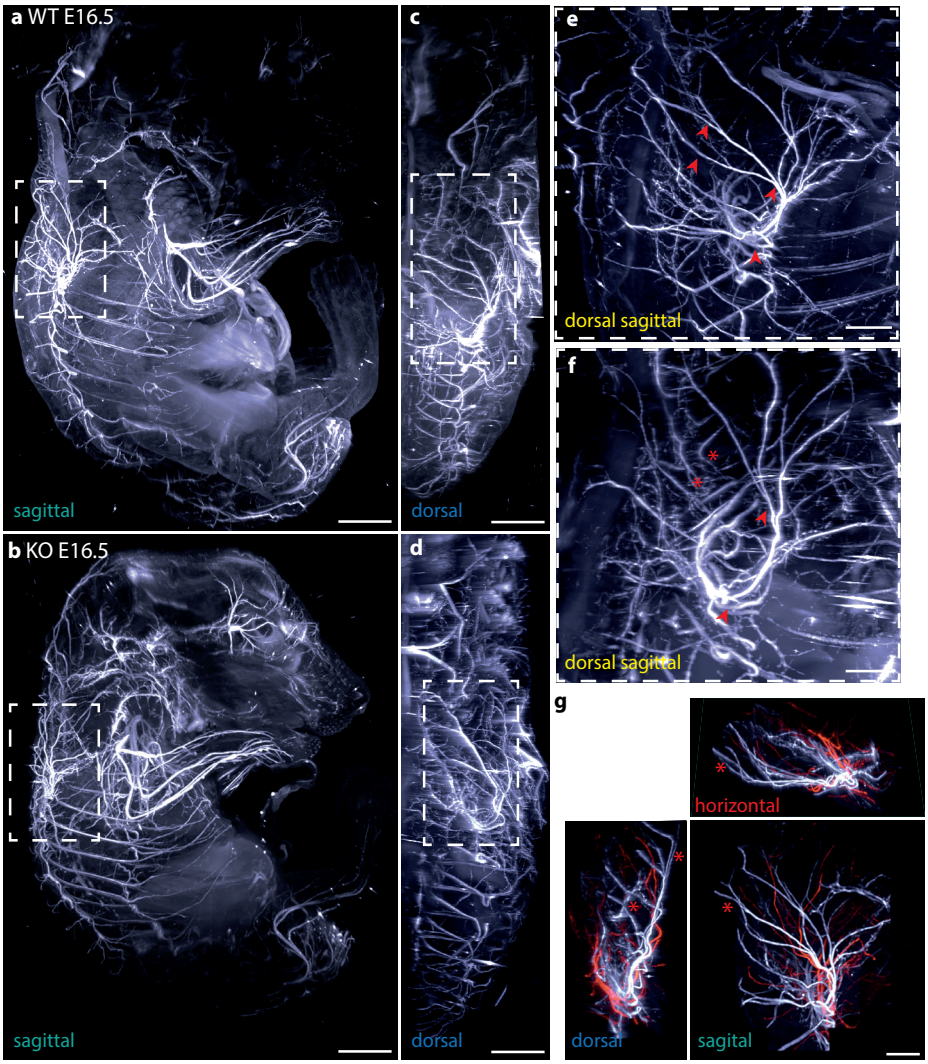

Figure 7 | The PNS is largely intact in *Sema4F* KO mice.
Immunohistochemistry for tyrosine hydroxylase (Th) in combination with 3-Dimensional Imaging of Solvent-Cleared Organ (3DISCO) imaging to visualize sympathetic neurons in the peripheral nervous system (PNS) at E16.5. Sagittal and dorsal overview of the body of E16.5 *Sema4F* WT and KO mice (a-d). A blow-up at the level of the stellate ganglion where the plane is dorsal and sagittal tilted to reveal aberrant innervations in the *Sema4F* KO (e-f, red arrows for present fibers, red asterisks for missing fibers). An overlay of *Sema4F* WT (white fibers) and KO fibers (red fibers) at different planes (g), red asterisks indicate lack of innervation in *Sema4F* KO). A representation of planes used for visualization of the 3D embryos in this figure (h). $n = 3$ mice. Scale bars: (a-d) 1 mm, (e-g) 500 µm.

screen. The stellate ganglion may be an exception as subtle defects were visible in the *Sema4F* KO mouse (fig. 7). At E9.5 neural crest cells proliferate and migrate into the ganglion primordium to form the stellate ganglion at E18.5, consisting of neurons, glia and neural stem. Proliferation of the stellate ganglion cells enhances between E10.5 and E13.5 in mice [59]. Interestingly, expression of *Sema4F* in the brain is reported from E13.5 onwards, suggesting that Sema4F will not influence the proliferation and migration of stellate cells at early stages [9,41]. At E16.5 *Sema4F* KO mice showed aberrant axon tract formation compared to the WT suggesting that Sema4F could be involved in the outgrowth or guidance of these axons. Sema4F causes growth cone collapse in rat retinal ganglion cells *in vitro* [41].

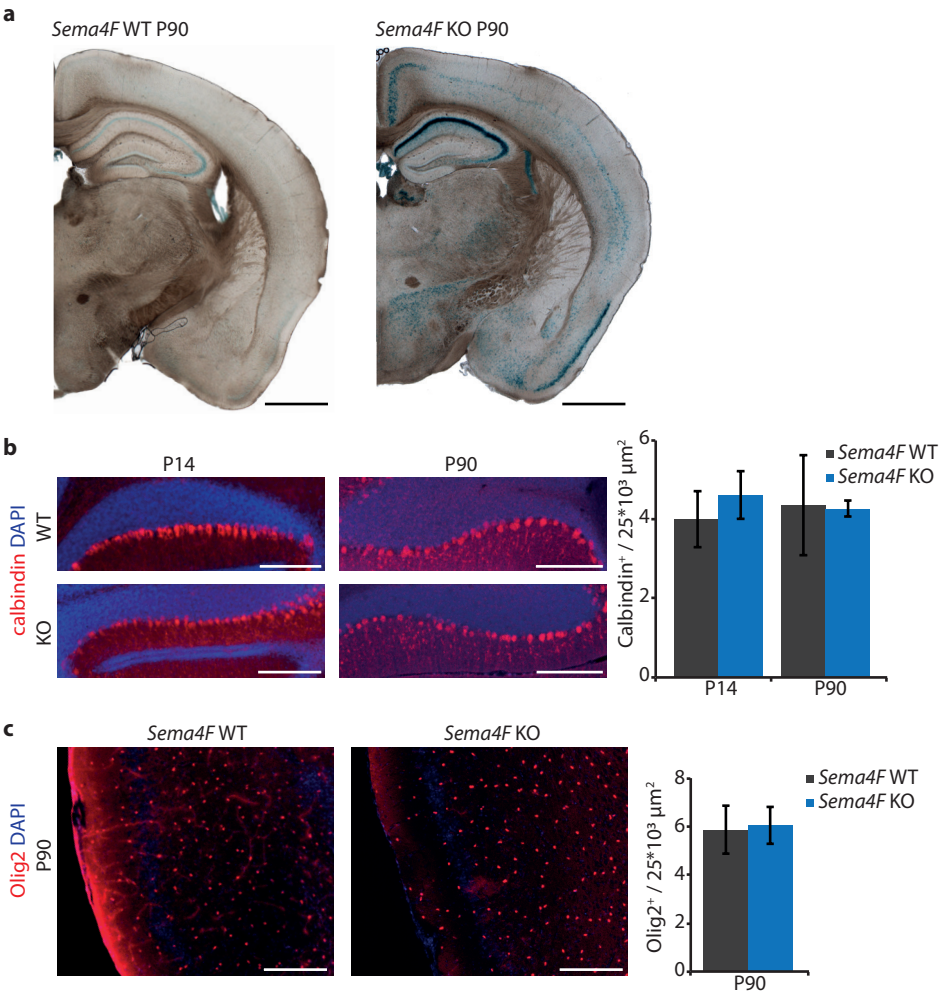

Figure 8 | No defects at postnatal stages in *Sema4F*F KO mice.
LacZ staining on coronal adult brain sections in*Sema4F* WT and KO mice (a). Immunohistochemistry for calbindin to visualize Purkinje cells in cerebellum for *Sema4F* WT and KO sections. Quantification shows no difference between WT and KO at P14 (unpaired *t* test: $p = 0.16$) or P90 (unpaired *t* test: $p = 0.90$) (b). Immunohistochemistry for Olig2 does not reveal differences in oligodendrocyte number, distribution or morphology at P90. Quantification of Olig2 positive cells per 25 mm² does not differ between genotypes (unpaired *t* test: $p = 0.73$) (c). $n = 3$ mice. Scale bars: (a) 1 mm, (b) 500 µm, (c) 500 µm.

Whether a similar response is found for stellate ganglion neurites needs to be determined. Overall, this first screen suggests that Sema4F is not required for general PNS development.

Overall, the *Sema4F* KO mouse is a valuable model to investigate the role of Sema4F *in vivo* but further and more detailed studies are needed to dissect the function of Sema4F during brain development and maturation.

The number of adult oligodendrocytes is unchanged in Sema4F KO mice

Sema4F promotes OPC differentiation. Addition of Sema4F to cultured OPCs enhances their differentiation, as measured by myelin production [9]. In the PNS, Sema4F is important for Schwann cell–peripheral axon contact, which is necessary for proper myelination of peripheral axons. Removal of *Sema4F* in rat Schwann cells via siRNA causes misalignment with axons *in vitro* [46]. These data prompted us to examine oligodendrocyte numbers in the *Sema4F* KO mouse. However, no differences in the number of oligodendrocytes were detected in KO mice. Next experiments should focus on OPC differentiation in the *Sema4F* KO mice, for instance, by determining oligodendrocyte numbers and myelin production at early postnatal stages.

Dedifferentiation of Schwann cells occurs following nerve injury [60]. Semaphorins are reported during these events, e.g. Sema4D deficiency leads to an increase in the number and migration of oligodendrocytes in injured mouse brains [28,61]. Perhaps Sema4F can influence Schwann cell–axon contact only after injury *in vivo*. Interestingly, *Sema4F* expression is upregulated 3 to 14 days after sciatic nerve injury in wild type mice but not in a mouse model that suppresses Wallerian degeneration suggesting a progressive de-myelination role for Sema4F [60]. Contrary, cell-axon contact is promoted by Sema4F as reported by Parrinello et al., (2008). Whether Sema4F exerts beneficial or adverse functional effects upon injury remains to be established.

Conclusive, the number of oligodendrocytes was not affected by *Sema4F* deletion in the adult brain. However, the differentiation and maturation of oligodendrocyte precursor cells need to be studied further in the *Sema4F* KO mouse model.

Is Sema4F involved in adult neurogenesis?

Distinct *Sema4F* expression is visible in the ventricular and subventricular zone at postnatal stages. The subventricular zone is important during early development for the generation of pyramidal cells in the cortex and at later stages for the generation of granule cells moving through the RMS to the olfactory bulb [62]. The subventricular zone and the subgranular zone are the only two regions in the adult mammalian brain where neurogenesis still occurs [62–65]. Interestingly, expression of *Sema4F* mRNA is high in the RMS and the granular layer of the olfactory bulb at P14 (figure 5, Armendáriz et al., 2012). In line with this, Sema4F expression is reported in the olfactory bulb and RMS [9]. Other Semaphorins can influence adult neurogenesis by regulating proliferation and development. For example, Sema7A inhibits the proliferation of adult granular progenitors in the dentate gyrus and promotes dendrite formation of newly born neurons [13]. Sema5A influences the development of adult born granule cells by inhibiting synaptogenesis [11]. However, the effects of Sema4F in adult neurogenesis are unknown. Sema4F may influence proliferation as increased BrdU incorporation is detected in prostate cell lines transfected with *Sema4F* [66]. Furthermore, expression of PlexinB1, a receptor for Sema4F, is found in proliferating cells in the ventricular and subventricular zones in adult mice but is not found in postnatal neurons [58]. This suggests that Sema4F could interact via PlexinB1 to influence adult neurogenesis. It will be interesting to determine whether Sema4F has a role in adult neurogenesis by

testing BrdU uptake in the OB and RMS in the *Sema4F* KO mouse. The *Sema4F* KO mouse is a great model to further examine the role of Sema4F in adult neurogenesis.

Heterogeneity and redundancy in Semaphorin class 4 signalling

The canonical receptors for class 4 Semaphorins are the PlexinB1-3, PlexinD1, Neuropilin1 and 2, CD72 and TIM2 [67]. It is likely that Sema4F can bind to multiple interactors. Indeed, a cell binding screen revealed binding between Sema4F and PlexinB1 and B3 and Neuropilin 1 and 2. Binding of CD72 and TIM2 were not tested [30]. Future *in vitro* and *in vivo* studies have to validate these findings.

The preliminary *Sema4F* KO screen did not reveal developmental abnormalities. Similar to our observation, other Sema4 or PlexinB KO mice do not show obvious brain defects [25,68]. For example, PlexinB3 deficiency does not affect the development of the brain nor does it induce behavioural defects [68]. Further, Sema4G KO mice do not show obvious neural phenotypes [25]. These observations suggest that deletion of a single Sema4 or PlexinB is insufficient to induce defects due to redundancy with other family members. This idea is supported by the finding that PlexinB1 and PlexinB2 double KO mice show a reduced neural progenitor pool in the subventricular zone which is not detected in single KO mice [19]. Similarly, deletion of Sema4C induces defects in cerebellar development which are enhanced in double KO for Sema4C and Sema4G, while single Sema4G KO mice do not show any defects [25]. Sema4C and Sema4G bind PlexinB2 [25,30,67]. However, PlexinB2 KO mice have more pronounced cerebellar defects than Sema4C/4G double KO mice. This suggests that yet another ligand may act as a PlexinB2 ligand in this process [69]. It is tempting to speculate if Sema4F is this third ligand. To understand which Sema4 may compensate for *Sema4F* deletion, expression levels of the other class 4 members should be established in *Sema4F* KO mice. It seems likely that double or triple KO mice need to be generated to elucidate the role of Sema4F *in vivo*. It is interesting to speculate which Sema4 could be crossed with the *Sema4F* KO. The expression profiles and receptors of Sema4F and Sema4D are similar [9,27,41,42,61]. Furthermore, both proteins repel ganglion axons [41,58]. In addition, Sema4D deficiency results in an increase in the number of oligodendrocytes in the cerebral cortex [61]. The present data did not show brain alterations in the single *Sema4F* KO. Therefore, in the future this mouse line should be crossed with other Sema4 or receptor KO lines to study the role of these axon guidance molecules.

Conclusion

In summary, *Sema4F* is expressed during brain development ranging from oligodendrocytes and Schwann cells to neurons. Analysis of *Sema4F* KO mice did not reveal major neural defects but more detailed studies are needed to dissect the role of Sema4F *in vivo*. As different class 4 Semaphorins have been reported with overlapping functions it is plausible that double or triple knockout mouse models, deleting multiple Sema4s, are needed to reveal the functions of Sema4F. While we failed to detect defects in the intact brain it is possible that Sema4F is especially important following injury. The newly generated *Sema4F* KO mouse will be an invaluable tool for testing this hypothesis.

Acknowledgements

We would like to thank the members of the Pasterkamp laboratory and the Department of Translational Neuroscience for assistance and helpful discussions throughout this project. This work was financially supported by Stichting Parkinson Fonds and the Netherlands Organization for Scientific Research (ALW-VICI).

Author Contributions

S.L. and R.J.P designed all experiments. S.L. performed (3DISCO) immunohistochemistry, validation of *Sema4F* KO mouse, ISH, (3D) imaging, ISH, *LacZ* staining and PCRs. Y.A. performed and contributed to tissue clearing and 3DISCO. W.A.G.B. contributed to ISH. S.L, G.M.J.R. and R.J.P. wrote manuscript with input from all authors.

References

1. Jongbloets, B. C. & Pasterkamp, R. J. Semaphorin signalling during development. *Development* 141, 3292–3297 (2014).
2. Pasterkamp, R. J. Getting neural circuits into shape with semaphorins. *Nat Rev Neurosci* 13, 605–18 (2012).
3. van Battum, E. Y., Brignani, S. & Pasterkamp, R. J. Axon guidance proteins in neurological disease. *Lancet Neurol* 14, 532–546 (2015).
4. Haklai-Topper, L., Mlechkovich, G., Savariego, D., Gokhman, I. & Yaron, A. Cis interaction between Semaphorin6A and Plexin-A4 modulates the repulsive response to Sema6A. *EMBO J* 29, 2635–2645 (2010).
5. Sun, T. *et al.* A reverse signaling pathway downstream of Sema4A controls cell migration via Scrib. *J Cell Biol* 216, 199–215 (2017).
6. Ding, S., Luo, J. H. & Yuan, X. B. Semaphorin-3F attracts the growth cone of cerebellar granule cells through cGMP signaling pathway. *Biochem Biophys Res Commun* 356, 857–863 (2007).
7. Toyofuku, T. *et al.* Repulsive and attractive semaphorins cooperate to direct the navigation of cardiac neural crest cells. *Dev Biol* 321, 251–262 (2008).
8. Prasad, A. a & Pasterkamp, R. J. Axon guidance in the dopamine system. *Adv Exp Med Biol* 651, 91–100 (2009).
9. Armendáriz, B. G. *et al.* Expression of Semaphorin 4F in neurons and brain oligodendrocytes and the regulation of oligodendrocyte precursor migration in the optic nerve. *Mol Cell Neurosci* 49, 54–67 (2012).
10. Bernard, F. *et al.* Role of transmembrane semaphorin Sema6A in oligodendrocyte differentiation and myelination. *Glia* 60, 1590–1604 (2012).
11. Duan, Y. *et al.* Semaphorin 5A inhibits synaptogenesis in early postnatal- and adult-born hippocampal dentate granule cells. *Elife* 3, e04390 (2014).
12. Parkash, J. *et al.* Semaphorin7A regulates neuroglial plasticity in the adult hypothalamic median eminence. *Nat Commun* 6, 6385 (2015).
13. Jongbloets, B. C. *et al.* Stage-specific functions of Semaphorin7A during adult hippocampal neurogenesis rely on distinct receptors. *Nat Commun* 8, 14666 (2017).
14. Perälä, N., Sariola, H. & Immonen, T. More than nervous: The emerging roles of plexins. *Differentiation* 83, 77–91 (2012).
15. Perälä, N. M., Immonen, T. & Sariola, H. The expression of plexins during mouse embryogenesis. *Gene Expr Patterns* 5, 355–362 (2005).
16. Tamagnone, L. *et al.* Plexins are a large family of receptors for transmembrane, secreted, and GPI-anchored semaphorins in vertebrates. *Cell* 99, 71–80 (1999).
17. Waimey, K. E. Axon Pruning and Synaptic *Development*: How Are They per-Plexin? *Neurosci* 12, 398–409 (2006).
18. Azzarelli, R. *et al.* An antagonistic interaction between PlexinB2 and Rnd3 controls RhoA activity and cortical neuron migration. *Nat Commun* 5, 3405 (2014).
19. Daviaud, N., Chen, K., Huang, Y., Friedel, R. H. & Zou, H. Impaired cortical neurogenesis in Plexin-B1 and -B2 double deletion mutant. *Dev Neurobiol* 76, 882–99 (2015).
20. Vodrazka, P. *et al.* The semaphorin 4D-plexin-B signalling complex regulates dendritic and axonal complexity in developing neurons via diverse pathways. *Eur J Neurosci* 30, 1193–1208 (2009).
21. Yukawa, K. *et al.* Sema4A induces cell morphological changes through B-type plexin-mediated signaling. *Int J Mol Med* 25, 225–230 (2010).
22. Swiercz, J. M., Kuner, R., Behrens, J. & Offermanns, S. Plexin-B1 directly interacts with PDZ-RhoGEF/LARG to regulate RhoA and growth cone morphology. *Neuron* 35, 51–63 (2002).
23. Li, X., Law, J. W. S. & Lee, A. Y. W. Semaphorin 5A and plexin-B3 regulate human glioma cell motility and morphology through Rac1 and the actin cytoskeleton. *Oncogene* 31, 595–610 (2012).
24. Driessens, H. E. *et al.* Plexin-B semaphorin receptors interact directly with active Rac and regulate the actin cytoskeleton by activating Rho. *Curr Biol* 11, 339–344 (2001).
25. Maier, V. *et al.* Semaphorin 4C and 4G are ligands of Plexin-B2 required in cerebellar development. *Mol Cell Neurosci* 46, 419–431 (2011).
26. Kuzirian, M. S., Moore, A. R., Staudenmaier, E. K., Friedel, R. H. & Paradis, S. The class 4 semaphorin Sema4D promotes the rapid assembly of GABAergic synapses in rodent hippocampus. *J Neurosci* 33, 8961–73 (2013).

27. Raissi, A. J., Staudenmaier, E. K., David, S., Hu, L. & Paradis, S. Sema4D localizes to synapses and regulates GABAergic synapse development as a membrane-bound molecule in the mammalian hippocampus. *Mol Cell Neurosci* 57, 23–32 (2013).
28. Smith, E. S. *et al.* SEMA4D compromises blood-brain barrier, activates microglia, and inhibits remyelination in neurodegenerative disease. *Neurobiol Dis* 73, 254–268 (2015).
29. Ben-gigi, L. *et al.* Astrogliosis induced by brain injury is regulated by Sema4B phosphorylation. *eNeuro* 2, e0078 (2015).
30. Visser, J. J. *et al.* An extracellular biochemical screen reveals that FLRTs and Unc5s mediate neuronal subtype recognition in the retina. *Elife* 4, e08149 (2015).
31. Peng, H.-Y., Gao, W., Chong, F.-R., Liu, H.-Y. & Zhang, J. Semaphorin 4A enhances lung fibrosis through activation of Akt via PlexinD1 receptor. *Indian Acad Sci* 40, 855–862 (2015).
32. Toyofuku, T. *et al.* Semaphorin-4A, an activator for T-cell-mediated immunity, suppresses angiogenesis via Plexin-D1. *EMBO J* 26, 1373–1384 (2007).
33. Kumanogoh, A. *et al.* Identification of CD72 as a Lymphocyte Receptor for the Class IV Semaphorin CD100 : A Novel Mechanism for Regulating B Cell Signaling. *Immunity* 13, 621–631 (2000).
34. Kumanogoh, A. *et al.* Nonredundant roles of Sema4A in the immune system: Defective T cell priming and Th1/Th2 regulation in Sema4A-deficient mice. *Immunity* 22, 305–316 (2005).
35. Leitner, D. F., Todorich, B., Zhang, X. & Connor, J. R. Semaphorin4A Is Cytotoxic to Oligodendrocytes and Is Elevated in Microglia and Multiple Sclerosis. *ASN Neuro* 7, (2015).
36. Linder, G. E. *et al.* Semaphorin 4A is dynamically regulated during thymocyte development in mice. *Cell Immunol* 281, 150–158 (2013).
37. Nkyimbeng-Takwi, E. & Chapoval, S. P. Biology and function of neuroimmune semaphorins 4A and 4D. *Immunol Res* 50, 10–21 (2011).
38. Kuklina, E. M., Nekrasova, I. V., Baidina, T. V. & Danchenko, I. Y. The role of the sema4D/CD72-dependent signal in the regulation of B-cell activity in multiple sclerosis. *Dokl Biol Sci* 458, 316–318 (2014).
39. Roney, K., Holl, E. & Ting, J. Immune plexins and semaphorins: old proteins, new immune functions. *Protein Cell* 4, 17–26 (2013).
40. Smith, E. P. *et al.* Expression of neuroimmune semaphorins 4A and 4D and their receptors in the lung is enhanced by allergen and vascular endothelial growth factor. *BMC Immunol* 12, 30 (2011).
41. Encinas, J. a *et al.* Cloning, expression, and genetic mapping of Sema W, a member of the semaphorin family. *Proc Natl Acad Sci* U S A 96, 2491–6 (1999).
42. Schultze, W. *et al.* Semaphorin4F interacts with the synapse-associated protein SAP90/PSD-95. *J Neurochem* 78, 482–489 (2001).
43. Van Battum, E. Y. *et al.* The intracellular redox protein MICAL-1 regulates the development of hippocampal mossy fibre connections. *Nat Commun* 5, 4317 (2014).
44. Belle, M. *et al.* A Simple Method for 3D Analysis of Immunolabeled Axonal Tracts in a Transparent Nervous System. *Cell Rep* 9, 1191–1201 (2014).
45. Malvaut, S. & Saghatelyan, A. The Role of Adult-Born *Neurons* in the Constantly Changing Olfactory Bulb Network. *Neural Plast* 2016, 1614329 (2016).
46. Parrinello, S. *et al.* NF1 loss disrupts Schwann cell-axonal interactions: a novel role for semaphorin 4F. *Genes Dev* 22, 3335–48 (2008).
47. Abraira, V. E. & Ginty, D. D. The sensory neurons of touch. *Neuron* 79, 618–639 (2013).
48. Manousiouthakis, E., Mendez, M., Garner, M. C., Exertier, P. & Makita, T. Venous endothelin guides sympathetic innervation of the developing mouse heart. *Nat Commun* 5, 3918 (2014).
49. Renier, N. *et al.* Resource iDISCO : A Simple , Rapid Method to Immunolabel Large Tissue Samples for Volume Imaging. *Cell* 159, 896–910 (2014).
50. Liem, K. F., Bemis, W. E., Walker Jr., W. F. & Grande, L. Functional anatomy of the vertebrates. 3rd, 437-472 (2001).
51. Kandel, E. R., Schwartz, J. H. & Jessell, T. M. Principles of neural science. 4th, 960-981 (2000).
52. Asamoto, K. Network of the sympathetic nervous system: focus on the input and output of the cervical sympathetic ganglion. *Anat Sci Int* 80, 132–40 (2005).
53. Nedden, S. zur *et al.* Protein kinase N1 critically regulates cerebellar development and long-term function. *J Clin Invest* 128, 2076–2088 (2018).
54. Sturrock, R. R. Changes in neuron number in the cerebellar cortex of the ageing mouse. *J Himsforsch* 30, 499–503 (1989).
55. Nedelescu, H., Abdelhack, M. & Pritchard, A. T. Regional differences in Purkinje cell morphology in

the cerebellar vermis of male mice. *J Neurosci* Res 96, 1476–1489 (2018).
56. Tripathi, R. B. *et al.* Remarkable Stability of Myelinating Oligodendrocytes in Mice. *Cell Rep* 21, 316–323 (2017).
57. Oinuma, I., Ito, Y., Katoh, H. & Negishi, M. Semaphorin 4D/Plexin-B1 stimulates PTEN activity through R-Ras GTPase-activating protein activity, inducing growth cone collapse in hippocampal neurons. *J Biol Chem* 285, 28200–28209 (2010).
58. Moreau-Fauvarque, C. *et al.* The transmembrane semaphorin Sema4D/CD100, an inhibitor of axonal growth, is expressed on oligodendrocytes and upregulated after CNS lesion. *J Neurosci* 23, 9229–9239 (2003).
59. Gonsalvez, D. G. *et al.* Proliferation and Cell Cycle Dynamics in the Developing Stellate Ganglion. *J Neurosci* 33, 5969–5979 (2013).
60. Barrette, B., Calvo, E., Vallières, N. & Lacroix, S. Transcriptional profiling of the injured sciatic nerve of mice carrying the Wld(S) mutant gene: Identification of genes involved in neuroprotection, neuroinflammation, and nerve regeneration. *Brain Behav Immun* 24, 1254–1267 (2010).
61. Taniguchi, Y. *et al.* Sema4D deficiency results in an increase in the number of oligodendrocytes in healthy and injured mouse brains. *J Neurosci* Res 87, 2833–2841 (2009).
62. Whitman, M. C. & Greer, C. A. Adult neurogenesis and the olfactory system. *prog neurobiol* 89, 162–175 (2010).
63. Braun, S. M. G. & Jessberger, S. Adult neurogenesis : mechanisms and functional significance. *Co Biol* 141, 1983–1986 (2014).
64. Christian, K. M., Song, H. & Ming, G. Functions and Dysfunctions of Adult Hippocampal Neurogenesis. *Annu Rev Neurosci* 37, 243–63 (2014).
65. Urbán, N. & Guillemot, F. Neurogenesis in the embryonic and adult brain : same regulators , different roles. *Front Cell Neurosci* 8, 396 (2014).
66. Ding, Y. *et al.* Semaphorin 4F as a critical regulator of neuroepithelial interactions and a biomarker of aggressive prostate cancer. *Clin Cancer Res* 19, 6101–11 (2013).
67. Worzfeld, T. & Offermanns, S. Semaphorins and plexins as therapeutic targets. *Nat Rev Drug Discov* 13, 603–21 (2014).
68. Worzfeld, T. *et al.* Mice lacking Plexin-B3 display normal CNS morphology and behaviour. *Mol Cell Neurosci* 42, 372–81 (2009).
69. Friedel, R. H. *et al.* Plexin-B2 controls the development of cerebellar granule cells. *J Neurosci* 27, 3921–3932 (2007).

Supplementary Information

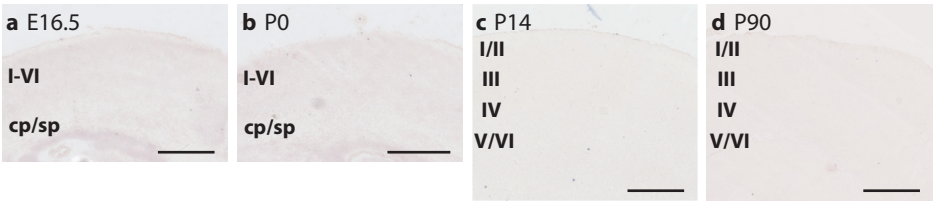

Supplementary Figure 1 | Validation ISH with sense *Sema4F* probe in the cortex.
In situ hybridization for sense *Sema4F* in coronal sections of the mouse cortex at E16.5 (a), P0 (b), P14 (c) and P90 (d). *n* = 3 mice. Scale bars: (a-d) 500µm. Pyramidal layer 1-6: I-VI, cp: cortical plate, sp: subplate.

Chapter 3

Stage-specific functions of Semaphorin7A during adult hippocampal neurogenesis rely on distinct receptors

Bart C. Jongbloets[1,*], Suzanne Lemstra[1,*], Roberta Schellino[2], Mark H. Broekhoven[1], Jyoti Parkash[3], Anita J.C.G.M. Hellemons[1], Tianyi Mao[4], Paolo Giacobini[5,6], Henriette van Praag[7], Silvia De Marchis[2,] Geert M.J. Ramakers[1], R. Jeroen Pasterkamp[1]

[1] Department of Translational Neuroscience, UMC Utrecht Brain Center, University Medical Center Utrecht, Utrecht University, Utrecht 3584 CG, the Netherlands. [2] Dipartimento di Scienze della Vita e Biologia dei Sistemi and Neuroscience Institute Cavalieri Ottolenghi, University of Torino, 10100 Torino, Italy. [3] Centre for Animal Sciences, School of Basic and Applied Sciences, Central University Punjab, City Campus, Mansa Road, Bathinda 151001, India. [4] Vollum Institute, Oregon Health & Science University, Portland, Oregon 97239, USA. [5] Inserm, Laboratory of Development and Plasticity of the Neuroendocrine Brain, Jean-Pierre Aubert Research Centre, U1172, 59045 Lille, France. [6] University of Lille, 59045 Lille, France. [7] Neuroplasticity and Behavior Unit, Laboratory of Neurosciences, Intramural Research Program, National Institute on Aging, National Institutes of Health, Baltimore, Maryland 21224, USA.

* These authors contributed equally to this work.

Published in Nature Communications, 2017, 8, 14666, doi: 10.1038/ncomms14666

Abstract

The guidance protein Semaphorin7A (Sema7A) is required for the proper development of the immune and nervous systems. Despite strong expression in the mature brain, the role of Sema7A in the adult remains poorly defined. Here we show that Sema7A utilizes different cell surface receptors to control the proliferation and differentiation of neural progenitors in the adult hippocampal dentate gyrus (DG), one of the select regions of the mature brain where neurogenesis occurs. PlexinC1 is selectively expressed in early neural progenitors in the adult mouse DG and mediates the inhibitory effects of Sema7A on progenitor proliferation. Subsequently, during differentiation of adult-born DG granule cells, Sema7A promotes dendrite growth, complexity and spine development through ß1-subunit-containing integrin receptors. Our data identify Sema7A as a key regulator of adult hippocampal neurogenesis, providing an example of how differential receptor usage spatiotemporally controls and diversifies the effects of guidance cues in the adult brain.

Introduction

Semaphorins comprise a large family of extracellular proteins that provide guidance to growing neurites and migrating cells during development [1,2]. Many semaphorins are prominently expressed in the embryonic nervous system, but their expression generally declines and becomes more restricted at adult stages. Semaphorin7A (Sema7A), the only glycophosphatidylinositol-linked member of the semaphorin family, is one of few semaphorins or guidance cues in general, that display markedly increased expression as the central nervous system (CNS) matures [3,4]. However, while the developmental roles of Sema7A have been well-characterized [5–10], the precise function of Sema7A in the adult nervous system remains poorly understood [11].

Two cell surface receptors mediate the biological effects of Sema7A: heterodimeric integrin receptors, composed of ß1 and α1or αV subunits, and plexinC1 (also known as VESPR or CD232) (ref. 12). ß1-subunit-containing integrins serve as well-characterized neuronal receptors for Sema7A (ref. 5), but also transduce the non-neuronal effects of Sema7A for example in the immune system [13,14]. Much less, however, is known about the role of plexinC1. Sema7A binds plexinC1 (refs 15,16) and in neurons Sema7A-plexinC1 signalling regulates synapse development and neuroglia plasticity [6,11]. Studies focusing on immune system function or cancer indicate roles for plexinC1 in cell migration and proliferation [17–19], but whether plexinC1 exerts similar cell biological effects in the CNS, and if so, whether these require Sema7A, remains to be determined.

In the adult CNS, cell proliferation is limited to two neurogenic regions, the subventricular zone (SVZ) of the lateral ventricles and the subgranular zone (SGZ) of the hippocampal dentate gyrus (DG). These neurogenic regions harbour adult neural progenitor cells (aNPCs), which give rise to astrocytes, intermediate progenitor cells (IPCs, also known as amplifying neural progenitors), and both immature and mature granule cells (GCs). Cell proliferation in the adult SVZ and SGZ is tightly controlled to avoid exhaustion of the neurogenic aNPC pool. This involves regulation of the balance between quiescent and active aNPCs and strict gating of the number of actively proliferating cells [20–22]. Interestingly, recent work reveals expression of plexinC1 in aNPCs within the SVZ [23], suggesting that plexinC1 may contribute to aNPC proliferation regulation.

New-born GCs in the adult brain (hereafter referred to as adult-born granule cells, or nGCs) need to integrate in a fully developed neural circuit. Although many of the key factors required for the regulation of aNPC proliferation in the SGZ have been identified, much less is known about the extracellular molecular signals that control the morphological development and integration of nGCs. Here we report that, in the adult mouse hippocampus, expression of plexinC1 is restricted to the SGZ and is largely confined to early progenitor cells. In line with this pattern of expression, Sema7A suppresses progenitor proliferation through plexinC1 *in vitro*, and *Sema7A* and *plexinC1* knockout mice display identical cell proliferation defects in the SGZ *in vivo*. At subsequent stages of adult neurogenesis, Sema7A is required for nGC dendrite outgrowth, spine development and functional integration of excitatory inputs to the nGCs. Remarkably, our data suggest that these morphological effects require ß1-integrins, but not plexinC1. Together, our data reveal a novel role for Sema7A in the adult brain, implicate semaphorins and plexins in the control of cell proliferation during adult hippocampal neurogenesis, and provide an example of how a single guidance cue can regulate multiple stages of adult neurogenesis via two, stage-specific, distinct receptors.

Methods

Animals. All experiments were approved by the DEC (Dutch Experimental Review Committee), performed in line with institutional guidelines of the University Medical Center Utrecht and Vrije University Amsterdam, and were conducted in agreement with Dutch law (Wet op de Dierproeven, 1996) and European regulation (Guideline 86/609/EEC). C57BL/6J mice were obtained from Jackson Laboratories. *ß1-integrin$^{fl/fl}$* and *nestin-Cre* mice were obtained from Jackson Laboratories. *Sema7A$^{-/-}$* and *plexinC1$^{-/-}$* mice were as described previously[5]. All mouse lines used in this study were backcrossed at least five times into a C57BL/6J genetic background. *ß1-integrin$^{fl/fl}$;nestin-Cre$^{+/-}$* mice were obtained by paternal inheritance of *nestin-Cre$^{+/-}$* to ensure efficient Cre recombination. All mice were raised by their mothers and weaned at the age of 4 weeks. Mice were kept in a controlled 12 h light-dark cycle with a temperature of 22±1 °C and were given unrestricted access to food (211 RMH-TM diet; Hope Farms) and water. Mice were housed in transparent plexiglas cages with wood-chip bedding and paper tissue for nest building.

BrdU-pulse labeling. BrdU-pulse labelling was performed as described previously[27]. For the analysis of cell proliferation in the adult SGZ, 8-week-old *plexinC1$^{-/-}$*, Sema7A$^{-/-}$, *ß1-integrin$^{fl/fl}$;nestin-Cre$^{+/-}$* and littermate control mice received intraperitoneal injections of 100mg kg^{-1} BrdU in saline. The 2 h post-injection groups received one injection of BrdU. The 3 days and 28 days post-injection (dpi) groups received two injections of BrdU separated by an 8 h interval. For Supplementary Fig. 6h, 6 and 18-month-old *plexinC1$^{-/-}$* and littermate control mice received two injections of BrdU and were treated identical to the 3 dpi group.

Viral vector production. Viral vector production was as described previously[35,37]. MMLV retrovirus was produced by transient transfection of CAG-GFP (Addgene plasmid #16664), CAG-GFP/Cre (Addgene plasmid #49054, encoding for GFP fused Cre recombinase; both were kind gifts of Fred Gage (Salk Institute for Biological Studies))[36], CAG-RFP, or CAG-GFP-IRES-Cre (Addgene plasmid #48201; 2.5 mg, encoding for GFP and Cre recombinase separately) with CMVGagPol (5 µg) and CMV-VSVG (2.5 µg) vectors using Lipofectamine 2000 in 90% confluent 293T cells[34]. Virus-containing supernatant was harvested 36 h after transfection. Supernatant was collected, filtered and concentrated by ultracentrifugation (two times 2 h at 19,400 r.p.m.). Viral titres were estimated to be ≈ 108 i.u. (infectious units) ml^{-1} as determined by infection of serially diluted virus in 293T cells.

Stereotaxic injections. Stereotaxic injections were performed as described previously[35,37]. Mice received pre-, peri- and post-surgically analgesia (5mg kg^{-1} Carprofen, subcutaneous injection; Lidocaine on the skull) and were anaesthetized using Isoflurane (4% induction, 1–2% maintenance). Stereotaxic surgery was performed to deliver 1.0 ml of retrovirus (104–105 i.u. ml^{-1}, MMLV) bilaterally to the DG using the following spatial coordinates relative to bregma: AP = -2.1mm, lateral = 1.5mm / - 1.5mm and ventral = -2.4mm. For some retroviral injections in *ß1-integrin$^{fl/fl}$* mice a mixture (1:1) of MMLV CAG-RFP and MMLV CAG-GFP/Cre or MMLV CAG-GFP-IRES-Cre was used.

Tissue collection and sectioning. For immunohistochemistry, adult mice (48 weeks) were deeply anesthetized with Euthanimal (Alfasan) and intracardially perfused with ice-cold phosphate-buffered saline (PBS) followed by 4% paraformaldehyde (PFA) in PBS. After dissection, brains were incubated overnight (ON) in 4% PFA in PBS at 4 °C. PFA-fixed brains

were then incubated in 30% sucrose in PBS until saturation, snap-frozen in -20 °C isopentane and stored at -80 °C. For non-radioactive *in situ* hybridization, mice were killed by cervical dislocation. Dissected brains were directly frozen on dry ice and stored at -80 °C. Frozen brains for expression analysis and BrdU-pulse assays were sectioned on a cryostat (Leica CM3050). For the BrdU-pulse assay, 40 µm coronal brain sections were collected in cryoprotectant solution and stored at -20 °C until use for free-floating immunohistochemistry. For immunohistochemistry and non-radioactive *in situ* hybridization expression analysis, coronal sections (16–20 µm) containing the hippocampus were collected on Superfrost slides (Merzel, Germany). Slides were stored at -20 °C until use for immunohistochemistry and -80 °C for non-radioactive *in situ* hybridization. Coronal sections (100 µm) of brains injected with MMLV were generated on a vibratome (VT1000S Leica), and stored in cryoprotectant solution, containing 40% PBS, 30% glycerol, 30% ethyleneglycol, at -20 °C until being subjected to free-floating immunohistochemistry.

Immunohistochemistry. Immunohistochemistry was performed as described[67]. In brief, all sections were blocked for 1 h in PBS containing 5% normal donkey serum or normal goat serum and 0.5–1.0% Triton X- 100. Prior blocking, BrdU immunohistochemistry required antigen-retrieval. Sections were incubated in 2N HCl at 37 °C for 30 min followed by 10 min incubation in 0.1M boric acid, pH 8.0. Then slices were treated with 0.3% peroxide in PBS to block endogenous peroxidase activity. Following incubation in blocking solution, all sections or coverslips were incubated overnight with primary antibodies in blocking solution at 4 °C. The following day, sections were incubated with appropriate secondary antibodies in blocking buffer for 2 h at room temperature (RT) (Alexa Fluor 488, 555, 568 or 596, 647, or biotin-conjugated (for BrdU staining)). Extensive washing in PBS was performed in between every incubation step. For BrdU immunohistochemistry, sections were incubated in ABC-staining solution (Pierce) for 2 h at RT, and developed with DAB (Sigma-Aldrich) in 0.05M Tris-buffer, pH 7.6. Immunofluorescent stained sections were counterstained with DAPI (Sigma-Aldrich) and mounted in DAPCO (Sigma-Aldrich) or Prolong Gold anti- fade reagent (Invitrogen). For plexinC1 immunohistochemistry antigen retrieval was required. Sections were incubated in 10 mM sodium citrate (pH 8.5) for 7min in the microwave at 180W followed by 2 h incubation in blocking solution. Sections were blocked for 2 h and incubated over night at 4 °C with primary antibodies. Incubation with secondary antibodies conjugated to biotin was followed by incubation with streptavidin-conjugated Alexa Fluor-488 for 2 h at RT. For differentiation assay immunocytochemistry, coverslips were fixed with 8% PFA and blocked for 1 h. Primary antibodies were incubated over night at 4 °C and secondary antibodies were incubated 1 h at RT. Sections or coverslips were digitized on an Axioskop epifluorescent microscope (Zeiss) or confocal FV1000 microscope (Olympus). Co-localization analysis of lineage-makers with plexinC1 immunohistochemistry was performed using the image-processing program FIJI [68]. Three to ten random locations along the SGZ were imaged with a confocal FV1000 microscope from at least three hippocampal sections per animal. Images were analysed twice by two observers, once based on marker-positive cells and once based on plexinC1-positive cells as reference cells. Observers were presented with single-channel fluorescent z-stacks for selection of the reference cells. After selection of the reference cells, overlap in immunostaining was assessed based on merged multiple-channel fluorescent z-stacks. Branch number and neurite length were determined with FIJI using the Simple Neurite Tracer plugin. To quantify expression of Sema7A in ß1-integrin WT and KO mice the intensity of Sema7A expression was measured in the molecular layer of the DG as

described previously[69]. In short, the molecular layer was defined as an ROI. In the ROI, median intensity levels were measured using FIJI. These levels were subtracted from the maximum intensity for an 8-bit image (250) to generate the reciprocal intensity, which was used to determine differences between genotypes.

Primary antibodies used were: sheep anti-plexinC1 (1:40, AF5375 R&D), goat anti-Sema7A (1:100, AF1835 R&D), rat anti-active ß1-integrin (1:100, 553715 BD Biosciences), mouse anti-NeuN (1:100, MAB377 Millipore), rat anti-BrdU (1:500, OBT0030 Accurate), rabbit anti-Ki-67 (1:100, ab15580 Abcam), mouse anti-GFAP (1:200, ab10062 Abcam), rabbit anti-GFAP (1:500, AB7260 Sigma), mouse anti- Sox2 (1:200, SC1002 Calbiochem), rabbit anti-TBR2 (1:300, AB2283 Millipore), guinea-pig anti-DCX (1:200, AB2253 Chemicon), rabbit anti-cleaved caspase 3 (1:500, 559565 BD Biosciences), rabbit anti-GFP (1:2,000, ab290 Abcam), chicken anti-GFP (1:400, ab13970 Abcam), rabbit anti-RFP (1:500, 600-401-379 Rockland), rabbit anti-Map2 (1:500, AB5622 Milipore) and mouse anti-Tuj1 (1:500, MMS-435P Covance).

Non-radioactive *in situ* hybridization. Non-radioactive *in situ* hybridization was performed on coronal brain sections (16 µm) of adult mice using digoxigenin-labelled RNA probes targeting *Sema7A* mRNA (rat *Sema7A*; NC_005107.4, nt 205–941 of coding region) or *ß1-integrin* mRNA (mouse ß1-integrin; NM_010578, nt 603–1205 of codion region). Probe design and synthesis, and non-radioactive *in situ* hybridization were performed as described previously[3]. In brief, sections were hybridized with 400 ng ml^{-1} RNA in 150 ml hybridization mixture containing 50% deionized formamide, 5% standard saline citrate (SSC), 1x Denhardt's solution, 0.25 mg ml^{-1} sonificated salmon sperm DNA, and 0.5 mg ml^{-1} tRNA baker's yeast. After overnight hybridization at 55 °C, slides were washed, incubated with anti-digoxigenin antibodies (1:2,500, 1093274 Boehringer Mannheim) and developed with BCIP/NBT (Boehringer Mannheim). Subsequently, sections were dehydrated and embedded in Entallan (Merck). For co-labelling of BrdU and *Sema7A*, 800 ng ml^{-1} RNA probe was used and Triton X- 100 was omitted during antibody incubation steps. Sections were embedded in 95% glycerol to avoid loss of *in situ* hybridization signal. Representative sections were digitized using an Axioskop2 light-microscope (Zeiss).

Western blotting. Specificity of different anti-plexinC1 and anti-Sema7A antibodies (Supplementary Fig. 1) was examined using western blotting as described[70]. In brief, fresh frozen tissue from *Sema7A*$^{-/-}$, *plexinC1*$^{-/-}$ or wild-type brains was homogenized in ice-cold RIPA buffer containing 10mM Tris-buffer pH 7.5, 150mM NaCl, 0.1% SDS, 1% Triton X- 100, 1% deoxycholate, 0.5mM EDTA, 1mM PMSF and complete protease inhibitor (Roche). Protein containing-supernatant was isolated after centrifugation at 12,000 r.p.m. at 4 °C for 15min. Tissue lysates (20µg of total protein) were separated by SDS-PAGE and transferred to nitrocellulose membrane. Blocking of the membrane and incubation of antibodies was performed in 3-5% ELK in TBS-T. To detect protein phosphorylation (Supplementary Fig. 3d–g), neurospheres from WT mice were cultured and treated with Fc (2nM, R&D) or Sema7A-Fc (2nM, R&D) proteins for 30min. Proteins were harvested by homogenization in ice-cold RIPA buffer followed by centrifugation at 12,000 r.p.m. at 4 °C for 15min. Protein lysates were incubated with sample buffer and 10% ß-mercaptoethanol and boiled for 5min at 95 °C. Samples (30µg of total protein) were separated in precast 3%-8% SDS-polyacrylamide Tris-acetate gels (Invitrogen). Proteins were transferred to Nitrocellulose membranes (0.2mm pore-size membranes, Invitrogen). For all membranes, membrane blocking and antibody incubation was performed in 5% ELK in TBS-T. Western blotting was

performed using the following antibodies: goat anti-Sema7A (1:1,000, AF1835 R&D), rabbit anti-Sema7A (1:500, ab23578 Abcam), goat anti-Sema7A (1:200, sc67969 Santa Cruz), rabbit anti-plexinC1 (1:200, sc25643 Santa Cruz), sheep anti-plexinC1 (1:200, AF5375 R&D), mouse anti-beta3-tubulin (1:1,000, MMS-435 P Convance), mouse anti-P-cofilin (1:500, sc271923 Santa Cruz Biotechnology), rabbit anti-cofilin (1:500, sc33779 Santa Cruz Biotechnology), rabbit anti-integrin ß1 (1:500, sc8978 Santa Cruz Biotechnology), rabbit anti-P-integrin ß1 (1:500, ab5189 Abcam) followed by incubation with HRP-conjugated secondary antibody (anti-rabbit (1:10,000), anti-goat (1:15,000) or anti-mouse (1:30,000)). After incubation with Pierce SuperSignal chemiluminescence kit, blots were exposed to ECL film (Pierce), developed and digitized using an Epson flatbed scanner (Perfection 4990, Epson America) for tissue lysates or detected via enhanced chemiluminescence (NEL101, PerkinElmer) for neurosphere lysates.

Isolation and culturing of aNPCs from the adult DG. Isolation and culture of adult NPCs (aNPCs) was performed as described previously[26,28]. aNPCs were isolated from 8–10 week-old *plexinC1*$^{-/-}$, *Sema7A*$^{-/-}$ or wild-type mice. The whole hippocampus was rolled out followed by microdissection of the DG. The isolated DG was dissociated by enzymatic digestion using the MACS Neural Tissue Dissociation kit (Miltenyi Biotech). Dissociated cells were passed through a 40 µm cell-strainer and seeded as a single-cell suspension in medium containing glutaMAX DMEM/F- 12 (Gibco), 20 ng ml^{-1} EGF (Invitrogen), 20 ng ml^{-1} FGF (Gibco), B-27 (Gibco) and penicillin/streptomycin (Gibco). Cultures were kept in a 5% CO_2 incubator at 37 °C. Neurospheres formed by proliferating aNPCs were passaged at a diameter of ±150–200 µm. Neurospheres were dissociated in Trypsin LE Express (Gibco) for 5min at 37 °C, passed through a 40 µm filter and cultured as a single-cell suspension. All differentiation and proliferation assays were performed using aNPCs with a passage number of 0–10 to avoid undesired side effects due to prolonged *in vitro* culture.

RT-PCR. Passage 10 neurospheres were collected and mRNA was isolated using the RNeasy micro kit (Qiagen). One-step RT-PCR was conducted, as described previously[3] on 100 ng µl^{-1} RNA using the following primers: *Sema7A* 5'-CGT GTATTCGCTTGGTGACAT-3', 5'-GTGGGTATGGGCTGCTTTTT-3' (product size of 120 bp) (ref. 71), *ß1-integrin* 5'-AATTTGCAACTGGTTTCCTG-3', 5'-GTT TGAGAGCCTCTGGGATT-3' (product size of 260 bp), *α1-integrin* 5'-CATCTGG CTTCTCACCGTTA-3', 5'-CTCTCTCTCCCAACTGGACAC-3' (product size of 219 bp), *av-integrin* 5'-GTCCTCCAGGATGTTTCTCC-3', 5'-ACCTCACAGAGG CTCCAAAC-3' (product size of 209 bp), and *plexinC1* 5'-TCTGGAACGGCAG TGTCTAC-3', 5'-GCCTGGATCTCACTCATCCT-3' (product size of 298 bp). HPRT primers were from Quantitect Primer Assay (product size of 107 bp, Qiagen). PCR cycle-sequence was as follows: 5min/95 °C, 30 s/95 °C, 30 s/54 °C, 45 s/72 °C (for 30, 35 and 40 cycles), 7min/72 °C.

Purification of AP-Fc-tagged Sema7A. Recombinant AP-Sema7A-Fc and AP-Fc control proteins[5] were freshly purified for each experiment as described previously[9]. HEK293 cells were cultured in 175cm^2 flasks at 70–80% confluency and transiently transfected with 32 µg DNA vector per flask (Sema7A-AP-Fc or AP-Fc) using PEI (Polyscience). Transfected cells were cultured in OptiMEM medium for 36–48 h before harvesting. Then medium was filtered and concentrated using filter spin column (50 kDa, Millipore) and Ultrafree 0.5 ml centrifugal filters (10 kDa, Millipore), respectively. Recombinant protein concentration was determined by measuring alkaline-phosphatase activity.

***In vitro* proliferation and differentiation assays.** For proliferation assays on aNPCs, passage 4–10 neurospheres were dissociated and seeded as a single-cell suspension at a density of 5,000 cells well^{-1} (24-wells plate, 500 ml growth volume) and allowed to form neurospheres for 8–10 days. Medium containing recombinant Sema7A-AP-Fc (2nM) or AP-Fc (2nM) was refreshed every other day. Experiments were terminated by addition of an equal volume, relative to medium, of 8% PFA in PBS and stored for analysis at 4 °C. Neurosphere number and diameter were determined using an upright light microscope (AxioVert, Zeiss) and the image-processing program FIJI.

For differentiation assays, small neurospheres (diameter of ±50µm) were seeded onto acid-etched coverslips coated with poly-L-lysine (500 mg ml^{-1}, Sigma-Aldrich) and laminin (40mg ml^{-1}, Sigma-Aldrich), and cultured in aNPC medium for 36 h. Subsequently, medium was changed to differentiation medium consisting of Neurobasal medium (Gibco) supplemented with 200mM L-Glut, B27, 1.8mM Hepes, and penicillin/streptomycin. Differentiation medium was supplemented with recombinant Sema7A-Fc (2nM, R&D) or Fc (2nM, R&D) and anti-rat IgG-control (25 µg ml^{-1}, 553968 BD bioscience) or anti-rat CD29 (25 µg ml^{-1}, 555002 BD biosciences) every other day. After 10 days, coverslips were processed for immunohistochemistry.

Stereology. BrdU-positive cells were counted as described previously[27], using a brightfield microscope (Zeiss) and Neurolucida (MBF Bioscience) and FIJI software. Cells were counted throughout the anterior-posterior extent of the GC layer in a series of 40 µm coronal sections spaced 240 µm apart. Total cell number in the DG per hippocampus was calculated based on the multiply of counted BrdU-positive cells, corrected for DG volume estimate and sampling frequency. Systematic random sampling with a dissector (625 µm^2) was used to determine the cell density of the DG granule layer (Supplementary Fig. 6e). GCs were counted in a series of 40 µm coronal sections with a vibratome advance of 240 µm. Total cell density was determined by correcting the total sum of counted GCs by dissector frame, sum of dissectors used, mean thickness of slice, vibratome advance and number of points associated with the dissector frame.

Morphometric analysis of adult-born GCs in the adult DG. Stained sections from MMLV-injected brains were scanned on a confocal microscope (FV1000, Olympus) using x40 (UPlanSApo UIS2 0.95 NA, Olympus) and oil-immersion x100 (UPlanSApo UIS2 1.40 NA, Olympus) objectives. Z-stack images were captured at a resolution of: x40 objective x/y-plane: 3.23 pixels µm^{-1}, z-plane: 1 µm and x100 objective x/y-plane: 8.06 pixels µm^{-1}, z-plane: 0.40 µm. Analysed nGCs extended their dendrites within the specimen section, avoiding the outer 5 µm of the section-depth. Images captured of GFP/RFP-positive adult-born GCs by using the x40 objective were used to identify (1) the inner molecular layer (IML), which was defined as the first 50 µm from and parallel to the outer border of DAPI-positive cells, and (2) the outer molecular layer (OML), which was defined as the last 70µm from and parallel to the outer border of the molecular layer. GFP-positive dendrites within the IML and OML were imaged, by using a x100 objective for spine density analysis. Analysis of dendritic branching was performed by using Neurolucida (MBF Bioscience) and spine density analysis and migration distance was performed using FIJI. Mushroom-like spines were defined as described earlier[40,41], that is, spines with a head diameter much greater than the diameter of the neck were judged mushroom-like.

Electrophysiology. Mice (WT and *Sema7A*$^{-/-}$) were injected at P54-P58 with 1 µl of MMLV virus encoding CAG-GFP in DG (as described in the section 'Stereotaxic injections'). Coronal brain slices were prepared 56–60 days later from mice sedated with isoflurane and perfused transcardially with ice-cold ACSF containing (in mM): NaCl (127), $NaHCO_3$ (25), D-glucose (25), KCl (2.5), $MgCl_2$ (1), CaCl2 (2), and NaH_2PO_4 (1.25), pH 7.25–7.35, ±310 mOsm, and bubbled with 95% O_2 / 5% CO_2, as described previously[37,72]. The brain was removed and placed into ice-cold cutting solution containing (in mM): choline chloride (110), $NaHCO_3$ (25), D-glucose (25), sodium ascorbate (11.5), $MgCl_2$ (7), sodium pyruvate (3), KCl (2.5), NaH_2PO_4 (1.25) and $CaCl_2$ (0.5). The ventral side of the brain was placed onto a 10° aluminium wedge, anterior side facing the inclining part of the slope and 300 µm thick horizontal slices were vibratome sectioned (Leica 1200S). Slices were incubated in oxygenated ACSF for 30 min at 34 °C, and then maintained in an oxygenated holding chamber for at least 30min at RT before commencing recording.

For recording of intrinsic properties of GCs oxygenated ACSF was supplemented with (in µM) $GABA_B$-receptor antagonist CGP 52432 (10), $GABA_A$-receptor antagonist SR 95531 (10), AMPA receptor antagonist NBQX (10) and NMDA receptor antagonist CPP (5). For recording of mEPSCs oxygenated ACSF was supplemented with (in µM) Na^+ channel blocker TTX (1) and $GABA_B$-receptor antagonist CGP 52432 (10), $GABA_A$-receptor antagonist SR 95531 (10), and NMDA receptor antagonist CPP (5). All compounds were purchased from Tocris.

Borosilicate pipettes (2.8–6 MΩ; Warner Instruments) were filled with potassium gluconate-based internal solution ((in mM) potassium sulfonate (120), KCl (20), $MgCl_2$ (4), NaCl (5), Hepes (10), EGTA (0.1), Na_2-phosphocreatine (10), Na_2ATP (4), Na_2GTP (0.3); pH 7.35–7.40; 290 mOsm) for recording of intrinsic properties and cesium methanesulfonate-based internal solution ((in mM) cesium methanesulfonate (135), NaCl (8), Hepes (10), EGTA (0.5), Na_2ATP (4), Na_2GTP (0.3); pH 7.35–7.40; 290 mOsm) for mEPSC recording. Both internal solutions contained 3mg ml^{-1} biocytin (Sigma) and 10 µM Alexa Fluor 594 dye (Invitrogen).

Whole-cell patch-clamp recordings were acquired at 10kHz using a Multiclamp 700B with an online 2 kHz low pass filter (Molecular Devices) and *Ephus* software (www.ephus.org). Data analysis was performed in Matlab, R (http://cran.r-project. org), Igor Pro (Wavemetrics) and Excel (Microsoft). Recordings were corrected for a liquid junction potential of 7.6 and 15mV, for the potassium gluconate-based and the cesium methanesulfonate-based internal solution, respectively. Series resistance was typically 15–35 MOhm. Resting membrane potentials were measured immediately after break-in. R_{input} was measured using a linear-regression of voltage deflections (±15mV from resting potential) in response to 200ms current steps of eight different amplitudes (increments, 25 pA). The time constant (Tau_m) was calculated fitting a single exponential function to the mean voltage responses to three hyperpolarizing and three depolarizing current steps (- 25pA and 25 pA, 200 ms). Membrane capacitance (C_m) was calculated according to $C_m = Tau_m/R_m$. mEPSCs were detected using template fitting, generated by manual setting of rise- and decay-time constants, in a custom-written Matlab routine (by Haining Zhong). Visual validation was performed after automatic detection of mEPSCs. Rise- and decay time were calculated based on 10-90% of mEPSC peak value. Instantaneous frequency of individual events was calculated based on the inverse of the time interval (in seconds) to the previous event. Amplitude and instantaneous frequency histograms of mEPSC were fitted with a single lognormal distribution using the following equation: $Y = A \cdot exp\ (- (ln(X) - \mu)^2 / (2 \cdot \sigma^2)) / (\sigma \cdot X \cdot \sqrt{(2\pi)})$, where Y represents number of instantaneous frequency / amplitude events, A relative area under the curve, X the measured instantaneous frequency / amplitude, m is the mean and σ is the s.d. of the underlying normal distribution. The mean of the lognormal

distribution (*m*) was then calculated using the equation: $m = exp\ (\mu + \sigma^2 \cdot 0.5)$.

Action potential (AP) kinetics was determined on isolated APs elicited at rheobase current injection. AP threshold was determined during a current ramp (165pA s^{-1}), for which AP onset was defined as $V_{membrane}\ s^{-1} > V\ s^{-1}$. Spike analysis was performed automatically by selecting individual APs based on AP onset ($V_{membrane}\ s^{-1} > V\ s^{-1}$), and peak amplitude ($V_{membrane} > 0$ mV), and subsequent manual validation. Inter-spike-interval was calculated for each AP and used for firing rate and firing adaptation index, 1- (F_{last} / $F_{initial}$) calculation, for which $F_{initial}$ is the averaged inter-spike-interval of the first two spike intervals and F_{last} is the averaged inter-spike-interval of the last three spike intervals.

Blinding methods and statistical analyses. To avoid observer bias, all quantitative assessments in this manuscript were performed while being unaware of genotype or condition. During analysis, raw data were named in a descriptive way, without revealing experimental group information. (Fluorescent) microscopic imaging was always done with the same settings within experiments, and analysis techniques were standardized.

A single person analysed all data obtained within the experiments. All experiments were replicated at least three times. All statistical analyses were performed using Excel (Microsoft Office, Microsoft, USA), Igor Pro (Version 6.0, Wavemetrics, USA), SPSS (Version 21.0, IBM Inc., USA), or R (version 3.1.2, http://cran.r-project.org). Thresholds of significance were set at $\alpha = 0.05$. Sholl-analyses were statistically tested using repeated-measures ANOVA, with Student's *t*-test *post-hoc* per radii. Two-way ANOVA with *post-hoc* Student's *t*-test was used where multi-factorial comparisons were made and specifically mentioned in the text. Homogeneity of variance was tested with the Levene's test. Paired-testing was performed where littermate-controls or technical-replicate were compared and specifically mentioned in the text, otherwise unpaired Student's *t*-test was used. The number of experiments performed with independent cultures or mice, (*n*) unless otherwise stated, is indicated in the legends. Error bars represent s.e.m..

Data availability. The data sets generated and analysed during the current study are available from R. Jeroen Pasterkamp on request.

Results

PlexinC1 is confined to the neurogenic niche of the adult DG

Expression of *Sema7A* in the brain increases as development progresses [3]. However, the precise role of this and the expression of many other semaphorins in the adult brain remains incompletely understood. Sema7A exerts its biological effects via two unrelated receptors, plexinC1 and ß1-subunit-containing integrins [12]. Whereas expression of ß1-integrins in the mature rodent brain is rather strong and ubiquitous [24], expression of *plexinC1* is much more restricted [3]. Therefore, to unravel specific function(s) of Sema7A in the adult brain we first focused on plexinC1 and performed immunohistochemistry for this receptor at adult stages. In line with our previous work showing restricted *plexinC1* expression in the adult mouse brain [3], plexinC1 immunolabelling was detected in a small number of brain regions, including the olfactory bulb, rostral migratory stream (RMS), cerebellum and DG of the hippocampus (Supplementary Fig. 1a–g;). Mature GCs in the DG are lined up within the granular cell layer (GCL) and project their axons to the CA3 region of the hippocampus. Beneath the GCL is a layer termed the SGZ, which harbours proliferating neuronal progenitor cells (aNPCs). aNPCs give rise to nGCs throughout adult

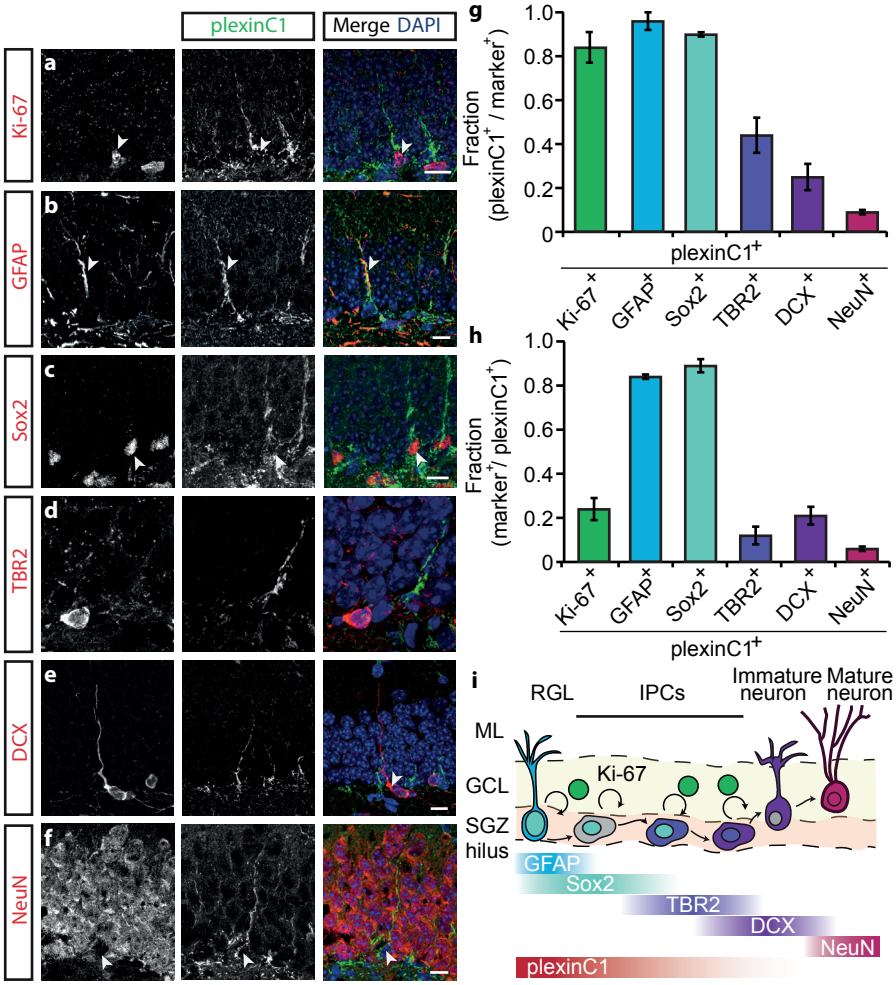

Figure 1 | PlexinC1 expression in the subgranular zone is largely confined to early progenitors. (a–f) Double immunohistochemistry for plexinC1 and Ki-67 (a), glial fibrillary acidic protein (GFAP; b), sex determining region Y-box 2 (Sox2; c), T-box brain 2 (TBR2; d), doublecortin (DCX; e) or neuronal nuclei (NeuN; f) in sections of the adult mouse dentate gyrus (DG). The majority of plexinC1-positive cells express Ki-67, GFAP and Sox2 but not TBR2, DCX or NeuN. Arrowheads indicate cells expressing specific markers. Arrows indicate plexinC1-positive cells not expressing the indicated marker. (g,h) Quantification of the fraction of cells expressing a specific marker that also express plexinC1 (g) or the fraction of plexinC1-positive cells that also express the indicated marker protein (h). Data are presented as means ± s.e.m. $n \geq 3$ (mice). (i) Schematic representation of lineage-marker and plexinC1 expression in cell lineage subtypes during neuronal differentiation in the adult DG. Ki-67 is a marker for proliferating cells during all active phases of the cell cycle. PlexinC1 is expressed in GFAP-positive and Sox2-positive radial glia-like cells (RGLs) and early intermediate progenitor cells (IPCs). Ki-67-positive proliferating cells express plexinC1. In contrast, only a small fraction of TBR2-, DCX- or NeuN-positive intermediate progenitor cells and (immature) granule cells express plexinC1. Scale bars: 10 µm.

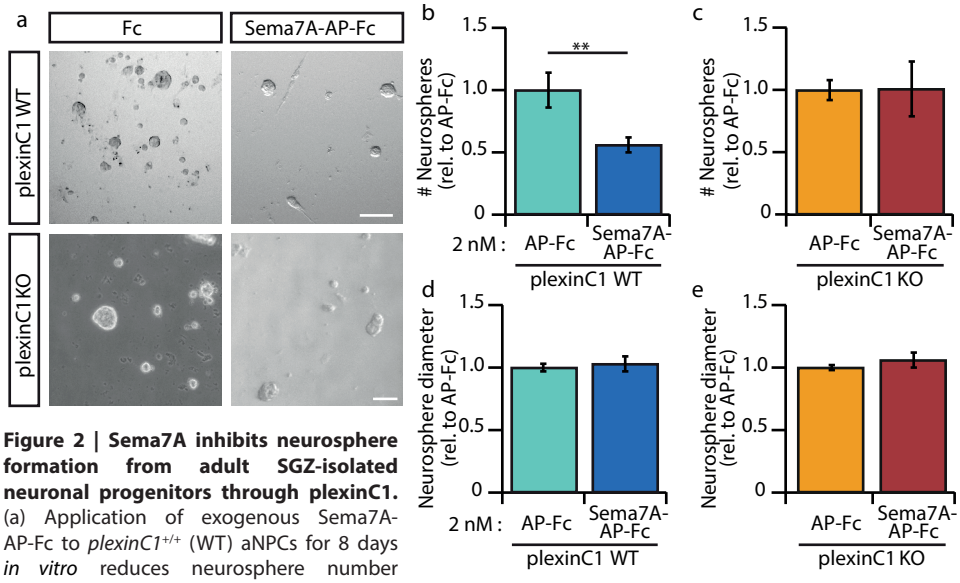

Figure 2 | Sema7A inhibits neurosphere formation from adult SGZ-isolated neuronal progenitors through plexinC1. (a) Application of exogenous Sema7A-AP-Fc to *plexinC1*$^{+/+}$ (WT) aNPCs for 8 days *in vitro* reduces neurosphere number compared to AP-Fc control treatment. This reduction is lost in *plexinC1*$^{-/-}$ (KO) aNPCs. (b–e) Quantification of WT neurosphere growth in the presence of Sema7A-AP-Fc reveals a significant reduction in neurosphere number (replicate-paired Student's *t*-test; b) but not diameter ($p = 0.0674$, $n = 5$ mice; d). aNPCs from KO mice are not sensitive to the proliferation inhibiting effects of Sema7A-AP-Fc (replicate-paired Student's *t*-test: $p_{(diameter)} = 0.9484$, $p_{(number)} = 0.7738$, $n = 5$ mice; c,e). Data are presented as means ± s.e.m. ** $p < 0.01$. Scale bar: 100 µm.

life (Fig. 1i). Immunohistochemistry showed that expression of plexinC1 in the DG GCL is confined to cells located in the SGZ (Supplementary Fig. 1c). In contrast to the specific expression of plexinC1, Sema7A was expressed throughout the adult DG (Supplementary Fig. 1h–j). The SGZ consists of aNPCs, such as radial glia-like cells (RGLs) and multiple types of IPCs, as well as immature nGCs (Fig. 1i). To reveal which cells in the SGZ express plexinC1, we performed double and triple immunohistochemistry experiments with several cell-type specific markers including Ki-67, GFAP and Sox2 (Fig. 1, Supplementary Fig. 2). Ki-67 labels proliferating cells and most Ki-67þ cells showed plexinC1 expression (Fig. 1a,g,h). However, plexinC1 expression was not restricted to proliferating cells, because only a small fraction of all plexinC1þ cells expressed Ki-67 (Fig. 1h). RGLs, which express GFAP and Sox2 (Fig. 1b,c), are recognizable by their short process extending into the GCL (ref. 25). This morphology is reminiscent of the majority of plexinC1þ cells in the SGZ (Fig. 1a–f, Supplementary Figs. 1c and 2a–e). Indeed, co-labelling showed that most GFAP$^+$ and Sox2$^+$ cells express plexinC1, and also that most plexinC1-expressing cells displayed GFAP and Sox2 immunolabelling (Fig. 1b,c,g,h, Supplementary Figs. 1c and 2a,c,d,f). About half of these cells were proliferating as evidenced by Ki-67 expression (Supplementary Fig. 2c,d,g). Only a small fraction of T-box brain protein (TBR2)-positive IPCs (Fig. 1d,g, Supplementary Fig. 2b,f) or doublecortin (DCX)-positive IPCs and immature nGCs (Fig. 1e,g, Supplementary Fig. 2b,f) expressed plexinC1, and we found that only a small subset of plexinC1$^+$ cells displayed TBR2 or DCX labelling (Fig. 1h, Supplementary Fig. 2f,g). Finally, most NeuN$^+$ mature GCs did not express plexinC1, while plexinC1$^+$ cells only rarely displayed NeuN signals (Fig. 1f–h). Together, these results indicate that in the neurogenic niche of the DG plexinC1 is mostly confined to early progenitor cells, including RGLs and early IPCs, independent of their proliferation state (Fig. 1i).

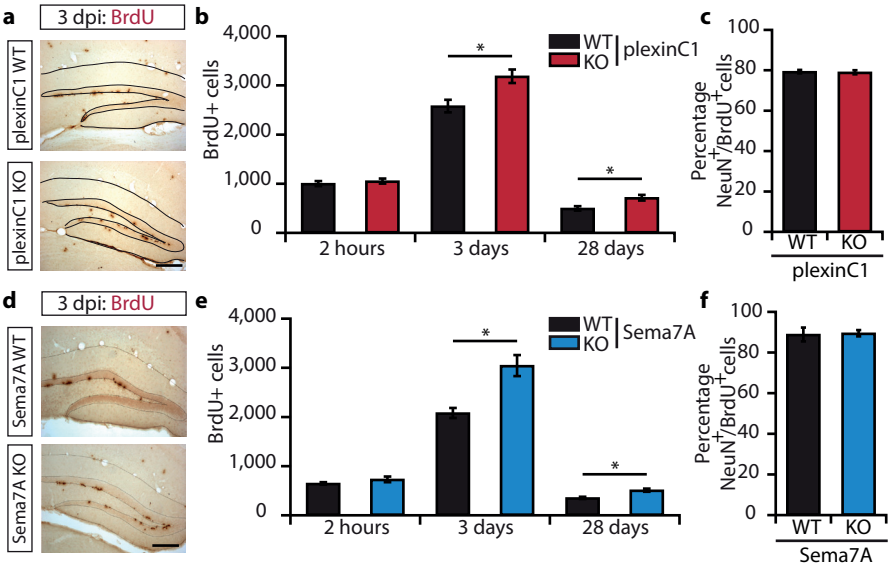

Figure 3 | *PlexinC1*$^{-/-}$ and *Sema7A*$^{-/-}$ mice display increased cell proliferation in the adult DG. (a,d) Representative examples of BrdU immunostaining in the dentate gyrus (DG) of adult wild-type littermates (WT), *plexinC1*$^{-/-}$ or *Sema7A*$^{-/-}$ mice at 3 days after BrdU injection (dpi). KO, knockout. (b,e) Adult mice were injected with BrdU and processed for immunohistochemistry for BrdU at 2 h, 3 days and 28 days post-injection. An increase in the number of BrdU-positive cells was detected at 3 and 28 dpi in *plexinC1*$^{-/-}$ and *Sema7A*$^{-/-}$ mice as compared to WT (two-way ANOVA, *post-hoc t*-test, 2 h: $n_{(WT,\ plexinC1\text{-}/\text{-})} = 4$, $n_{(Sema7A\text{-}/\text{-})} = 3$, 3 days: $n_{(WT,\ Sema7A\text{-}/\text{-})} = 4$, $n_{(plexinC1\text{-}/\text{-})} = 7$, 28 days: $n_{(plexinC1\text{-}/\text{-},WT)} = 5$, $n_{(Sema7A\text{-}/\text{-})} = 4$, $n_{(Sema7A\text{-}WT)} = 3$). (c,f) Quantification of the number NeuN/BrdU-positive cells in the indicated mouse models at 28 dpi (Wilcoxon-Mann-Whitney test, Sema7A: $n_{(Ki\text{-}67,\ DCX)} = 4$, plexinC1: $n_{(WT:\ Ki\text{-}67,\ DCX)} = 3$, $n_{(plexinC1\text{-}/\text{-}:\ Ki\text{-}67,\ DCX)} = 4$, $p_{(plexinC1)} = 0.8728$, $p_{(Sema7A)} = 0.7114$). Data are presented as means ± s.e.m., ** $p < 0.01$, * $p < 0.05$. Scale bars: 250µm.

Sema7A inhibits proliferation of aNPCs through plexinC1

The specific expression of plexinC1 in aNPCs (Fig. 1) led us to hypothesize that Sema7A and plexinC1 regulate cell proliferation during adult neurogenesis. To examine this model, we performed experiments with neurosphere cultures. Proliferation of aNPCs in dissociated *in vitro* suspension culture leads to the formation of neurospheres, which express *plexinC1* (Supplementary Fig. 3a). Neurosphere size and number are routinely used as a measure for aNPC proliferation [26]. We first assessed whether Sema7A could modulate aNPC proliferation. Indeed, application of 2 nM Sema7A-AP-Fc to wild-type aNPCs for 8 days strongly reduced the number of neurospheres (Fig. 2a,b,d; $n = 5$ mice, Student's *t*-test: $p = 0.0172$), as compared to control (AP-Fc, 2 nM). In contrast, the number and diameter of neurospheres formed from *Sema7A*$^{-/-}$ aNPCs resembled *Sema7A*$^{+/+}$ control (Supplementary Fig. 3b,c; $n = 5$ mice, Student's *t*-test: $p_{(number)} = 0.4515$, $p_{(diameter)} = 0.8900$). To determine whether exogenous Sema7A affects aNPC proliferation via plexinC1, *plexinC1*$^{-/-}$ aNPCs were exposed to Sema7A. Application of Sema7A reduced the number of neurospheres derived from *plexinC1*$^{+/+}$ but not *plexinC1*$^{-/-}$ aNPCs (Fig. 2a–e; $n = 5$ mice, Student's *t*-test: $p_{(number)} = 0.7738$, $p_{(diameter)} = 0.9484$). Genetic depletion of plexinC1 by itself did not affect neurosphere number (n = 3 mice, *plexinC1*$^{+\backslash+}$ = 1.000±0.0156, *plexinC1*$^{-/-}$ = 1.005 ± 0.1383, Student's *t*-test: $p = 0.9712$ (mean normalized to *plexinC1*$^{+/+}$ ± s.e.m.)). Together, these results suggest that Sema7A-plexinC1 signalling negatively regulates aNPC proliferation *in vitro*.

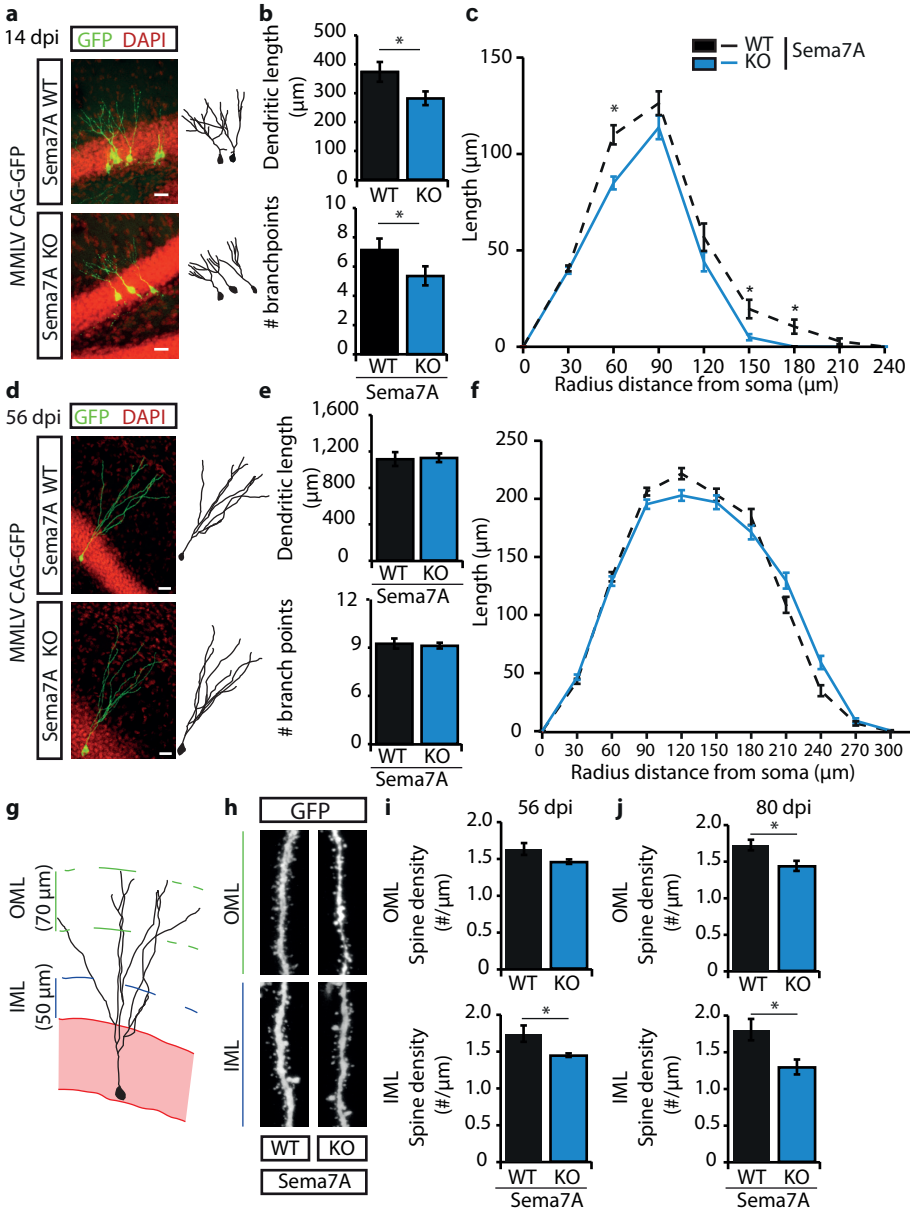

Figure 4 | Sema7A is required for dendritic growth and spine development in adult-born DG granule cells. (a,d) The dentate gyrus of adult *Sema7A*$^{+/+}$ (WT) or *Sema7A*$^{-/-}$ (KO) mice was injected with MMLV CAG-GFP to label adult-born granule cells and immunostained for GFP at 14 or 56 days post-injection (dpi). DAPI is shown in red. Right panels depict representative tracings based on confocal z-stack images. (b,e) Quantification of dendritic length and number of branch points in WT (black bars) and KO (blue bars) littermates (two-way ANOVA, *post-hoc t*-test, 14 dpi: $n = 3$, 56dpi: $n = 4$, $p_{(56\text{ dpi: length})} = 0.150$ and $p_{(56\text{ dpi: branch points})} = 0.868$). (c,f) Sholl analysis of the dendritic tree of GFP-labelled cells in WT (black dashed-lines) and KO mice (blue lines). Dendritic length per radius distance from soma (30µm radius interval) at 14 dpi, but not at 56 dpi, was decreased in KO mice (14 dpi: $n = 117$ WT cells/3 mice, $n = 120$ KO cells/3 mice, 56 dpi: $n = 134$ WT cells/4 mice, $n = 151$ KO cells/4 mice. Repeated-measures ANOVA 14 dpi: $F_{(7, 1645)} = 3.219$, 56dpi: $F_{(9, 1224)} =$

2.2560, $p = 0.056$). (g) Schematic representation of the DG indicating the regions selected for spine density quantification. IML, inner molecular layer; OML, outer molecular layer. (h) Representative images showing spine-bearing dendritic segments in the OML and IML in WT and KO mice. (i) Quantification of spine density on adult-born granule cells (nGCs) at 56dpi shows differences between WT($n = 5$) and KO ($n = 5$) mice in the IML (*post-hoc t*-test: $p_{(OML)} = 0.081$). (j) Quantification of spine density on nGCs at 80dpi shows differences between WT ($n = 3$) and KO ($n = 3$) mice in the IML and OML (Student's *t*-test). Data are presented as means ± s.e.m. * $p < 0.05$. Scale bars: (a,d) 25µm; (h) 10µm.

Sema7A-plexinC1 inhibit proliferation in the adult DG in vivo

To confirm these *in vitro* observations and to examine whether Sema7A and plexinC1 can regulate aNPC proliferation *in vivo*, bromodeoxyuridine (BrdU)-pulse labelling was performed in adult mice. Proliferating cells incorporate BrdU during DNA-replication allowing quantification of the number of proliferating cells [27]. At 2 h after a BrdU injection, the number of BrdU$^+$ cells in the DG was similar in *plexinC1*$^{+/+}$ and *plexinC1*$^{-/-}$ mice (Fig. 3a,b; $n = 4$ mice, *post-hoc t*-test: $p_{(2\ h)} = 0.335$; Supplementary Fig. 5a–d). In contrast, the number of BrdU$^+$ cells in *plexinC1*$^{-/-}$ mice was significantly increased 3 and 28 days after BrdU injections (Fig. 3a,b; $n \geq 4$ mice, two-way ANOVA: genotype x time $F_{(2,15)} = 0.003$, *post-hoc t*-test: $p_{(3\ days)} = 0.0208$, $p_{(28\ days)} = 0.0208$). To confirm these data, immunohistochemistry for Ki-67 and DCX was performed. In line with the BrdU data, quantification showed an increase in Ki-67$^+$ proliferating cells and DCX$^+$ immature nGCs in adult *plexinC1*$^{-/-}$ mice (Supplementary Fig. 6a,b; $n \geq 3$ mice, Student's *t*-test: $p_{(Ki\text{-}67)} = 0.0445$, $p_{(DCX)} = 0.0121$). These data, together with the selective expression of plexinC1 in the SGZ (Fig. 1), our *in vitro* observations (Fig. 2) and previous work revealing an inhibitory effect of plexinC1 on cell proliferation [18], suggest that plexinC1 negatively regulates aNPC proliferation *in vivo*. In addition, quantification revealed that the relative number of differentiated (NeuN$^+$) BrdU$^+$ cells was similar in *plexinC1*$^{+/+}$ and *plexinC1*$^{-/-}$ mice (Fig. 3c; $n = 3$ mice, Student's *t*-test: $p = 0.8728$). This suggests that plexinC1 is not required for the differentiation of aNPCs into nGCs.

Because Sema7A strongly reduced neurosphere formation via plexinC1 and *plexinC1*$^{-/-}$ mice showed enhanced proliferation, we next examined aNPC proliferation in adult *Sema7A*$^{-/-}$ mice. Analogous to our observations in *plexinC1*$^{-/-}$ mice, no changes in the number of BrdU$^+$ cells were found at 2 h after injection in *Sema7A*$^{-/-}$ mice (Fig. 3d,e; $n \geq 3$ mice, *post-hoc t*-test: $p = 0.5141$), while significantly more BrdU$^+$ cells were detected at 3 and 28 days post-injection (dpi, Fig. 3d,e; $n = 3$ mice, two-way ANOVA: genotype x time $F_{(2,22)} = 0.0129$, *post-hoc t*-test: $p_{(3\ days)} = 0.0313$, $p_{(28\ days)} = 0.0313$). Quantification of Ki-67$^+$ and DCX$^+$ cells confirmed these results, showing an increase in proliferating cells and immature nGCs in the adult DG of *Sema7A*$^{-/-}$ mice (Supplementary Fig. 6c,d; $n = 4$ mice, Student's *t*-test: $p_{(Ki\text{-}67)} = 0.0279$, $p_{(DCX)} = 0.0294$). In contrast, no change in the number of BrdU$^+$ cells expressing NeuN was observed (Fig. 3f; $n = 3$ mice, Student's *t*-test: $p = 0.7114$). Together, these results indicate that Sema7A inhibits aNPC proliferation in the adult DG.

Next we addressed the consequence of the increased aNPC proliferation observed in *plexinC1*$^{-/-}$ and *Sema7A*$^{-/-}$ mice. Increased proliferation could lead to an increase in GC density in the DG, faster depletion of the aNPC pool and/or a larger pool of immature cells during aging [28]. To assess the specific effect of loss of Sema7A-plexinC1 signalling, we focused on *plexinC1*$^{-/-}$ mice. First, we observed that GC density in the DG was unchanged but found an increase in the number of cleaved caspase-3$^+$ cells in the mature DG of *plexinC1*$^{-/-}$ mice (Supplementary Fig. 6e–g; $n_{(cell\ density)} = 3$ and $n_{(Caspase3)} = 6$ mice, Student's *t*-test: $p_{(cell\ density)} = 0.141$, $p_{(Caspase3)} = 0.039$). Second, we analysed aNPC proliferation at older ages to examine aNPC pool depletion. BrdU injection and quantification at 3 dpi in ageing *plexinC1*$^{-/-}$ mice (2, 6 and 18 months of age) revealed a comparable decrease in the number

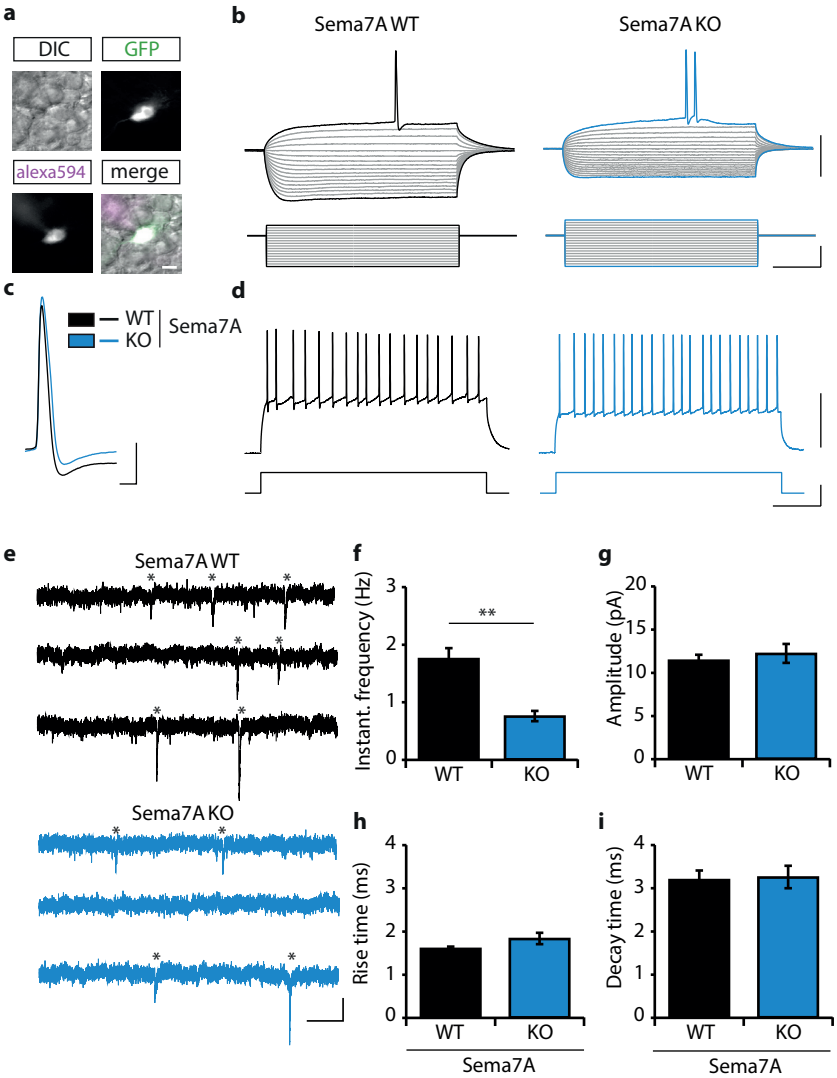

Figure 5 | Sema7A is required for the functional integration of adult-born DG granule cells. (a) Representative images of an MMLV CAG-GFP infected adult-born granule cell (nGC) used for recording of electrophysiological properties and miniature excitatory post-synaptic currents (mEPSCs). Healthy cells were identified using differential interference contrast (DIC). Recording of nGCs (GFP-positive cells) was confirmed by the presence of recording pipet-dye Alexa Fluor 594 in the same cell. (b) Representative traces of membrane potential (upper traces) in response to current injections (lower traces) in *Sema7A*$^{+/+}$ (WT, black) or *Sema7A*$^{-/-}$ (KO, blue) nGCs. Note the reduced hyperpolarization of the membrane potential during hyperpolarizing current injections in KO nGCs. (c) Representative traces of action potentials in WT and KO nGCs. (d) Representative traces for action potential firing rates (upper trace) in response to a 200 pA current injection (lower trace) in WT and KO nGCs. (e) Representative traces of mEPSC recordings in WT and KO nGCs. Asterisks indicate identified mEPSC events. (f–i) Quantification of mEPSC instantaneous frequency (f), amplitude (g), rise- (h) and decay- (i) time ($n_{(WT)}$ = 9 cells / 3 mice, $n_{(KO)}$ = 8 cells / 3 mice, Student's *t*-test). Data are presented as means ± s.e.m. ** $p < 0.01$. Scale bars: (a)10µm, (b,d) horizontal: 220ms, vertical: 50mV (upper traces) or 200 pA (bottom traces), (c) horizontal: 2 ms, vertical: 20mV, (e) horizontal: 200ms, vertical: 10 pA.

of BrdU$^+$ cells during ageing. However, at every age examined a larger number of BrdU$^+$ cells were detected in *plexinC1*$^{-/-}$ mice as compared to WT littermates (Supplementary Fig. 6h; $n = 3$ mice, two-way ANOVA: genotype time $F_{(2,19)} = 0.0283$, *post-hoc t*-test: $p_{(2\ months)} = 0.0469$, $p_{(6\ months)} = 0.0469$, $p_{(18\ months)} = 0.0469$). Third, the number of GFAP$^+$ RGL cells and DCX$^+$ cells, that is, late progenitor cells and immature GCs, was also elevated at 18 months of age in *plexinC1*$^{-/-}$ mice (Supplementary Fig. 6i,j; $n = 3$ mice, Student's *t*-test: $p_{(GFAP)} = 0.036$ $p_{(DCX)} = 0.023$). Thus, loss of plexinC1 leads to an increased number of progenitor cells and immature GCs at older age and triggers caspase-3-dependent apoptosis without altering overall cell density in the adult DG.

Several of the reported Sema7A effects on neurons are mediated by ß1-subunit-containing integrin receptors. ß1-integrins are expressed in the SGZ of the DG and have been implicated in stem cell proliferation and survival (Supplementary Fig. 7a–c)[24,29–31]. To determine whether ß1-integrins cooperate with plexinC1 to mediate the effects of Sema7A on aNPCs, BrdU-pulse labelling was performed in *ß1-integrin* knockout mice. Null mutant *ß1-integrin* mice do not survive into adulthood, so we generated neural-specific *ß1-integrin* knockout mice by crossing *nestin-Cre* with *ß1-integrin*$^{fl/fl}$ mice. As reported previously, adult *ß1-integrin*$^{fl/fl}$*;nestin-Cre* mice displayed cortical layering defects, subtle changes in the organization of the DG infrapyramidal blade and abnormal positioning and orientation of a small subset of DCX$^+$ cells (Supplementary Fig. 7d–f)[32,33]. However, we did not detect significant changes in the number of BrdU$^+$ cells in *ß1-integrin*$^{fl/fl}$*;nestin-Cre* mice at 2 h and 3 days after BrdU injection (Supplementary Fig. 7g,h; $n = 3$, Student's *t*-test: $p_{(2\ h)} = 0.8302$ $p_{(3\ days)} = 0.4199$). Similarly, the number of Ki-67$^+$ cells in the SGZ of *ß1-integrin*$^{fl/fl}$*;nestin-Cre* mice was normal (Supplementary Fig. 7i; $n = 8$ mice, Student's *t*-test: $p = 0.1064$). These results contrast with our observations in *plexinC1*$^{-/-}$ and *Sema7A*$^{-/-}$ mice, which displayed changes in BrdU$^+$ and Ki-67$^+$ cell number at 3 dpi. While proliferation appeared intact in *ß1-integrin*$^{fl/fl}$*;nestin-Cre* mice, neural-specific ablation of ß1-integrin caused a pronounced increase in DCX$^+$ cell number in the DG (Supplementary Fig. 7j; $n = 3$ mice, Student's *t*-test: $p = 0.0270$). Thus, although ß1-integrins do indeed affect specific aspects of adult neurogenesis, the early role of Sema7A during aNPC proliferation that we observe appears to be independent of ß1-integrins.

Dendritic development of nGCs requires Sema7A

Expression of Sema7A in the adult DG is not restricted to the SGZ but is also found in more superficial layers of the DG that contain immature nGCs and their dendrites. This observation, together with the fact that Sema7A can regulate dendritic growth of embryonic neurons[10], prompted us to examine whether Sema7A controls dendrite development in nGCs. Retroviral labelling of proliferating cells (aNPCs) with Moloney murine leukaemia virus (MMLV)-based retroviral vectors allows for tracing and analysis of the dendritic morphology of nGCs (refs 34–36). Adult *Sema7A*$^{-/-}$ mice and littermate controls were injected with MMLV CAG-GFP in the DG to selectively visualize nGCs (Fig. 4a). Quantification of the position of GFP$^+$ nGC cell bodies relative to the SGZ, a measure of nGC migration, at 14 dpi did not reveal significant differences between wild-type and mutant littermates (Supplementary Fig. 8a–c; littermate-paired Student's *t*-test $n = 4$ mice, $p_{(distance)} = 0.1645$, $p_{(relative\ distance)} = 0.2246$). However, analysis of dendritic morphology revealed a reduction in total dendritic length and the number of dendritic branch points in GFP$^+$ nGCs in *Sema7A*$^{-/-}$ mice (Fig. 4a,b; $n = 3$ mice, *post-hoc t*-test: $p_{(dendritic\ length)} = 0.045$ and $p_{(branch\ points)} = 0.0499$). Sholl-analysis confirmed this reduction in dendritic length and branch points (Fig. 4c, Supplementary Fig. 8f; $n = 3$ mice, repeated-measures ANOVA: Sholl length; $F_{(7,}$

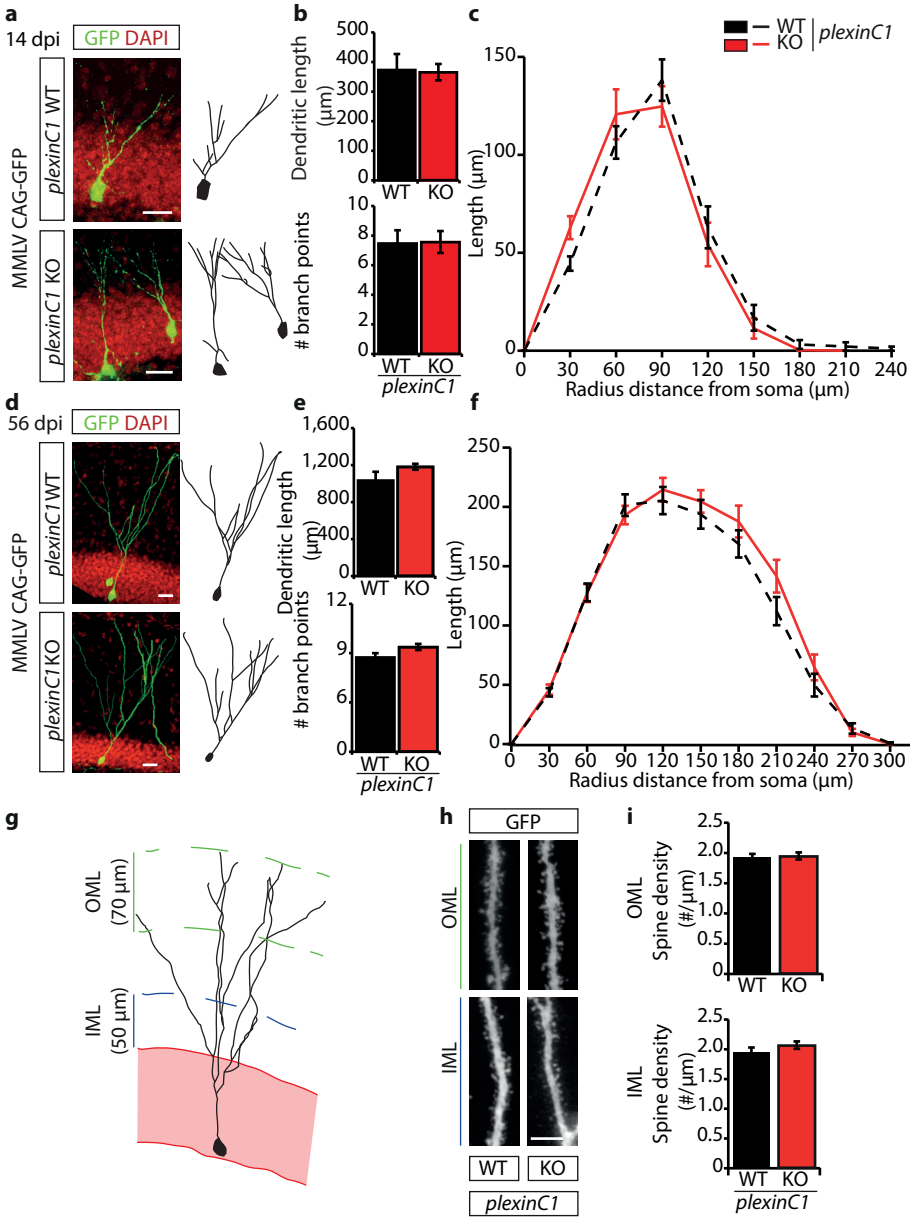

Figure 6 | Dendritic growth and spine development are intact in adult-born DG granule cells in *plexinC1*$^{-/-}$ mice. (a,d) The dentate gyrus (DG) of adult *plexinC1*$^{+/+}$ (WT) or *plexinC1*$^{-/-}$ (KO) mice was injected with MMLV CAG-GFP to label adult-born granule cells and immunostained for GFP at 14 or 56 days post-injection (dpi). DAPI is shown in red. Right panels depict representative tracings based on confocal z-stack images. (b,e) Quantification of dendritic length and number of branch points in WT (black bars) and KO (red bars) littermates (two-way ANOVA, *post-hoc t*-test, 14 dpi: $n = 4$, $p_{(length)} = 0.898$ and $p_{(branch\ points)} = 0.944$, 56 dpi: $n = 5$, $p_{(length)} = 0.344$ and $p_{(branch\ points)} = 0.159$). (c,f) Sholl-analysis of the dendritic tree of GFP-labelled cells in WT (black dashed-lines) and KO mice (red lines). Dendritic length per radius distance from soma (30µm radius interval) was unchanged in KO mice (14 dpi: $n = 45$ WT cells/4 mice, $n = 47$ KO cells/4 mice, 56dpi: $n =$

40 WT cells/5 mice, $n = 38$ KO cells/5 mice. Repeated-measures ANOVA 14 dpi: $F_{(7, 630)} = 1.833$, $p = 0.139$, 56 dpi: $F_{(9, 684)} = 1.075$, $p = 0.364$). (g) Schematic representation of the DG indicating the regions selected for spine density quantification. IML, inner molecular layer; OML, outer molecular layer. (h) Representative images showing spine-bearing dendritic segments in the OML and the IML in WT and KO mice. (i) Quantification of spine density on adult-born granule cells at 56dpi did not reveal differences between WT ($n = 5$) and KO ($n = 5$) mice (Student's *t*-test, $p_{(OML)} = 0.8858$ and $p_{(IML)} = 0.2825$). Whiskers represent s.e.m. Scale bars: (a,d)25 µm; (h)10 µm.

$_{1,645)} = 2.800$, $p = 0.045$, Sholl intersections; $F_{(7, 1,645)} = 3.219$, $p = 0.025$). This effect of Sema7A ablation was no longer observed at 56 dpi (Fig. 4d–f, Supplementary Fig. 8g; $n = 4$ mice, two-way ANOVA, dendritic length: dpi $F_{(1, 10)} = 205.078$, $p < 0.001$, *post-hoc t*-test: $p_{(dendritic\ length)} = 0.150$, brachpoints: dpi $F_{(1, 10)} = 12.448$, $p = 0.0006$; *post-hoc t*-test: $p_{(branch\ points)} = 0.868$, repeated- measures ANOVA: Sholl length; $F_{(9, 1,224)} = 2.560$, $p = 0.056$, Sholl intersections; $F_{(9, 1,224)} = 2.202$, $p = 0.082$). These data indicate that Sema7A is required for the initial phase of dendritic outgrowth and ramification of nGCs in the adult DG.

Sema7A controls dendritic spine number in nGCs

Although the role of Sema7A in the adult brain remains poorly characterized, recent work implicates this semaphorin in the regulation of dendritic spines in the postnatal cerebellum[6]. We therefore explored the effect of Sema7A ablation on dendritic spine density in nGCs in the adult DG. Dendritic spines begin to emerge from 16 days after MMLV-GFP injection and their density rapidly increases until 56 dpi. Spine density stabilizes at 56 dpi, although specific subtypes of spines continue to develop until 126 dpi (ref. 36). nGCs receive functional inputs from the entorhinal cortex, septum and hippocampal subfields[37]. Therefore, we determined nGC spine density in the inner- molecular layer (IML) and the outer-molecular layer (OML) where afferent inputs contact nGCs (refs 38,39) (Fig. 4g,h). In line with previous work, wild-type nGCs exhibited an average spine density of ±1.6 spines μm^{-1} at 56 dpi of MMLV CAG-GFP (Fig. 4i) (ref. 39). Loss of Sema7A resulted in a mild but consistent decrease in spine density on GFP-labelled nGCs in the IML. Although spine density appeared to be also reduced in the OML of *Sema7A* mutants, this effect was not statistically significant (Fig. 4i; $n = 5$ mice, *post-hoc t*-test: $p_{(OML)} = 0.0812$ and $p_{(IML)} = 0.0320$). Quantification of mushroom-like spine density, a hallmark of matured spines[40,41], in both the IML and OML revealed reduced mushroom-like spine density in the IML of *Sema7A*$^{-/-}$ nGCs ($n = 5$ mice, Student's *t*-test: *Sema7A*$^{+/+}{}_{(IML)} = 0.200 \pm 0.011$, *Sema7A*$^{-/-}{}_{(IML)} = 0.160 \pm 0.010$, $p = 0.033$, *Sema7A*$^{+/+}{}_{(OML)} = 0.200 \pm 0.021$, *Sema7A*$^{-/-}{}_{(OML)} = 0.170 \pm 0.017$, $p = 0.674$ (mean ± s.e.m.)). At 80 dpi, spine density was still reduced in the IML of *Sema7A* mutants and was also significantly decreased in the OML (Fig. 4j; $n = 3$ mice, two-way ANOVA IML: genotype $F_{(1, 12)} = 15.094$, $p = 0.0022$, OML: genotype $F_{(1,12)} = 10.57$, $p = 0.0069$, *post-hoc t*-test: $p_{(IML)} = 0.0458$ $p_{(OML)} = 0.0463$). Thus, Sema7A positively regulates dendritic spine density in nGCs.

Sema7A is required for functional integration of nGCs

The hampered dendritic development and spinogenesis of nGCs observed in *Sema7A*$^{-/-}$ mice may affect the functional integration of nGCs into the adult DG. To test this hypothesis, we performed an electrophysiological characterization of nGCs in the DG at 56 days after MMLV-GFP injection (Fig. 5a–d, Supplementary Table 1). Normal resting membrane potential, action potential membrane threshold and action potential properties were recorded in nGCs of *Sema7A*$^{-/-}$ mice (Supplementary Table 1). In *Sema7A*$^{-/-}$ mice, nGCs had lower input resistance and required higher current injections to reach the action potential threshold (Supplementary Table 1; $n = 3$mice, Student's *t*-test with Benjamini-Hochberg

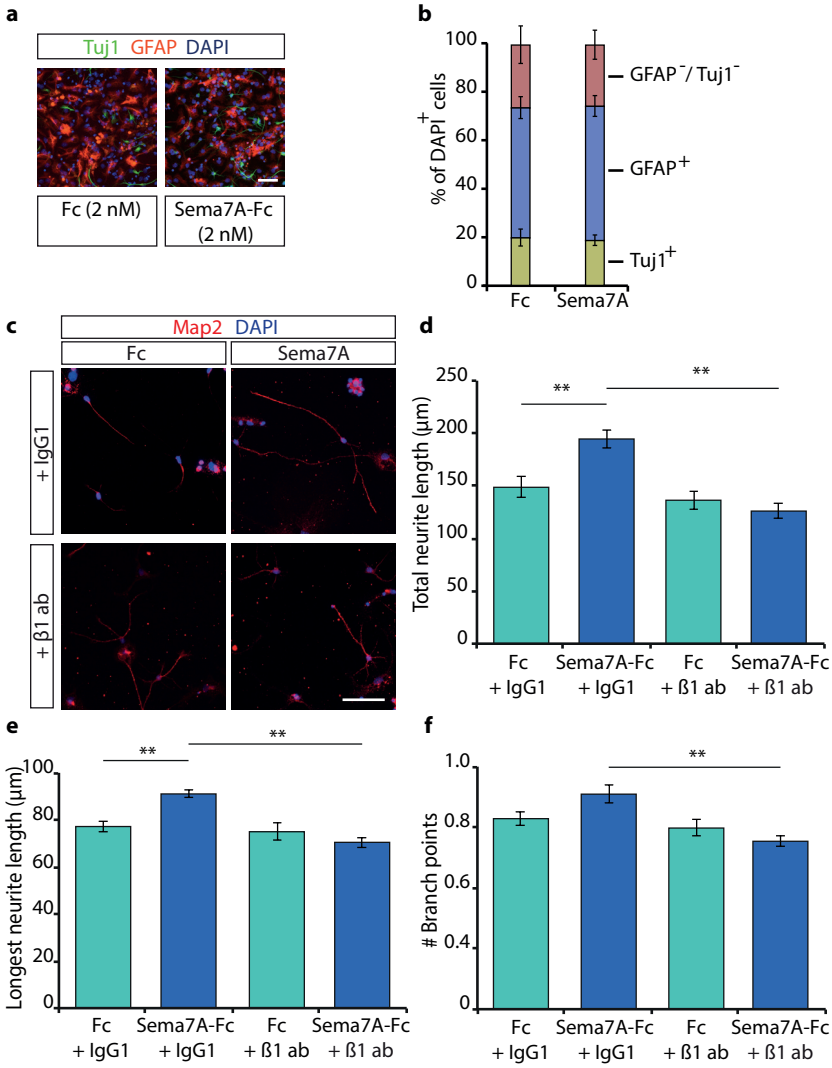

Figure 7 | Sema7A promotes neurite growth from differentiated adult SGZ neuronal progenitors *in vitro*. **(a)** Immunocytochemistry for Tuj1 and glial fibrillary acidic protein (GFAP) on cultures of differentiated SGZ neuronal progenitors at 3 days post-differentiation in the presence of 2 nM Fc control or Sema7A-Fc protein. (b) Quantification of the number of GFAP-negative/Tuj1-negative, GFAP-positive (astrocytes) or Tuj1-positive (neurons) cells in cultures of differentiated SGZ neuronal progenitors. Addition of Sema7A-Fc does not alter the relative number of neurons and astrocytes in the cultures. (c) Immunocytochemistry for microtubule-associated protein 2 (Map2) to label dendrites on cultures of differentiated SGZ neuronal progenitors at 10 days post-differentiation in the presence of 2nM exogenous Fc control or Sema7A-Fc protein in the presence of a ß1-integrin blocking antibody or control IgG1 antibody. (d–f) Quantification of total Map2$^+$ neurite length (d), longest Map2$^+$ neurite length (e) or the number of Map2$^+$ branch points (f) in cultures as in c (two-way ANOVA, *post-hoc* Replicate-paired *t*-test). Data represent means ± s.e.m. from at least three independent experiments. * $p < 0.05$ and ** $p < 0.01$. Scale bars: 50µm.

correction for multiple testing: $p_{\text{(input resistance)}} = 0.007$, $p_{\text{(hyperpolarization during -300 pA injection)}} = 0.001$, $p_{\text{(action potential current threshold)}} = 0.017$). To test whether decreased dendritic development and spinogenesis resulted in reduced functional inputs onto nGCs in *Sema7A*$^{-/-}$ mice, we next recorded miniature excitatory post-synaptic currents (mEPSCs) (Fig. 5e–i). Quantification of mEPSCs showed normal amplitudes, rise- and decay times (Fig. 5g–i; $n = 3$ mice, Student's *t*-test: $p_{\text{(amplitude)}} = 0.553$, $p_{\text{(rise time)}} = 0.112$, $p_{\text{(decay time)}} = 0.855$). However, the instantaneous frequency of the recorded mEPSCs was reduced in *Sema7A*$^{-/-}$ mice nGCs (Fig. 5f; Student's *t*-test: $p < 0.001$). To test whether Sema7A is also required for the function of adult GCs, we determined electrophysiological properties of putative mature GCs (GFP-negative GCs in the outer layer of the DG GCL). Normal electrophysiological properties and excitatory synaptic inputs were observed in adult GCs of *Sema7A*$^{-/-}$ mice (Supplementary Fig. 9, Supplementary Table 2). Overall these observations suggest that Sema7A, as expected on basis of delayed dendritic development and reduced (mature) spine density, is required for the proper functional integration of nGCs and their excitatory inputs.

Stage-specific receptor interactions control neurogenesis

Our data indicate that Sema7A controls cell proliferation in the SGZ of the DG through the plexinC1 receptor. However, given the restricted expression of plexinC1 in early progenitors in the adult DG (Fig. 1, Supplementary Fig. 2), it seemed unlikely that this receptor could also mediate regulation of dendritic outgrowth and spine development by Sema7A in nGCs. Indeed, injection of adult *plexinC1*$^{-/-}$ mice with MMLV CAG-GFP followed by tracing of the dendritic tree of nGCs at 14 dpi and 56 dpi did not reveal defects in cell migration or dendritic outgrowth and ramification (Fig. 6a–f, Supplementary Fig. 8d,e,h,i). Furthermore, spine densities of nGC dendrites within the IML and OML of adult *plexinC1*$^{-/-}$ mice were reminiscent of those found in wild-type littermates (Fig. 6g–i).

To determine whether ß1-integrin receptors are involved in Sema7A-mediated dendritic outgrowth in nGCs, we first differentiated aNPCs *in vitro* and measured neurite growth and branching. Importantly, differentiation of cultured aNPCs in the presence of Sema7A-Fc (2nM) for 3 days did not alter the percentage of GFAP$^+$ or Tuj1$^+$ cells compared to control treatment (Fig. 7a,b; $n = 3$ independent experiments, Chi-squared test: $p = 0.3008$, $X^2 = 2.4024$). This observation is in line with our finding that the number of NeuN$^+$/BrdU$^+$ cells is unchanged in *Sema7A*$^{-/-}$ mice *in vivo* (Fig. 3). To confirm that Sema7A stimulates neurite outgrowth of differentiated aNPCs, we quantified the length of Map2$^+$ neurites at DIV10 (Fig. 7c–e). In line with a reduction in dendrite growth in *Sema7A*$^{-/-}$ mice *in vivo* (Fig. 4), exposure to Sema7A (2nM) significantly enhanced total neurite length and longest neurite length *in vitro* (Fig. 7c–e; $n = 3$ independent experiments, *post-hoc t*-test: $p_{\text{(total)}} = 0.008$ and $p_{\text{(longest)}} = 0.007$). Functional blockage of ß1-integrins by incubation with a well-characterized ß1-integrin blocking antibody[5] prevented Sema7A's positive effect on neurite outgrowth (Fig. 7c–e, $n = 3$ independent experiments, two-way ANOVA total: protein x antibody treatment $F_{(1, 8)} = 13.353$, $p = 0.006$, longest: protein x antibody treatment $F_{(1, 8)} = 10.515$, $p = 0.012$, *post-hoc t*-test: $p_{\text{(total)}} = 0.002$ and $p_{\text{(longest)}} = 0.001$). Analysis of neurite ramification was hindered by the relatively small number of branch points per neurite on differentiated nGCs even at DIV 10 (Fig. 7f). While no statistical significant effect of Sema7A-Fc on number of branch points was observed, ß1-integrin blocking antibody treatment reduced the number of branch points on neurites compared to Sema7A-Fc treated cells (Fig. 7f; $n = 3$ independent experiments, two-way ANOVA branch points: protein x antibody treatment $F_{(1, 8)} = 6.077$, $p = 0.039$, *post-hoc t*-test: $p = 0.001$). In all, these data show that Sema7A is not required for neuronal differentiation but that it stimulates dendrite outgrowth of differentiated nGCs

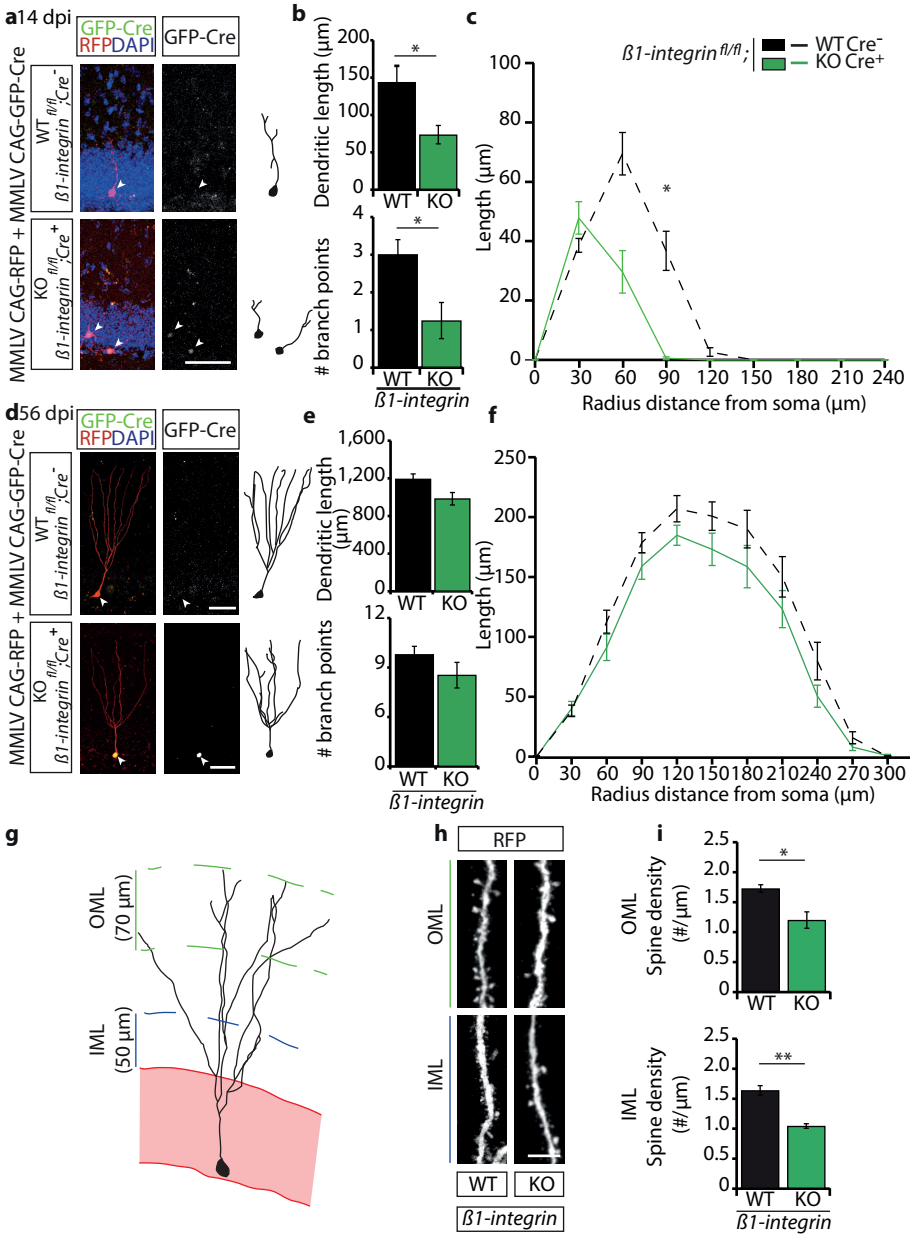

Figure 8 | ß1-integrins are required for dendritic growth and spine development in adult-born DG granule cells. (a,d) The dentate gyrus of *ß1-integrin*$^{fl/fl}$ mice was injected with MMLV CAG-RFP and MMLV CAG-GFP-Cre and immunostained for RFP and GFP at 14 or 56 days post-injection (dpi). Despite underestimation of the dendritic length and complexity due to low expression of RFP at 14 dpi, cell-autonomous ablation of ß1-integrin in GFP-positive, RFP-positive cells induces a clear reduction in dendritic morphology at 14dpi. DAPI is shown in blue. WT, GFP-negative, RFP-positive cell; KO, GFP-positive, RFP-positive cell. Right panels depict representative tracings based on confocal z-stack images. (b,e) Quantification of dendritic length and number of branch points in WT (black bars, $n = 4$) and KO (green bars, $n = 4$) littermates (two-way ANOVA, *post-hoc t*-test, 56dpi: $p = 0.176$ and $p = 0.336$). (c,f) Sholl-analysis of the dendritic tree of WT (black dashed-

lines) and KO cells (green lines). Dendritic length per radius distance from soma (30 µm radius interval) was decreased in KO adult-born granule cells (nGCs) (14 dpi: $n = 20$ WT cells/4 mice, $n = 9$ KO cells/4 mice, 56 dpi: $n = 27$ WT cells/4 mice, $n = 20$ KO cells/4 mice. Repeated-measures ANOVA 14 dpi: $F_{(7, 175)} = 2.625$, 56dpi: $F_{(9, 405)} = 0.724$, $p = 0.533$). (g) Schematic representation of the DG indicating the regions selected for spine density quantification. IML, inner molecular layer; OML, outer molecular layer. (h) Representative images showing spine-bearing dendritic segments in the OML and the IML in WT and KO nGCs. (i) Quantification of spine density on nGCs at 56 dpi reveals differences between WT ($n = 4$) and KO ($n = 4$) granule cells (two-way ANOVA, *post-hoc t*-test). Data are represented as means ± s.e.m. * $p < 0.05$ and ** $p < 0.01$. Scale bars: (a,d) 25µm; (h)10µm.

via ß1-integrins. To confirm this model a mix of retroviral MMLV CAG-GFP/Cre and MMLV CAG-RFP viruses was injected in adult *ß1-integrin*$^{fl/fl}$ mice. The RFP signal in nGCs allows for tracing and analysis of dendritic morphology and spine density, whereas co-expression of the Cre-vector, reported by nuclear GFP immunostaining, induces cell-autonomous ablation of *ß1-integrin* in individual nGCs (ref. 35). Similar to *Sema7A*$^{-/-}$ mice (Fig. 4), cell-autonomous loss of *ß1-integrin* in nGCs induced a reduction in dendritic outgrowth and complexity at 14 dpi (Fig. 8a–c; $n = 4$ mice, two-way ANOVA length: genotype $F_{(1,12)} = 9.738$, $p = 0.0088$, branch points: genotype $F_{(1,12)} = 6.205$, $p = 0.0284$ *post-hoc t*-test: $p_{(\text{dendritic length})} = 0.0307$ and $p_{(\text{branch points})} = 0.0292$, Supplementary Fig. 10a; $n = 4$ mice, repeated-measures ANOVA: Sholl length; $F_{(7, 175)} = 2.625$, $p = 0.013$, Sholl intersections; $F_{(7, 175)} = 5.273$, $p < 0.001$). Unilateral injection of MMLV CAG-GFP-IRES-Cre or MMLV CAG-GFP in a separate *ß1-integrin*$^{fl/fl}$ cohort confirmed that the observed defects were not caused by a potential increased cellular burden due to infection with two viral constructs (Supplementary Fig. 10c,d; $n = 4$ mice, Student's *t*-test: $p_{(\text{length})} = 0.0445$ and $p_{(\text{branch points})} = 0.0254$). Intriguingly, the temporally restricted requirement for Sema7A during early stages (14 dpi, Fig. 4a–c) of dendritic outgrowth but not at later stages (56 dpi, Fig. 4d–f) was also observed in virus-injected *ß1-integrin*$^{fl/fl}$ mice. No significant change in total dendritic length, number of branch points or dendritic complexity, was observed at 56 dpi in *ß1-integrin*$^{-/-}$ nGCs (Fig. 8d–f, Supplementary Fig. 10b). Thus, ß1-integrins are required at early stages of dendritic outgrowth in nGCs.

Loss of Sema7A, but not plexinC1, caused reduced spine density in nGCs (Fig. 4). To determine whether or not ß1-integrin knockout induces similar defects, spine densities were analysed within the IML and OML of *ß1-integrin*$^{-/-}$ nGCs at 56 dpi (Fig. 8g,h). Cell-autonomous ablation of ß1-integrin in nGCs resulted in a marked reduction of spine density both in the IML and OML (Fig. 8h,i; $n = 4$ mice, two-way ANOVA genotype $F_{(1,12)} = 37.235$, $p < 0.0001$ *post-hoc t*-tests: $p_{(\text{OML})} = 0.012$ and $p_{(\text{IML})} = 0.002$). A significant reduction in mushroom-like spine density was observed in the OML but not in the IML (n = 5 mice, Student's *t*-test: $ß1\text{-}integrin^{+/+}{}_{(\text{IML})} = 0.248 \pm 0.029$, $ß1\text{-}integrin^{-/-}{}_{(\text{IML})} = 0.211 \pm 0.020$, $p = 0.341$, $ß1\text{-}integrin^{+/+}{}_{(\text{OML})} = 0.319 \pm 0.026$, $ß1\text{-}integrin^{-/-}{}_{(\text{OML})} = 0.205 \pm 0.017$, $p = 0.011$ (mean ± s.e.m.)). These data together with our *in vitro* experiments (Fig. 7) suggest that Sema7A-ß1-integrin signalling controls dendritic development and spine density of nGCs within the adult DG.

Discussion

Sema7A contributes to the formation of neuronal connections during development. Although neural expression of Sema7A increases as development progresses, the precise role of this semaphorin in the adult brain remains poorly understood. Here, we report several stage-specific roles for Sema7A during adult hippocampal neurogenesis. At early stages, Sema7A and its receptor plexinC1 cooperate to suppress early progenitor

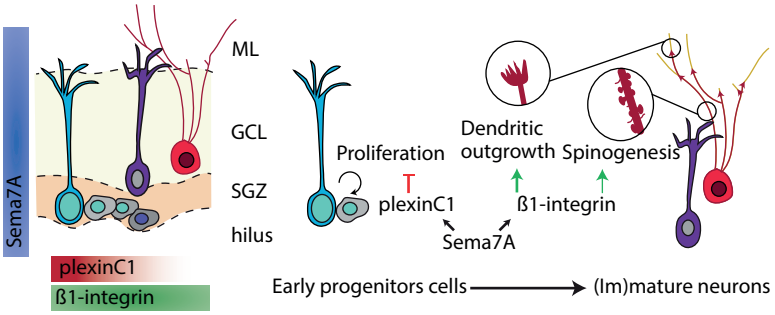

Figure 9 | Sema7A regulates cell proliferation and dendritic morphology during adult hippocampal neurogenesis via distinct receptors. In the adult dentate gyrus (DG), expression of plexinC1 is largely confined to early progenitor cells in the subgranular zone (SGZ). In contrast, Sema7A and ß1-subunit-containing integrin receptors are expressed throughout the SGZ and granular cell layer (GCL). On basis of our *in vitro* and *in vivo* results we propose a model in which Sema7A, through plexinC1, inhibits proliferation of early progenitor cells in the SGZ during early stages of adult hippocampal neurogenesis, while at later stages Sema7A utilizes ß1-subunit-containing integrin receptors to promote dendritic growth, complexity and spine development in differentiated adult-born GCs. While our data suggest that ß1-subunit-containing integrin receptors are required cell autonomously in adult-born GCs, further work is needed to determine the cellular origin of the Sema7A that activates these receptors. Sema7A could be expressed in nGCs and activate ß1-subunit-containing integrin receptors in cis. Alternatively, Sema7A may be expressed in neighbouring nGCs and act in *trans* either via cell-cell interactions or following cleavage of its GPI domain, resulting in a soluble Sema7A ectodomain. Similarly, the cellular origin of Sema7A molecules that activate plexinC1 receptors remains to be determined. Sema7A is broadly expressed in the GC layer, including strongly in immature and mature granule cells. These cells could represent a cellular source of Sema7A for aNPCs in the adjacent SGZ.

cell proliferation in the adult SGZ. At later stages, Sema7A regulates dendrite growth, complexity and spine development of adult-born GCs. These morphological effects require ß1-subunit-containing integrin receptors but not plexinC1. In addition, loss of Sema7A results in reduced excitatory inputs to nGCs but not to adult GCs. These data support a functional role for Sema7A signalling during adult neurogenesis. Our data establish a novel role for Sema7A and plexinC1 in the adult brain and, more generally, implicate semaphorins and plexins in the control of cell proliferation during adult hippocampal neurogenesis. Moreover, they provide further insight into the function and mechanisms of ß1-integrins during adult neurogenesis. Recent work shows that regulation of neuroglial plasticity at the adult median eminence by Sema7A also requires plexinC1 and ß1-integrins[11]. Our data are, however, conceptually distinct from these previous observations: here we find that stage-specific neuronal expression of Sema7A receptors is required for adult neurogenesis, rather than a requirement for receptor expression in axons (plexinC1) and ensheating glia (ß1-integrins). Further, while it is known that semaphorins can regulate multiple, distinct steps of neuronal development[1], our data present one of the first examples in which stage-specific expression of structurally unrelated semaphorin receptor proteins (that is, plexins and integrins) in the same neuron is required to mediate these steps.

Integration of nGCs in mature hippocampal circuitry constitutes an important form of structural plasticity that contributes to hippocampal function and, if perturbed, to disease[20,42–44]. Most aNPCs in the adult DG are maintained in a quiescent state to secure tissue homeostasis and avoid stem cell exhaustion, with proliferation induction occurring. The neurogenic niche is composed of various cell types and molecular signals that tightly control aNPC quiescence and proliferation[21,22]. Our data identify Sema7A and plexinC1

as new players in the regulation of aNPC proliferation in the adult DG and suggest that Sema7A acts through plexinC1 to inhibit aNPC proliferation in the SGZ (Fig. 9). Strong *plexinC1* expression has recently been detected in quiescent, as compared to active aNPCs in the SVZ (ref. 23). Our data suggest that plexinC1 protein is present in both quiescent and active aNPCs. This indicates that plexinC1 may act to retain aNPCs in a quiescent state but may also serve other functions, for example to negatively control transiently amplifying cells, or IPCs. In contrast to plexinC1, which is largely confined to early progenitor cells, Sema7A is expressed in both aNPCs and their immediate environment. The observation that application of exogenous Sema7A inhibits neurosphere formation *in vitro* while genetic ablation of Sema7A has no effect hints at a non-cell autonomous role for Sema7A in aNPC proliferation. Sema7A is broadly expressed in the GC layer, including strongly in immature and mature GCs. These cells could represent a cellular source of Sema7A for aNPCs in the adjacent SGZ. Additional studies will examine these possible non-cell autonomous effects and dissect the precise plexinC1 mechanism-of-action in the SGZ.

Regulation of cell proliferation by plexinC1 is likely not restricted to the SGZ. PlexinC1 is prominently expressed in different neurogenic niches in the embryonic and adult mouse brain[3,23] (Supplementary Fig. 1a–f). Further, plexinC1 is a tumour suppressor for melanoma. Loss of plexinC1 increases melanocyte proliferation thereby promoting melanoma progression[18]. Interestingly, another plexin family member, plexinB2, is expressed in adult progenitor cells in the SVZ. PlexinB2 promotes cell proliferation in the adult SVZ and neuroblast migration in the RMS and olfactory bulb[45]. These results coupled with our data detailing a role for plexinC1 in adult hippocampal neurogenesis reveal that plexins can have opposing effects on aNPC proliferation and highlight a more general role for these receptors in adult neurogenesis. Plexins other than plexinB2 and plexinC1 regulate cell proliferation in normal and diseased tissues[46–49], and it will be interesting to determine whether or not these receptors contribute to adult neurogenesis.

The best-characterized neuronal receptors for Sema7A are ß1-subunit-containing integrins. ß1-integrins transduce Sema7A-mediated effects on axonal and dendritic growth, neuron migration and synapse elimination[5,6,9–11]. ß1-integrins contribute to adult neurogenesis and their selective inactivation affects cell proliferation, neuroblast migration and neuronal differentiation in the adult DG or SVZ/RMS (refs 29,30,50). In the postnatal cerebellum, plexinC1 and ß1-integrins cooperate to mediate the synaptic effects of Sema7A (ref. 6). Therefore, we examined whether, in addition to plexinC1, ß1-integrins regulate aNPC proliferation. We found that cell proliferation in the SGZ is intact in adult *ß1-integrin$^{fl/fl}$;nestin-Cre* mice at 2 h and 3 days following BrdU labelling. Thus, while the two known Sema7A receptors plexinC1 and ß1-integrins are both expressed in aNPCs, our data suggest that plexinC1 is required for mediating the proliferation suppressive effects of Sema7A. First, plexinC1 and Sema7A mutant mice, but not *ß1-integrin$^{fl/fl}$;nestin-Cre* mice, display similar changes in the number of proliferating cells in the SGZ using different approaches. Second, a negative effect of Sema7A on neurosphere growth is seen in wild-type but not *plexinC1$^{-/-}$* neurospheres. Third, neurospheres exposed to Sema7A show increased phosphorylation of cofilin, but not of ß1-integrin receptors (Supplementary Figs 3d–g and 4). Normally activation of plexinC1 by Sema7A leads to phosphorylation of cofilin, while binding of Sema7A to ß1-integrins triggers their phosphorylation[11,12]. Thus, Sema7A activates cofilin but not ß1-integrins in neurosphere cultures. Together our observations indicate that the interaction of Sema7A with plexinC1, but not with ß1-subunit containing integrin receptors, triggers downstream signalling during Sema7A-induced suppression of aNPC proliferation. This is in line with previous work showing normal cell proliferation

in the SVZ of adult *ß1-integrin*$^{fl/fl}$*; nestin-Cre* mice[50]. It should be noted, however, that acute inactivation of ß1-integrins in the SVZ by *in vivo* injection of function blocking antibodies causes an increase in aNPC proliferation[30]. One explanation for these seemingly disparate results is that compensatory mechanisms mediated by other classes of integrins, for example, ß8-integrins[51], or other molecules in the neurogenic niche mask putative effects of genetic ß1-integrin ablation on aNPC proliferation. Thus, while our data implicate plexinC1 in Sema7A's inhibitory effects on aNPC proliferation, further work is needed to examine the role of ß1-integrins and to understand how Sema7A signals through plexinC1, but not ß1-integrins, in aNPCs despite the presence of both receptors in these cells.

A large body of previous work has identified key factors for the regulation of aNPC proliferation in the SGZ, but the extracellular molecular signals that control the morphological development of adult-born GCs are less well-understood (for example, refs 52–56). Our data help to fill this void by showing that Sema7A is indispensable for the early development of dendrites and dendritic spines in adult-born GCs and that this effect cell-autonomously requires ß1-integrins but not plexinC1. Interestingly, we find that genetic ablation of ß1-integrins leads to a larger decrease in dendritic length and spine number as compared to knockout of Sema7A. This suggests that different ß1-integrin ligands may cooperate to control dendritic morphology during adult hippocampus neurogenesis. Multiple different ß1-integrin ligands have been implicated in adult neurogenesis[57]. Recent work further indicates that, in contrast to Sema7A, Sema5A acts to inhibit spine density and synaptic integration of nGCs via plexinA2 (ref. 55). This suggests that semaphorins and their receptors can exert opposing effects on developing spines during the integration of nGCs into the adult DG.

All steps of adult hippocampal neurogenesis occur in the SGZ and DG in relative close proximity and many of the factors regulating multiple distinct steps, such as Sema7A, are expressed constantly. Intriguingly, our study, and work of others[56] reveals that these non-selectively expressed cues can exert stage-specific effects because of the stage-dependent expression and function of their receptors: plexinC1 expression is restricted to aNPCs and regulates the effects of Sema7A on proliferation, while ß1-integrins serve as a Sema7A receptor in differentiated adult-born GCs. Stage-specific receptor expression not only allows spatiotemporal control over the biological effects of Sema7A during adult neurogenesis, but it also diversifies the effects of this semaphorin, enabling it to exert control over proliferation and morphogenesis. In contrast to GCs generated at embryonic stages, adult-born GCs integrate into a fully developed neural circuit. However, many of the molecular cues that help to establish neural circuitry during development are no longer present in the adult brain. During embryonic development, the effects of semaphorins, and other cues, are diversified allowing them to control a disproportionally large number of cells and cellular events[58–65]. Whether similar diversification mechanisms operate in the adult CNS and, if so, whether these would contribute to the regulation of adult neurogenesis was not known. Our data suggest that diversification mechanisms for semaphorins operate in the adult brain and help to explain how a relatively limited set of molecular cues can spatiotemporally control the birth and integration of adult-born GCs. It will be interesting to determine whether similar mechanisms act to control other roles of semaphorins in the adult brain, such as in synaptic function[66].

In summary, the data presented here show novel stage-specific effects of Sema7A during adult hippocampal neurogenesis. Remarkably, these effects, including suppression of aNPC proliferation and promotion of dendritic development, require stage-specific expression of structurally unrelated Sema7A receptors (plexinC1 and ß1-integrins). This

tight regulation of receptor expression not only provides spatiotemporal control over Sema7A's effects during adult neurogenesis, but also diversifies the biological effects of this semaphorin.

Acknowledgements

We thank members of the Pasterkamp laboratory for assistance and helpful discussions throughout the course of this project, and Alex Kolodkin and Guo-liMing for comments on the manuscript. We thank Luca Tamagone for kindly providing *plexinC1*$^{-/-}$ mice, Onur Basak and Tamar Smit for assistance with setting up aNPC cultures, Haining Zhong for providing custom-written Matlab routines for mEPSC analysis, Wouter Beenker for assisting with immunohistochemistry, Emmeke Aarts for statistical advice, and Matthijs Verhage and Joke Wortel for help with mouse breeding. This work was supported by the Netherlands Organization for Health Research and Development (VIDI, ZonMW-TOP, ALW-VICI), Epilepsiefonds (NEF 17^{-1}0), Neuroscience and Cognition Utrecht (NCU), Stichting ParkinsonFonds to R.J.P., and in part by the National Institute on Aging, Intramural Research Program (to H.v.P.).

Author contributions

B.C.J. designed and performed immunostaining, non-radioactive ISH, colocalization, aNPC proliferation and differentiation, western blot and RT-PCR, BrdU-pulse/ stereology, morphometric analysis and spine count, and electrophysiology experiments. S.L. designed and performed immunostaining, western blot, colocalization, stereology, aNPC proliferation and differentiation experiments. R.S. and S.D.M. designed and performed BrdU-pulse/stereology experiments. M.H.B. performed stereotactic injections of MMLV. A.J.C.G.M.H. performed immunostaining and colocalization experiments. J.P. and P.G. designed and performed western blot experiments. H.v.P., T.M., G.M.J.R. provided reagents and contributed to the design and planning of experiments. B.C.J., S.L. and R.J.P. wrote the manuscript with input from all authors.

References

1. Pasterkamp, R. J. Getting neural circuits into shape with semaphorins *Nat Rev Neurosci* 13, 605–618 (2012).
2. Yoshida, Y. Semaphorin signaling in vertebrate neural circuit assembly. *Front Mol Neurosci* 5, 71 (2012).
3. Pasterkamp, R. J., Kolk, S. M., Hellemons, A. J. C. G. M. & Kolodkin, A. L. Expression patterns of semaphorin7A and plexinC1 during rat neural development suggest roles in axon guidance and neuronal migration. *BMC Dev Biol* 7, 98 (2007).
4. Xu, X. *et al.* Human semaphorin K1 is glycosylphosphatidylinositol-linked and defines a new subfamily of viral-related semaphorins. *J Biol Chem* 273, 22428–22434 (1998).
5. Pasterkamp, R. J., Peschon, J. J., Spriggs, M. K. & Kolodkin, A. L. Semaphorin 7A promotes axon outgrowth through integrins and MAPKs. *Nature* 424, 398–405 (2003).
6. Uesaka, N. *et al.* Retrograde semaphorin signaling regulates synapse elimination in the developing mouse brain. *Science* 344, 1020–1023 (2014).
7. Fukunishi, A. *et al.* The action of Semaphorin7A on thalamocortical axon branching. *J Neurochem* 118, 1008–1015 (2011).
8. Carcea, I. *et al.* Maturation of cortical circuits requires Semaphorin 7A. Proc. *Natl Acad Sci USA* 111, 13978–13983 (2014).
9. Messina, A. *et al.* Dysregulation of Semaphorin7A/b1-integrin signaling leads to defective GnRH-1 cell migration, abnormal gonadal development and altered fertility. *Hum Mol Genet* 20, 4759–4774 (2011).
10. Moresco, E. M. Y., Donaldson, S., Williamson, A. & Koleske, A. J. Integrin-mediated dendrite branch maintenance requires Abelson (Abl) family kinases. *J Neurosci* 25, 6105–6118 (2005).
11. Parkash, J. *et al.* Semaphorin7A regulates neuroglial plasticity in the adult hypothalamic median eminence. *Nat Commun* 6, 6385 (2015).
12. Jongbloets, B. C., Ramakers, G. M. J. & Pasterkamp, R. J. Semaphorin7A and its receptors: pleiotropic regulators of immune cell function, bone homeostasis, and neural development. *Semin Cell Dev Biol* 24, 129–138 (2013).
13. Suzuki, K. *et al.* Semaphorin 7A initiates T-cell-mediated inflammatory responses through alpha1beta1 integrin. *Nature* 446, 680–684 (2007).
14. Kang, S. *et al.* Intestinal epithelial cell-derived semaphorin 7A negatively regulates development of colitis via avb1 integrin. *J Immunol* 188, 1108–1116 (2012).
15. Tamagnone, L. *et al.* Plexins are a large family of receptors for transmembrane, secreted, and GPI-anchored semaphorins in vertebrates. *Cell* 99, 71–80 (1999).
16. Liu, H. *et al.* Structural basis of semaphorin-plexin recognition and viral mimicry from Sema7A and A39R complexes with PlexinC1. *Cell* 142, 749–761 (2010).
17. Scott, G. A., McClelland, L. A., Fricke, A. F. & Fender, A. Plexin C1, a receptor for semaphorin 7a, inactivates cofilin and is a potential tumor suppressor for melanoma progression. *J Invest Dermatol* 129, 954–963 (2009).
18. Chen, Y., Soong, J., Mohanty, S., Xu, L. & Scott, G. The neural guidance receptor Plexin C1 delays melanoma progression. *Oncogene* 32, 4941–4949 (2013).
19. König, K. *et al.* The plexin C1 receptor promotes acute inflammation. Eur *J Immunol* 44, 2648–2658 (2014).
20. Christian, K. M., Song, H. & Ming, G. Functions and dysfunctions of adult hippocampal neurogenesis. *Annu Rev Neurosci* 37, 243–262 (2014).
21. Kempermann, G., Song, H. & Gage, F. H. Neurogenesis in the adult hippocampus. *Cold Spring Harb Perspect Biol* 7, a018812 (2015).
22. Urbán, N. & Guillemot, F. Neurogenesis in the embryonic and adult brain: same regulators, different roles. *Front Cell Neurosci* 8, 396 (2014).
23. Codega, P. *et al.* Prospective identification and purification of quiescent adult neural stem cells from their in vivo niche. *Neuron* 82, 545–559 (2014).
24. Pinkstaff, J. K., Lynch, G. & Gall, C. M. Localization and seizure-regulation of integrin beta 1 mRNA in adult rat brain. *Brain Res Mol Brain* Res 55, 265–276 (1998).
25. Bonaguidi, M. A. *et al.* In vivo clonal analysis reveals self-renewing and multipotent adult neural

stem cell characteristics. Cell 145, 1142–1155 (2011).
26. Guo, W., Patzlaff, N. E., Jobe, E. M. & Zhao, X. Isolation of multipotent neural stem or progenitor cells from both the dentate gyrus and subventricular zone of a single adult mouse. *Nat Protoc* 7, 2005–2012 (2012).
27. van Praag, H., Kempermann, G. & Gage, F. H. Running increases cell proliferation and neurogenesis in the adult mouse dentate gyrus. *Nat Neurosci* 2, 266–270 (1999).
28. Lugert, S. *et al.* Quiescent and active hippocampal neural stem cells with distinct morphologies respond selectively to physiological and pathological stimuli and aging. *Cell Stem Cell* 6, 445–456 (2010).
29. Porcheri, C., Suter, U. & Jessberger, S. Dissecting integrin-dependent regulation of neural stem cell proliferation in the adult brain. *J Neurosci* 34, 5222–5232 (2014).
30. Kazanis, I. *et al.* Quiescence and activation of stem and precursor cell populations in the subependymal zone of the mammalian brain are associated with distinct cellular and extracellular matrix signals. *J Neurosci* 30, 9771–9781 (2010).
31. Leone, D. P. Regulation of neural progenitor proliferation and survival by 1 integrins. *J Cell Sci* 118, 2589–2599 (2005).
32. Förster, E. *et al.* Reelin, Disabled 1, and beta 1 integrins are required for the formation of the radial glial scaffold in the hippocampus. *Proc Natl Acad Sci USA* 99, 13178–13183 (2002).
33. Graus-Porta, D. *et al.* Beta1-class integrins regulate the development of laminae and folia in the cerebral and cerebellar cortex. *Neuron* 31, 367–379 (2001).
34. van Praag, H. *et al.* Functional neurogenesis in the adult hippocampus. *Nature* 415, 1030–1034 (2002).
35. Tashiro, A., Zhao, C. & Gage, F. H. Retrovirus-mediated single-cell gene knockout technique in adult newborn neurons in vivo. *Nat Protoc* 1, 3049–3055 (2006).
36. Zhao, C., Teng, E. M., Summers, R. G., Ming, G.-L. & Gage, F. H. Distinct morphological stages of dentate granule neuron maturation in the adult mouse hippocampus. *J Neurosci* 26, 3–11 (2006).
37. Vivar, C. *et al.* Monosynaptic inputs to new neurons in the dentate gyrus. *Nat Commun* 3, 1107 (2012).
38. Witter, M. P. The perforant path: projections from the entorhinal cortex to the dentate gyrus. *Prog Brain Res* 163, 43–61 (2007).
39. Amaral, D. G., Scharfman, H. E. & Lavenex, P. *The Dentate Gyrus: A Comprehensive Guide to Structure, Function, and Clinical Implications. Progress in brain research* Vol. 163 (Elsevier, 2007).
40. Harris, K. M., Jensen, F. E. & Tsao, B. Three-dimensional structure of dendritic spines and synapses in rat hippocampus (CA1) at postnatal day 15 and adult ages: implications for the maturation of synaptic physiology and long-term potentiation. *J Neurosci* 12, 2685–2705 (1992).
41. Gao, F. *et al.* Dendritic morphology, synaptic transmission, and activity of mature granule cells born following pilocarpine-induced status epilepticus in the rat. *Front Cell Neurosci* 9, 384 (2015).
42. Sahay, A. & Hen, R. Adult hippocampal neurogenesis in depression. *Nat Neurosci* 10, 1110–1115 (2007).
43. Aimone, J. B. *et al.* Regulation and function of adult neurogenesis: from genes to cognition. *Physiol Rev* 94, 991–1026 (2014).
44. Braun, S. M. G. & Jessberger, S. Adult neurogenesis: mechanisms and functional significance. *Development* 141, 1983–1986 (2014).
45. Saha, B., Ypsilanti, A. R., Boutin, C., Cremer, H. & Chédotal, A. Plexin-B2 regulates the proliferation and migration of neuroblasts in the postnatal and adult subventricular zone. *J Neurosci* 32, 16892–16905 (2012).
46. Granziero, L. *et al.* CD100/Plexin-B1 interactions sustain proliferation and survival of normal and leukemic CD5þ B lymphocytes. *Blood* 101, 1962–1969 (2003).
47. Rehman, M. & Tamagnone, L. Semaphorins in cancer: biological mechanisms and therapeutic approaches. Semin. *Cell Dev Biol* 24, 179–189 (2013).
48. Andrews, W. D., Davidson, K., Tamamaki, N., Ruhrberg, C. & Parnavelas, J. G. Altered proliferative ability of neuronal progenitors in PlexinA1 mutant mice. *J Comp Neurol* 524, 518–534 (2015).
49. Kigel, B., Rabinowicz, N., Varshavsky, A., Kessler, O. & Neufeld, G. Plexin-A4 promotes tumor progression and tumor angiogenesis by enhancement ofVEGF and bFGF signaling. *Blood* 118, 4285–4296 (2011).

50. Belvindrah, R., Hankel, S., Walker, J., Patton, B. L. & Müller, U. Beta1 integrins control the formation of cell chains in the adult rostral migratory stream. *J Neurosci* 27, 2704–2717 (2007).
51. Mobley, A. K., Tchaicha, J. H., Shin, J., Hossain, M. G. & McCarty, J. H. Beta8 integrin regulates neurogenesis and neurovascular homeostasis in the adult brain. *J Cell Sci* 122, 1842–1851 (2009).
52. Ge, S. *et al.* GABA regulates synaptic integration of newly generated neurons in the adult brain. *Nature* 439, 589–593 (2006).
53. Teixeira, C. M. *et al.* Cell-autonomous inactivation of the reelin pathway impairs adult neurogenesis in the hippocampus. *J Neurosci* 32, 12051–12065 (2012).
54. Ng, T. *et al.* Class 3 semaphorin mediates dendrite growth in adult newborn neurons through Cdk5/FAK pathway. *PLoS ONE* 8, e65572 (2013).
55. Duan, Y. *et al.* Semaphorin 5A inhibits synaptogenesis in early postnatal- and adult-born hippocampal dentate granule cells. *Elife* 3, e04390 (2014).
56. Schafer, S. T. *et al.* The Wnt adaptor protein ATP6AP2 regulates multiple stages of adult hippocampal neurogenesis. *J Neurosci* 35, 4983–4998 (2015).
57. Faissner, A. & Reinhard, J. The extracellular matrix compartment of neural stem and glial progenitor cells. *Glia* 63, 1330–1349 (2015).
58. Toyofuku, T. *et al.* Guidance of myocardial patterning in cardiac development by Sema6D reverse signalling. *Nat Cell Biol* 6, 1204–1211 (2004).
59. Toyofuku, T. *et al.* Dual roles of Sema6D in cardiac morphogenesis through region-specific association of its receptor, Plexin-A1, with off-track and vascular endothelial growth factor receptor type 2. *Genes Dev* 18, 435–447 (2004).
60. Chauvet, S. *et al.* Gating of Sema3E/PlexinD1 signaling by neuropilin1 switches axonal repulsion to attraction during brain development. *Neuron* 56, 807–822 (2007).
61. Komiyama, T., Sweeney, L. B., Schuldiner, O., Garcia, K. C. & Luo, L. Graded expression of semaphorin1a cell-autonomously directs dendritic targeting of olfactory projection neurons. *Cell* 128, 399–410 (2007).
62. Jeong, S., Juhaszova, K. & Kolodkin, A. L. The control of semaphorin-1a- mediated reverse signaling by opposing pebble and RhoGAPp190 functions in drosophila. *Neuron* 76, 721–734 (2012).
63. Hsieh, H.-H., Chang, W.-T., Yu, L. & Rao, Y. Control of axon-axon attraction by Semaphorin reverse signaling. *Proc Natl Acad Sci USA* 111, 11383–11388 (2014).
64. Sun, L. O. *et al.* Functional assembly of accessory optic system circuitry critical for compensatory eye movements. *Neuron* 86, 971–984 (2015).
65. Andermatt, I. *et al.* Semaphorin 6B acts as a receptor in post-crossing commissural axon guidance. *Development* 141, 3709–3720 (2014).
66. Koropouli, E. & Kolodkin, A. L. Semaphorins and the dynamic regulation of synapse assembly, refinement, and function. *Curr Opin Neurobiol* 27, 1–7 (2014).
67. Schmidt, E. R. E. *et al.* Subdomain-mediated axon-axon signaling and chemoattraction cooperate to regulate afferent innervation of the lateral habenula. *Neuron* 83, 372–387 (2014).
68. Schindelin, J. *et al.* Fiji: an open-source platform for biological-image analysis. *Nat Methods* 9, 676–682 (2012).
69. Nguyen, D. H. *et al.* Quantifying chromogen intensity in immunohistochemistry via reciprocal intensity. *Cancer InCytes* 2, 1 (2013).
70. Koppers, M. *et al.* C9orf72 ablation in mice does not cause motor neuron degeneration or motor deficits. *Ann Neurol* 78, 426–438 (2015).
71. Morote-Garcia, J. C., Napiwotzky, D., Köhler, D. & Rosenberger, P. Endothelial Semaphorin 7A promotes neutrophil migration during hypoxia. *Proc Natl Acad Sci USA* 109, 14146–14151 (2012).
72. Mao, T. *et al.* Long-range neuronal circuits underlying the interaction between sensory and motor cortex. *Neuron* 72, 111–123 (2011).

Supplementary Information

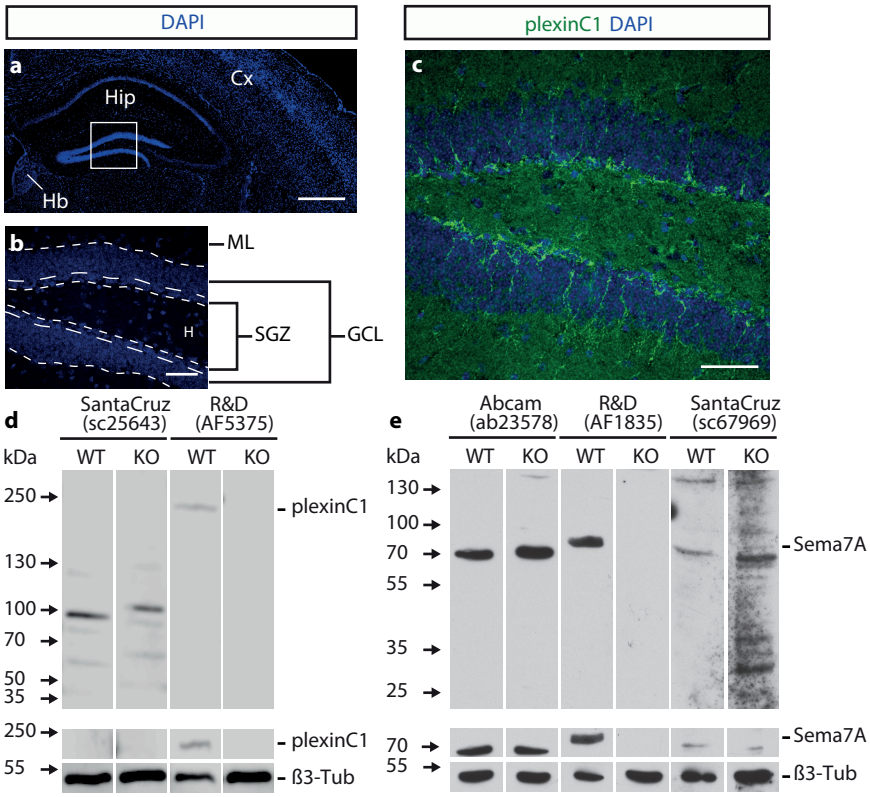

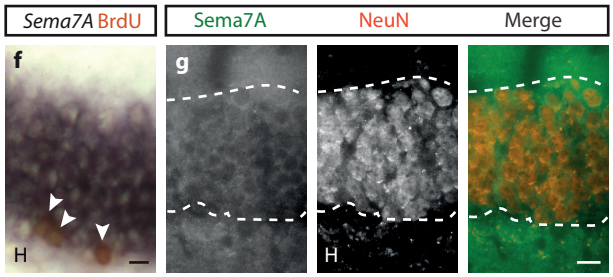

Supplementary Figure 1 | Analysis of antibody specificity and plexinC1 - Sema7A expression in the adult dentate gyrus. (a, b) Mature granule cells reside within the two blades of the granular cell layer (GCL) in the dentate gyrus (DG) of the hippocampus (Hip). A neurogenic niche exists beneath the GCL, called the subgranular zone (SGZ). Boxed area in a is shown at higher magnification in b. DAPI in blue. Cx, cortex; H, hilus; Hb, habenula; ML, molecular layer. (c-f) Immunohistochemistry for plexinC1 on coronal (c) and sagittal (d-f) sections of the adult mouse brain. In the adult DG, shown in panel c, plexinC1 expression is restricted to a subpopulation of cells beneath the GCL. (d) Expression of plexinC1 is largely confined to the glomerular layer (GloL) of the olfactory bulbs, while the external plexiform layer (EpL) and the mitral cell layer (MiL) show sparse labelling. (e) Progenitors from the subventricular zone migrate to the olfactory bulbs through the rostral migratory stream (RMS), situated between the Cx and the striatum (Str). Robust expression of plexinC1 is observed in the RMS. (f) Purkinje cells and granule cells situated in the cerebellar purkinje cell layer (PCL) and GCL, respectively, express high levels of plexinC1 protein. DAPI in blue. (g) Western blotting of *plexinC1*$^{-/-}$ (KO) and *plexinC1*$^{+/+}$ (WT) brain lysates with different anti-plexinC1 antibodies. Upper panels show whole immunoblots, lower panels show cropped immunoblots at predicted size (± 206 kDa) and tubulin loading- control (ß3-Tub, ± 50 kDa). The R&D antibody specifically detects plexinC1. (h) Western blotting of *Sema7A*$^{-/-}$ (KO) and *Sema7A*$^{+/+}$ brain lysates with different anti-Sema7A antibodies. Upper panels show whole immunoblots, lower panels

show cropped immunoblots at predicted size (±80 kDa) and tubulin loading-control (ß3- Tub, ± 50kDa). The R&D antibody specifically detects Sema7A. (i) *In situ* hybridization for *Sema7A* (purple) combined with immunohistochemistry for BrdU (brown) in the adult DG at 2 hrs after BrdU injection. Proliferating, BrdU-positive cells (arrowheads) express *Sema7A*. (j) Double immunohistochemistry for Sema7A and NeuN, a marker for mature granule cells, on sections of the adult DG. Sema7A is expressed throughout the DG GCL (indicated by dotted lines) in NeuN-positive and -negative cells. Scale bars: a 250 µm; b, c 50 µm; e-h 100 µm; i, j 10 µm.

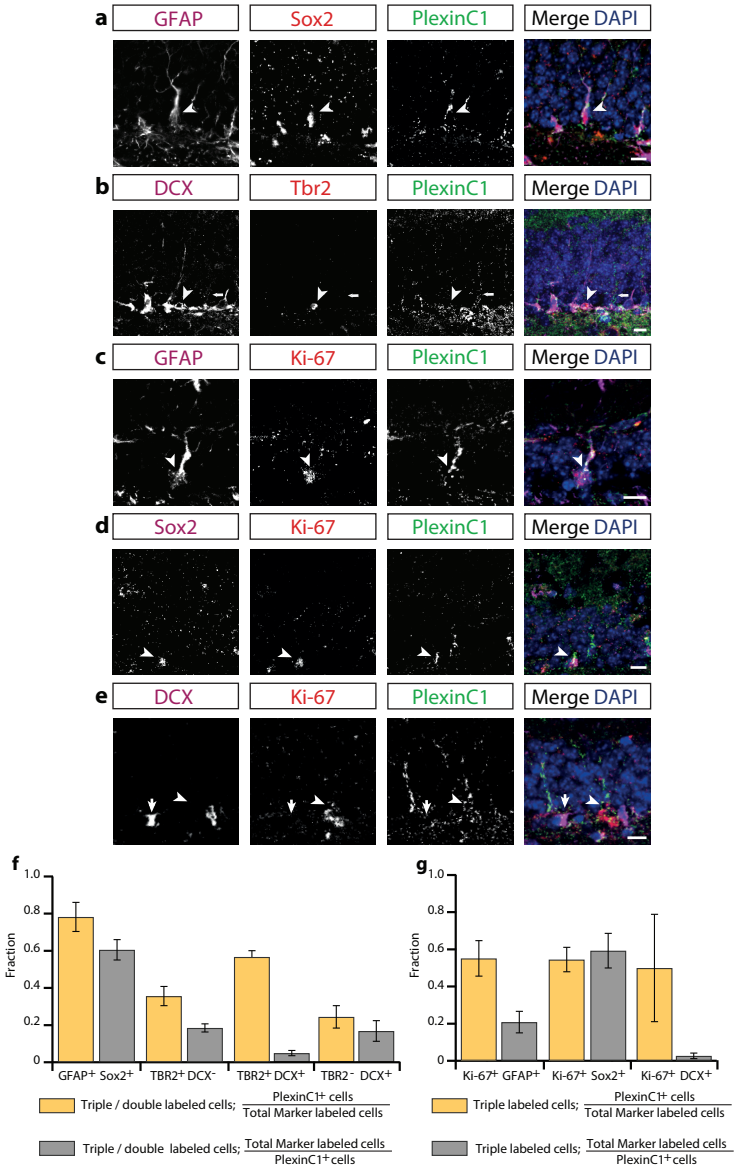

Supplementary Figure 2 | PlexinC1 is enriched in radial glial cells and early immediate progenitor cells of the dentate gyrus subgranular zone. (a-e) Triple immunohistochemistry for plexinC1 and different marker proteins. (f, g) Quantification of the fraction of cells expressing specific markers that also express plexinC1 (yellow) or the fraction of plexinC1-positive cells that also express the indicated marker proteins (grey). A large fraction of cells expressing glial fibrillary acidic protein (GFAP) and sex determining region

Y-box 2 (Sox2) also express plexinC1. Similarly, a large portion of plexinC1-positive cells express GFAP and Sox2. A small fraction of immediate progenitors (t-box brain 2 (TBR2)-positive and doublecortin (DCX)-negative), neuroblasts (TBR2-positive and DCX-positive), and immature neurons (TBR2-negative and DCX-positive) express plexinC1. A small fraction of plexinC1-positive cells are identified as immediate progenitors, neuroblasts or immature neurons. (g) A large fraction cells positive for Ki-67 and GFAP, Sox2 or DCX express plexinC1. A large number of plexinC1-positive cells show Ki-67 and Sox2 co-expression. In contrast, small numbers of plexinC1-positive cells also express Ki-67 and GFAP or Ki-67 and DCX. All data are obtained from $n = 3$ mice and presented as means ± SEM. Scale bar: 10 µm.

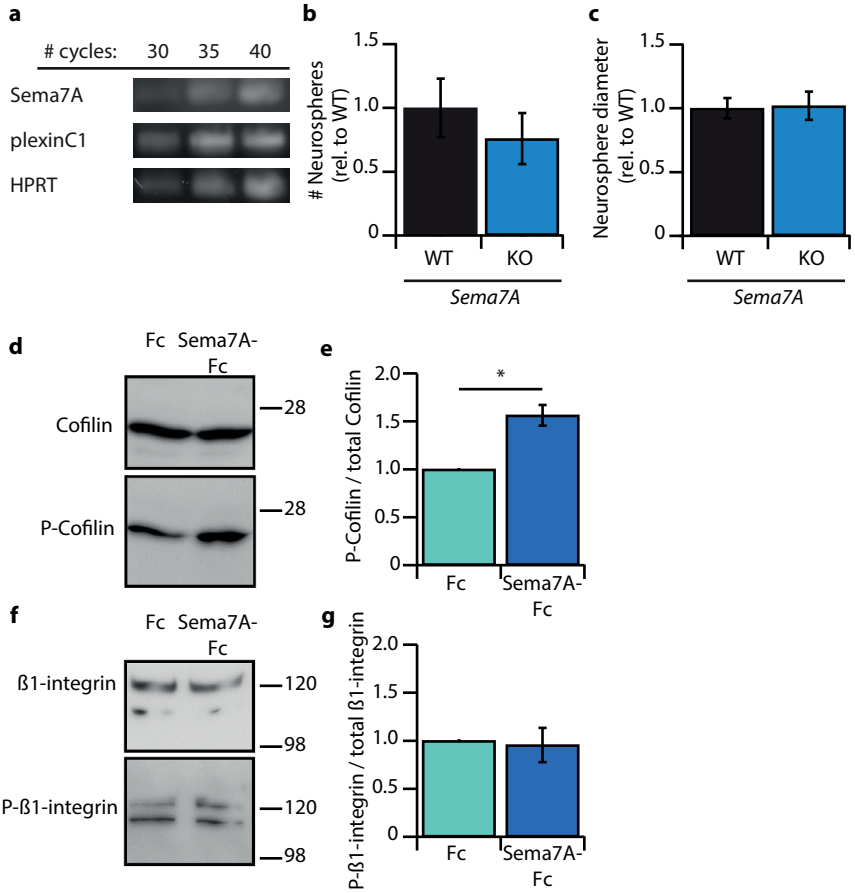

Supplementary Figure 3 | Adult subgranular zone-derived neurospheres do not cell-autonomously require Sema7A for growth and Sema7A induces phosphorylation of cofilin but not β1-integrins in neurospheres. (a) RT-PCR for *Sema7A, plexinC1*, and the house-keeping gene *HPRT* in passage 10 neurospheres. (b, c) Neurosphere number and size are unchanged in *Sema7A*$^{-/-}$ (KO) mouse cultures (Littermate-paired Student's *t*-test: $n = 5$ mice, $p_{(number)} = 0.4515$, $p_{(diameter)} = 0.8900$). WT, *Sema7A*$^{+/+}$. (d-g) Wild-type neurospheres were treated with exogenous Sema7A-Fc (2 nM) or Fc (2 nM) for 30 minutes followed by cell lysis and western blot analysis using the indicated antibodies (d, f). (e, f) Quantification of band intensity of experiments as shown in d and f was performed by scanning densitometry. Signals were normalized to an internal loading control and then to the Fc condition and are represented as the fraction of phosphorylated protein of total protein ($n = 3$ independent neurosphere cultures, replicate-paired Student's *t*-test: $p_{(P\text{-}ß1\text{-}integrin)} = 0.827$). All data are presented as means ± SEM, * $p < 0.05$. Sema7A treatment leads to an increase in the phosphorylation of cofilin but not β1-integrins.

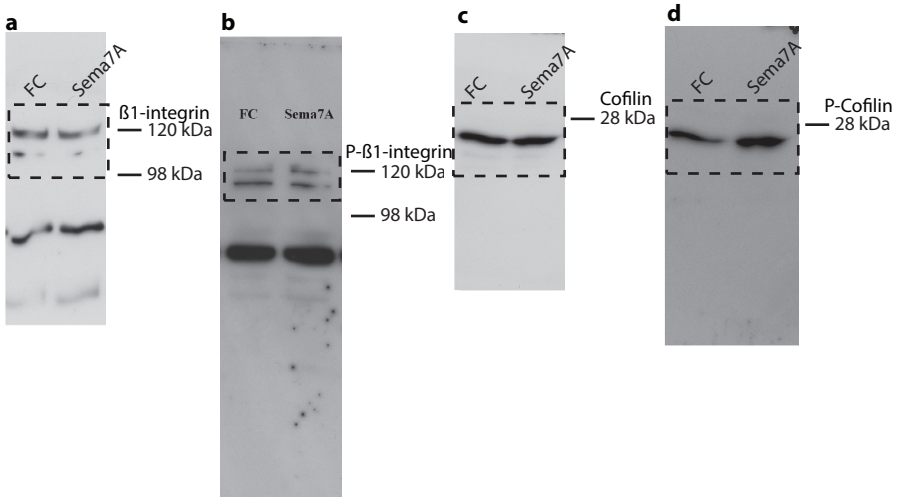

Supplementary Figure 4 | Uncropped western blots from the experiments shown in Supplementary Fig. 3.

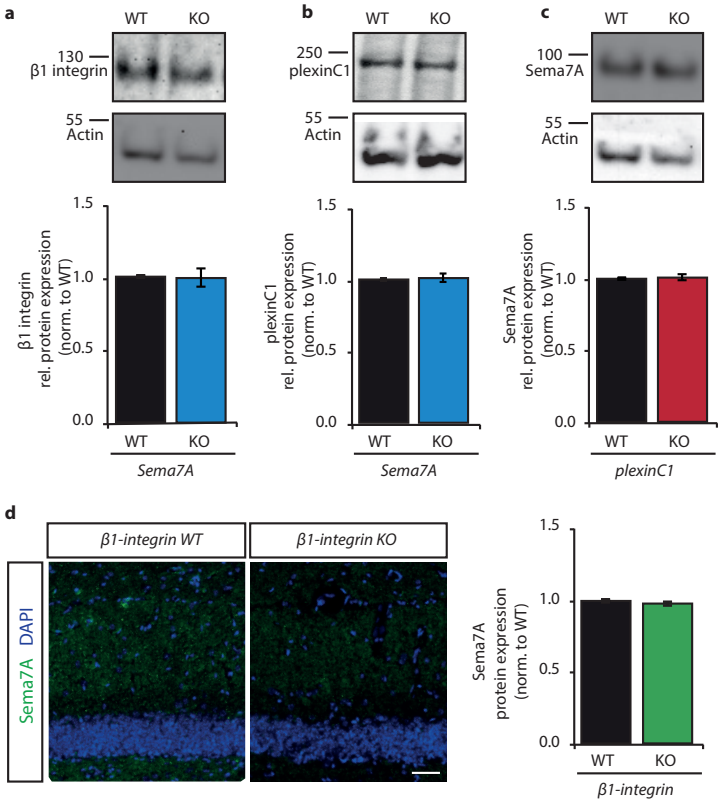

Supplementary Figure 5 | Expression analysis of Sema7A, plexinC1 and ß1- integrin in different knockout mice. Expression of plexinC1 (a) and β1-integrin (b) was determined in adult *Sema7A*$^{+/+}$ (WT) and *Sema7A*$^{-/-}$ (KO) brain lysates using Western blotting. Upper panels show bands for β1-integrin and plexinC1 at the predicted size. Lower panels show actin as a loading control. Graphs show quantification of

normalized levels between genotypes. No differences were observed (Student's *t*-test: $p_{(plexinC1)} = 0.5936$ and $p_{(\beta1\text{-integrin})} = 0.7698$). Data are presented as means ± SD. (c) Brain lysates of *plexinC1*$^{+/+}$ (WT) and *plexinC1*$^{-/-}$ (KO) were used to determine Sema7A expression by Western blotting. Upper panel shows a band for Sema7A at the predicted size. Lower panel shows actin as a loading control. Graph shows quantification of normalized Sema7A levels between genotypes. No difference was detected (Student's *t*-test: $p_{(Sema7A\ in\ plexinC1)} = 0.5499$). (d) Sections of *nestin-Cre;β1-integrin*$^{+/+}$ (WT) and *nestin-Cre;β1-integrin*$^{fl/fl}$ (KO) mice were immunostained for Sema7A and DAPI (left panel). Images show dentate gyrus (strongly labeled DAPI-positive cell bodies in blue in the lower part of the image and molecular layer on top of the GC layer in upper part of the image (strongly stained for Sema7A in green). Right panel shows quantification of the intensity of normalized Sema7A immunostaining. No difference was found between WT and KO immunostainings (Student's *t*-test $p_{(Sema7A\ in\ \beta1\text{-integrin})} = 0.2540$). Data are obtained from $n = 3$ mice and presented as means ± SEM. Scale bar: 50 µm.

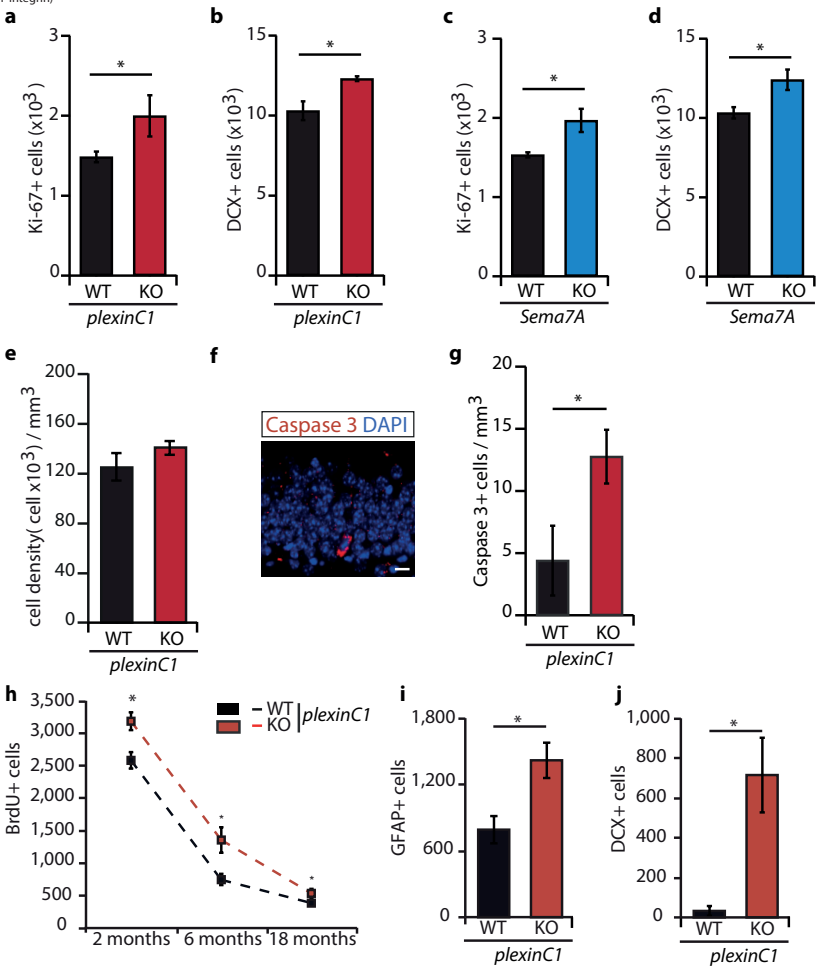

Supplementary Figure 6 | Increased cell proliferation in the subgranular zone of the DG in *plexinC1* and *Sema7A*-deficient mice. (a-d) Quantification of the number of Ki-67$^+$ or DCX$^+$ cells in *plexinC1*$^{-/-}$ mice (a, b; KO), *Sema7A*$^{-/-}$ mice (c, d; KO) or littermate controls (WT)($n = 3$ *plexinC1*$^{+/+}$, $n = 4$ *plexinC1*$^{-/-}$, *Sema7A*$^{+/+}$, and *Sema7A*$^{-/-}$ mice; Student's *t*-test). The number of Ki-67$^+$ and DCX$^+$ cells is increased in *plexinC1*$^{-/-}$ and *Sema7A*$^{-/-}$ mice. (e) Cell density measurements in the dentate gyrus (DG) granule cell layer (GCL) in *plexinC1*$^{-/-}$ mice or littermate controls (WT) ($n = 3$ mice, Student's *t*-test, $p = 0.141$). Granule cell density is unchanged in *plexinC1*$^{-/-}$ mice. (f) Immunohistochemistry for cleaved caspase-3 in the DG GCL. DAPI in blue. (g) Quantification of experiments as in f shows that cleaved caspase-3 levels are increased in *plexinC1*$^{-/-}$ mice compared to littermate controls (WT; $n = 6$ mice, Student's *t*-test). * $p < 0.05$. (h) Quantification of BrdU-

positive cells in *plexinC1*$^{-/-}$ mice and littermate controls (WT) at 2, 6 and 18 months of age. *PlexinC1*$^{-/-}$ mice show increased levels of BrdU at all ages examined ($n = 7$ *plexinC1*$^{-/-}$ and $n = 4$ *plexinC1*$^{+/+}$ mice for 2 months; $n = 3$ *plexinC1*$^{+/+}$ and *plexinC1*$^{-/-}$ mice for 6 months; $n = 4$ *plexinC1-/-* and $n = 5$ *plexinC1*$^{+/+}$ mice for 18 months, two-way ANOVA dpi x genotype $F_{(2, 19)} = 4.325$ $p = 0.028$, *post-hoc t*-tests). (i, j) Quantification of the number of GFAP^{+} or DCX^{+} cells in 18 months old *plexinC1*$^{-/-}$ mice shows an increased number of GFAP^{+} (i) ($n = 3$ mice, Student's *t*-test) and DCX^{+} (j) ($n = 3$ mice, Student's *t*-test) cells in *plexinC1*$^{-/-}$ mice. All data are presented as means ± SEM. Scale bar: 10 µm.

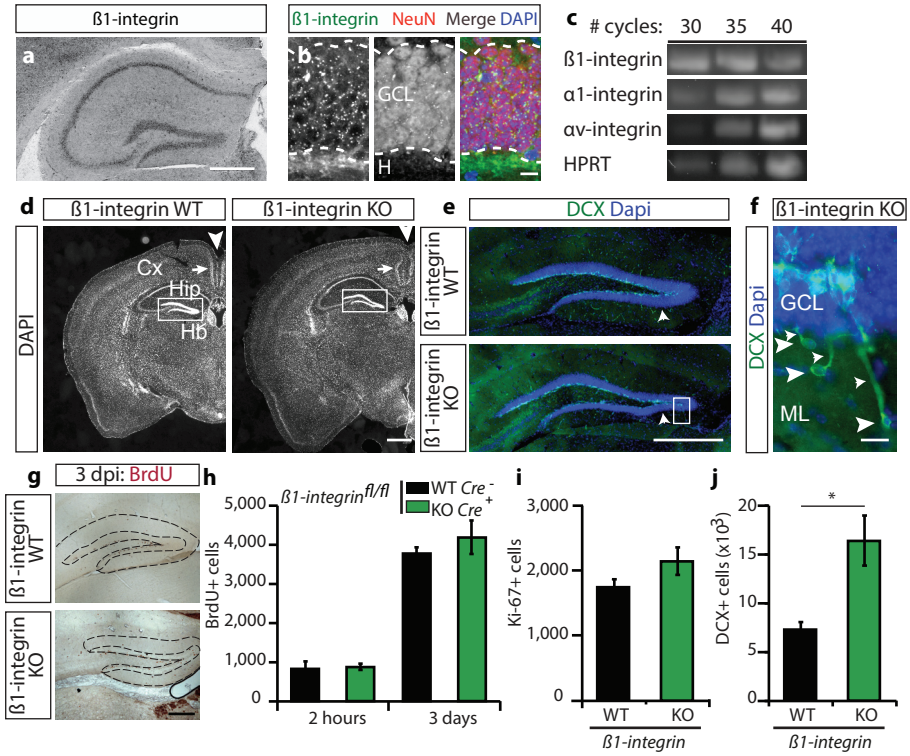

Supplementary Figure 7 | Expression of ß1-integrin in the adult DG is required for proper development and the number of immature granule cells. (a) *In situ* hybridization for *ß1-integrin* reveals broad expression in the adult hippocampus. (b) Double immunohistochemistry using an antibody against active ß1-integrin (green) and NeuN (red) shows that the majority of granule cells, both NeuN-positive and -negative, express ß1-integrin protein. DAPI in blue. GCL, granular cell layer; H, hilus (c) RT-PCR for *ß1-, α1-,* and *αv-integrin* receptor subunits and the housekeeping gene HPRT, as shown in Supplementary Fig. 3a, from passage 10 neurospheres. (d) DAPI-stained coronal sections from *ß1-integrin*$^{fl/fl}$*;nestin-Cre*$^{+/-}$ (KO) brains show abnormal cell alignment in the cortex (Cx, arrow) and hemisphere separation (arrowhead) as compared to *ß1-integrin*$^{fl/fl}$*;nestin-Cre*$^{-/-}$ control mice (WT). Boxed area in d is shown at higher magnification in e. Hip, hippocampus; Hb, habenula. (e) Immunostaining for immature granule cells (DCX, green) and cell nuclei (DAPI, blue) in the DG in *ß1-integrin*$^{fl/fl}$*;nestin-Cre*$^{+/-}$ (KO) mice shows disrupted alignment of the GCL within the infrapyramidal blade (arrow) compared to *ß1-integrin*$^{fl/fl}$*;nestin-Cre*$^{-/-}$ (WT). (f) Higher magnification of the boxed area in e reveals misplaced DCX+ cells (arrowheads) in the molecular layer (ML) of the DG with disoriented dendrites (arrows) facing the GCL. (g) Representative examples of BrdU immunostaining in *ß1-integrinfl/fl;nestin-Cre*+/- (KO) and *ß1-integrin*$^{fl/fl}$*;nestin-Cre*$^{-/-}$ (WT) mice. (h) Quantification of the number of BrdU-positive cells at 2 hours and 3 days post- injection in the DG of *ß1-integrin*$^{fl/fl}$*;nestin-Cre*$^{+/-}$ (KO) and *ß1-integrin*$^{fl/fl}$*;nestin-Cre*$^{-/-}$- (WT) mice ($n = 3$ mice, Student's *t*-test: $p_{(2\ hours)} = 0.8302$ $p_{(3\ days)} = 0.4199$). (i, j) Quantification of the number of Ki-67^{+} or DCX^{+} cells in *ß1-integrin*$^{fl/fl}$*;nestin-Cre*$^{+/-}$ (KO) and *ß1-integrin*$^{fl/fl}$*;nestin-Cre*$^{-/-}$ (WT) mice (($n_{(Ki\text{-}67)} = 9$ WT, $n_{(Ki\text{-}67)} = 8$ KO, $n_{(DCX)} = 3$ WT and KO mice: Student's *t*-test: $p_{(Ki\text{-}67)} = 0.1046$). The number of DCX-positive cells is increased in KO mice. Data are presented as means ± SEM. * $p < 0.05$. Scale bars: d, e 500 µm; f 100 µm; g 250 µm.

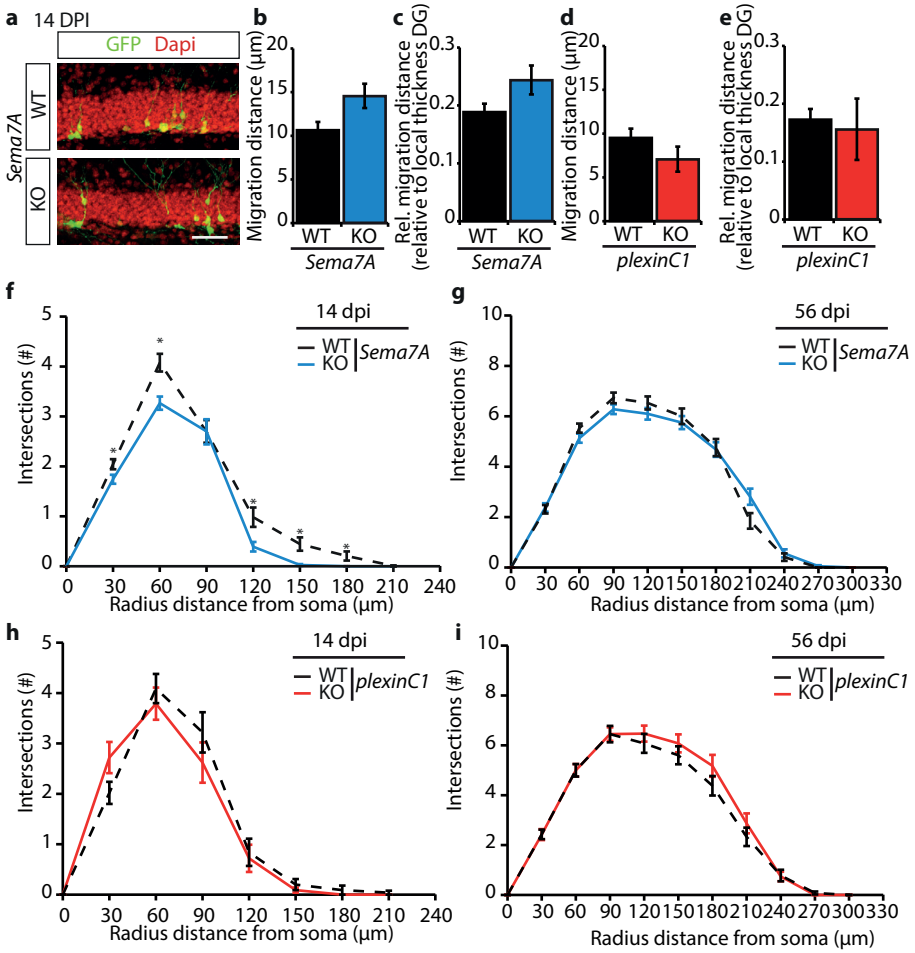

Supplementary Figure 8 | Migration of adult-born granule cells in the DG of *plexinC1*$^{-/-}$ and *Sema7A*$^{-/-}$ mice is intact but Sema7A is required for early stages of dendrite development during adult neurogenesis. (a) Representative examples of adult-born cells infected with MMLV CAG-GFP and visualized at 14 days post-infection (dpi) in *Sema7A*$^{-/-}$ (KO) and *Sema7A*$^{+/+}$ (WT) mice. (b, d) Quantification of the migration of adult-born granule cells as shown in a (distance between the edge of subgranular zone (SGZ) and center of GFP-positive cell) in KO ($n = 4$) and WT ($n = 4$) mice (Student's *t*-test $p_{(Sema7A)} = 0.1645$, $p_{(plexinC1)} = 0.2801$). (c, e) Quantification of the migration of adult-born granule cells relative to the local width of the SGZ (Student's *t*-test: $p_{(plexinC1)} = 0.5265$). (f-i) Sholl-analysis of the dendritic trees of adult-born granule cells at 14 or 56 dpi with MMLV CAG-GFP in *Sema7A*$^{-/-}$ (KO), *plexinC1*$^{-/-}$ (KO) and wild-type littermates (WT) mice. (Sema7A: KO, $n = 120$ cells/3 mice (f), $n = 79$ cells/3 mice (g), WT, $n = 117/4$ mice cells (f), 60 cells/4 mice (g). f: repeated-measures ANOVA $F_{(7, 1645)} = 2.204$, g: repeated-measures ANOVA $F_{(9, 1224)} = 2.202$, $p = 0.082$. plexinC1: KO, $n = 47$ cells/ 4 mice (h), $n = 38$ cells/5 mice (i), WT, $n = 45$ cells/4 mice (h), 40 cells/5 mice (i). h: repeated-measures ANOVA $F_{(7, 630)} = 1.362$ $p = 0.219$, i: repeated- measures ANOVA $F_{(9, 684)} = 0.815$ $p = 0.510$). Whiskers represent SEM. * $p < 0.05$. Scale bar: 50 µm.

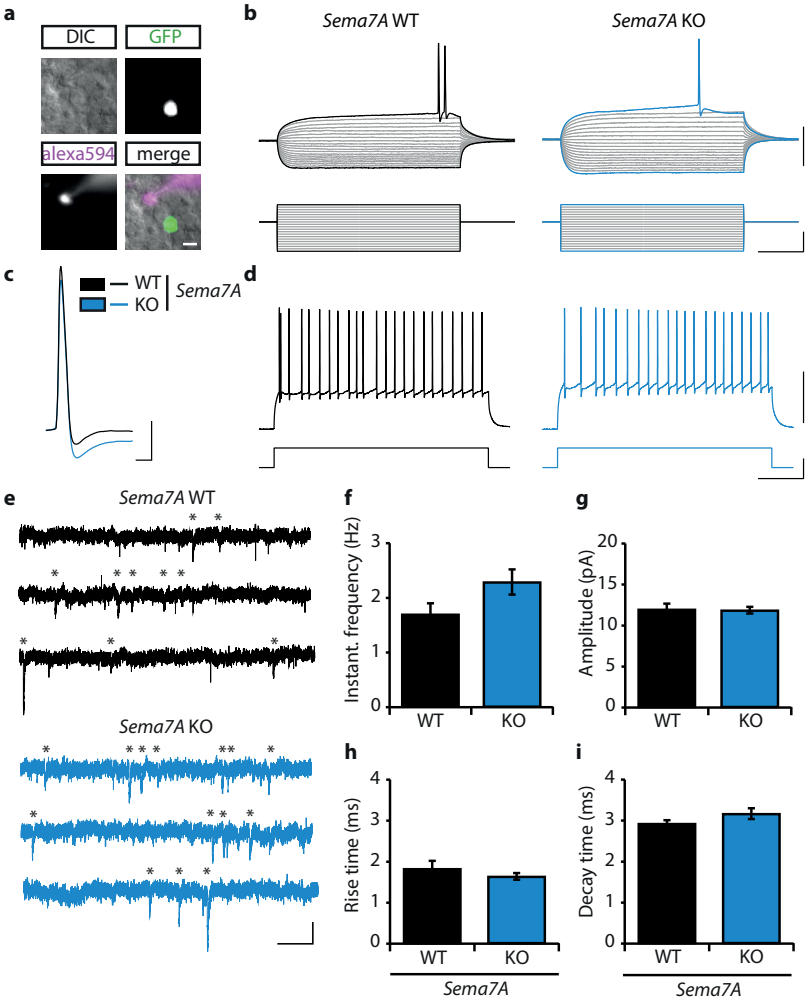

Supplementary Figure 9 | Electrophysiological characterization of mature granule cells in the DG of Sema7A knockout mice. (a) Representative image of a mature granule cell (GC) used for recording of electrophysiological properties and miniature excitatory post-synaptic currents (mEPSCs). Healthy cells in the outer layer of the granule cell layer were identified using differential interference contrast (DIC). Recording of mature GCs (GFP- negative cells) was confirmed by the presence of recording pipet-dye Alexa Fluor 594. (b) Representative traces of membrane potential (upper traces) in response to current injections (lower traces) in *Sema7A*$^{+/+}$ (WT, black) or *Sema7A*$^{-/-}$ (KO, blue) mature GCs. (c) Representative traces of action potentials in WT and KO nGCs. (d) Representative traces for action potential firing rates (upper trace) in response to a 200 pA current injection (lower trace) in WT and KO mature GCs. (e) Representative traces of mEPSC recordings in WT and KO mature GCs. Asterisks indicate identified mEPSC events. (f-i) Quantification of mEPSC instantaneous frequency (f), amplitude (g), rise- (h) and decay- (i) time ($n_{(WT)}$ = 6 cells/3 mice, $n_{(KO)}$ = 9 cells/4 mice, Student's *t*-test: $p_{(instantaneous\ frequency)}$ = 0.091, $p_{(amplitude)}$ = 0.886, $p_{(rise\ time)}$ = 0.307, $p_{(decay\ time)}$ = 0.201). Scale bars: a 10 µm, b, d horizontal: 220 ms, vertical: 50 mV (upper traces) or 200 pA (bottom traces), c horizontal: 2 ms, vertical: 20 mV, e horizontal: 200 ms, vertical: 10 pA. All data are presented as means ± SEM.

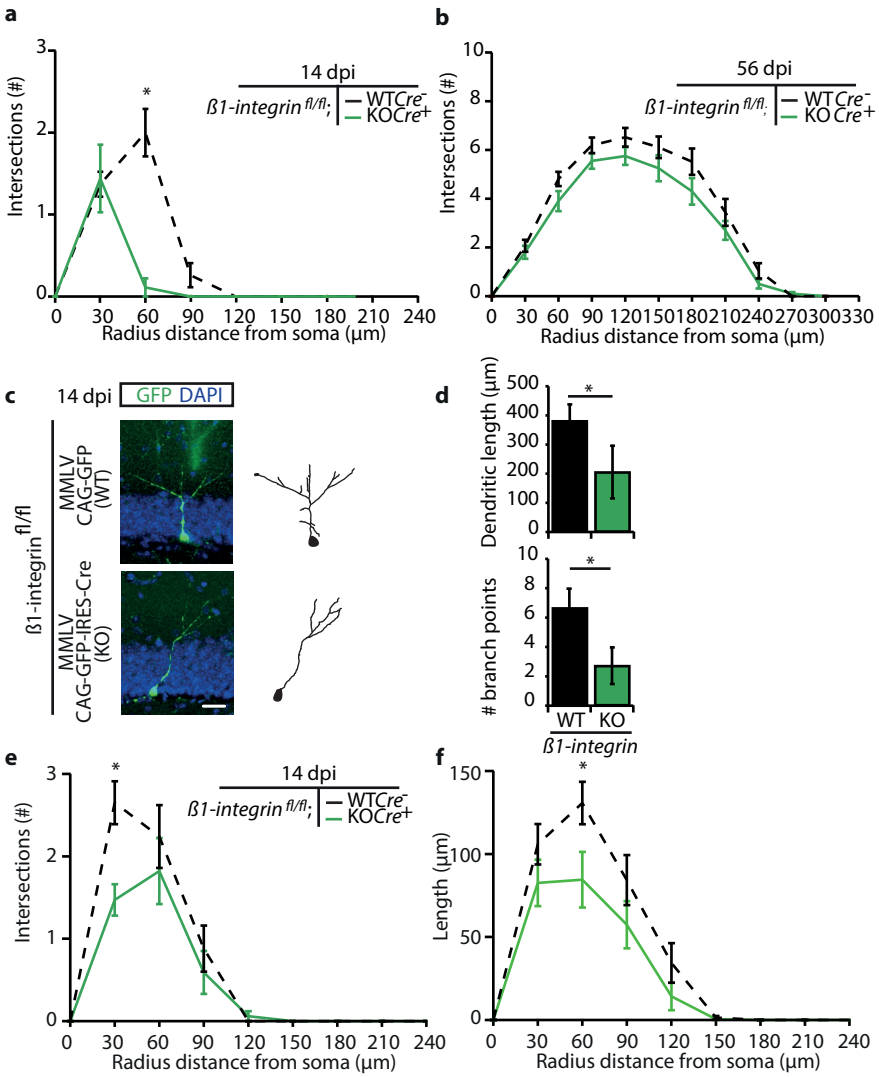

Supplementary Figure 10 | Reduced dendritic complexity in *ß1-integrin*$^{-/-}$ adult-born granule cells. (a, b) Sholl-analysis of the dendritic trees of adult-born granule cells (nGCs) at 14 or 56 days post-injection (dpi) with MMLV CAG-GFP-Cre and MMLV CAG-RFP in *ß1-integrin*$^{fl/fl}$ mice. (14 dpi: KO, n = 7 cells/4 mice, WT, n = 20 cells/4 mice; 56 dpi: KO, n = 20 cells/4 mice, WT, n = 27 cells/4 mice. a: repeated-measures ANOVA $F_{(7,175)} = 2.822$ $p < 0.0001$, b: repeated-measures ANOVA $F_{(9, 405)} = 0.783$ $p = 0.513$). WT, ß1- integrin$^{fl/fl}$ + MMLV CAG-RFP; KO, *ß1-integrin*$^{fl/fl}$ + MMLV CAG-GFP-Cre and MMLV CAG-RFP. Cell-autonomous knockout of ß1-integrin in adult-born granule cells reduces dendritic complexity at 14 dpi. (c) Representative z-stack projection from confocal images of MMLV CAG-GFP- IRES-Cre or CAG-GFP infected nGCs in *ß1-integrin*$^{fl/fl}$ mice. Right panel depicts corresponding tracings. (d) Quantification of dendritic length (top panel) and number of branch points (bottom panel) of KO nGCs (*ß1-integrin*$^{fl/fl}$ + MMLV CAG-GFP-IRES-Cre, green bars, n = 4 mice) compared to WT nGCs (*ß1-integrin*$^{fl/fl}$ +t MMLV CAG-GFP, black bars, n = 4 mice) shows decreased dendritic length and branch points following cell-autonomous loss of ß1-integrin. Scale bar: 25 µm. (e-f) Sholl-analysis of the dendritic tree of nGCs at 14 dpi with MMLV CAG-GFP- IRES-Cre (KO), green lines, n = 17 cells/4 mice, and MMLV CAG-GFP (WT), dashed lines, n = 26 cells/4 mice. (e: number of intersections per radius distance from soma (30 µm radius interval), repeated-measures ANOVA: $F_{(7, 287)} = 7.09$, $p < 0.0001$. f: dendritic length

per radius distance from soma, repeated-measures ANOVA: $F_{(7, 287)} = 6.898$, $p < 0.0001$). Asteriks represent significant difference Student's *t*-test: * $p < 0.05$ and ** $p < 0.01$. All data are presented as means ± SEM.

Supplementary Table 1 | Electrophysiological properties of adult-born 56 dpi GCs in *Sema7A*$^{+/+}$ and *Sema7A*$^{-/-}$ mice.

Electrophysiological property	*Sema7A* WT	*Sema7A* KO	Statistical significance (*P*)
Resting potential (mV)	-69.59 (1.11)	-68.43 (0.97)	0.4664
Input resistence (MOhm)	245.12 (11.49)	197.47 (9.63)	0.0069*
Time constant (ms)	13.63 (0.92)	11.10 (1.06)	0.1304
Membrane capacitance (pF)[†]	56.61 (5.00)	55.18 (2.78)	0.7886
Hyperpolarization (mV)[§]	-134.97 (2.35)	-123.03 (1.85)	0.0011*
Sag (mV)[§§]	1.78 (0.41)	1.42 (0.16)	0.3354
SagArea (mV•ms)	60.34 (20.98)	40.93 (5.77)	0.2686
Action potential property			
Threshold (mV)	-33.72 (0.93)	-33.93 (1.21)	0.9069
Threshold (pA)	120.56 (6.61)	151.45 (7.95)	0.0167*
Amplitude (mV)	68.00 (3.62)	65.10 (4.03)	0.6191
Width (ms)	2.50 (0.24)	2.72 (0.13)	0.4078
Rise time (ms)	0.86 (0.08)	0.86 (0.05)	0.9725
Fall time (ms)	1.54 (0.16)	1.76 (0.10)	0.2473
Afterhyperpolarization (mV)	9.43 (1.10)	6.20 (0.89)	0.0359
Firing rate (Hz)[‡]	25.07 (2.95)	27.07 (4.27)	0.7311
Firing adaptation index[‡‡]	0.32 (0.09)	0.17 (0.12)	0.3801

Data are presented as means with standard error of the mean between parantheses. Statistical significance (*p*) was calculated with *t*-test. *n* Sema7A WT = 7, *n* Sema7A KO = 13.
* $p <$ Benjamini-Hochberg (BH) critical value after correction for multiple testing, BH-correction, FDR = 0.1.
[†] Calculated from the time constant and input resistence, as Cm = τm/Rin
[§] Steady-state hyperpolarization, measured in response to a -300 pA current injection step
[§§] Initial hyperpolarization overshoot relative to steady-state hyperpolarization§
[‡] Calculated from the averaged inter-spike-interval in response to a 200 pA current injection step
[‡‡] Calculated from the averaged last three inter-spike-intervals (F_{last}) and first two inter-spike-intervals ($F_{initial}$), as 1-(F_{last}/$F_{initial}$)

Supplementary Table 2 | Electrophysiological properties of mature GCs in *Sema7A*$^{+/+}$ and *Sema7A*$^{-/-}$ mice.

Electrophysiological property	*Sema7A* WT	*Sema7A* KO	Statistical significance
Resting potential (mV)	-71.14 (1.22)	-72.76 (1.15)	0.3471
Input resistence (MOhm)	185.73 (18.43)	205.79 (12.36)	0.3596
Time constant (ms)	12.56 (1.34)	13.17 (0.89)	0.6956
Membrane capacitance (pF) [†]	68.04 (3.76)	65.48 (4.45)	0.6733
Hyperpolarization (mV)[§]	-122.71 (4.26)	-128.42 (2.99)	0.2697
Sag (mV)[§§]	1.64 (0.25)	1.85 (0.20)	0.5191
SagArea (mV•ms)	59.25 (10.01)	62.12 (8.04)	0.8226
Action potential property			
Threshold (mV)	-36.11 (2.25)	-33.81 (0.95)	0.3204
Threshold (pA)	151.14 (11.04)	143.26 (8.97)	0.5803
Amplitude (mV)	70.52 (5.05)	76.08 (2.19)	0.2981
Width (ms)	3.28 (0.89)	2.25 (0.15)	0.2293
Rise time (ms)	0.80 (0.06)	0.75 (0.04)	0.5559
Fall time (ms)	2.38 (0.89)	1.39 (0.12)	0.2480
Afterhyperpolarization (mV)	8.25 (1.51)	10.19 (1.30)	0.3376
Firing rate (Hz)[‡]	23.64 (4.83)	26.40 (3.46)	0.6398
Firing adaptation index[‡‡]	0.25 (0.12)	0.07 (0.12)	0.3159

Data are presented as means with standard error of the mean between parantheses. Statistical significance (*p*) was calculated with *t*-test. *n* Sema7A WT = 13, *n* Sema7A KO = 16.

[†] Calculated from time constant and input resistence, as $Cm = \tau_m/R_{in}$

[§] Steady-state hyperpolarization, measured in response to a -300 pA current injection step

[§§] Initial hyperpolarization overshoot relative to steady-state hyperpolarization[§]

[‡] Calculated from the averaged inter-spike-interval in response to a 200 pA current injection step

[‡‡] Calculated from the averaged last three inter-spike-intervals (F_{last}) and first two inter-spike-intervals ($F_{initial}$), as $1-(F_{last}/F_{initial})$

Chapter 4

Transcriptional repression of Plxnc1 by Lmx1a and Lmx1b directs topographic dopaminergic circuit formation

Audrey Chabrat[1,2], Guillaume Brisson[1,2], Hélène Doucet-Beaupré[1,2], Charleen Salesse[1,2], Marcos Schaan Profes[1,2], Axelle Dovonou[1,2], Cléophace Akitegetse[1,2], Julien Charest[1,2], Suzanne Lemstra[3], Daniel Côté [2,4], R. Jeroen Pasterkamp [3], Monica I. Abrudan[5,6], Emmanouil Metzakopian[5], Siew-Lan Ang[7] & Martin Lévesque[1,2]

[1.] Department of Psychiatry and Neurosciences, Faculty of Medicine, Université Laval, Québec, Quebec G1V 0A6, Canada. [2.] CERVO Brain Research Centre, 2601, chemin de la Canardière, Québec, Quebec, Canada G1J 2G3. [3.] Department of Translational Neuroscience, Brain Center Rudolf Magnus, University Medical Center Utrecht, 3584 CG Utrecht, The Netherlands. [4.] Département de Physique, Genie Physique et Optique, Université Laval, Québec, Quebec G1V 0A6, Canada. [5.] Wellcome Trust Sanger Institute, Wellcome Trust Genome Campus, Hinxton, Cambridge CB10 1SA, UK. [6.] Faculty of Medicine, School of Public Health, Imperial College, London, W2 1PG, UK. [7.] The Francis Crick Institute, 1 Midland Road, London, NW1 1AT, UK.

Published in Nature Communications, 2017, 8, 933, doi: 10.1038/s41467-017-01042-0

Abstract

Mesodiencephalic dopamine neurons play central roles in the regulation of a wide range of brain functions, including voluntary movement and behavioral processes. These functions are served by distinct subtypes of mesodiencephalic dopamine neurons located in the substantia nigra pars compacta and the ventral tegmental area, which form the nigrostriatal, mesolimbic, and mesocortical pathways. Until now, mechanisms involved in dopaminergic circuit formation remained largely unknown. Here, we show that Lmx1a, Lmx1b, and Otx2 transcription factors control subtype-specific mesodiencephalic dopamine neurons and their appropriate axon innervation. Our results revealed that the expression of Plxnc1, an axon guidance receptor, is repressed by Lmx1a/b and enhanced by Otx2. We also found that Sema7a/Plxnc1 interactions are responsible for the segregation of nigrostriatal and mesolimbic dopaminergic pathways. These findings identify Lmx1a/b, Otx2, and Plxnc1 as determinants of dopaminergic circuit formation and should assist in engineering mesodiencephalic dopamine neurons capable of regenerating appropriate connections for cell therapy.

Introduction

Subsets of midbrain neurons forming the ventral tegmental area (VTA) and the substantia nigra pars compacta (SNpc) produce the majority of dopamine in the central nervous system. Despite sharing a common neurotransmitter phenotype, these neurons innervate different brain regions, serve different functions, and are differentially susceptible to degeneration. In Parkinson's disease (PD), mesodiencephalic dopamine (mDA) neurons from SNpc are the most affected population, whereas VTA neurons degenerate at much later stages of the disease1. Dopaminergic axons from SNpc neurons target the dorsal striatum forming the nigrostrial pathway that controls motor behavior. Dopaminergic neurons from the VTA innervate numerous brain structures including the ventral striatal region, the nucleus accumbens, and the prefrontal cortex. VTA neurons are involved in a variety of behavioral processes such as reward and motivation, and they are referred to as the mesolimbic and the mesocortical pathways. Despite the absence of clear boundaries between these two groups of neurons, single axon tracing studies reported that ascending projections from the SNpc and VTA are topographically organized [2–5].

The differential expression of the guidance cue Netrin-1 in the striatum has been shown to contribute to the topographic organization of mDA neuron innervation [6]. However, although some guidance molecules have been shown to influence mDA neurons targeting (see ref. 7 for a review), how the different mDA neuronal subpopulations establish their specific connections remains unclear.

Recent progress has led to the identification of transcription factors expressed in mDA progenitors that are required for their differentiation. Two LIM-homeodomain transcription factors, Lmx1a and Lmx1b (Lmx1a/b), are specifically expressed in mDA progenitors, and this expression persists in post-mitotic and adult mDA neurons. We and others have recently shown that Lmx1a and Lmx1b were required for the survival of adult mDA neurons [8, 9]. Although some evidence suggests that Lmx1a/b might also be involved in axon growth and guidance [10–12], no studies have yet determined their role in the formation of dopaminergic circuits.

Here, we show that Lmx1a and Lmx1b are required for the topographical organization of dopaminergic innervation in the striatum. Our gene expression profiling experiments identified Plxnc1 as a downstream target gene of Lmx1a/b in mature mDA neurons. Using *in vivo* and *in vitro* approaches, we found that the interaction of Plxnc1 with its ligand semaphorin 7a (Sema7a) segregates the nigrostriatal and mesolimbic pathways. Moreover, we show that another transcription factor, Otx2, well characterized for its role during mDA neurons development, promotes Plxnc1 expression. Our findings elucidate a central mechanism leading to the establishment of key ascending circuits in the brain and pave the way to the development of a more efficient cell replacement therapy for PD.

Methods

Animals. All animal experiments were performed in accordance with the Canadian Guide for the Care and Use of Laboratory Animals and were approved by the Université Laval Animal Protection Committee. *Lmx1a*$^{f/f}$ [9, 15], *Lmx1b*$^{f/f}$ [43], *Dat*$^{Cre/+}$ [18], *Pitx3*$^{Gfp/Gfp}$ [30], and *Sema7a* KO [28] mice were genotyped as previously described. *Lmx1a/b c*KO mice were generated by intercrossing *Dat*$^{Cre/+}$*;Lmx1a*$^{f/f}$*; Lmx1b*$^{f/f}$ male and *Lmx1a*$^{fl/fl}$*;Lmx1b*$^{fl/fl}$ female animals. *Plxnc1-Ires-td-Tomato* mice were generated by standard procedures using pronuclear microinjection into fertilized single-cell mouse embryos as previously described [44].

Transgenes contained the 9-Kb TH promoter [45] (gift from Dr. Kazuto Kobayashi), the full coding sequence of mouse Plxnc1 (NM_018797.2), and td-Tomato (Plateforme d'outils moléculaires, IUSMQ). Transgenic mice were identified by PCR with forward primer in Plxnc1 sequence, 5'–GGCTGGAAGAAGCTCAGAAA–3'; and reverse primer in IRES sequence, 5'–TACGCTTGAGGAGAGCCATT–3'. Sema7a KO and Plxnc1-Ires-td-Tomato mice are kept in C57BL/6 background, while all other mice were kept in a mixed genetic background. The number of mice used in data quantifications was at least three per groups. No mice were excluded from our analysis. No randomization was applied.

Tissue analysis. Mouse brains at P1 were incubated in 4% paraformaldehyde in PBS at 4°C, followed by cryoprotection in 30% sucrose in PBS, before freezing on dry ice. For mice older than P1, perfusion using 4% paraformaldehyde in PBS was instead performed. After cryostat sectioning at 60 µm, sections were washed in PBS, then blocked with 1% normal donkey serum (NDS) and 0.2% Triton X-100 for at least 30 min. Primary antibodies used in this study unless specified otherwise: Rabbit anti-TH (1:1000, Pel-FreezBiologicals P40101-0), Sheep anti-TH (1:1000, Millipore, AB1542), Rat anti-DAT (1:500, Millipore, MAB369), Sheep anti-Plxnc1 (1:150, R&D Systems, AF5375), Rabbit anti-Lmx1a (1:1000, Millipore, AB10533), Guinea-pig anti-Lmx1b (1:100, gift of Dr Carmen Birchmeier, Max Delbruck Center of Molecular Medicine, Berlin, Germany), Goat anti-Otx2 (1:200, R&D Systems, AF1979), Mouse anti-Tyrosine tubuline (1:3000, Sigma, T9028), Mouse anti-Actin (1:1000 & 1:10000, Millipore, MAB1501), Chicken anti-GFP (1:500, Aves Labs, GFP-1020), Rabbit anti-Sema7A (1:500, Abcam, ab23578). Secondaries used in this study unless specified otherwise: Donkey anti-mouse Alexa-Fluor-680 (1:5000, JacksonImmunoResearch, 715-625-150), Donkey anti-sheep Alexa-Fluor-680 (1:5000, JacksonImmunoResearch, 713-625-147), Donkey anti-rabbit Alexa-Fluor-790 (1:5000, JacksonImmunoResearch, 711-655-152), Donkey anti-mouse Alexa-Fluor-790 (1:5000, JacksonImmunoResearch, 715-655-150), Donkey Alexa-Fluor-488 (1:200, JacksonImmunoResearch), Donkey Alexa-Fluor-555 (1:200, JacksonImmunoResearch), Donkey Alexa-Fluor-647 (1:200, JacksonImmunoResearch), HRP-conjugated Goat anti-mouse (1:5000, Life Technologies, G-21040), HRP-conjugated Goat anti-rabbit (1:3000, Cell Signaling Technology, 7074P2).

Optical density measurements on sections. Striatal sections were co-labeled with TH and actin or with Plxnc1 and actin, and then incubated with infrared fluorescent conjugated secondary antibodies (donkey anti-mouse Alexa-Fluor-680, donkey anti-mouse Alexa-Fluor-790, donkey anti-sheep Alexa-Fluor-680, donkey anti-rabbit Alexa-Fluor-790, 1:5000, Jackson ImmunoResearch). Sections were then mounted on glass slides, coverslipped, and scanned using an infrared imaging system (Odyssey CLx; LI-COR Biosciences, Lincoln, NE, USA [46,47]). Optical density measurements were done using Image Studio Lite Ver 5.2 software after delineatingthe striatal areas with the software's freehand tool. Although there is no clear boundaries between SNpc and VTA target regions in the striatum, the dorsal half of the striatum receive mostly DA projections from SNpc, whereas the ventral half receives mostly projections from VTA. The distinction between dorsal vs. ventral striatum areas was thus determined by dividing the striatum in two halves, which represent the major striatal target regions for SNpc and VTA [2, 3, 5, 48].

***In situ* hybridization**. *In situ* hybridization was performed as previously described [8, 16]. Brains were dissected in diethylpyrocarbonate (DEPC)-treated PBS, and fixed in 4% PFA (DEPC) overnight. After an overnight incubation in 30% sucrose (DEPC), brains were frozen with

dry ice and then cryosectioned in 20-µm thick coronal sections. Sections were collected on superfrost plus slides (Fisher Scientific). The complementary DNA (cDNA) templates were generated from E18.5 whole-brain RNA and used to generate RNA probes for Plxnc1, Lmx1a, and Lmx1b using RT-PCR following the protocol described previously [11].

Quick TH staining and LCM. The experiment was performed as described in ref. 49. Briefly, E15.5 or P1 mouse brains were quickly dissected and snap-frozen in liquid nitrogen. The 12-µm thick cryostat sections were collected on membrane-coated glass-slides (Leica Biosystems), allowed to dry, before being fixed in 70% ethanol at −20 °C. The fixed sections were quickly stained (20 min) using rabbit anti-TH (Pel-Freez, 1:25) as a first antibody, washed with PBS, and then exposed to a biotinylated anti-rabbit secondary antibody (Vector Labs, 1:100). The slides were subsequently incubated in avidin/biotinylated enzyme complex HRP (Vectastain; Vector Laboratories), and the staining was detected with the diaminobenzidine substrate. The stained slides were stored frozen at −80 °C. After defrosting, the SNpc and VTA areas were collected using a LCM microscope (Leica). For single-cell LCM experiment, slides were co-labeled using a rabbit anti-TH and a goat anti-Otx2, and then exposed to secondary antibodies donkey anti-rabbit Alexa-Fluor- 488 and donkey anti-goat Alexa-Fluor-555 (1:100, Jackson ImmunoResearch).

cDNA library production. Cells from the SNpc and VTA respectively were isolated using LCM (Leica AS-LMD) from stained frozen sections of control and *Lmx1a/b c*KO mice as described above. Microdissected cells were collected in lysis buffer, and total RNA isolation was carried out using an RNA isolation kit (Arcturus PicoPure, Applied Biosystems) according to the manufacturer's instructions. RNA was reverse-transcribed using Superscript III (Life Technologies) and the cDNA obtained was used for RT-qPCR.

RNA sequencing. RNA sequencing was performed on three biological replicates for the control and four biological replicates for *Lmx1a/b c*KO mice. For each sample, two technical replicates were performed. For each E15.5 embryo used, VTA and SNpc were dissected from eight antero–posterior levels across the entire DA domain as revealed by TH immnostaining. Following RNA extraction, RNA-seq libraries were constructed using the Illumina TruSeq Stranded RNA protocol with oligo dT pulldown and sequenced on Illumina HiSeq2500 by 150-bp paired-end sequencing. One sample was excluded before the sequencing because the amount of RNA was too low to measure the RNA quality. Reads were aligned using STAR aligner (version 2.4.2a) to the mouse genome assembly GRCm38. Raw read counts per gene were obtained using featureCount in the R package Rsubread with the GENCODE annotation vM8. The gene differential expression analysis was done using DeSeq2 [50]. We only considered genes with >10 reads across all of the samples. A total of 225 genes with adjusted *p* value <0.2 were reported as being significantly differentially expressed. Data are available at Array Express under accession number E-MTAB-5986.

RT-qPCR. Quantitative RT-PCR was performed using a cDNA library obtained from the LCM experiment. Analysis of expression levels of mRNAs was achieved with Platinum SYBR Green Super Mix (Invitrogen) and performed in triplicate using the LightCycler 480 (Roche Diagnostics). Primers for amplification were designed in the 3' region of each gene using the online Primer3 tool (http://www. bioinfo.ut.ee/primer3/). The primer sequences are available upon request. Ampli- fications were performed in 20 µl containing 0.5 µM of each primer, 0.5 µl SYBR Green (Invitrogen), and 2 µl of 50-fold diluted cDNA, with 40 cycles at 94

°C for 15s, 60°C for 1min, 72°C for 30s, and 79°C for 5s. Analysis of real-time quantitative RT-PCR triplicate reactions was performed with the LCS 480 software (Roche Applied Science; version 1.5.0.39); outliers were removed according to the method described by ref. 51. The "Advanced Relative Quantification" mode of the LCS 480 software was used to estimate relative gene expression; the 2−ΔCT formula was used to calculate relative quantifications. Values were normalized using the amount of target gene for at least two or three reference genes (*GAPDH, TBP,* and *RPL13*). To confirm homogeneous product formation, a melting curve analysis was performed. Data are represented as the mean ± SEM of the fold change normalized against reference genes.

Brain injections. The anterograde virus AAV2-mCBA-FLEx-EGFP-WPRE (9 e12 genome copy per ml; from Plateformed'OutilsMoléculaires, IUSMQ) was injected into the SNpc of *Dat*$^{Cre/+}$ *Lmx1a/b*$^{f/f}$ or *Dat*$^{Cre/+}$ mice at P10. Mice were anesthetized using isoflurane and immobilized in a stereotaxic apparatus (Stoelting, Wood Dale, IL, USA). Then, 200 nl of this virus was injected at the following coordinates: +1 mm anteroposterior (AP) from lambda; 1.1 mm mediolateral (ML); −3.2 mm dorsoventral (DV, taken from the surface of the brain)[52]. Mice were killed 17 days after surgery for immunohistochemistry analysis. Injection of AAV2-Retro-GFP (2 e13 genome copy per ml; from Plateforme d'Outils Moléculaires, IUSMQ) was performed in the striatum of the *Dat*$^{Cre/+}$ *Lmx1a/b*$^{f/f}$ or $^{Dat+/+}$ $^{Lmx1a/bf/f}$ mice, *Sema7a* KO, or WT at P10. Two hundred nanoliters was injected in both hemispheres at the following coordinates for the ventral striatum: bregma: +0.7 mm AP; ±1 mm ML; −3.5 mm DV; and for the dorsal striatum: bregma: +0.7 mm AP; 1.6 mm ML; −2 mm DV [52]. Mice were killed 17 days after surgery for analysis. For the Fluorogold injections in the ventral striatum, we used the same coordinates, but we injected 1 µl of Fluorogold (2% in 0.9% sodium chloride, Millipore) in both hemispheres and mice were killed 3 days after.

Stereological neuron counting. Stereological methods (optical fractionator method, StereoInvestigator, MBF Bioscience) [53–55] were used to compare the number of TH-positive neurons within the ventral midbrain of control and mutant mice at P1 and P15. Contours were traced at ×5 magnification to define the area of interest, and counting was performed at ×40 magnification at one in two section intervals. Coefficients of error (Gundersen, m = 1) were <0.08.

Western blot. Striata from control *Pitx3*$^{GFP/+}$ mice brains at P1 were dissected by cutting a 1-mm coronal slice, followed by dissection of samples from dorsal and ventral striata. These samples were then snap-frozen. Sample lysis was performed in radioimmunoprecipitation buffer complemented with protease inhibitor and phosphatase inhibitor cocktails (Roche) (50 mM Tris-HCl, 150 mM NaCl, 1% NP-40, 0.5% sodium deoxycholate, 0.1% SDS, 2 mM EDTA, 50 mM NaF, pH 7.4). Quantification of protein content in the samples was carried out using a DC-protein assay (Bio-Rad). Fifteen micrograms of protein extracts were separated by SDS-polyacrylamide gel electrophoresis (12% SDS-PAGE Tris-glycine gels). Nitrocellulose membranes (Bio-Rad) were used for the transfer. Blots were immunostained overnight at 4 °C with primary antibodies. The primary antibodies were diluted in blocking solution containing TBS and 0.01% Tween-20 (Sigma). Blots were washed three times (5 min each) with TBS and 0.01% Tween-20, and immune complexes were detected with species-appropriate secondary antibody conjugated to HRP. Membranes were covered with ECL for 5 min (Western Lightning Plus-ECL, PerkinElmer), and chemiluminescence was then

documented by exposing the membranes to Pierce CL-Xposure film (Thermo Scientific). Films were scanned and analyzed using the ImageJ64 program.

In vitro ventral midbrain cell cultures and explant cultures. Primary ventral midbrain cell cultures were prepared as previously described [8]. In brief, embryonic ventral midbrains were dissected from E18.5 *Pitx3-GFP* embryos in chilled L15 containing 5% fetal bovine serum (FBS). After one DIV, cells were transfected using Lipofectamine 2000 (Life Technologies) with either the control plasmid pCMV-mCherry (Plateformed'OutilsMoléculaires, IUSMQ), or a plasmid allowing overexpression of Otx2 (gift from S.-L.A.), Lmx1a (pCAGGS-Lmx1a-IRES2- nucEGFP, Addgene), or Lmx1b (pCMV-Lmx1b-RFP, Applied Biological Materials Inc.). Cells were collected after three DIVs and processed for RT-qPCR.

Explants of embryonic ventral midbrain were dissected from E14.5 *Pitx3*$^{GFP/+}$ embryos in chilled L15, 5% FBS. Explants were grown on 12-mm diameter glass coverslips coated with 7 µl of MatrigelTM (BD Biosciences, Mississauga, ON, Canada) in 24-well plates. Then, explants were each covered by 7 µl of Matrigel and cultured in 1 ml of neurobasal medium complemented with B27, PenStrep, Glutamax, sodium pyruvate, and FBS (86.8% neurobasal medium, 5% P/ S, 2% B27, 0.2% Glutamax, 1% Na-Pyruvate, and 5% FBS) for 2 days at 37 °C, 5% CO2. After two DIVs, the medium was replaced by the same complemented medium without FBS. Then, explants were exposed to Sema7a (0.5 µg/ml) for 2 h, and fixed for 30 min at 4 °C in fixative solution (3.5% PFA, 4% sucrose, in PBS 1×). The actin was stained by incubating the explants for 40 min at room temperature with a buffer solution containing 1% rhodamine-phalloidin (Life Technologies) and 1% BSA, while TH was immunostained by incubating overnight with rabbit anti-TH (Pel-Freez, 1:1000) in 5% NDS and 0.1% Triton X-100 in PBS. Axonal outgrowth analysis was performed on confocal images of the TH signal using the Neurite-J plug-in [56].

Stripe assay. The stripe assay was performed as previously described [57]. Alternating stripes (IgG or Sema7a 100 µg/ml, R&D system) were applied to glass coverslips. These stripes were then covered by laminin (20 µg/ml). Approximately three to four explants from *Pitx3*$^{GFP/+}$ embryos or from *Lmx1a/b c*KO and control littermates were seeded in the middle and at the left and right extremities of each coverslip. These explants were then cultured for 3 days, and fixed with 3.5% PFA, 4% sucrose, in DPBS (1×) before immunostaining. For quantification, the number of neurites terminating on control vs. Sema7a stripes was counted for each explant.

iDISCO. Mice brains were dissected at P1 and then processed as described in the iDISCO protocol [20]. Briefly, after tissue collection and fixation, a pretreatment with methanol was performed before immunostaining. Then, permeabilization and blocking of the tissue were performed before incubation in primary antibodies at the following concentration: rabbit anti-TH (Pel-Freez, 1:250) for 7 days. After 1 day of washing in buffer PTwH (100 ml PBS 10×, 2 ml Tween-20, 1 ml of 10 mg/ml heparin stock solution), brains were incubated in the secondary antibody Alexa Fluor 594 donkey anti-rabbit (Life Technologies, 1:400) for 6 days. After washing, brains were transferred in a clearing solution for further imaging.

Light-sheet imaging. Whole hemisphere three-dimensional (3D) images were obtained using a two-photon light-sheet microscope. An excitation light-sheet was generated by scanning a long, thin near-infrared (800 nm) Bessel beam into the sample through a long working distance objective (Olympus, XLFLUOR4X/340, NA 0.28, WD 29.5 mm). The length

and thickness of the beam were decoupled, thereby achieving a large field of illumination (2.5 mm × 2.5 mm) without compromising the axial resolution (2 µm). To produce a light-sheet with sufficient energy, a femtosecond titanium-sapphire laser source (Coherent Mira 900) was used with an amplifier (Coherent RegA 9000). The emitted two-photon fluorescence was detected by a scientific CMOS camera (Hamamatsu Orca-Flash4.0 V2) through a long working distance multi-immersion objective (Olympus XLPLN10XSVMP, NA 0.6, WD 8 mm) placed perpendicular to the scanning plane, achieving an effective field of view of 1.3 mm by 1.3 mm. The whole-brain images were obtained by moving the sample using a motorized stage (Sutter MPC-385), thus generating 3D images. These images were stitched together using a custom Matlab script to form a 3D image of the entire sample.

Electrophysiological recordings. Sagittal whole-brain slices (300 µm thick) were prepared from *Dat*$^{Cre/+}$ *Lmx1a/b*$^{f/f}$ *c*KO mice and control littermates (P9–14). Animals were lightly anesthetized with isoflurane and brains were dissected and sliced in ice-cold (0–4 °C) solution containing (in mM): 250 sucrose, 2 KCl, 1.25 NaH_2PO_4, 26 $NaHCO_3$, 7 $MgSO_4$, 0.5 $CaCl_2$, and 10 glucose, saturated with 95% O_2 and 5% CO_2, 340–350 mOsm. Slices were immediately transferred to a heated (34 °C) oxygenated solution containing (in mM): 126 NaCl, 2.5 KCl, 1.4 NaH_2PO_4, 26 $NaHCO_3$, 2.4 $MgCl_2$, 1.2 $CaCl_2$, and 11 glucose (60 min, after which they were kept at room temperature until use). During recordings, slices were continuously perfused at 2 ml per min with a standard artificial cerebrospinal fluid (126 mM NaCl; 2.5 mM KCl; 1.4 mM NaH_2PO_4; 25 mM $NaHCO_3$; 1.2 mM $MgCl_2$; 2.4 mM $CaCl_2$; and 11 mM D-glucose; osmolarity adjusted to 295–305 mOsm) saturated with 95% O_2 and 5% CO_2 at near-physiological temperature (30–32 °C). Whole-cell voltage-clamp recordings were obtained from visually identified cells. For recordings, 3.5–5 MΩ borosilicate glass pipettes were filled with a 115 mM $CsMeSO_3$, 20 mM CsCl, 10 mM diNa-phosphocreatine, 10 mM HEPES, 2.5 mM $MgCl_2$, 0.6 mM EGTA, 4 mM ATP-Mg, and 0.4 mM GTP-Na (pH 7.25; osmolarity adjusted to 275–285 mOsm). Data acquisition (filtered at 2–3 kHz; digitized at 10 kHz) was performed using a Multiclamp 700B amplifier and Clampex 10.6 software (Molecular Devices, Union City, CA, USA). Data were analyzed using Clampfit 10.6 (Molecular Devices). Spontaneous and miniature events were analyzed using the search event algorithm in Clampfit 10.6 and fitted with a double exponential.

Statistical analysis. Statistical analyses were performed using GraphPad Prism 4.0 (GraphPadSoftware, La Jolla, CA, USA) software. The differences between two groups were determined by Student's *t* test or Mann–Whitney U test when variance was different between groups. Explant and mDA cell intersection profiles were analyzed by two-way analysis of variance, and the Sidak test was used for post hoc comparisons. All data are represented as means ± SEM, and significance is defined as * $p < 0.05$, ** $p < 0.01$, or *** $p < 0.001$.

Microscopes. All immunofluorescence images were acquired using a Zeiss LSM5 Pascal confocal microscope ora Zeiss LSM700 confocal microscope, then processed using Zen software and Adobe Photoshop CS4. Brightfield pictures were acquired using a Leica DMRB equipped with a digital camera. Tiled brightfield images were also acquired using an Olympus BX51 equipped with a motorized stage and stitched with Surveyor Software for Real-Time Mosaic Imaging (Objective Imaging, Cambridge, UK).

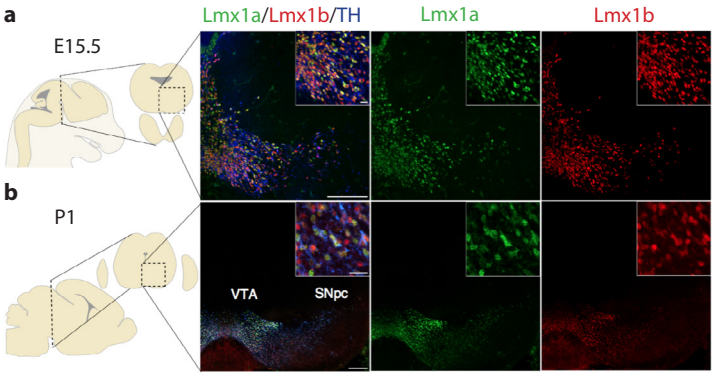

Fig. 1 | Ventral midbrain expression of transcription factors Lmx1a and Lmx1b at early stage of development. Representative confocal stitched images of immunohistochemical staining of the transcription factors Lmx1a and Lmx1b in TH-positive neurons in midbrain coronal sections at E15.5 (a) and P1 (b). Although Lmx1a and Lmx1b are present in all mDA neurons, the staining intensity for Lmx1a and Lmx1b varies in mDA neurons. Scale bars: a, 200 µm and 10 µm for high-magnification inserts; b, 200 µm, and 20 µm for high-magnification inserts. SNpc, substantia nigra pars compacta; VTA, ventral tegmental area.

Data availability. All data generated and analyzed during the current study are available from the corresponding author on request. RNA sequencing data are available at Array Express under accession number E-MTAB-5986.

Results

Lmx1a/b are required for appropriate mDA axon projections

During midbrain development, Lmx1a/b are among the first transcription factors expressed by mDA progenitors [13, 14]. Previous studies showed that Lmx1a/b are required for the specification, proliferation, and differentiation of dopaminergic progenitors [15, 16]. Immunostaining of mouse embryonic and post-natal midbrain sections shows that all post-mitotic mDA neurons express both Lmx1a and Lmx1b as previously reported (Fig. 1) [16]. Given the functional redundancy established between these two factors in mDA progenitors [16], we generated *Dat*$^{Cre/+}$; *Lmx1a*$^{flox/flox}$;*Lmx1b*$^{flox/flox}$ (referred to henceforth as *Lmx1a/b c*KO) mice to study potential roles of Lmx1a/b in regulating axon pathfinding of mDA neurons. *Lmx1a/b c*KO animals were born at the expected Mendelian frequency, fertile and morphologically indistinguishable from their control littermates (*Dat*$^{+/+}$; *Lmx1a/b*$^{f/f}$).

In agreement with previous studies [17–19], the Cre recombinase expressed from the Dat promoter is efficient at deleting Lmx1a and Lmx1b in the ventral midbrain (Supplementary Fig. 1). Inactivation of Lmx1a and Lmx1b using the Dat-Cre line starts around embryonic day E14 [19], which corresponds to the developmental period where mDA neurons initiate their axonal growth toward the forebrain [7]. Histological analysis and stereological counting of mDA neurons in *Lmx1a/b c*KO and control mice did not reveal any significant difference in the total number and the distribution of mDA neurons (Fig. 2a–c). However, analysis of tyrosine hydroxylase (TH) immunostaining in the striatum of *Lmx1a/b c*KO mice revealed an obvious lack of dopaminergic (DA) axons innervating the dorsal and caudal portion of the striatum at post-natal day 1 (P1) and in 2-week-old mice (Fig. 2d–g and Supplementary Figs. 2 and 3). Accordingly, quantification of TH-positive axonal innervation in the striatum

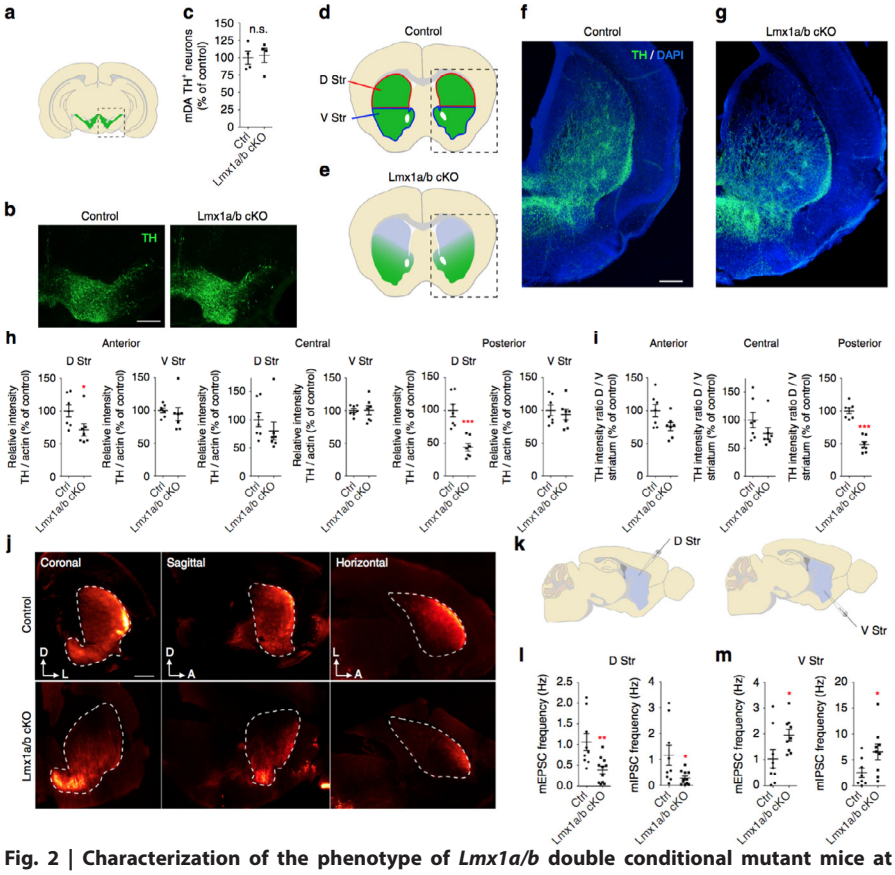

Fig. 2 | Characterization of the phenotype of *Lmx1a/b* double conditional mutant mice at P1. a Schematic representation of coronal section of mouse brain at the midbrain level at post-natal day 1 (P1). Dashed line indicates the delimitation of the pictures shown in b. Distribution (b) and number (c) of mDA neurons in the midbrain were not different between controls and *Lmx1a/b* cKO at P1 ($n = 4$, two-tailed unpaired t test, $p = 0.8134$). d, e Schematic representations of axonal innervation in the striatum in control and *Lmx1a/b* cKO mice brains at P1. f, g Representative confocal images of control and *Lmx1a/b* cKO mice brain sections showing a loss of dopaminergic innervation in dorso-posterior striatum for *Lmx1a/b* cKO mice (green = TH and blue = DAPI). h, i Optical density measurements of TH axons in the striatum. Graphs (i) show the ratio of TH intensity in dorsal vs. ventral striatum (n = 7, two-tailed unpaired t test, $p_{(Ant D)} = 0.0483$, $p_{(Cent D)} = 0.3398$, $p_{(Cent V)} = 0.9596$, $p_{(Post D)} = 0.0003$, $p_{(Post V)} = 0.5914$, $p_{(Ant D/V)} = 0.0526$, $p_{(Cent D/V)} = 0.1863$, $p_{(Post D/V)} \leq 0.0001$, Mann–Whitney U, $p_{(Ant V)} = 0.1649$). j Light-sheet scans of the TH immunostaining in the striatum of iDISCO-cleared brains from control and *Lmx1a/b* cKO mice. The panels show single optical planes in coronal and reconstructed sagittal and horizontal planes showing the lack of TH axons in the dorsal striatum of the *Lmx1a/b* cKO mice brains. Dotted lines delineate the border of the striatum. k Schematic representation of the location of electrophysiological recordings in the striatum. l, m Analysis of the frequency of miniature excitatory post-synaptic currents (mEPSC) and miniature inhibitory post-synaptic currents (mIPSC) in dorsal and ventral striatum (dorsal striatum: $n = 9$ cells for controls and $n = 11$ cells for *Lmx1a/b* cKO, Mann–Whitney U, $p_{(mEPSC)} = 0.0078$; $p_{(mIPSC)} = 0.0275$; ventral striatum: $n = 9$; two-tailed unpaired t test; $p_{(mEPSC)} = 0.0408$; $p_{(mIPSC)} = 0.0444$). Scale bars: 250 µm for b, f, g and 500 µm for j. D, dorsal; L, lateral; N.S., not significant; Str, striatum; V, ventral.

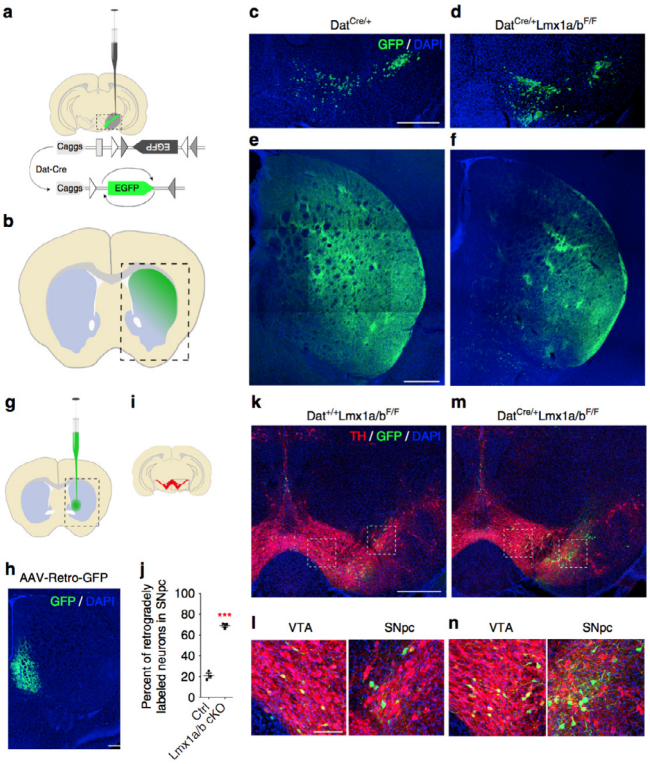

Fig. 3 | Anterograde and retrograde axonal tracing experiments showing aberrant dopaminergic axonal connections in Lmx1a/b conditional mutants. a, b Schematic description of the AAV-FLEx-EGFP experiment showing injection of the viral vector in the SNpc at P10 and the labeling of the axonal projections in the striatum. c, d Representative confocal images of the GPF-positive cells in the midbrain (AAV-FLEx-EGFP in green and DAPI in blue), and the resulting GFP-positive axons at the striatal level in the control (e) and in the *Lmx1a/b* cKO mice (f) 17 days after injection. g Schematic representation of the injection site of the AAV-retro-GFP in the ventral striatum. h Representative confocal images of the injection site in the ventral striatum. i Schematic representation of a coronal section of mouse brain at the midbrain level indicating the delimitation of the pictures shown in k–n. j Quantification of the percentage of retrogradely labeled neurons in SNpc (GFP+ TH+ in SNpc on total GFP+ TH+; $n = 3$, two-tailed unpaired t test, $p < 0.0001$). k–n Representative confocal images of the retrogradely labeled cells in control (k) and in *Lmx1a/b* cKO mice (m) 17 days after injection in the ventral striatum at P10 (TH in red, AAV-Retro-GFP in green and DAPI in blue). l, *n* Higher magnification in the VTA and SNpc as indicated by the dashed boxes in upper images k, m. Scale bars: c, d, e, f, 250µm; h, k, m, 500µm; l, n, 100µm.

shows a decrease of mDA axon density in the dorso-posterior striatal region (Fig. 2h, i and Supplementary Fig. 2g). No significant defect was observed in other known regions innervated by mDA neurons (Supplementary Fig. 4). We also used iDISCO brain clearing [20] combined with TH immunostaining and light-sheet whole-brain imaging to further analyze the DA system. The whole-brain analysis of TH immunostaining confirmed the lack of DA axons in the dorso-posterior striatum, but no other obvious defect could be detected in *Lmx1a/b* cKO mice brains (Fig. 2j).

Since dopamine was shown to induce synapse formation *in vitro* [21], we evaluated the physiological consequences of a lack of DA axons in dorsal striatum. Post-synaptic currents (PSCs) were recorded in the dorsal and ventral striatum of *Lmx1a/b* cKO mice and control littermates using whole-cell patch-clamp recordings (Fig. 2k–m). Analysis of miniature inhibitory and excitatory PSC in the dorsal striatum revealed a decrease in the frequency of both excitatory and inhibitory synaptic inputs (Fig. 2l). These data are consistent with a lack of DA innervation in the dorsal striatum observed in *Lmx1a/b* cKO mice. Inversely, we found an increase in the frequency of excitatory and inhibitory synaptic inputs in the ventral striatum of *Lmx1a/b* cKO mice (Fig. 2m). To confirm a potential axon-targeting defect, we examined specific axon projections of DA neurons from the SNpc and VTA. We performed both anterograde and retrograde tracing experiments. First, we used a

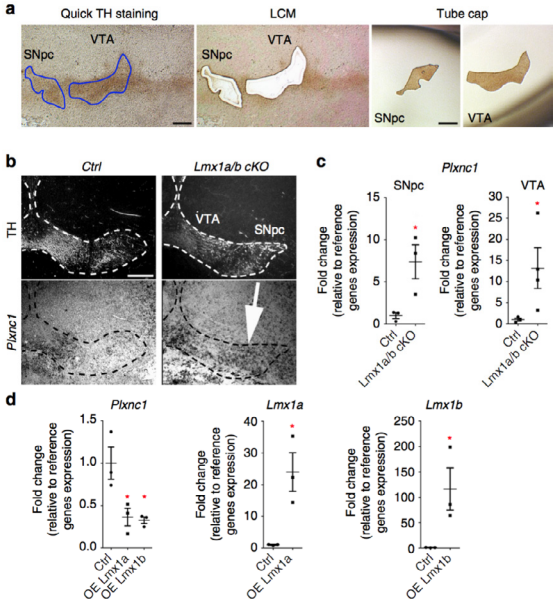

Fig. 4 | Lmx1a/b regulate the expression of the axon guidance receptor Plxnc1. a Images of brain tissue section following quick TH staining, before LCM and in the tube cap after LCM. b *In situ* hybridization for Plxnc1 expression in ventral midbrain coronal sections of control and *Lmx1a/b cKO* mice at P1. c RT-qPCR analysis of Plxnc1 expression specifically in SNpc and VTA neurons isolated with LCM (SNpc: n = 3, two-tailed unpaired t test, p = 0.0353; VTA: n = 3 controls and 4 *Lmx1a/b cKO*, one-tailed Mann–Whitney U, p = 0.0286). d RT-qPCR quantification of Plxnc1 expression after Lmx1a and Lmx1b overexpression in ventral midbrain primary cell cultures at P1 (n = 3 independent cultures; for Plxnc1: one-way ANOVA with Tukey's post test, * $p < 0.05$; for Lmx1a and Lmx1b: one-tailed Mann–Whitney U, p = 0.05). Scale bars: 200 µm.

Cre recombinase-dependent viral vector expressing green fluorescent protein (GFP) for labeling mDA neurons and their axonal projections [22, 23]. Ten days after birth, *Lmx1a/b cKO* and control (*Dat*$^{cre/+}$) mice received stereotaxic injections of AAV-FLEx-GFP in the SNpc (Fig. 3a–f). Upon Cre-mediated recombination, infected DA neurons expressed GFP. Histological analyses showed that in both the controls and *Lmx1a/b cKO* mice SNpc and part of the VTA neurons expressed GFP following AAV-FLEx-GFP injection (Fig. 3c, d). Analysis of GFP axons innervating the striatum corroborates with the axon-targeting defect observed with TH immunostaining in *Lmx1a/b cKO* mice. In control animals, GFP axons could be found in the entire striatal region, whereas in *Lmx1a/b cKO* mice, GFP axons were absent from the dorsal striatal region (Fig. 3e, f). We next confirmed this phenotype by performing stereotaxic injections of a retrograde adeno-associated viral vector (AAV-Retro-GFP [24]) in the ventral striatum (Fig. 3g–n). When injected in control animals, backfilled neurons were observed predominantly in the VTA (Fig. 3j–l). In contrast, injection of AAV-Retro-GFP in the

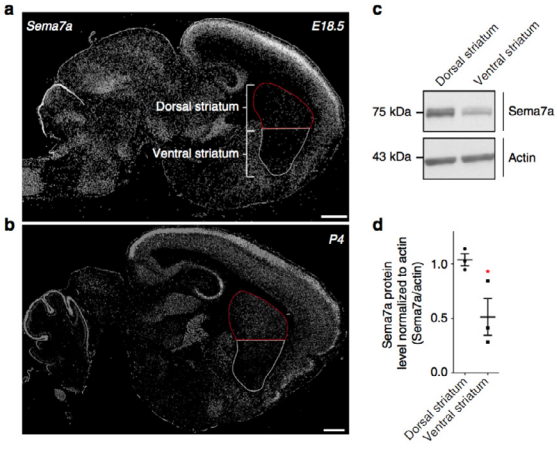

Fig. 5 | The axonal guidance repellent cue Sema7a shows higher expression in the dorsal than in the ventral striatum. a, b *In situ* hybridization for Sema7a on a sagittal section from embryonic day 18.5 and from post-natal day 4 mouse brains (from Allen Brain Atlas). The dorsal striatum (delineated in red) expresses more Sema7a than the ventral striatum. c, d Western blot and quantification of Sema7a protein level in the dorsal and ventral striatum at P1 (n = 3, two-tailed unpaired t test, p = 0.0418). Scale bar: 500 µm.

ventral striatum of *Lmx1a/b c*KO mice resulted in numerous labeled neurons not only in the VTA but also in the SNpc (Fig. 3m, n). Accordingly, we observed the same result using the retrograde tracer Fluorogold (Supplementary Fig. 5).

Lmx1a and Lmx1b regulate Plxnc1 expression

Transcription factors can positively or negatively regulate the expression of hundreds of genes [8, 25, 26]. To identify the genes regulated by Lmx1a/b during the axonal development of mDA neurons, we performed gene expression profiling of *Lmx1a/b* mutant and control embryos at E15.5. We used laser-capture microdissection (LCM) to isolate TH-immunolabeled regions of the SNpc and VTA from controls and *Lmx1a/b c*KO mice (Fig. 4a), followed by next-generation RNA sequencing (RNA-seq). We found 225 genes differently expressed between *Lmx1a/b c*KO and control animals (Supplementary Table 1 and Supplementary Fig. 6). We then searched our RNA-seq list to find genes related to axon development. Among the differently expressed genes, RNA for the axon guidance receptor *Plxnc1* was found to be significantly more abundant in *Lmx1a/b* mutants than in controls. To confirm the messenger RNA (mRNA) sequencing data, we performed *in situ* hybridization for *Plxnc1* on midbrain sections at P1 (Fig. 4b). As previously reported for mDA neurons of wild-type mice, *Plxnc1* expression was found restricted to the VTA [27], with no apparent expression detected in the SNpc (Fig. 4b). In contrast, mDA neurons from both the VTA and SNpc expressed significantly higher levels of *Plxnc1* in *Lmx1a/b c*KO mice (Fig. 4b). Quantification of relative *Plxnc1* mRNA transcript levels in either the SNpc or VTA regions revealed that *Plxnc1* was, respectively, seven and 11-fold more abundant in these two regions in *Lmx1a/b* mutant mice at P1 (Fig. 4c). Gain-of-function experiments by overexpressing Lmx1a or Lmx1b in ventral midbrain primary cell cultures also induced a significant decrease in *Plxnc1* mRNA levels, confirming the repressive role of Lmx1a/ b on *Plxnc1* (Fig. 4d).

Sema7a/Plxnc1 interaction mediates repulsion of VTA neurons

Plxnc1 is a known guidance receptor for the membrane-associated GPI (glycosylphosphatidylinositol)-linked semaphorin 7a (Sema7a). Semaphorins are a large family of soluble and membrane bound proteins largely known for their repulsive function on developing axons [28]. *In vitro* studies have shown that Sema7a binds directly to Plxnc1 [29]. However, the functional significance of Sema7a interaction with Plxnc1 expressed by mDA neurons from the VTA remains unknown. Using protein extracts from dorsal and ventral striatum, we quantified the relative abundance of Sema7a protein and found that it was three times more abundant in the dorsal striatum than in the ventral striatum (Fig. 5 and Supplementary Fig. 7). On the basis of the respective level of expression of Plxnc1 in the VTA and Sema7a in the dorsal striatum, we hypothesized that Sema7a acts as a repellent cue on mDA axons from the VTA, and consequently restricts their projections to the ventral striatum. To address this hypothesis, we tested *in vitro* the effect of Sema7a on ventral midbrain primary cells coming from either the VTA or SNpc. We precisely dissected ventral midbrain regions containing the SNpc and VTA from 1-day-old *Pitx3*$^{Gfp/+}$ mice and cultured them separately for 2 days. In these mice, all mDA neurons express GFP [30], allowing a more accurate dissection of the VTA and SNpc regions. We then exposed these cultures to Sema7a for 2h and measured the axonal and dendritic arborization of mDA neurons. Sholl analysis revealed a decrease in both dendritic and axonal complexity of mDA neurons from the VTA but not from the SNpc (Fig. 6a–c). We obtained the same results using VTA and SNpc explants cultured in collagen gel matrix and exposed to Sema7a for 2h. Both the

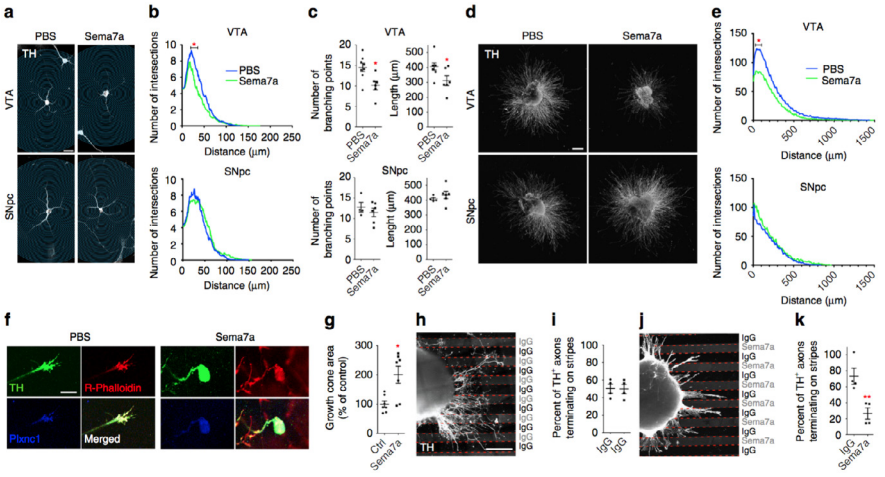

Fig. 6 | In vitro experiments showing the effect of Sema7a on VTA and SNpc neurons. a, c Sholl analysis on ventral midbrain primary VTA or SNpc neuron cultures exposed to PBS or Sema7a. a Examples of confocal images of VTA and SNpc neurons with their respective Sholl intersection circle mask. b, c Quantitative analysis of the VTA and SNpc neurite intersection profiles, number of branches, and neurite length (SNpc: 71 neurons analyzed from 5 independent cultures; VTA: 114 neurons analyzed from 7 independent cultures; b: two-way ANOVA, and the Sidak test was used for post hoc comparisons, * $p < 0.05$; c: two-tailed unpaired *t* test, $p_{(VTA\ Branch)} = 0.0137$, $p_{(VTA\ length)} = 0.0335$, $p_{(SNpc\ Branch)} = 0.4370$, $p_{(SNpc\ length)} = 0.4395$). d Examples of embryonic ventral midbrain explants from E14.5 Pitx3-GFP embryos grown in collagen matrix then exposed to PBS (control) or Sema7a. e Sholl analysis of the neurite intersection profiles for the VTA and SNpc explants exposed to PBS or Sema7a (a total of 34 explants from 8 independent cultures, 20 explants from VTA and 14 from SNpc; two-way ANOVA, and the Sidak test was used for post hoc comparisons, *p < 0.05). f Confocal images of growth cones from VTA explants exposed to Sema7a or PBS. g Growth cone size measurements expressed as a percentage of control ($n = 7$ independent cultures; 65 growth cones for Sema7a and control were used in each of the 7 experiments, Mann–Whitney U, $p = 0.0175$). h–k Confocal images of stripe assay and quantification of the number of axons terminating on stripes for VTA explants grown on the control alternating IgG stripes and the Sema7a stripes alternating with IgG stripes. Dotted lines delineate the stripes (i, $n = 29$ explants in 4 independent experiments, two-tailed unpaired *t* test, $p = 0.9349$; k, $n = 27$ explants in 4 independent experiments, two-tailed unpaired *t* test, $p = 0.0091$). Scale bars: a, 20 µm; d, f, h, 250 µm; j, 10 µm.

length and complexity of axons from VTA explants were reduced in the presence of Sema7a, while Sema7a had no effect on mDA axons from SNpc explants (Fig. 6d, e). Interestingly, we also observed a significant enlargement of mDA growth cones from VTA explants following treatment with Sema7a (Fig. 6f, g). Because Sema7a is a membrane-associated GPI-anchored protein and not a diffusible cue, we also tested the axon response of VTA explants grown on alternating stripes of Sema7a. Control stripes had no effect on mDA axons from the VTA as they grew randomly from the explant (Fig. 6h, i). In contrast, mDA axons displayed a clear avoidance for Sema7a stripes when provided with a choice between the control and Sema7a substrate (Fig. 6j, k). We then further assess if the ectopic expression of Plxnc1 observed in SNpc mDA neurons of *Lmx1a/b c*KO mice has a functional impact on axonal response to Sema7a. We cultured SNpc explants from control and *Lmx1a/b c*KO mice on alternating stripes of Sema7a and quantified mDA axons terminating on Sema7a. Explants from control SNpc grew randomly on either Sema7a or IgG stripes, confirming that Sema7a has no guidance effect on mDA axons from the SNpc. In contrast, mDA axons from SNpc explants of *Lmx1a/b c*KO mice displayed a clear avoidance for Sema7a stripes (Supplementary Fig. 8). Altogether, these experiments showed that Sema7a functions as

a chemorepulsive and/or non-permissive signal for mDA axons from the VTA. The specific expression of Sema7a in dorsal striatum may therefore contribute to the dorsal vs. ventral organization of the nigrostriatal and mesolimbic pathways, respectively.

mDA projections in the striatum is altered in Sema7a KO mice

To further study the role of Sema7a on the development of mDA axons, we analyzed the axon projections of mDA neurons in the absence of Sema7a (Fig. 7a–j). Because Plxnc1 expression is restricted to VTA mDA neurons, loss of Sema7a should affect mDA axon projections to the ventral striatum and nucleus accumbens. As expected, detailed analysis of Sema7a KO mice revealed that mDA axons expressing Plxnc1 were more widely distributed in the dorsal striatum than in control mice (Fig. 7a–d). Quantification of TH and Plxnc1 axonal density in dorsal and ventral striatal regions suggest that TH positive and Plxnc1 positive axons extend more dorsally in *Sema7a* KO mice (Fig. 7e–g and Supplementary Fig. 9). Stereological counting of mDA neurons in *Sema7a* KO and control mice did not reveal any significant difference in the total number, the distribution of mDA neurons (Fig. 7h–j), or in the expression of Plxnc1 (Supplementary Fig. 10). To confirm a potential axon-targeting defect of VTA DA neurons in the dorsal striatum, we examined the specific axon projections of DA neurons by injecting an AAV-Retro-GFP into the dorsal striatal region (Fig. 7k, l). When injected in control animals, backfilled neurons were observed predominantly in the SNpc (Fig. 7m, n). However, injection of AAV-Retro-GFP in the dorsal striatum of *Sema7a* KO mice resulted in numerous labeled neurons in VTA (Fig. 7o–q). These data suggest that Sema7a in the dorsal striatum functions as a repellent factor for Plxnc1-containing axons.

Forced expression of Plxnc1 mimics Lmx1a/b cKO phenotype

Our *in vitro* and *in vivo* experiments suggest that the interaction of Sema7a with Plxnc1 could be responsible for the topographical segregation between the two main DA circuits: the nigrostriatal and mesolimbic pathways. To determine whether the aberrant Plxnc1 expression observed in SNpc neurons of the *Lmx1a/b c*KO mice could lead to axon targeting defects, we generated a transgenic mouse in which Plxnc1 is produced by all DA neurons. These animals were generated by pronuclear injection of a plasmid in which the TH promoter drives *Plxnc1* and td-Tomato expression (TH-Plxnc1-Ires-tdTomato; Fig. 7r–x). In these mice, the expression of the td-Tomato reporter gene was visualized in virtually all mDA neurons (Fig. 7r, s). We also measured the expression level of *Plxnc1* by RT-qPCR from 1-mm thick ventral midbrain sections and found that these mice showed a more than fivefold increase of the normal level of *Plxnc1* expression (Fig. 7t). Stereological counting of mDA neurons labeled for TH and td-Tomato showed no difference in the total mDA neuron number or distribution (Fig. 7u). However, analysis of DA axon projections of these mutant animals revealed a very similar axon-targeting defect to the one observed in *Lmx1a/b c*KO mice (Figs. 2, 7v, w). The density of DA axons innervating the dorsal and posterior striatal region of these mutants was also reduced (Fig. 7x), thus indicating that the nigrostriatal circuits were defective in these mutants.

Otx2 and Lmx1a/b regulate Plxnc1 expression in mDA neurons

Among the transcription factors expressed by mDA neurons, very few have a restricted localization in either the VTA or SNpc [31]. The transcription factor Otx2 is restricted to VTA neurons and has been shown to regulate the subtype identity of mDA neurons [32, 33]. In contrast to Otx2, Lmx1a and Lmx1b are found in both SNpc and VTA neurons. Our results show that Lmx1a/b are repressing Plxnc1, but because Plxnc1 remains expressed in the

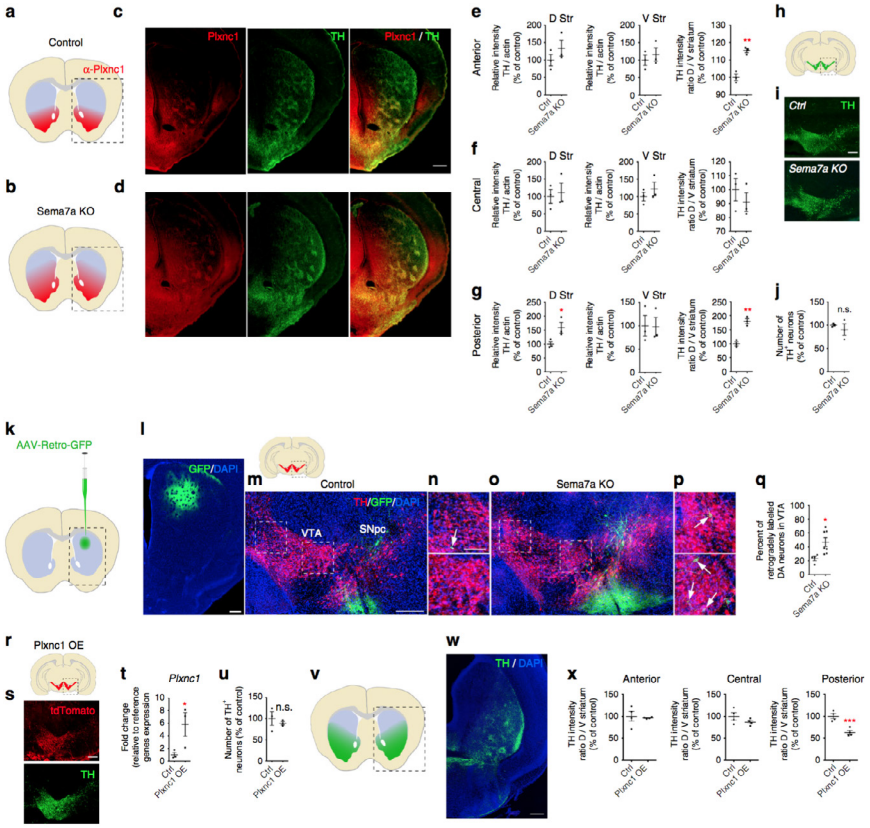

Fig. 7 | Sema7a/Plxnc1 interaction regulates mDA axon guidance. a, b Schematic representations of coronal views of the axonal projections in the striatum showing that Plxnc1 mDA axons (in red) are more numerous in the dorso-posterior striatal region of *Sema7a* KO mice (b) compared to control animals (a). c, d Confocal images of TH and Plxnc1 immunostained striatal sections from control and *Sema7a* KO mice. e–g Quantification of TH relative optical density at different striatum levels ($n = 3$, two-tailed unpaired t test, $p_{(Ant\ D)} = 0.2855$, $p_{(Ant\ V)} = 0.5355$, $p_{(Cent\ D)} = 0.7461$, $p_{(Cent\ V)} = 0.3933$, $p_{(Post\ D)} = 0.0491$, $p_{(Post\ V)} = 0.9514$, $p_{(Ant\ D/V)} = 0.0023$, $p_{(Cent\ D/V)} = 0.4418$, $p_{(Post\ D/V)} = 0.0023$). h Schematic representation of coronal section of mouse brain at the midbrain level. Dashed line indicates the boundaries of the pictures shown in i. i Representative confocal images of the VTA and SNpc for Control and *Sema7a* KO mice. j Stereological counts of mDA neurons in control and *Sema7a* KO mice at P1 ($n = 3$, two-tailed unpaired t test, $p = 0.4843$). k Schematic representation of the injection site of the AAV-retro-GFP in the dorsal striatum. l Representative confocal images of the injection site in the dorsal striatum. m–p Representative confocal images of the retrogradely labeled cells in control (m, n) and in *Sema7a* KO mice (o, p) 17 days after injection in the dorsal striatum at P30 (TH in red, AAV-Retro-GFP in green and DAPI in blue). n,p Higher magnifications in the VTA as indicated by the dashed boxes in m, o. q Quantification of the percentage of retrogradely labeled neurons in VTA ($GFP^+\ TH^+$ in VTA on total $GFP^+\ TH^+$; $n = 4$ for controls and $n = 7$ for *Sema7a* KO mice; two-tailed unpaired t test, $p = 0.0245$). r, s Schematic and confocal images of TH labeling in Plxnc1 overexpression mice showing a loss of DA innervation in dorso-posterior striatum. t RT-qPCR quantification of *Plxnc1* from the ventral midbrain section of control and Plxnc1 overexpression mice at P1 ($n = 3$, one-tailed unpaired t test, $p = 0.0322$). u Stereological counts of mDA neurons in control and Plxnc1 overexpression mice at P1 ($n = 3$, two-tailed unpaired t test, $p = 0.5431$). v, w Schematic and confocal images of TH and td-Tomato in the VTA and SNpc for one hemisphere. The reporter tdTomato indicates that all mDA neurons express the transgene (Plxnc1-ires-tdTomato). x Optical density measurements of TH-positive axons in the striatum at three antero–posterior levels ($n = 4$, two-tailed unpaired t test, $n = 4$, Mann–Whitney U, $p_{(Ant\ D/V)} = 0.6857$, two-tailed unpaired t test, $p_{(Cent\ D/V)} = 0.1945$, $p_{(Post\ D/V)} = 0.0019$). Scale bars: 200 µm except n, p, 100 µm.

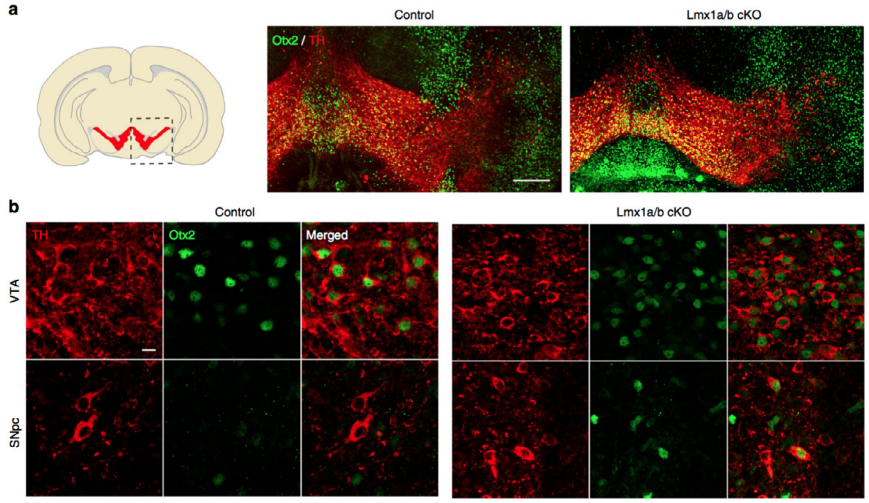

Fig. 8 | Otx2 and Lmx1a/b control Plxnc1 expression in the VTA. a, b Confocal images of Otx2 immunostaining in TH-positive cells in coronal midbrain sections of control and *Lmx1a/b c*KO mutant mice showing ectopic Otx2 expression in SNpc mDA neurons. c Quantification of the number of mDA neurons in SNpc with ectopic expression of Otx2 ($n = 3$, two-tailed unpaired *t* test, $p = 0.0015$). d Rt-qPCR quantification of Otx2 in VTA and SNpc isolated from control and *Lmx1a/b c*KO with LCM (VTA: $n = 3$ for control and $n = 5$ for *Lmx1a/b c*KO, two-tailed unpaired *t* test, $p = 0.9128$; in SNpc $n = 3$, one- tailed Mann–Whitney U, $p = 0.05$). e Overexpression of Otx2 in primary cell cultures leads to an increase of Plxnc1 expression as quantified by RT-qPCR ($n = 3$ independent cultures; for Plxnc1: two-tailed unpaired *t* test, $p = 0.03$; for Otx2: Mann–Whitney U, $p = 0.0286$). f RT-qPCR quantification of Otx2 in mDA primary cell cultures following Lmx1a and Lmx1b overexpression ($n = 8$ for control, $n = 7$ for Lmx1a and $n = 5$ for Lmx1b; one-way ANOVA with Tukey's multiple comparison test, not significant). g Representative images of TH and Otx2 immunolabeling from E15.5 *Lmx1a/b c*KO embryo at E15.5 showing SNpc neurons co-expressing Otx2 and TH (arrows) before and after LCM. Right panels are high magnification of the left panels. h RT-qPCR quantification of Plxnc1 expression from LCM isolated cells co-expressing Otx2 and TH in VTA and SNpc from control and *Lmx1a/b c*KO embryos. For control SNpc, TH-positive cells were isolated ($n = 3$, 5–8 cells per embryo, one-way ANOVA with Tukey's multiple comparison test, not significant between groups expressing Plxnc1). Image on the right is a representative image of the gel showing the RT-qPCR product. Plxnc1 was not detected in mDA neurons of SNpc from control. Scale bars: a, 200 µm; b, 10 µm; g (left), 100 µm, (right), 10 µm.

VTA, we also determined whether Otx2 could contribute to the regulation of *Plxnc1* expression in the VTA. First, we performed double immunolabeling to determine whether Otx2 could also be ectopically expressed in the SNpc of *Lmx1a/b c*KO mice. As previously reported, Otx2 was restricted to DA neurons of the VTA in control mice [34, 35]. However, we observed numerous DA neurons co-expressing Otx2 and TH in the SNpc of *Lmx1a/b c*KO mice at P1 (Fig. 8a–c). We next validated if Otx2 expression is upregulated in *Lmx1a/b c*KO by quantifying Otx2 expression in the VTA and SNpc samples obtained by LCM at P1. We found that Otx2 expression was significantly higher in the SNpc of *Lmx1a/b c*KO mice compared to the control animals (Fig. 8d). However, Otx2 transcript levels were not significantly changed in the VTA of *Lmx1a/b c*KO animals. We then overexpressed Otx2 using transient transfection in ventral midbrain primary cell cultures and measured *Plxnc1* expression by RT-qPCR. Overexpression of Otx2 induced a significant increase of *Plxnc1* transcript levels (Fig. 8e). Finally, to understand the mechanisms controlling subtype identity in mDA neurons, we overexpressed Lmx1a and Lmx1b in ventral midbrain primary cell cultures and measured *Plxnc1* and *Otx2* expression by RT-qPCR. As predicted, Lmx1a

and Lmx1b overexpression led to a decrease in *Plxnc1* transcripts (Fig. 4e). However, Lmx1a and Lmx1b overexpression seemed not to be sufficient to repress *Otx2* (Fig. 8f). To test if the ectopic Otx2 + mDA neurons in SNpc of *Lmx1a/b c*KO mice express Plxnc1, we performed rapid double immunolabeling for TH and Otx2, followed by LCM to isolate double-labeled neurons (Fig. 8g). RT-qPCR quantification revealed that similarly to VTA mDA neurons, Otx2- and TH-expressing neurons in SNpc of *Lmx1a/b c*KO mice also express *Plxnc1* (Fig. 8h). Remarkably, we could not detect *Plxnc1* expression in mDA neurons of SNpc from control animals. Altogether these results indicate that *Plxnc1* expression in the VTA is maintained by the transcriptional control of Otx2, while in SNpc, Lmx1a and Lmx1b repress *Plxnc1* expression. Consequently, the specific topography of VTA and SNpc axon projections to the striatum appears to be established by the presence or the absence of Plxnc1 in mDA axons.

Discussion

The proper functioning of the brain's DA system depends on the precise organization of DA circuits during development. Here, we show that transcriptional regulation of Plxnc1 by Lmx1a/b and Otx2 controls the formation and the topographical organization of the nigrostriatal and mesolimbic pathways. We found that the inactivation of Lmx1a/b in post-mitotic mDA neurons leads to aberrant nigrostriatal axon projections. We also discovered that Lmx1a/b function as a transcriptional repressor (directly or indirectly) of *Plxnc1* expression. Our *in vitro* data and mutant mice analysis revealed a new mechanism whereby the interaction of Sema7a/Plxnc1 regulates the striatal innervation.

In addition to their roles in the early development of mDA progenitors [15, 16], we showed here that Lmx1a and Lmx1b have other functions in post-mitotic mDA neurons. By controlling Plxnc1 expression, Lmx1a, Lmx1b, and Otx2 regulate the proper organization of nigrostriatal and mesolimbic axon projections. In SNpc, Lmx1a and Lmx1b are required and sufficient to repress Plxnc1. Lmx1a and Lmx1b are also required for the repression of Otx2 in the SNpc, but were not sufficient to repress Otx2 in primary ventral midbrain cell cultures. In the VTA, Lmx1a/b are required and sufficient for Plxnc1 repression, but they are not required or sufficient to repress Otx2. Our gain-of-function experiments also showed that Otx2 can drive Plxnc1 expression in mDA primary cultures. Altogether, our data indicate that Plxnc1 expression is precisely controlled in mDA neurons by the coordinated action of Lmx1a, Lmx1b, and Otx2. In the VTA, all three transcription factors are present. Lmx1a/b repress Plxnc1, but Otx2 promotes and possibly maintains Plxnc1 expression. In the SNpc, Otx2 is normally absent, and both Lmx1a and Lmx1b repress Plxnc1. Following Lmx1a/b ablation, we found ectopic Otx2 expression in mDA neurons located in the SNpc and these neurons also express Plxnc1. In addition, RT-qPCR experiments in *Lmx1a/b c*KO mice revealed that *Otx2* expression was only increased in the SNpc, whereas in the VTA, *Otx2* expression was unchanged. According to these results, it is likely that another transcription factor, only present in the SNpc, cooperatively contributes to Otx2 repression in the SNpc.

Previous anatomical studies described the expression of Sema7a in the striatum and Plxnc1 in the VTA, thus suggesting a possible role of these proteins in the guidance of mDA neurons [7, 27]. We showed here that Sema7a is more abundant in the dorsal compared to the ventral striatal region and found that Sema7a repels Plxnc1-containing mDA axons from the VTA. In Sema7a knockout mutant mice, Plxnc1 axons extend more dorsally in the striatum, whereas transgenic mice overexpressing Plxnc1 in mDA neurons lack DA innervations in the dorsal striatum. These *in vivo* data indicate that the Sema7a/Plxnc1

interaction controls DA axon targeting in the striatum. In addition, our *in vitro* assays revealed that Sema7a functions as a repellent cue for VTA axons expressing Plxnc1. The repellent function of Sema7a on mDA axons from the VTA reported here represents a major mechanism assuring the proper topographical innervation of the main mDA target region, the striatum. It is reasonable to think that other axon guidance cues contribute to attract mDA neurons in the striatum. Indeed, a gradient of Netrin-1 is present in the striatum. The latero-ventral region of the striatum is rich in Netrin-1, whereas the medio-dorsal striatum is poor in Netrin-1. Although all mDA neurons express the receptor DCC [36], VTA axons prefer a higher Netrin-1 concentration than the SNpc axon [6]. Accordingly, null mice for Netrin-1 show a loss of innervation in the dorsal striatum [6]. These data suggest that mDA neurons require both Sema7a and Netrin-1 cues to correctly innervate their striatal targets. SNpc neurons, which do not express Plxnc1, are not repelled by the high concentration of Sema7a in the dorsal striatum, but require Netrin-1 to attract them toward the dorsal striatum. The mechanism by which Netrin-1 differently attracts VTA and SNpc DA axons is not fully understood, but the convergence of guidance signals could direct the trajectory of mDA neurons. A recent study showed that motor growth cones synergistically integrate both Netrin-1 and Ephrin signals. Receptors for these ligands can form a complex that acts in synergy on a common downstream effector [37]. In the striatum, Sema7a and Netrin-1 could also synergistically interact at the receptor level and control mDA innervation in the striatum. In *Lmx1a/b c*KO mice, we found SNpc axons redirected ventrally. Although our electro- physiological recordings suggested an increase in DA in the ventral striatum, we did not observe a significant increase in DA axon density in this region. One possible explanation is that SNpc axonal branching is limited by another cue such as the high Netrin-1 concentration. It is also possible that although SNpc axons are repelled ventrally, they compete with VTA axons for the synaptic space, which in turn limits the number of SNpc axons ventrally.

The mechanism regulating DA innervation in the striatum reported here sheds new light on how the VTA and SNpc establish their connections with the striatum. However, anatomical and genetic evidence indicate that mDA neurons can be subdivided into more distinct subpopulations [2, 3, 38, 39]. In the striatum, subregions can be divided based on their neurochemical content and two main compartments can be defined, the striosomes and the surrounding matrix [40]. In the SNpc, neurons from the ventral tier are believed to preferentially innervate the striosomes, whereas the ones from the dorsal tier preferentially innervate the matrix compartment [38]. In our study, we did not observe any changes in the striosomes and matrix innervation in either *Lmx1a/b c*KO, *Sema7A* KO, or *Plxnc1* overexpressing mice. These data suggest that the specific DA projections toward these striatal compartments are regulated by other developmental mechanisms. On the basis of gene expression, multiple molecularly distinct subgroups of mDA neurons have been identified [39], but the precise axon projections of these subpopulations and the guidance mechanisms regulating these subpopulations remain to be discovered.

Our findings have important implications for stem cell engineering and transplantation for PD. This chronic progressive neurodegenerative disorder is characterized by the selective loss of DA-containing neurons in the SNpc. The identification of Plxnc1 as a main guidance receptor allowing subset-specific axon targeting of mDA neurons provides a valuable tool to improve the efficiency of reconnection of newly generated neuron grafts. Indeed, to replace degenerated SNpc mDA neurons that will innervate and integrate specifically in the dorsal striatum, newly generated neurons should not express Plxnc1. In a recent study, forced expression of Otx2 has been used in human embryonic stem cells (hESCs) to

generate DA neurons. When grafted in the SNpc, these hESC-derived DA neurons were able to innervate the forebrain structures, but displayed a strong preference for VTA-specific target regions with few axons innervating the dorsal striatum [41]. According to our results, Otx2 promotes Plxnc1 expression, and thus it is likely that the grafted neurons in this study innervated VTA target regions because they express Plxnc1. Further studies are needed to test the efficiency of a cell replacement therapy using mDA neurons that lack Plxnc1 expression.

In sum, our work shows a new mechanism for Lmx1a and Lmx1b during mid-gestational stages to control the DA innervation of the striatum. Other mechanisms involved in the development of the dopamine circuits still remain largely unknown, despite the involvement of these circuits in important physiological functions and in various mental disorders such as schizophrenia. Interestingly, three SNIPs in LMX1A and one in LMX1B were found associated with schizophrenia, and were the same as those previously identified in PD [42]. However, further studies will be necessary to evaluate the role of these SNIPs in regulating Plxnc1 expression and the development of the DA system.

Acknowledgements

This work was mainly supported by a grant from the Natural Sciences and Engineering Research Council of Canada (NSERC: 418391-2012) and by Canadian Institutes of Health Research Grants MOP 311120 to M.L. A.C. received a scholarship from the Fondation de l'institut universitaire en santé mentale de Québec, and from the Centre thématique de recherche en neurosciences (CTRN). M.L. is a FRSQ Chercheur-Boursier. R.J.P. received funding from Stichting ParkinsonFonds and the Netherlands Organization for Scientific Research (ALW-VICI). S.-L.A. is supported by the Fran*cis* Crick Institute, which receives its core funding from Cancer Research UK (FC001089), the UK Medical Research Council (FC001089), and the Wellcome Trust (FC001089); and by Parkinson's UK research grant G0617. E.M. is funded by Parkinson's Disease UK (F1501). We thank Veronique Rioux for technical assistance. We thank Meng Li for sharing Pitx3-GFP mice and Thomas Perlmann for Lmx1a flox mice. We thank Dr Armen Saghatelyan for his useful comments and Dr Louis-Eric Trudeau for sharing Sema7a KO mice. We also thank the Plateforme d'Outils Moléculaires (https://www. neurophotonics.ca/fr/pom) for the production of the viral vectors used in this study.

Author contributions

A.C. analyzed mutant mice, performed, and analyzed most of the histological preparations, *in situ* hybridization, immunostainings, explants and stripe assay, and retrograde and anterograde tracing experiments, and performed dissection and genotyping for all mice used in this study. A.C. and M.L. wrote the article. A.C. and H.D.-B. performed the LCM and made the cDNA library for LCM samples; H.D.-B. and E.M. performed and analyzed qRT-PCR experiments. G.B. performed and analyzed explant experiments. A.D. performed retrograde labeling experiments on Sema7a KO. C.S. performed and analyzed electrophysiological experiments. E.M., M.I.A., and M.L. performed and analyzed mRNA sequencing at E15.5. M.S.P. performed and analyzed western blot experiments, neuron counting at P15, and stripe assay on *Lmx1a/b c*KO embryos. A.C., G.B. and J.C. performed mDA primary cell culture experiments. C.A., D.C. and M.L. built the light- sheet microscope and C.A. performed imaging of transparent brains. S.L. and R.J.P. performed Plxnc1 expression analysis on

Sema7a KO. Funding acquisition, M.L.; S.-L.A., E.M. and M.L.. supervised the study. All authors contributed to manuscript preparation, read and approved the final manuscript.

References

1. Bjorklund, A. & Dunnett, S. B. Dopamine neuron systems in the brain: an update. *Trends Neurosci* 30, 194–202 (2007).
2. Prensa, L. & Parent, A. The nigrostriatal pathway in the rat: a single-axon study of the relationship between dorsal and ventral tier nigral neurons and the striosome/matrix striatal compartments. *J Neurosci* 21, 7247–7260 (2001).
3. Aransay, A. *et al.* Long-range projection neurons of the mouse ventral tegmental area: a single-cell axon tracing analysis. *Front Neuroanat* 9, 59 (2015).
4. Gauthier, J. *et al.* The axonal arborization of single nigrostriatal neurons in rats. *Brain Res* 834, 228–232 (1999).
5. Matsuda, W. *et al.* Single nigrostriatal dopaminergic neurons form widely spread and highly dense axonal arborizations in the neostriatum. *J Neurosci* 29, 444–453 (2009).
6. Li, J. *et al.* Evidence for topographic guidance of dopaminergic axons by differential Netrin-1 expression in the striatum. *Mol Cell Neurosci* 61, 85–96 (2014).
7. Prestoz, L., Jaber, M. & Gaillard, A. Dopaminergic axon guidance: which makes what? *Front Cell Neurosci* 6, 32 (2012).
8. Doucet-Beaupre, H. *et al.* Lmx1a and Lmx1b regulate mitochondrial functions and survival of adult midbrain dopaminergic neurons. *Proc Natl Acad Sci USA* 113, E4387–E4396 (2016).
9. Laguna, A. *et al.* Dopaminergic control of autophagic-lysosomal function implicates Lmx1b in Parkinson's disease. *Nat Neurosci* 18, 826–835 (2015).
10. Millen, K. J., Millonig, J. H. & Hatten, M. E. Roof plate and dorsal spinal cord dl1 interneuron development in the dreher mutant mouse. *Dev Biol* 270, 382–392 (2004).
11. Krawchuk, D. & Kania, A. Identification of genes controlled by LMX1B in the developing mouse limb bud. *Dev Dyn* 237, 1183–1192 (2008).
12. Szabo, N. E. *et al.* Hoxb8 intersection defines a role for Lmx1b in excitatory dorsal horn neuron development, spinofugal connectivity, and nociception. *J Neurosci* 35, 5233–5246 (2015).
13. Andersson, E. *et al.* Identification of intrinsic determinants of midbrain dopamine neurons. *Cell* 124, 393–405 (2006).
14. Ono, Y. *et al.* Differences in neurogenic potential in floor plate cells along an anteroposterior location: midbrain dopaminergic neurons originate from mesencephalic floor plate cells. *Development* 134, 3213–3225 (2007).
15. Deng, Q. *et al.* Specific and integrated roles of Lmx1a, Lmx1b and Phox2a in ventral midbrain development. *Development* 138, 3399–3408 (2011).
16. Yan, C. H. *et al.* Lmx1a and lmx1b function cooperatively to regulate proliferation, specification, and differentiation of midbrain dopaminergic progenitors. *J Neurosci* 31, 12413–12425 (2011).
17. Kadkhodaei, B. *et al.* Nurr1 is required for maintenance of maturing and adult midbrain dopamine neurons. *J Neurosci* 29, 15923–15932 (2009).
18. Zhuang, X. *et al.* Targeted gene expression in dopamine and serotonin neurons of the mouse brain. *J Neurosci Methods* 143, 27–32 (2005).
19. Stott, S. R. *et al.* Foxa1 and foxa2 are required for the maintenance of dopaminergic properties in ventral midbrain neurons at late embryonic stages. *J Neurosci* 33, 8022–8034 (2013).
20. Renier, N. *et al.* iDISCO: a simple, rapid method to immunolabel large tissue samples for volume imaging. *Cell* 159, 896–910 (2014).
21. Fasano, C. *et al.* Dopamine facilitates dendritic spine formation by cultured striatal medium spiny neurons through both D1 and D2 dopamine receptors. *Neuropharmacology* 67, 432–443 (2013).
22. Saunders, A., Johnson, C. A. & Sabatini, B. L. Novel recombinant adeno- associated viruses for Cre activated and inactivated transgene expression in neurons. *Front Neural Circuits* 6, 47 (2012).
23. Schnutgen, F. *et al.* A directional strategy for monitoring Cre-mediated recombination at the cellular level in the mouse. *Nat Biotechnol* 21, 562–565 (2003).
24. Tervo, D. G. *et al.* A designer AAV variant permits efficient retrograde access to projection neurons. *Neuron* 92, 372–382 (2016).
25. Metzakopian, E. *et al.* Genome-wide characterization of Foxa2 targets reveals upregulation of

floor plate genes and repression of ventrolateral genes in midbrain dopaminergic progenitors. *Development* 139, 2625–2634 (2012).
26. Veenvliet, J. V. *et al.* Specification of dopaminergic subsets involves interplay of En1 and Pitx3. *Development* 140, 3373–3384 (2013).
27. Pasterkamp, R. J. *et al.* Expression patterns of semaphorin7A and plexinC1 during rat neural development suggest roles in axon guidance and neuronal migration. BMC *Dev Biol* 7, 98 (2007).
28. Pasterkamp, R. J. & Kolodkin, A. L. Semaphorin junction: making tracks toward neural connectivity. *Curr Opin Neurobiol* 13, 79–89 (2003).
29. Tamagnone, L. *et al.* Plexins are a large family of receptors for transmembrane, secreted, and GPI-anchored semaphorins in vertebrates. *Cell* 99, 71–80 (1999).
30. Zhao, S. *et al.* Generation of embryonic stem cells and transgenic mice expressing green fluorescence protein in midbrain dopaminergic neurons. *Eur J Neurosci* 19, 1133–1140 (2004).
31. Doucet-Beaupré, H. & Lévesque, M. The role of developmental transcription factors in adult midbrain dopaminergic neurons. *OA Neurosci* 1, (2013).
32. Di Salvio, M. *et al.* Otx2 controls neuron subtype identity in ventral tegmental area and antagonizes vulnerability to MPTP. *Nat Neurosci* 13, 1481–1488 (2010).
33. Panman, L. *et al.* Sox6 and Otx2 control the specification of substantia nigra and ventral tegmental area dopamine neurons. *Cell Rep*. 8, 1018–1025 (2014).
34. Chung, C. Y. *et al.* The transcription factor orthodenticle homeobox 2 influences axonal projections and vulnerability of midbrain dopaminergic neurons. *Brain* 133(Pt 7), 2022–2031 (2010).
35. Chung, C. Y. *et al.* Cell type-specific gene expression of midbrain dopaminergic neurons reveals molecules involved in their vulnerability and protection. *Hum Mol Genet* 14, 1709–1725 (2005).
36. Xu, B. *et al.* Critical roles for the netrin receptor deleted in colorectal cancer in dopaminergic neuronal precursor migration, axon guidance, and axon arborization. *Neuroscience* 169, 932–949 (2010).
37. Poliak, S. *et al.* Synergistic integration of Netrin and ephrin axon guidance signals by spinal motor neurons. *Elife* 4, (2015).
38. Gerfen, C. R., Herkenham, M. & Thibault, J. The neostriatal mosaic: II. Patch- and matrix-directed mesostriatal dopaminergic and non-dopaminergic systems. J. Neurosci. 7, 3915–3934 (1987).
39. Poulin, J. F. *et al.* Defining midbrain dopaminergic neuron diversity by single- cell gene expression profiling. *Cell Rep* 9, 930–943 (2014).
40. Gerfen, C. R. The neostriatal mosaic: multiple levels of compartmental organization. *Trends Neurosci* 15, 133–139 (1992).
41. Grealish, S. *et al.* Human ESC-derived dopamine neurons show similar preclinical efficacy and potency to fetal neurons when grafted in a rat model of Parkinson's disease. *Cell Stem Cell* 15, 653–665 (2014).
42. Bergman, O. *et al.* Preliminary evidence that polymorphisms in dopamine- related transcription factors LMX1A, LMX1B and PITX3 are associated with schizophrenia. *Prog Neuropsychopharmacol Biol Psychiatry* 34, 1094–1097 (2010).
43. Zhao, Z. Q. *et al.* Lmx1b is required for maintenance of central serotonergic neurons and mice lacking central serotonergic system exhibit normal locomotor activity. *J Neurosci* 26, 12781–12788 (2006).
44. Scardigli, R. *et al.* Crossregulation between Neurogenin2 and pathways specifying neuronal identity in the spinal cord. *Neuron* 31, 203–217 (2001).
45. Iwawaki, T., Kohno, K. & Kobayashi, K. Identification of a potential nurr1 response element that activates the tyrosine hydroxylase gene promoter in cultured cells. *Biochem Biophys Res Commun* 274, 590–595 (2000).
46. Petryszyn, S. *et al.* The number of striatal cholinergic interneurons expressing calretinin is increased in Parkinsonian monkeys. *Neurobiol Dis* 95, 46–53 (2016).
47. Eaton, S. L. *et al.* Quantitative imaging of tissue sections using infrared scanning technology. *J Anat* 228, 203–213 (2016).
48. Gauthier, J. *et al.* The axonal arborization of single nigrostriatal neurons in rats. *Brain Res* 834, 228–232 (1999).
49. Chabrat, A., Doucet-Beaupre, H. & Levesque, M. RNA isolation from cell specific subpopulations using laser-capture microdissection combined with rapid immunolabeling. *J Vis Exp* (2015).
50. Love, M. I., Huber, W. & Anders, S. Moderated estimation of fold change and dispersion for RNA-seq data with DESeq2. *Genome Biol* 15, 550 (2014).

51. Bookout, A. L. *et al.* High-throughput real-time quantitative reverse transcription PCR. *Curr Protoc Mol Biol* (2006).
52. Paxinos, G. & Franklin, K. B. J. in Paxinos and Franklin's The Mouse brain in Stereotaxic Coordinates 4th edn (Elsevier Academic Press, 2013).
53. Ma, J., Shaw, V. E. & Mitrofanis, J. Does melatonin help save dopaminergic cells in MPTP-treated mice? *Parkinsonism Relat Disord* 15, 307–314 (2009).
54. Peoples, C. *et al.* Photobiomodulation enhances nigral dopaminergic cell survival in a chronic MPTP mouse model of Parkinson's disease. *Parkinsonism Relat Disord* 18, 469–476 (2012).
55. Wallace, B. A. *et al.* Survival of midbrain dopaminergic cells after lesion or deep brain stimulation of the subthalamic nucleus in MPTP-treated monkeys. *Brain* 130(Pt 8), 2129–2145 (2007).
56. Torres-Espin, A. *et al.* Neurite-J: an image-J plug-in for axonal growth analysis in organotypic cultures. J. *Neurosci Methods* 236, 26–39 (2014).
57. Knoll, B. *et al.* Stripe assay to examine axonal guidance and cell migration. *Nat Protoc* 2, 1216–1224 (2007).

Supplementary Information

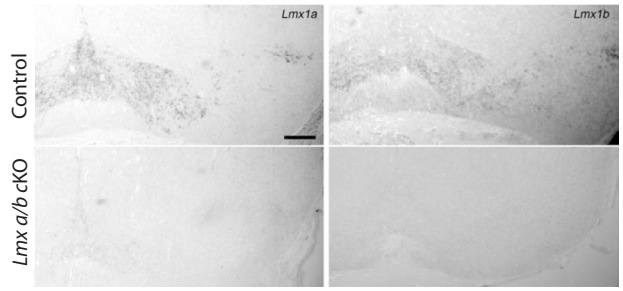

Supplementary Figure 1 | *Lmx1a* and *Lmx1b* are deleted in mDA neurons of Lmx1a/b cKO mice. *In situ* hybridization for *Lmx1a* and *Lmx1b* on *Lmx1a/b* cKO and control midbrain sections at P1 showing the absence of *Lmx1a* and *Lmx1b* expression in the *Lmx1a/b* cKO midbrain. Scale bar: 250 µm.

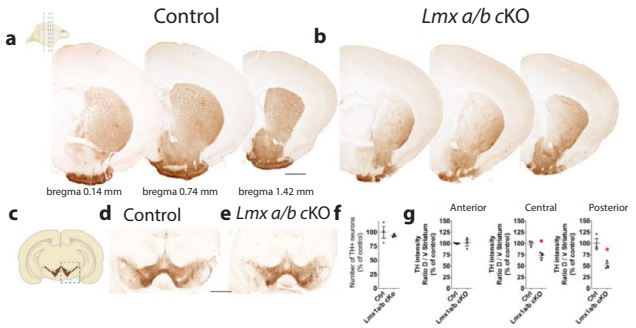

Supplementary Figure 2 | Phenotype analysis of *Lmx1a/b* cKO mutant mice at P15. (a and b) Representative images of TH immunostaining of coronal striatal sections at P15 in control (a) and double conditional mutant mice for *Lmx1a/b* (b) showing a loss of innervation in the dorsal striatum for the mutant. (c-e) Schematic and representative images of TH immunostaining of coronal midbrain sections for the control and *Lmx1a/b* cKO mutant showing no change in the number of mDA cells as quantified by stereological counting of TH-positive cells in (f) (n =3, Mann-Whitney U, p = 0.700). (g) Optical density measurements of TH axons in the striatum. Graphs show the ratio of TH intensity in dorsal vs ventral striatum (n =3, Mann-Whitney U, $p_{\text{(Ant D/V)}}$ = 0.7000, two-tailed unpaired t-test, $p_{\text{(Cent D/V)}}$ = 0.0140, $p_{\text{(Post D/V)}}$ = 0.0138). Scale bar: 250 µm.

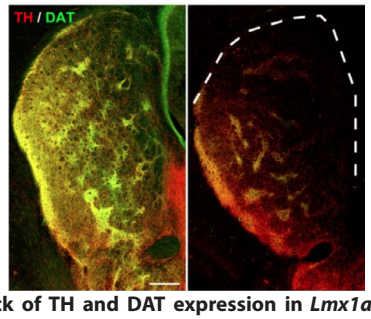

Supplementary Figure 3 | Lack of TH and DAT expression in *Lmx1a/b* cKO mutant mice. Confocal images of the dopaminergic markers TH (in red) and DAT (in green) in the striatum of control and *Lmx1a/b* cKO mutant were performed to show the loss of dopaminergic innervation using these two specific dopaminergic markers. Scale bar: 200 µm.

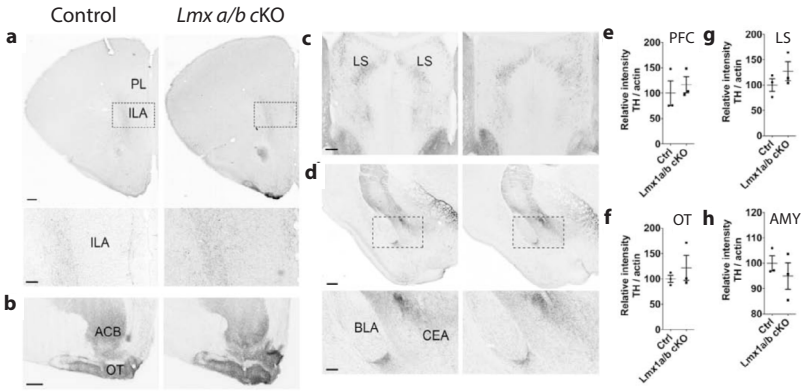

Supplementary Figure 4 | Extrastriatal targets in Lmx1a/b cKO mutant mice and control at P15. (a-d) Representative images of TH-stained coronal sections in the extrastriatal dopaminergic targets do not show abnormal DA innervation in *Lmx1a/b c*KO mice as shown in (a) at the PFC level; (b) Olfactory tubercule; (c) Septum; (d) Amygdale. (e-h) Optical density measurement of extrastriatal targets at P15 comparing controls and *Lmx1a/b c*KO (n =3, two-tailed unpaired t-test: $p_{(PFC)} = 0.5986, p_{(OT)} = 0.4489, p_{(LS)} = 0.2931, p_{(Amy)} = 0.4472$). Optical density measurements in the prefrontal cortex were performed at 3 different antero-posterior levels in prelimbic and infralimbic areas (Bregma +2.22 mm, +1.98 mm and +1.70 mm). Dashed boxes in a and d delineate the higher magnification images in the lower panels. The optical density measurements in the septum were performed at 3 different antero-posterior levels (Bregma +1.18mm, +0.62mm; and +0.14mm) in the area located between the 2 lateral ventricles and between the corpus callosum (upper border) and the zona limitans (lower border). The optical density measurements in the olfactory tubercule were performed at 3 different antero-posterior levels (Bregma +1.73mm, +1.10mm and +0.62mm). For the Amygdala, measurements were performed in the central amygdaloid nucleus (Bregma -1.80mm). Abbreviations: Prelimbic area of the prefrontal cortex (PL), Infralimbic area of the prefrontal cortex (ILA), prefrontal cortex (PFC), Nucleus accumbens (ACS), olfactory tubercule (OT), lateral septum (LS), Basolateral amygdalar nucleus (BLA), Central amygdalar nucleus (CEA) and amygdale (Amy). Scale bars = 250 µm.

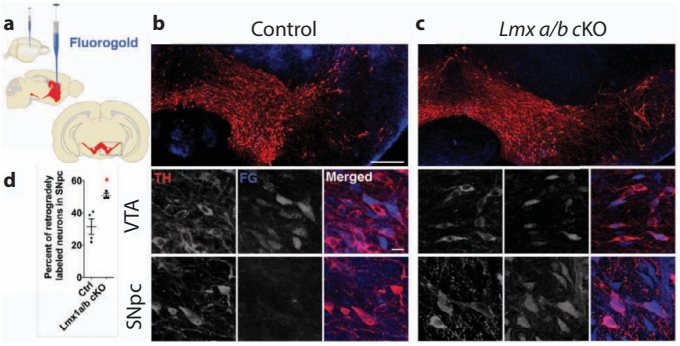

Supplementary Figure 5 | Retrograde tracing experiment showing aberrant DA connections in *Lmx1a/b c*KO. (a) Schematic representation of the injection site of the Fluorogold retrograde tracer in the ventral striatum. (b-c) Representative confocal images of the retrogradely labeled cells in control (b) (TH in red, Fluorogold in blue) and in *Lmx1a/b c*KO mutant mice (c). Lower panels show higher magnification in the VTA and SNpc. (d) Quantification of the percentage of retrogradely labeled neurons in SNpc (GFP^+TH^+ in SNpc on total GFP^+TH^+; n =4 for controls and n =3 for *Lmx1a/b c*KO mice; two-tailed unpaired t-test, p = 0.0208). Scale bars: b upper panel 250 µm, lower panels, 15 µm.

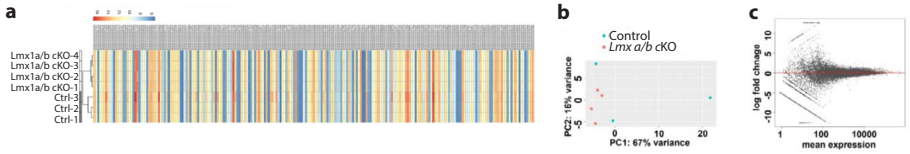

Supplementary Figure 6 | Gene expression profiling of control and Lmx1a/b cKO at E15.5. (a) A clustered heatmap showing transformed expression values of 225 differentially expressed genes, with adjusted *p* value of 0.2. The dendrogram on top shows the relationship between the control and the *Lmx1a/b c*KO samples. We had 3 biological replicates for the control and 4 biological replicates for the *Lmx1a/b c*KO mutants, with two technical replicates per sample. The map was produced with the function pheatmap in the R package pheatmap, and shows the relationships between the significantly differently expressed genes. (b) The principle component analysis (PCA) plot shows the relationship between the RNA-seq samples with respect to two axes, which explain 67% and respectively 16% of the variance. The plot indicates a good correlation between the *Lmx1a/b c*KO samples whereas we see slight differences in the control samples. The *Lmx1a/b c*KO samples cluster together with respect to PC1 and PC2, while the control samples are scattered with respect to these principal components. However, as seen from the heatmap in a, the mutant samples cluster together and so do the control samples. The PCA plot was obtained using the output of DEseq2 function rlog, which minimizes the differences between samples for rows with small counts and with respect to library size. (c) Scatterplot of log2 fold changes versus the mean of normalised counts. The graph shows unshrunken maximum likelihood estimates. Dots in red are the significantly differentially expressed genes.

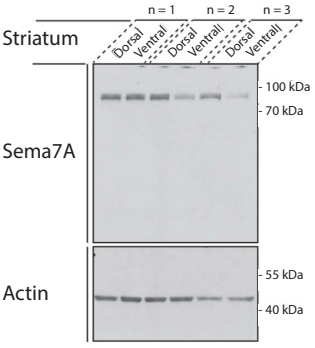

Supplementary Figure 7 | Full gel image for the western blot shown in Figure 5c.

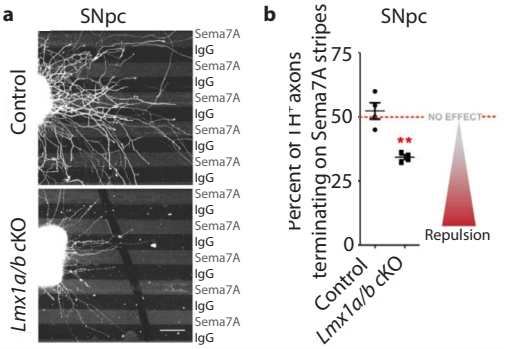

Supplementary Figure 8 | SNpc mDA axons from *Lmx1a/b c*KO embryos are repelled by Sema7a stripes. (a) Confocal images of stripes assay showing explants from SNpc of control (upper panel) and *Lmx1a/b c*KO embryos (lower panel). (b) Quantification of the number of DA axons terminating on Sema7a stripes or on IgG stripes (n =4 independent experiments, Mann-Whitney U, p = 0.0286). Scale bars: 150 µm.

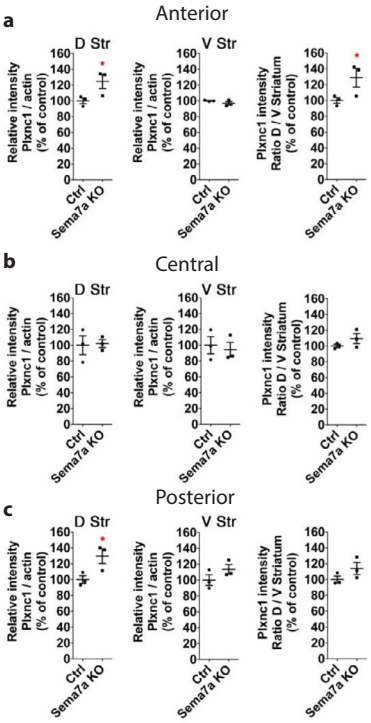

Supplementary Figure 9 | Quantification of Plxnc1 axonal density in dorsal and ventral striatal regions of WT and Sema7a KO. Graphs in a, b and c show the quantification at anterior, central and posterior striatal regions respectively. (n =3, one-tailed unpaired t-test, $p_{(\text{Ant D})} = 0.0321$, $p_{(\text{Ant V})} = 0.1060$, $p_{(\text{Cent D})} = 0.4404$, $p_{(\text{Cent V})} = 0.3586$, $p_{(\text{Post D})} = 0.0232$, $p_{(\text{Post V})} = 0.1046$, $p_{(\text{Ant D/V})} = 0.0399$, $p_{(\text{Cent D/V})} = 0.1179$, $p_{(\text{Post D/V})} = 0.0941$).

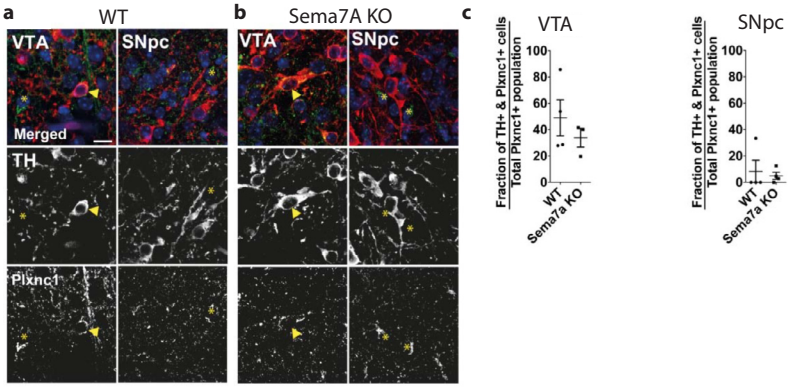

Supplementary Figure 10 | Plxnc1 levels are not altered in the SNpc or VTA of *Sema7A* KO mice. (a-b) Confocal images of Plxnc1 and TH immunostaining in coronal midbrain sections of WT and *Sema7a* KO mice. Plxnc1 staining barely localizes with TH staining in the SNpc in *Sema7A* WT and KO animals (asterisk). In the VTA co-localization between Plxnc1 and TH is more common (yellow arrow). Scale bar is 10µm. (c) Quantification of the fraction Plxnc1$^+$ cells also expressing TH is shown for the VTA and SNpc in *Sema7A* WT and KO mice. No difference in the amount of double positive cells were found (4 sections from two animals, two-tailed unpaired t-test: $p_{(\text{VTA})} = 0.418$, $p_{(\text{SNpc})} = 0.715$).

Supplementary Table 1 | Differentially expressed genes between Lmx1a/b cKO and control identified by RNA sequencing from laser capture micro-disected midbrain dopamine region at E15.5.

Gene symbol	baseMean	log2Fold Change	lfcSE	stat	pvalue	padj
Tec	132.63489	1.7691725	0.3127767	5.6563444	1.55E-08	0.0001223
Kank4	648.28329	1.6044785	0.2788192	5.7545482	8.69E-09	0.0001223
Gxylt2	117.22443	1.5751485	0.3160579	4.9837336	6.24E-07	0.0013313
Mroh7	119.47238	1.5390824	0.3083197	4.9918395	5.98E-07	0.0013313
Jade2	135.62344	1.5075358	0.3080761	4.8933875	9.91E-07	0.0016111
Gm26697	108.43484	1.5008836	0.3074238	4.8821323	1.05E-06	0.0016111
Fam83d	104.09539	1.4250111	0.3053186	4.6672922	3.05E-06	0.0037123
Pls1	116.17728	1.336951	0.3023687	4.421592	9.80E-06	0.0103287
Dusp27	88.542255	1.2799397	0.3004672	4.2598312	2.05E-05	0.0179725
	680.38792	1.2758896	0.233943	5.4538485	4.93E-08	0.0002598
Slc38a4	122.74667	1.2447294	0.2988226	4.1654455	3.11E-05	0.0258622
Nmrk1	88.305915	1.2396087	0.2988412	4.148052	3.35E-05	0.0265118
Nsun7	499.66734	1.2243704	0.2830788	4.3251925	1.52E-05	0.0141758
Klhl3	286.16943	1.2144639	0.3040753	3.9939581	6.50E-05	0.0356607
Spata45	79.635073	1.2049569	0.2974424	4.0510598	5.10E-05	0.0315814
Gm13563	78.827415	1.2025212	0.3040513	3.9549938	7.65E-05	0.0390411
Dcaf12l2	66.998171	1.161501	0.2956036	3.9292518	8.52E-05	0.0421073
Plvap	94.530995	1.0947537	0.2972602	3.6828127	0.0002307	0.0703543
Slc7a2	67.063699	1.0887315	0.2918965	3.7298547	0.0001916	0.0688549
Gm26759	64.540308	1.076117	0.2912438	3.6949013	0.00022	0.0703543
Slc25a54	101.58176	1.062969	0.2901577	3.6634178	0.0002489	0.0703543
Foxl2os	78.250002	1.0510832	0.2896624	3.628649	0.0002849	0.0758937
Chrnb3	6008.0655	1.0471264	0.2721203	3.8480283	0.0001191	0.0537969
Slc6a3	28823.34	1.0385222	0.2904993	3.5749566	0.0003503	0.0814569
Lrrc10b	88.673347	1.0353744	0.2886568	3.5868702	0.0003347	0.0801841
Col11a1	4465.2647	1.0344368	0.2823915	3.6631301	0.0002492	0.0703543
Otor	64.590052	1.018518	0.2878937	3.5378262	0.0004034	0.0898525
Gm12504	77.068838	1.0181349	0.3058569	3.3287943	0.0008722	0.1231434
Cubn	74.348658	1.0067295	0.2877886	3.498156	0.0004685	0.0988909
Gm10340	58.21414	1.004274	0.2871122	3.4978453	0.000469	0.0988909
Katnal2	466.15254	1.003239	0.3060688	3.2778216	0.0010461	0.1331852
Irak4	217.69105	0.9969763	0.2873165	3.4699583	0.0005205	0.1028911
Dgka	1936.8967	0.9782067	0.2008982	4.8691661	1.12E-06	0.0016111
Gm14830	68.297434	0.9770787	0.2931843	3.3326428	0.0008603	0.1231434
Sgsh	86.299609	0.9756349	0.2849641	3.4237113	0.0006177	0.107911
Csf2rb2	141.73976	0.9754252	0.2846984	3.4261708	0.0006122	0.107911
Dsc2	70.851927	0.9746244	0.2850363	3.4192995	0.0006278	0.107911
Apobec2	79.340696	0.9743161	0.2849364	3.4194164	0.0006276	0.107911
Slc19a3	60.934841	0.9737366	0.2851052	3.4153589	0.000637	0.1083072

Ulk3	1392.9883	0.9694674	0.3025048	3.2048003	0.0013516	0.1444071
Rec8	66.644822	0.9657843	0.2845039	3.3946257	0.0006872	0.1143904
Map2k1	2399.5915	0.9656409	0.2520367	3.8313509	0.0001274	0.053914
1700001C19Rik	63.791484	0.9648832	0.2854211	3.38056	0.0007234	0.1191547
Pus7	1076.7408	0.9585332	0.2859686	3.3518826	0.0008026	0.1231434
Slc12a7	1860.8765	0.9545708	0.2390951	3.9924307	6.54E-05	0.0356607
Eif2ak2	54.959731	0.9530543	0.2838164	3.3579958	0.0007851	0.1217133
Serpine1	148.70353	0.9473531	0.294872	3.212761	0.0013147	0.1431303
Gm14966	64.669717	0.939529	0.2827349	3.3230029	0.0008905	0.1231434
Slc43a1	63.916405	0.9391906	0.2827214	3.3219646	0.0008939	0.1231434
Gatsl3	74.656523	0.9288374	0.2818733	3.2952303	0.0009834	0.1331852
Ankdd1a	57.406495	0.9279085	0.2820173	3.2902539	0.001001	0.1331852
Cfap45	52.008411	0.9242172	0.2818455	3.279163	0.0010412	0.1331852
Slc6a20a	78.811181	0.9191505	0.2811447	3.2693151	0.0010781	0.1331852
Fgf10	97.224732	0.9156243	0.2812816	3.2551875	0.0011332	0.1367855
3300002I08Rik	75.486992	0.909309	0.2804578	3.2422313	0.001186	0.1374793
Nrg4	57.192668	0.9082436	0.280593	3.2368722	0.0012085	0.1374793
Hace1	1396.2043	0.9056106	0.3013946	3.0047346	0.0026581	0.1913704
Cntnap4	4563.081	0.901953	0.1804086	4.9995007	5.75E-07	0.0013313
Gm29443	86.114214	0.8989346	0.2796083	3.2149781	0.0013045	0.1431303
Gm15834	51.699951	0.8975923	0.2798937	3.2069044	0.0013417	0.1443303
Adamts4	58.464507	0.8946289	0.2795561	3.2001768	0.0013734	0.1447873
C230014O12Rik	672.44857	0.8927198	0.2946038	3.0302382	0.0024436	0.1884917
Fbln1	887.92113	0.8888746	0.2471092	3.5970924	0.0003218	0.0801841
Necab1	1946.1597	0.8850782	0.2361742	3.7475658	0.0001786	0.065664
Htr5a	765.2541	0.884484	0.2628474	3.3650094	0.0007654	0.1217133
1700047F07Rik	46.416472	0.8742544	0.2792779	3.1304104	0.0017456	0.1577344
Gm3411	40.804494	0.8711275	0.2874008	3.0310545	0.002437	0.1884917
Oit1	68.536755	0.8691295	0.2774688	3.1323506	0.0017341	0.1575962
Agfg2	1570.7873	0.8673752	0.2131904	4.0685464	4.73E-05	0.0315814
Gm2897	46.016702	0.8615516	0.2869817	3.0021137	0.0026811	0.1913704
Prpf39	2756.7653	0.856514	0.2072244	4.1332683	3.58E-05	0.0269304
Irgm1	66.55605	0.8433621	0.2754112	3.0621931	0.0021972	0.1814455
AF529169	1622.9676	0.8428367	0.2440478	3.4535722	0.0005532	0.1053973
Adgrg3	57.070368	0.8419657	0.2754121	3.0571123	0.0022348	0.1814455
Med12	4334.9881	0.8416678	0.2667436	3.1553446	0.0016031	0.1501429
Zfp937	77.945504	0.8330366	0.2744545	3.0352445	0.0024034	0.1884917
Gm23455	46.155624	0.8317904	0.2747444	3.0275064	0.0024658	0.1888374
Rasip1	1855.5569	0.8270402	0.1858381	4.4503265	8.57E-06	0.0096843
Phldb2	1442.6985	0.8257672	0.2643365	3.1239239	0.0017846	0.1603372
Klf10	608.40906	0.8245077	0.2475375	3.3308394	0.0008658	0.1231434
Pigl	585.68591	0.8173411	0.2489093	3.2836909	0.0010246	0.1331852
Atg4c	758.67684	0.8059936	0.2483192	3.2457963	0.0011712	0.1374793

Pakap	3089.6065	0.8055926	0.2639465	3.0521058	0.0022724	0.1824049
Trpm7	3483.4636	0.8009433	0.252056	3.1776405	0.0014848	0.1464889
Ntsr1	1769.0789	0.7682348	0.2231693	3.4423862	0.0005766	0.1060218
9330182L06Rik	2540.2536	0.7591052	0.239802	3.1655496	0.0015479	0.1478222
Mdn1	5277.8838	0.7495314	0.2290041	3.2730043	0.0010641	0.1331852
Nbeal2	2439.9825	0.7247411	0.2081758	3.4813907	0.0004988	0.1024389
Tnfrsf19	2651.0312	0.7079271	0.1902176	3.7216702	0.0001979	0.0690217
Abcg4	5679.8077	0.6941309	0.1914374	3.6258907	0.000288	0.0758937
Gm15952	1098.9068	0.6722274	0.1943233	3.4593248	0.0005415	0.1044297
Gm45837	2147.9732	0.6678855	0.2146904	3.1109238	0.001865	0.1666199
Htt	1771.5858	0.653338	0.1767462	3.6964754	0.0002186	0.0703543
Xpo1	8722.7451	0.650828	0.2037043	3.1949646	0.0013985	0.1450659
Pdzrn4	5923.5491	0.6412071	0.2122079	3.0215991	0.0025144	0.1889355
Pcgf6	4844.3849	0.6255757	0.143456	4.3607501	1.30E-05	0.0128102
Plxnc1	8780.4919	0.6254371	0.1802095	3.4706121	0.0005193	0.1028911
Gna13	2681.98	0.6111642	0.1894431	3.226109	0.0012549	0.1417359
Gpd2	2977.2057	0.5904261	0.1715085	3.4425476	0.0005763	0.1060218
Kcnn2	2435.1412	0.5467289	0.1808873	3.0224832	0.0025071	0.1889355
Chst1	8781.1933	0.5416485	0.1649311	3.2840906	0.0010231	0.1331852
Cdh4	12776.909	0.5202046	0.1468081	3.5434325	0.000395	0.0892202
Pfkp	57113.287	0.5063947	0.1586659	3.1915785	0.001415	0.1452924
Slc9a3r2	4692.6263	0.5046352	0.1249382	4.0390793	5.37E-05	0.0315814
Bicdl1	11749.212	0.4973351	0.130162	3.8208927	0.000133	0.053914
Mef2d	4361.6344	0.4937621	0.1599727	3.0865405	0.002025	0.1730885
Syn1	18533.855	0.4798082	0.1462833	3.2799925	0.0010381	0.1331852
Xbp1	6605.8528	0.4534775	0.1426002	3.1800625	0.0014724	0.1464889
Plekha5	20895.762	0.4436007	0.1449669	3.0600136	0.0022133	0.1814455
Ano6	6652.3748	0.4407902	0.146064	3.0177874	0.0025463	0.1899257
Sos1	4905.0622	0.4137507	0.1275603	3.2435706	0.0011804	0.1374793
Iqsec3	8639.7475	0.4081129	0.1335791	3.0552149	0.002249	0.1814455
Arhgap39	9568.5596	0.3691208	0.1219528	3.0267509	0.002472	0.1888374
Lingo1	15684.562	0.3672232	0.1089274	3.3712645	0.0007482	0.1209287
Wdr82	22052.507	-0.231293	0.0770595	-3.001485	0.0026867	0.1913704
Cdc16	11971.295	-0.274198	0.0796512	-3.442483	0.0005764	0.1060218
Stip1	16039.935	-0.343856	0.1085787	-3.166879	0.0015408	0.1478222
Slc30a9	10966.921	-0.361795	0.105251	-3.437451	0.0005872	0.1067316
Klhdc2	13104.46	-0.362343	0.0886787	-4.086023	4.39E-05	0.0315419
Arfip2	9436.2949	-0.36931	0.1032279	-3.577616	0.0003467	0.0814569
Pmpcb	5703.8052	-0.376154	0.1218673	-3.086584	0.0020247	0.1730885
Stoml1	9440.9333	-0.37891	0.1140804	-3.321434	0.0008956	0.1231434
Hsp90aa1	17776.487	-0.42089	0.1405934	-2.993669	0.0027565	0.1954609
Ldhb	14923.915	-0.434539	0.140344	-3.096244	0.0019599	0.1712668
Fkbp4	31362.249	-0.437285	0.145586	-3.003616	0.0026679	0.1913704

Elp5	10174.683	-0.451532	0.1403834	-3.216422	0.001298	0.1431303
Ranbp1	16985.812	-0.483263	0.1523219	-3.172644	0.0015106	0.1474491
Aamp	10485.908	-0.484909	0.1560144	-3.108106	0.0018829	0.1672721
Dnajc8	13813.461	-0.485091	0.1571407	-3.086988	0.002022	0.1730885
Ubxn6	9882.8166	-0.487475	0.1456868	-3.346048	0.0008197	0.1231434
Msantd3	2305.7181	-0.488881	0.1503843	-3.25088	0.0011505	0.1374793
Gpx4	5278.8232	-0.489146	0.1556935	-3.141725	0.0016796	0.1544117
Map3k7	6738.7591	-0.490067	0.1363892	-3.59315	0.0003267	0.0801841
Atp5d	15609.958	-0.514091	0.1682309	-3.055864	0.0022441	0.1814455
Enpp2	2759.819	-0.523814	0.1734022	-3.020803	0.0025211	0.1889355
Gpat4	13488.82	-0.524783	0.1652165	-3.176337	0.0014915	0.1464889
1700025G04Rik	3412.5692	-0.528299	0.1586236	-3.33052	0.0008668	0.1231434
Trak2	3620.9587	-0.534041	0.1724843	-3.096172	0.0019604	0.1712668
Zbtb8b	2497.156	-0.534141	0.1584601	-3.37082	0.0007494	0.1209287
Pycr2	3781.4407	-0.537003	0.1639172	-3.276062	0.0010527	0.1331852
Rgs2	7293.9668	-0.542005	0.1802151	-3.007547	0.0026337	0.1913704
Phax	9629.9696	-0.545997	0.1816663	-3.005496	0.0026515	0.1913704
Ccnh	4711.3792	-0.546421	0.1423826	-3.837699	0.0001242	0.053914
Tbl3	4946.6772	-0.546734	0.1796033	-3.044118	0.0023336	0.1854362
Cdc34	7285.2973	-0.547387	0.138286	-3.958365	7.55E-05	0.0390411
Nubp2	3904.3301	-0.563735	0.1772675	-3.180138	0.001472	0.1464889
Gm6485	9866.6399	-0.568901	0.1546199	-3.679352	0.0002338	0.0703543
Tpgs1	5931.4605	-0.583849	0.1665095	-3.506401	0.0004542	0.0983894
Mkks	1463.1873	-0.585822	0.1631668	-3.590326	0.0003303	0.0801841
Ttc9b	5257.3612	-0.585825	0.1856507	-3.155524	0.0016021	0.1501429
Coprs	6198.7942	-0.609322	0.201665	-3.021456	0.0025156	0.1889355
Gm12396	2177.1325	-0.619672	0.1922448	-3.223351	0.001267	0.1420929
Tmem120a	4570.7877	-0.625684	0.2077577	-3.011605	0.0025987	0.1913704
Zmat5	1332.6763	-0.628298	0.1921183	-3.27037	0.0010741	0.1331852
Fez2	2739.019	-0.629224	0.195799	-3.21362	0.0013107	0.1431303
Mgst3	6982.0183	-0.631221	0.2074869	-3.04222	0.0023484	0.1856762
Foxo3	3028.9986	-0.660803	0.2146216	-3.078921	0.0020775	0.1756779
Polr2e	8290.4618	-0.672718	0.2075794	-3.240776	0.001192	0.1374793
2010107E04Rik	7787.1436	-0.679603	0.2030118	-3.347604	0.0008151	0.1231434
Uqcr10	7751.0754	-0.681152	0.2281915	-2.985	0.0028358	0.199299
Rplp0	54659.937	-0.684637	0.2131984	-3.211267	0.0013215	0.1431303
Mul1	2376.2704	-0.685379	0.2109351	-3.249241	0.0011571	0.1374793
2410015M20Rik	4596.6937	-0.695344	0.2184111	-3.183647	0.0014543	0.1464889
Dpf3	1994.5975	-0.695847	0.2035029	-3.419347	0.0006277	0.107911
Rnf213	550.34675	-0.698045	0.21896	-3.188001	0.0014326	0.146153
Nedd8	16238.713	-0.700818	0.2311376	-3.032036	0.0024291	0.1884917
Srp9	4614.9831	-0.70677	0.21182	-3.336653	0.0008479	0.1231434
Gm10221	10624.915	-0.709061	0.1837048	-3.859783	0.0001135	0.0527818

Gm10221	10624.915	-0.709061	0.1837048	-3.859783	0.0001135	0.0527818
Gm12350	3700.0572	-0.744447	0.2470567	-3.013264	0.0025845	0.1913704
Timm8b	8773.3091	-0.747128	0.2336557	-3.197559	0.001386	0.1450659
Rpl34	5556.2326	-0.752002	0.250153	-3.006168	0.0026456	0.1913704
Tmem178	1636.4353	-0.756022	0.2250024	-3.360061	0.0007793	0.1217133
Ctdsp1	1139.025	-0.756189	0.2440974	-3.097897	0.001949	0.1712668
Fis1	23677.435	-0.775178	0.2523253	-3.07214	0.0021253	0.1768811
Tmem256	5462.202	-0.777676	0.2543954	-3.056956	0.002236	0.1814455
Fxn	1057.1254	-0.780662	0.2221675	-3.513843	0.0004417	0.0970026
Nlrc4	3124.3561	-0.780821	0.2573248	-3.034381	0.0024103	0.1884917
Hist3h2ba	13657.2	-0.785568	0.2071507	-3.792255	0.0001493	0.0562061
Mrpl41	6742.02	-0.785757	0.2400234	-3.273669	0.0010616	0.1331852
Rpl19	4207.8326	-0.791169	0.2499888	-3.16482	0.0015518	0.1478222
Itgb1bp1	1798.4161	-0.800114	0.2535967	-3.155062	0.0016046	0.1501429
Rnf7	7999.9667	-0.80564	0.2108462	-3.820983	0.0001329	0.053914
Gm1673	17436.238	-0.814416	0.2706502	-3.009108	0.0026202	0.1913704
Psmb4	18137.743	-0.822282	0.2620043	-3.138429	0.0016986	0.1552565
Alkbh4	1539.8707	-0.836233	0.2276993	-3.672534	0.0002402	0.0703543
Rpl13a	54654.197	-0.843804	0.2666012	-3.165041	0.0015506	0.1478222
Znrd1	3029.2497	-0.849079	0.1649199	-5.148429	2.63E-07	0.0010384
Fhl2	1065.4021	-0.857417	0.2570051	-3.336189	0.0008494	0.1231434
2310009A05Rik	753.18698	-0.857582	0.2475742	-3.463941	0.0005323	0.1039215
Uqcr11	8221.8771	-0.865363	0.2650204	-3.265268	0.0010936	0.1340555
Ust	452.53199	-0.883043	0.2680937	-3.293785	0.0009885	0.1331852
Tacr1	931.62202	-0.886526	0.2195494	-4.037935	5.39E-05	0.0315814
Fxyd2	516.49703	-0.893564	0.2760348	-3.237142	0.0012073	0.1374793
Gm10073	10897.628	-0.900213	0.2928964	-3.073485	0.0021157	0.1768811
Gm8186	7436.661	-0.910486	0.2943147	-3.093579	0.0019776	0.171821
Fmc1	3660.2474	-0.910743	0.2396009	-3.801082	0.0001441	0.0562061
Scand1	5486.2763	-0.912363	0.2675907	-3.409546	0.0006507	0.109465
Sdhaf1	921.41393	-0.915346	0.2978267	-3.073417	0.0021162	0.1768811
Cnp	2088.7242	-0.921781	0.1919947	-4.801078	1.58E-06	0.0020796
BC026585	338.98832	-0.942816	0.3156686	-2.986727	0.0028198	0.1990611
Gm5617	523.26568	-0.949182	0.3115639	-3.046508	0.0023152	0.1848973
Igfbpl1	2184.4764	-0.953839	0.3093933	-3.082934	0.0020497	0.1742583
Rps14	32336.088	-0.964627	0.2474953	-3.897556	9.72E-05	0.0465612
Med18	591.73258	-0.973819	0.264042	-3.688123	0.0002259	0.0703543
Snrpe	5563.4135	-0.97818	0.2712029	-3.606819	0.00031	0.0801841
Boll	2287.175	-0.981266	0.3065337	-3.201167	0.0013687	0.1447873
H19	12356.601	-0.982634	0.1977588	-4.968848	6.74E-07	0.0013313
Rpl5-ps2	76.775066	-0.984702	0.2951819	-3.335917	0.0008502	0.1231434
Cpa2	307.02543	-0.986434	0.3136498	-3.145016	0.0016608	0.1538591
Rpl9	2126.3451	-0.986685	0.2780452	-3.548651	0.0003872	0.0887385

Mdfi	320.78235	-0.987827	0.3107094	-3.179264	0.0014765	0.1464889
Tbc1d4	359.55886	-0.990889	0.3102433	-3.19391	0.0014036	0.1450659
Zfp335os	661.8285	-0.993406	0.2724853	-3.645724	0.0002666	0.0739715
Gm15286	212.83742	-0.994512	0.316272	-3.144481	0.0016638	0.1538591
Gm2199	611.87128	-1.002211	0.2870517	-3.491394	0.0004805	0.099977
Agt	108.33311	-1.005079	0.3085674	-3.257242	0.001125	0.1367855
Siva1	1284.0794	-1.029746	0.2778454	-3.706182	0.0002104	0.0703543
Zfp36l1	637.50493	-1.065304	0.3168151	-3.362541	0.0007723	0.1217133
Cd160	289.75252	-1.075188	0.3091582	-3.477792	0.0005056	0.1024931
Nol3	289.97327	-1.130848	0.3110404	-3.635694	0.0002772	0.0755843
Gm4876	150.26848	-1.137648	0.3169924	-3.588881	0.0003321	0.0801841
Chst7	485.80818	-1.159365	0.3160115	-3.668744	0.0002437	0.0703543
Gm9748	220.55359	-1.178057	0.31685	-3.718028	0.0002008	0.0690217
4933431K14Rik	248.92463	-1.203263	0.3168666	-3.797381	0.0001462	0.0562061
Loxl1	246.74786	-1.281964	0.3170186	-4.043814	5.26E-05	0.0315814

Abbreviations: baseMean: the base mean over all rows, lfcSE: Log Fold Standard Error, stat: Wald statistic, pvalue: Wald test *p*-value, padj: Benjamini-Hochberg (BH) adjusted *p*-values.

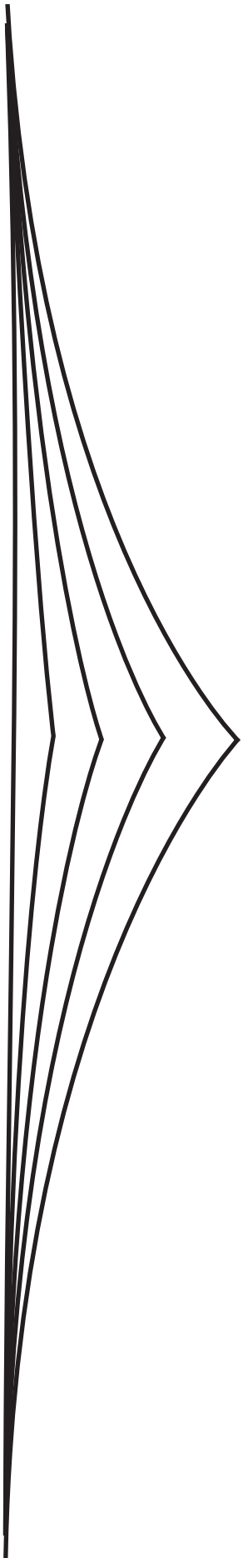

Chapter 5

Characterization of Sema6A reverse signalling through the identification of Sema6A-interacting proteins

Suzanne Lemstra[1], Marieke G. Verhagen[1], Aikaterini Koutourlou[1], Kati Rehberg[1], Erikjan Rijkers[2], Jeroen A. A. Demmers[2], Geert M. J. Ramakers[1], R. Jeroen Pasterkamp[1]

[1.] Department of Translational Neuroscience, UMC Utrecht Brain Center, University Medical Center Utrecht, Utrecht University, Utrecht 3584 CG, the Netherlands. [2.] Center for Proteomics, Erasmus MC, 3000 CA Rotterdam, The Netherlands

Abstract

Semaphorin signalling is important for brain development and involves complex signalling cascades. Semaphorin 6A (Sema6A) is a transmembrane member of the Semaphorin family, involved in migration, axon outgrowth and actin remodelling. Sema6A can act both as a ligand and as a receptor. As a ligand, Sema6A induces forward signalling via its receptors PlexinA2 and PlexinA4. As a receptor, via so-called reverse signalling, Sema6A initiates downstream intracellular signalling cascades. However, these downstream reverse signalling cascades remain poorly understood. In this study, Sema6A constructs were created to study reverse signalling. A truncated construct of Sema6A (*Sema6AΔcyto-GFP*), lacking the intracellular domain, was used to study loss of reverse signalling. Comparing Sema6AΔcyto-GFP to the full-length Sema6A (Sema6A-GFP) neuronal cell lines and primary cortical neurons did not reveal changes in expression levels and ligand function of Sema6A. Next, to identify the interactome of Sema6A, these constructs were used in immunoprecipitation (IP) experiments followed by mass spectrometry analysis comparing Sema6A-GFP to GFP and Sema6AΔcyto-GFP. 21 of the 925 identified proteins were significantly enriched in the interactome of Sema6A. Gene- ontology analysis revealed amongst others enrichment in biological processes important for actin dynamics and the Arp 2/3 complex. This study is the first that robustly links class 6 Semaphorins to the Arp2/3 complex through novel Sema6A-interacting proteins. Although future studies need to validate and examine these hits, this study provides interesting candidates that might be involved in the complex downstream signalling cascade involved in Sema6A reverse signalling.

Introduction

The Semaphorin guidance cue family instructs cells to migrate, differentiate, form synapses and integrate into neuronal networks and if disturbed can lead to neurological disorders [1–4]. Transmembrane Semaphorins can act via forward and reverse signalling cascades [5–8]. During forward signalling, Semaphorins bind to Plexins to execute their neuronal effects [1,9]. Each subunit of a Semaphorin dimer binds a monomeric Plexin [10,11], consequently leading to conformational changes and downstream activation of the signalling complex [12]. Plexins contain GTPase-activated protein (GAP) domains that can regulate actin modelling, e.g. through inhibition of Ras GTP-binding protein 1 (Rap1) or Ras-related protein (R-Ras) [13,14]. Interestingly, during development, a limited number of Semaphorins and Plexins are expressed in specific spatiotemporal patterns, leading to specialised and diversified Sema-Plexin signalling events. Certain transmembrane Semaphorins can act as receptors to induce so-called reverse signalling via their intracellular domain [15]. Reverse signalling has been established for mammalian Semaphorin 4 and 6 subclasses [7,16–21]. Reverse signalling of transmembrane Semaphorins plays a pivotal role in brain development by influencing cell migration and differentiation, axonal guidance and actin remodelling [7,19,20,22–25]. However, the mechanisms-of-action necessary to achieve these cellular events are obscure.

Currently, five Semaphorin 6A (Sema6A)-interacting proteins are identified. Each of these proteins are involved in actin formation or modulation. Sema6A contains an intracellular zyxin-like carboxy-terminal domain that interacts directly with the VASP-like protein / Vasodilator stimulated phosphoprotein (EVL/VASP)-pathway [26]. Activation of the EVL/VASP pathway promotes the formation of filopodia [27,28]. Interestingly, other proteins that can modulate the EVL/VASP-pathway were also found in the interactome of Sema6A by immunoprecipitations in COS-7 cells: Abelson (Abl) and Murine ena (Mena) [7,26], both contribute to the filopodia formation via the EVL-VASP pathway. The tyrosine kinase Abl (*Drosophila* homologous to Enable) modulates the EVL/VASP pathway by phosphorylating Mena to promote cell migration and actin remodelling [7,29–31]. Noteworthy, recently two other Sema6A-interacting proteins were identified, membrane palmitoylated protein 6 (Mpp6) and Filamins (Flns A-C) [32]. The actin modulation capacity of Mpp6 is not well defined, while Filamins are cross-linking proteins that stabilize branched actin [33–35]. Downstream signalling of Sema6A can regulate actin remodelling e.g. by decreasing cerebellar migration or axon length of cultured cerebellar granular explants or neurons, respectively [7]. Although, the precise mechanism-of-action is obscure of Sema6A-induced actin remodelling, the current identified Sema6A-interacting proteins indicate a major role for the EVL/VASP-pathway.

Examination of Sema6A-interacting proteins will provide novel insights into the mechanisms and function of reverse signalling in actin remodelling. In this study, the interactome downstream of Sema6A was further characterized by overexpression of GFP, full-length (Sema6A-GFP) or a truncated Sema6A (Sema6AΔcyto-GFP) constructs in Neuro2A (N2A) cells and primary cortical neurons. The constructs were first validated for protein production, localization and ligand function. Next, immunoprecipitation of Sema6A constructs followed by mass spectrometry and Gene-Ontology (GO)-analysis comparing Sema6A-GFP to GFP and Sema6AΔcyto-GFP identified Cortactin, Coronin1C, Capping Actin Protein Of Muscle Z-Line Subunit Beta (CapZb) and Twinfilin as new intracellular interactors in Sema6A signalling. Our findings indicate novel Sema6A-interacting proteins that might be key regulators in Sema6A-induced actin remodelling in reverse signalling.

Methods

Animals. All animal research was approved by and performed in accordance to the CDC (Central Committee for Animal research, the Netherlands) and the University Medical Center Utrecht, the Dutch law (Wet op de Dierproeven 1996) and European regulation (Guideline 86/609/EEC). From Jackson Laboratories the C57BL/6J mice were obtained. Mice were raised by their mothers and weaned at 4-5 weeks of age. Mice were kept at 22 ±1°C on wood-chip bedding with tissue paper for nest building in a 12 hours light cycle. Animals had ad libitum access to food (211 RMG—TH diet, Hope Farms) and water and constant sound from the radio.

Cell cultures. To validate that Sema6AΔcyto-GFP protein is expressed, constructs were brought into N2A cells through PEI transfections. In short, 12 mm coverslips were coated with poly-L-lysine (PLL) (20 µg/ml, Sigma-Aldrich) and exposed to UV for 20 minutes. N2A cells were plated 1000 cells/well in a 24 wells plate and cultured in DMEM high glucose containing fetal calf serum, L-glutamine and penicillin/ streptomycin. On the day of transfections, cells (70-80% confluent) were switched to DMEM high glucose – antibiotic free media at least 1 hour prior to transfections. 1 µg of *CAG-GFP, CAG-Sema6A-GFP* or *CAG-Sema6AΔcyto-GFP* constructs were mixed 1:3 with PEI (Polyscience) in H_2O containing 150 mM NaCl and incubated at room temperature for >20 minutes. The following day, media without antibiotics were refreshed. 48-72 hours post-transfections cells were fixated and processed for immunochemistry or western blot.

The constructs were also examined for surface expression in primary cortex neurons. To obtain primary cortex neurons, the upper layer of the cortex was dissected from P0 - P3 brains and collected in Krebs buffer containing 0.7% NaCl, 0.04% KCl, 0.02% KH_2PO_4, 0.2% $NaHCO_3$, 0.25% glucose and 0.001% phenol red. Cells were dissociated for 20 min in 0.25% trypsin in Krebs buffer at 37°C. Tissue was triturated using fire-polished Pasteur pipettes. Adding 2 mg of soybean trypsin inhibitor and 20 µg/mL DNAse stopped the dissociation and cells were triturated using fire-polished Pasteur pipettes. Dissociated cells were buffered in Krebs buffer supplemented with 1 mM $MgSO_4$ and µM $CaCl_2$ and collected via centrifugation at 800 RPM for 10 min at 4°C. Cells were resuspended in neurobasal medium supplemented with B-27, L-glutamine, penicillin/streptomycin and β-mercaptoethanol and plated onto poly-L-lysine- (PLL; 20 mg/ml) and laminin (40 mg/ml)-coated coverslips in 24 well plates at 37°C and 5% CO_2 for 24 hours. Primary cortex neurons were transfected with lipofectamine 2000 (Life Technologies, 11668019) and incubated for 45 min. Cells were quickly dipped in neurobasal medium and cultured for 48 hours after transfection. Primary cortex neurons were fixated and labelled for surface expression of constructs.

Primary explants were used to assess ligand function of the CAG-Sema6A-GFP or CAG-Sema6AΔcyto-GFP constructs [7]. Explants were generated from P2-P4 C57BL/6J mice that were killed via decapitation. Brains were taken out and placed on a round table to cut coronal slices with a tissue chopper set at 350 µm. Slices were taken and the upper part of the cortex was dissected and cut into small pieces of 100-300 µm. Explants were plated on NIH3T3 cells transiently expressing either *CAG-GFP, CAG-Sema6A-GFP* or *CAG-Sema6AΔcyto-GFP* constructs in Neurobasal medium supplemented with B27, L-glutamine, penicillin/streptomycin, HEPES and β-mercaptoethanol for 72 hours on coverslips previous coated with PLL (20 mg/mL) and laminin (40 mg/mL). Primary explants were fixated and processed by immunochemistry.

Western blot. To validate protein expression of Sema6A-GFP and Sema6AΔcyto-GFP, transfected N2As were lysed using RIPA buffer (10 mM Tris-buffer pH 7.5, 150 mM NaCl, 0.1% SDS, 1% Triton X-100, 1% Deoxycholate, 0.5 mM EDTA, 1 mM PMSF and complete protease inhibitor (Roche) and spun down for 15 min at 12.000 RPM at 4°C. The protein containing supernatant was isolated and sample buffer (NuPage, 1:4) containing DTT (5 mM) was added. Samples were boiled for 10 min at 70°C and loaded on an 8% gel for SDS-polyacrylamide gel electrophoresis. Protein was transferred from gel to a nitrocellulose membrane (Bio-Rad). Blots were incubated with goat-anti-Sema6A (1:1000, R&D Systems, AF1615) or rabbit-anti-GFP (1:1000, Life Technologies, A11122) followed by the appropriate HRP-conjugated secondary antibody in 1.5% milk in TBS-T. Immunoblots were exposed to Pierce ECL substrate (Thermo Fisher Scientific, 32106) and digitized using an Epson flatbed scanner (Epson America, Perfection 4990).

Immunochemistry. To visualize cell surface expression of Sema6A-GFP and Sema6AΔcyto-GFP on N2A and primary cortex neurons, cells were labelled with goat-anti-Sema6A (1:1000, R&D Systems, AF1615) for 10 min at 37°C and 5% CO_2 in an incubator. Cells were carefully washed and fixated in 4% PFA and 10% sucrose for 1 hour at 37°C. Coverslips were blocked (PBS with 3% BSA) for 30 min and incubated with donkey-anti-goat 555 (Alexa Fluor, 1:750) in 50% blocking buffer with PBS for 1 hour at room temperature. Subsequently, cells were fixated for 10 min with 4% PFA and permeabilised with blocking buffer containing 3% BSA and 0.1% Triton X-100 for 30 min. The cytosolic pool of Sema6A-GFP or Sema6AΔcyto-GFP was visualised using rabbit-anti-GFP (1:1000, Life Technologies, A11122) followed by donkey-anti-rabbit 488 (Alexa Fluor, 1:750), both incubated in 50% blocking buffer for 1 hour. For primary cortical neurons tubulin was visualized using mouse-anti-Tuj1 (1:500, Covance, MMS-435P) with an Alexa-conjugated secondary donkey-anti-mouse 647 (1:750) to specifically label neurons. Hoechst (1:1000, Thermo fisher scientific, H3569) was used to visualize cell nuclei. Coverslips were washed extensively between steps and mounted using fluorsave (VWR international) or prolong gold antifade (Invitrogen), respectively of imaging processing. Axioskop EPI-fluorescent microscope (Zeiss) or confocal FV1000 microscope (Olympus) were used for imaging. FIJI was used for image processing.

NIH3T3 cells and primary explants were processed for immunocytochemistry similarly to cytosolic pool as mentioned above. Antibodies used: rabbit-anti-GFP (1:1000, Life Technologies, A11122), mouse-anti-Tuj1 (1:500, Covance, MMS-435P) labelled with donkey-anti-rabbit 488 (1:750, Alexa Fluor) and donkey-anti-mouse 555 (1:750, Alexa Fluor), respectively, combined with Hoechst. Coverslips were mounted using Fluorsave, imaged on an Axioskop EPI-fluorescent microscope (Zeiss) and processed using FIJI.

Immunoprecipitation and mass spectrometry. Immunoprecipitation for Sema6A-GFP complexes was conducted as reported previously [36,37]. In short, N2A cells were transiently transfected with *CAG-GFP, CAG-Sema6A-GFP* or *CAG-Sema6AΔcyto-GFP* constructs for 48 hours at 37°C and 5% CO_2. Cells were lysed using (1% Triton X-100 (Sigma-Aldrich, 10789704001), 1% Nonidet P-40 (Merck), 1% Lauryl Maltosid (Invitrogen, BN2005), 1x protease inhibitor (Sigma-Aldrich, 11873580001), 1x phosphatase inhibitor (Sigma-Aldrich, P5726) and 50% glycerol in PBS) followed by 15 min centrifugation at 12.000 RPM. With GFP-trap beads (ChromoTek, gtma-20) proteins were specifically pulled down and analysed on western blot via immunochemistry, silver staining and coomassie staining.

For all procedures, SDS-polyacrylamide gel electrophoresis with 4-12% Bis-Tris gels (Thermo fisher scientific, NP0323BOX) was conducted by loading 5 µg or 15 µg protein

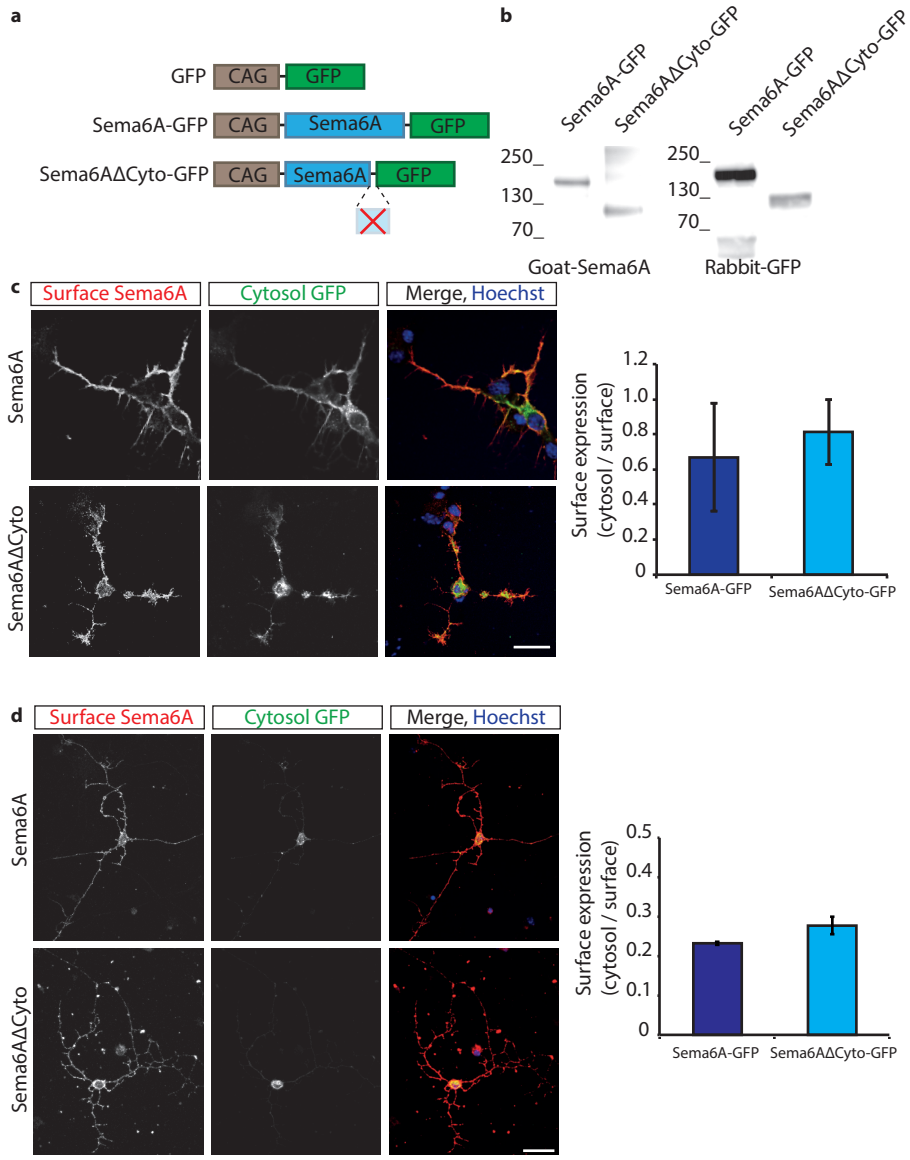

Figure 1 |Generation and validation of Sema6AΔcyto-GFP construct.
(a) Constructs containing *CAG-GFP, CAG-Sema6A-GFP* and *CAG-Sema6AΔCyto-GFP* were created. (b) Sema6a-GFP and Sema6AΔcyto-GFP N2A lysates were stained for Goat-anti-Sema6A and Rabbit-anti-GFP on western blot. (c) Surface and cytosolic expression of Sema6A-GFP and Sema6AΔcyto-GFP constructs via immunocytochemistry in N2A. Quantification revealed no differences in surface expression in Sema6AΔcyto-GFP compared to Sema6A-GFP full-length. (d) Transient expression of Sema6A-GFP and Sema6AΔcyto-GFP in primary cortex neurons. Via immunocytochemistry the surface and cytosolic expression were labelled. Quantification did not show alterations in surface or cytosolic expression between Sema6A-GFP and Sema6AΔcyto-GFP. $n = 3$ experiments. Data are presented as means ± s.e.m. Scale bar (c,d) 20 µm.

per condition for immunochemistry and silver or coomassie staining, respectively. Immunoprecipitation samples were visualized using rabbit-anti-GFP (1:1000, Life Technologies, A11122) in 2.5% milk. For silver and coomassie gels, all steps were performed on an orbital shaker. For silver staining, gels were fixated in 50% methanol followed by several washing steps. Gels were incubated with 10 µM DTT for 20 min and soaked in 0.1% $AgNO_3$ for 20 min. A developer solution (3% Na_2CO, 1.85% formaldehyde in H_2O) was used to visualize protein bands for ±2 min followed by addition of citric acid ($C_6H_8O_7$ monohydrate, 5%) to stop the development. For coomassie staining, gels were fixated (50% MeOH, 7% Acetic acid in H_2O) and washed with H_2O. Gelcode staining solution (Thermo fisher, 24590) was left overnight at room temperature. Extensive washing steps using H_2O were performed for silver and coomassie gels.

Coomassie gels were sent for mass spectrometry as reported previously [36–38]. Mass spec data was analysed using MaxQuant software suite (v1.6.5.0) via a Mus musculus reference proteome (Swiss-Prot, Uniprot) as previously reported [39,40]. Briefly, to identify positive protein hits a false discovery rate (FDR) of 1% is used. Hits were not considered as Sema6A-interacting proteins when they appeared as a positive hit in either GFP or Sema6AΔcyto-GFP samples. Hits were considered significantly enriched if (1) the difference was statistically significant ((false discovery rate (FDR) < 0.05), (2) the fold-change was higher than 1.0 and (3) proteins were detected in triplicate within one group. GO-analysis was performed via PANTHER overrepresentation test (v14.1) with the Mus Musculus gene ontology reference list [41]. Biological processes were found significant if (1) the fold enrichment exceeded 1.0 and (2) with a FDR < 0.01.

Statistics. The expression of GFP, Sema6A-GFP and Sema6AΔcyto-GFP were quantified using FIJI. Mean grey values (representing grey values divided by pixel of 16-bit images) were measured from GFP positive cells followed by subtraction of background grey values. The total GFP intensity was compared between constructs and quantified using a two-tailed unpaired Student's *t*-test.

For surface localization of Sema6A-GFP and Sema6AΔcyto-GFP, images were processed in FIJI. The fluorescent intensity of the cytosolic pool and surface pool was measured using mean grey value per cell. A ratio between these represents cell surface expression. A two-tailed unpaired Student's *t*-test revealed significant changes between conditions.

For explant cultures the images were stitched and analysed with FIJI by measuring the surface of the outgrowth of explants and the area of the explant itself. The outgrowth ratio represents the ratio between the outgrowth surface and explant's area. The outgrowth ratio was calculated for all conditions and used for quantification. A two-tailed unpaired Student's *t*-test was used to show significant changes between conditions.

Results

Full-length Sema6A and Sema6A lacking the intracellular domain are processed similarly

Sema6A full-length protein can function as a ligand and as a receptor [5–8]. In the present study, we created three constructs to study reverse signalling of Sema6A (Fig. 1a). A *CAG-Sema6A-GFP* (Sema6A-GFP) construct was created to study full-length protein function. In addition, a truncated form of Sema6A, *CAG-Sema6AΔcyto-GFP* (Sema6AΔcyto-GFP), lacking the intracellular domain, was generated. More specifically, Sema6AΔcyto-GFP encodes the first 1267 residues of the mature protein, thus lacking amino acids encoded by exon [20-21]. The constructs were expressed in N2A cells and protein levels were assessed using western

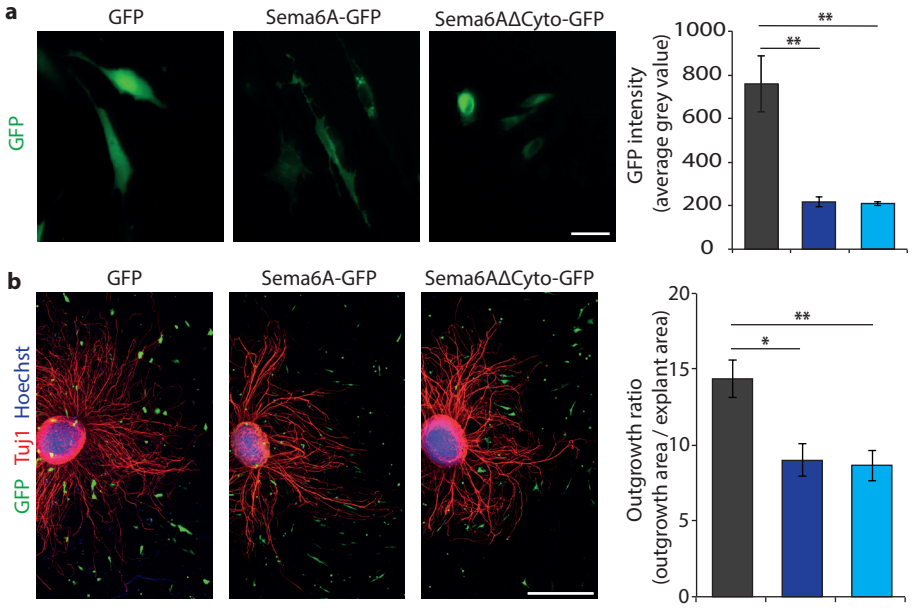

Figure 2 | Sema6AΔcyto retains its ligand function in vitro.
(a) Expression levels of GFP, Sema6A-GFP and Sema6AΔcyto-GFP in NIH3T3 cells. Quantification showed decreased expression of Sema6A-GFP and Sema6AΔcyto-GFP compared to GFP. No difference was found between Sema6A-GFP and Sema6AΔcyto-GFP. $n = 3$ coverslips. Data are presented as means ± standard deviation. (b) Outgrowth of cortex neurons was decreased when challenged with Sema6A-GFP or Sema6AΔcyto-GFP. Primary cortex neurons were grown on NIH3T3 cells transiently expressed with GFP, Sema6A-GFP or Sema6AΔcyto-GFP. The ratio between the spanning region and area of the explant was used to assess the outgrowth of cortical neurons. Quantification showed reduced outgrowth when neurons interacted with Sema6A-GFP or Sema6AΔcyto-GFP compared to GFP. Bar graphs represent SEM. $n = 5$ experiments. Student's *t*-test, * $p > 0.05$, ** $p > 0.01$. Data are presented as means ± s.e.m. Scale bar (a) 40 µm, (b) 500 µm.

blot. Blots showed a ±160 kDa band for Sema6A-GFP and a ±120 kDa band for truncated Sema6AΔcyto-GFP using Sema6A- or GFP-specific antibodies (Fig. 1b). Next, Sema6A-GFP or Sema6AΔcyto-GFP was transiently overexpressed in N2A cells to validate protein production and membrane-localization of Sema6A-GFP and Sema6AΔcyto-GFP (Fig. 1c). Both proteins showed cell surface expression and no differences in surface expression were found between Sema6A-GFP and Sema6AΔcyto-GFP ($n = 3$ experiments, Student's *t*-test, $p_{(\text{Sema6A-GFP, Sema6AΔcyto-GFP})} = 0.293$). Accumulation of protein was absent in the cytoplasm. To establish whether the constructs were similarly processed *in vitro* in neurons, primary cultures were used. Sema6A is endogenously expressed in pyramidal cells of the cortex [42]. Therefore, Sema6A-GFP and Sema6AΔcyto-GFP were transiently overexpressed in primary cortical neurons to assess protein distribution (Fig. 1d). Both proteins showed normal (cell surface) expression patterns. This was confirmed by quantifying cell surface expression for Sema6A-GFP and Sema6AΔcyto-GFP in relation to cytosolic expression ($n = 3$ experiments, Student's *t*-test, $p_{(\text{Sema6A-GFP, Sema6AΔcyto-GFP})} = 0.122$). This shows that Sema6AΔcyto-GFP is expressed and localized similar to Sema6A-GFP.

The Sema6AΔcyto-GFP truncated protein lacks the intracellular domain containing activation sites for downstream signalling. Consequently, the receptor function of the Sema6AΔcyto-GFP is compromised [7]. However, whether the ligand function of

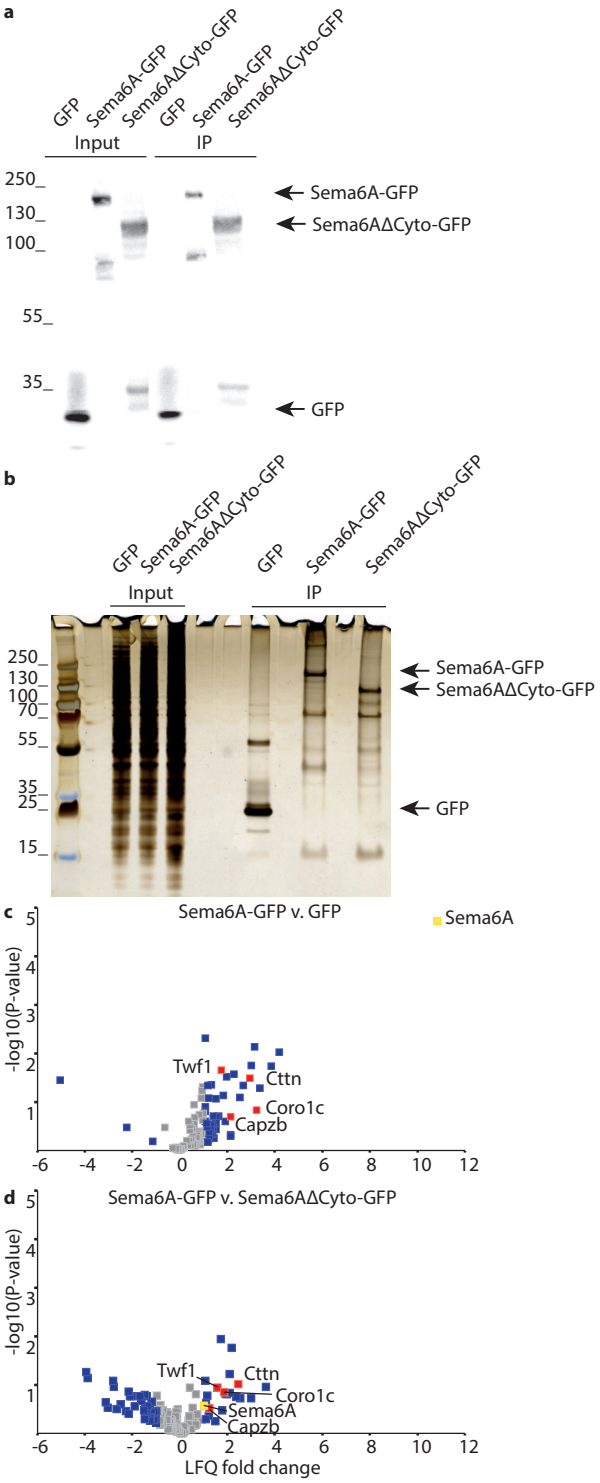

Figure 3 | Identifying novel Sema6A-interacting proteins via mass spectrometry. (a) GFP-trap pulldown of GFP, Sema6A-GFP and Sema6AΔcyto-GFP from transient expressed N2A cells. Immunoblots were labelled with rabbit-anti-GFP. Numbers indicate protein size in kDa. *n* = 3 experiments. (b) Silver gel from immunoprecipitated samples. Numbers show protein size in kDa. *n* = 3 experiments. (c-d) Volcano plot denoting differentially bound protein interactors for Sema6A-GFP compared to GFP (c) and Sema6AΔcyto-GFP (d). Each point represents a protein. Proteins are considered significant (blue) when three valid values were measured within one group, FDR < 0.01 and intensity differences exceeded 1.0. The bait (Sema6A) is depicted in yellow and the candidate interactors are shown in red. In grey are not significant hits.

Table 1 | Gene-ontology analysis of the Sema6A-interactome.

Biological Process	GO ID	Mouse REF list	# proteins	# proteins expected by chance	Fold Enrichment	Raw p-value	FDR
translation	GO:0006412	241	66	10,19	6,48	2,10E29-	3,76E26-
metabolic process	GO:0008152	4091	301	173,03	1,74	1,73E22-	6,18E20-
protein folding	GO:0006457	101	27	4,27	6,32	1,39E12-	3,10E10-
cellular component organization	GO:0016043	1748	134	73,93	1,81	1,05E10-	1,56E08-
organic acid biosynthetic process	GO:0016053	84	22	3,55	6,19	2,29E10-	2,56E08-
carboxylic acid biosynthetic process	GO:0046394	84	22	3,55	6,19	2,29E10-	2,73E08-
intracellular protein transport	GO:0006886	663	67	28,04	2,39	6,94E10-	6,21E08-
organelle organization	GO:0006996	762	73	32,23	2,27	9,16E10-	7,45E08-
cellular process	GO:0009987	6139	347	259,65	1,34	1,37E09-	1,07E07-
cellular protein localization	GO:0034613	799	73	33,79	2,16	4,46E09-	3,33E07-
protein ubiquitination	GO:0016567	208	29	8,8	3,3	1,27E07-	6,49E06-
gene expression	GO:0010467	1771	122	74,9	1,63	2,80E07-	1,39E05-
tricarboxylic acid cycle	GO:0006099	24	10	1,02	9,85	6,23E07-	2,79E05-
protein-containing complex assembly	GO:0065003	175	25	7,4	3,38	6,17E07-	2,83E05-
cytoskeleton organization	GO:0007010	227	29	9,6	3,02	6,54E07-	2,85E05-
cellular component biogenesis	GO:0044085	213	28	9,01	3,11	6,08E07-	2,86E05-
protein modification by small protein conjugation or removal	GO:0070647	228	29	9,64	3,01	7,09E07-	3,02E05-
protein-containing complex subunit organization	GO:0043933	218	28	9,22	3,04	9,22E07-	3,75E05-
cellular amino acid biosynthetic process	GO:0008652	50	13	2,11	6,15	1,19E06-	4,61E05-
ribonucleoprotein complex biogenesis	GO:0022613	135	21	5,71	3,68	1,44E06-	5,49E05-
organic substance biosynthetic process	GO:1901576	268	31	11,33	2,73	1,85E06-	6,77E05-
aerobic respiration	GO:0009060	36	11	1,52	7,22	2,11E06-	7,56E05-
positive regulation of transcription initiation from RNA polymerase II promoter	GO:0060261	6	6	0,25	23,64	3,29E06-	1,13E04-
positive regulation of protein complex assembly	GO:0031334	7	6	0,3	20,27	5,90E06-	1,96E04-
organelle assembly	GO:0070925	127	19	5,37	3,54	7,45E06-	2,26E04-
nucleoside triphosphate biosynthetic process	GO:0009142	26	9	1,1	8,18	7,82E06-	2,33E04-

coenzyme biosynthetic process	GO:0009108	52	12	2,2	5,46	8,71E06-	2,56E04-
RNA splicing	GO:0008380	180	23	7,61	3,02	9,14E06-	2,64E04-
purine ribonucleoside triphosphate biosynthetic process	GO:0009206	21	8	0,89	9,01	1,43E05-	3,66E04-
purine nucleoside triphosphate biosynthetic process	GO:0009145	21	8	0,89	9,01	1,43E05-	3,71E04-
cofactor biosynthetic process	GO:0051188	58	12	2,45	4,89	2,26E05-	5,46E04-
oxidation-reduction process	GO:0055114	127	18	5,37	3,35	2,47E05-	5,88E04-
actin filament organization	GO:0007015	129	18	5,46	3,3	2,97E05-	6,48E04-
energy derivation by oxidation of organic compounds	GO:0015980	105	16	4,44	3,6	3,14E05-	6,54E04-
cellular respiration	GO:0045333	105	16	4,44	3,6	3,14E05-	6,62E04-
phosphorylation	GO:0016310	32	9	1,35	6,65	3,12E05-	6,64E04-
ribosome biogenesis	GO:0042254	117	17	4,95	3,44	3,10E05-	6,68E04-
actin filament depolymerization	GO:0030042	11	6	0,47	12,9	3,70E05-	7,61E04-
regulation of RNA polymerase II transcriptional preinitiation complex assembly	GO:0045898	6	5	0,25	19,7	4,10E05-	8,06E04-
regulation of transcription initiation from RNA polymerase II promoter	GO:0060260	6	5	0,25	19,7	4,10E05-	8,15E04-
cell cycle	GO:0007049	539	45	22,8	1,97	4,27E05-	8,21E04-
ATP biosynthetic process	GO:0006754	19	7	0,8	8,71	5,92E05-	1,10E03-
DNA replication	GO:0006260	124	17	5,24	3,24	5,97E05-	1,10E03-
RNA processing	GO:0006396	229	25	9,69	2,58	6,84E05-	1,21E03-
protein homooligomerization	GO:0051260	7	5	0,3	16,89	6,79E05-	1,22E03-
COPII-coated vesicle budding	GO:0090114	13	6	0,55	10,91	7,57E05-	1,33E03-
localization	GO:0051179	2123	128	89,79	1,43	7,99E05-	1,39E03-
establishment of localization	GO:0051234	1372	90	58,03	1,55	8,70E05-	1,48E03-
response to oxidative stress	GO:0006979	21	7	0,89	7,88	9,92E05-	1,57E03-
protein complex oligomerization	GO:0051259	8	5	0,34	14,78	1,07E04-	1,66E03-
purine nucleobase biosynthetic process	GO:0009113	8	5	0,34	14,78	1,07E04-	1,68E03-
regulation of protein complex assembly	GO:0043254	32	8	1,35	5,91	1,73E04-	2,51E03-
Arp3/2 complex-mediated actin nucleation	GO:0034314	10	5	0,42	11,82	2,33E04-	3,23E03-
generation of precursor metabolites and energy	GO:0006091	25	7	1,06	6,62	2,45E04-	3,35E03-
cellular macromolecule biosynthetic process	GO:0034645	141	17	5,96	2,85	2,43E04-	3,35E03-
cellular homeostasis	GO:0019725	36	8	1,52	5,25	3,45E04-	4,50E03-
actin filament polymerization	GO:0030041	57	10	2,41	4,15	3,51E04-	4,55E03-

cellular protein catabolic process	GO:0044257	279	26	11,8	2,2	3,60E04-	4,64E03-
pigment biosynthetic process	GO:0046148	19	6	0,8	7,47	4,01E04-	5,13E03-
neuron projection development	GO:0031175	49	9	2,07	4,34	5,12E04-	6,40E03-
movement of cell or subcellular component	GO:0006928	61	10	2,58	3,88	5,64E04-	6,92E03-
response to heat	GO:0009408	22	6	0,93	6,45	7,69E04-	8,93E03-

All 925 proteins identified in this mass spectrometry were analysed using Panther and categorized by biological process. The biological processes were depicted when they were enriched in Sema6A-GFP and showed an FDR > 0.01.

Sema6AΔcyto-GFP is intact is unknown. *In vitro*, Sema6A can function as a ligand by attenuating cerebellar granule cellular outgrowth [7] and genetic ablation of Sema6A leads to cortical defects *in vivo* [42]. Sema6A-GFP and Sema6AΔcyto-GFP are processed regularly in cortical neurons (Fig. 1). An exploratory study using cortical explants grown on NIH3T3 expressing Sema6A confirmed that Sema6A forward signalling attenuates neurite outgrowth in cortical neurons (data not shown). To assess whether a similar effect occurs for the truncated Sema6A, cortical explants were placed on NIH3T3 cells expressing GFP, Sema6A-GFP or Sema6AΔcyto-GFP for 48 hours (Fig. 2). First, expression of GFP, Sema6A-GFP and Sema6AΔcyto-GFP was assessed in NIH3T3 cells (Fig. 2a). Quantification showed higher protein expression for GFP compared to Sema6A-GFP and Sema6AΔcyto-GFP (n = 3 coverslips, Student's t-test, $p_{(GFP, Sema6A\text{-}GFP)} = 0.006$, $p_{(GFP, Sema6A\Delta cyto\text{-}GFP)} = 0.005$). However, expression levels were not different between Sema6A-GFP and Sema6AΔcyto-GFP ($n = 3$ coverslips, Student's t-test, $p_{(Sema6A\text{-}GFP, Sema6A\Delta cyto\text{-}GFP)} = 0.770$). This indicates that Sema6A-GFP and Sema6AΔcyto-GFP show similar expression, as shown in Figure 1b-d. Next, cortical explants were cultured for 48 hours on transiently transfected NIH3T3 to assess forward signalling of Sema6A (Fig. 2b). The outgrowth ratio was similarly decreased for Sema6A-GFP and Sema6AΔcyto-GFP compared to GFP ($n = 5$ experiments, Student's t-test, $p_{(GFP, Sema6A\text{-}GFP)} = 0.011$, $p_{(GFP, Sema6A\Delta cyto\text{-}GFP)} = 0.007$). No difference was found between Sema6A-GFP and Sema6AΔcyto-GFP ($n = 5$ experiments, Student's t-test, $p_{(Sema6A\text{-}GFP, Sema6A\Delta cyto\text{-}GFP)} = 0.833$) indicating intact ligand function for Sema6AΔcyto-GFP.

Together these results indicate that Sema6A-GFP and Sema6AΔcyto-GFP are normally processed and expressed in cells and both exert forward signalling events.

Novel Sema6A-interacting proteins identified with mass spec and GO-analysis

To study the intracellular signalling cascade of Sema6A, novel Sema6A-interacting protein were identified via GFP-trap immunoprecipitation followed by mass spectrometry analysis. GFP, Sema6A-GFP and Sema6AΔcyto-GFP were overexpressed in N2A cells and lysates were blotted for GFP showing pull down of these proteins (Fig. 3a). In the mass spec data, specific enrichment was found for Sema6A-interactor proteins compared to controls. GFP served as a negative control while Sema6AΔcyto-GFP controlled for Sema6A interacting proteins, non-specific for the intracellular domain (Fig. 3b). Mass spectrometry analysis identified 925 proteins (insignificant hits in grey) of which 43 were significantly enriched (in blue) in Sema6A-GFP complexes compared to GFP (Fig. 3c). Further comparisons revealed 21 proteins significantly enriched in Sema6A-GFP to Sema6AΔcyto-GFP complexes (Fig. 3d). GO-analysis via overrepresentation with a Mus Musculus gene ontology reference list 41 revealed strong enrichment for biological processes in which Sema6A is known to play a role, such as Actin related proteins (Arp) 2/3 complex-mediated actin nucleation

Table 2 | Table of novel potential Sema6A-interacting proteins.

Protein Name	GO ID	Biological process	GFP v. Sema6A-GFP		Sema6A-GFP v. Sema6AΔcyto	
			Intensity difference	-log p-value	Intensity difference	-log p-value
Actr2	*GO:0034314*	*Arp2/3 complex-mediated actin nucleation*	*4.17*	*2.03*	*3.53*	*0.95*
Arpc1b	*GO:0034314*	*Arp2/3 complex-mediated actin nucleation*	*3.83*	*1.73*	*2.89*	*0.72*
Arpc2	*GO:0034314*	*Arp2/3 complex-mediated actin nucleation*	*3.37*	*1.28*	*2.468*	*0.72*
Coro1c	***GO:0007015***	***Actin filament organization***	***3.22***	***0.83***	***1.91***	***0.80***
Arpc1a	*GO:0034314*	*Arp2/3 complex-mediated actin nucleation*	*3.14*	*2.13*	*1.846*	*0.81*
Arpc3	*GO:0034314*	*Arp2/3 complex-mediated actin nucleation*	*3.01*	*1.76*	*2.28*	*0.74*
Cttn	***GO:0008154***	***Actin polymerization or depolymerization***	***2.95***	***1.49***	***2.38***	***1.02***
Actr3	*GO:0034314*	*Arp2/3 complex-mediated actin nucleation*	*2.66*	*1.34*	*2.02*	*0.83*
CapZb	***GO:0030833***	***Regulation of actin filament polymerization***	***2.15***	***0.70***	***1.17***	***0.52***
Twf1	***GO:0008154***	***Actin polymerization or depolymerization***	***1.75***	***1.66***	***1.51***	***0.93***
Hspa5	GO:0051130	Positive regulation of cellular component organization	2.54	1.09	1.07	0.77
Luc7l2	GO:0009987	Cellular process	1.08	0.90	2.08	1.75
Adprh	GO:0009987	Cellular process	1.10	0.27	2.02	1.22
Hmgb2	GO:2001234	Negative regulation of apoptotic signaling pathway	1.32	1.36	1.79	0.85
Mapk1	GO:1903829	Positive regulation of cellular protein localization	1.29	0.43	1.69	0.47
Cpsf6	GO:0006397	mRNA processing	1.08	2.31	1.65	1.93
Fn3krp	N.D.	N.D.	1.52	0.44	1.42	0.25
Hnrnph1	GO:0006397	mRNA processing	1.52	0.57	1.13	0.36
Ppib	GO:0006457	Protein folding	1.38	0.54	1.02	0.62
Hmgb1	GO:0080135	Regulation of cellular response to stress	1.19	1.34	1.01	1.08
Ddx3x	GO:0006417	Regulation of translation	1.13	0.56	1.03	0.30

List of 21 novel candidates in Sema6A signalling depicted with their GO ID, biological process and mass spectrometry intensity difference score.

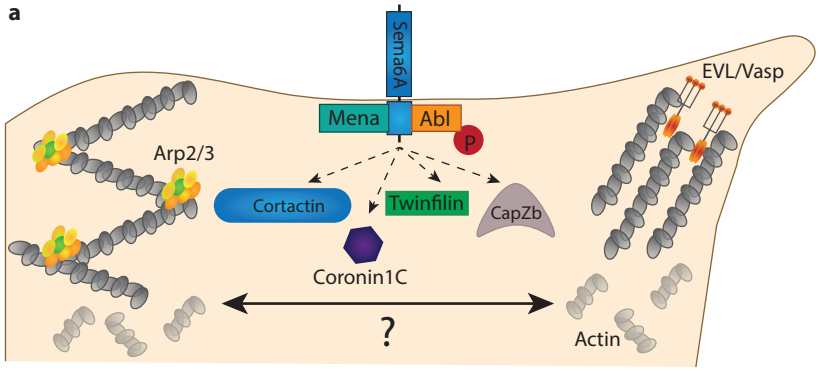

Figure 4 | Schematic overview of Sema6A intracellular signalling in actin remodelling.
The formation of lamellipodia and filopodia are tightly controlled and are greatly influenced by Arp2/3 complex and EVL/VASP pathway, respectively. Arp2/3 complex and EVL/VASP pathway compete for available actin to promote lamellipodia or filopodia formation. During lamellipodia formation, coordinated action of Arp2/3 complex proteins, Cortactin and WAVE promote actin branching, which are stabilized Twinfilin-CapZb. Actin turnover is controlled by Cofilin and Coronin. The EVL/VASP-pathway is crucial for filopodia where binding of EVL proteins, like Mena, bundle actin filaments. Abl modulates the phosphorylation of Mena. Twinfilin-CapZb do not cap the filaments to allow for actin polymerization. Cross-talk between the Arp2/3 complex and EVL/VASP-pathway is observed through Cortactin, Abl and Mena. Novel Semaphorin 6A (Sema6A)-interacting proteins are involved in the Arp2/3 complex and EVL/VASP pathway. How Sema6A influences these proteins and how this can affect actin remodelling through Arp2/3 complex or EVL/VASP pathway is unknown. WAVE; WASP-family verprolin-homologous protein, CapZb: Capping Actin Protein Of Muscle Z-Line Subunit Beta, EVL/VASP: VASP-like protein / Vasodilator stimulated phosphoprotein, Arp2/3: Actin related proteins 2/3, Mena: Murine ena, Abl: Abelson.

(FDR, $p = 0.003$) and various actin-regulating processes (FDR, $p_{\text{(actin lament organization)}} = 0.0006$, $p_{\text{(actin lament depolymerization)}} = 0.0007$, $p_{\text{(actin lament polymerization)}} = 0.005$) (Table 1). Together, these results identify multiple novel Sema6A-interacting proteins that have interesting roles in actin remodelling, protein localization, mRNA binding and Arp2/3 signalling (Table 2).

Discussion

Reverse signalling of Sema6A is essential during development. However, the precise mechanism and proteins involved in this process are incompletely understood. In this study, Sema6A constructs were generated to study reverse signalling. We found that Sema6A-GFP and Sema6AΔcyto-GFP were comparably processed and expressed in N2A cells and primary cortical neurons. Sema6A-GFP and Sema6AΔcyto-GFP decreased axon outgrowth of primary cortical explants to a similar extent indicating intact forward signalling for Sema6AΔcyto-GFP. Mass spectrometry analysis identified specific interactors in Sema6A-GFP. GO-analysis showed involvement of actin remodelling pathways and suggests candidates for further analysis in reverse signalling downstream of Sema6A.

Identification of novel Sema6A-interacting proteins

To study reverse signalling of Sema6A, full-length (Sema6A-GFP) and a truncated form of Sema6A lacking the intracellular domain (Sema6AΔcyto-GFP) were generated. We first validated the constructs to ensure proper protein expression, protein localization and intact forward signalling. First, we found similar expression for Sema6A-GFP and Sema6AΔcyto-

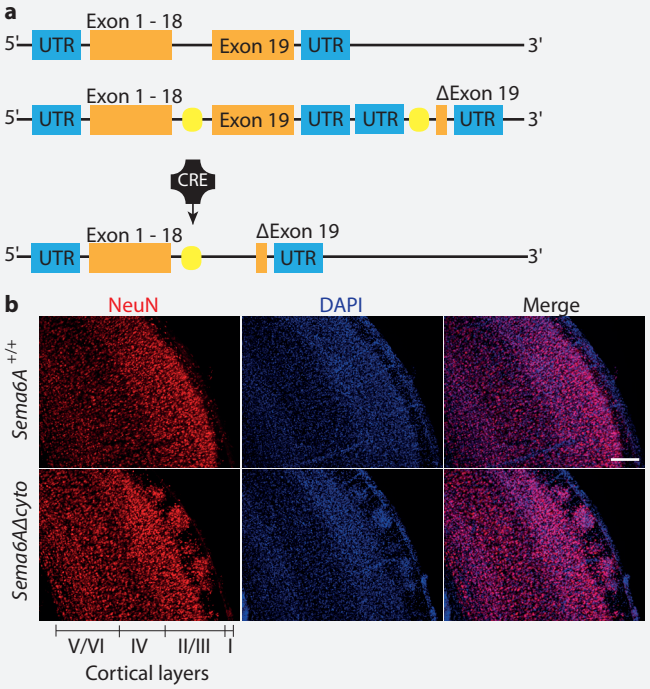

Box 1. Sema6A signalling in the cortex, have a look both ways.
Semaphorin 6A is a transmembrane protein that interacts with PlexinA2 or PlexinA4 to exert actin remodelling. Genetic ablation of full-length Sema6A revealed a defect in the cellular organisation of the cortex *in vivo* [42]. The otherwise cell-sparse border is now invaded with cells, seemingly from layer II/III. Cortical laminar organisation occurs between E13 and E18, at P0 all the layers are established [67,68]. Rünker et al., observed the defect from P3 onwards, suggesting that all the layers form initially in the Sema6A KO mouse. It is unclear how loss of Sema6A induces this disorganisation of the cortical layers postnatal. To study the contribution of forward and reverse signalling to Sema6A's function in the cortex, a mutated mouse was generated to express a truncated form of Sema6A (a). Using Cre-Lox recombination the intracellular domain 19 was deleted while a mutated, shorter exon 19 was inserted. This so-called *Sema6AΔcyto* mouse expresses Sema6A lacking the intracellular signalling domains, thus lacking reverse signalling. *Ex vivo* characterization of the mouse revealed an identical defect appearing in the first postnatal week and evident at P10 in cortical organisation. In conclusion, the *Sema6AΔcyto* mouse indicates the importance of Sema6A's reverse signalling during brain development. To deepen our understanding of reverse signalling of Sema6A, the complete downstream interactome need to be identified.

GFP. We showed that both proteins were expressed and localized to the cell membrane, independent of their intracellular domains (Fig. 1). Next, cortical explants were used to show that forward signalling was intact for Sema6A-GFP and Sema6AΔcyto-GFP. Both constructs reduced outgrowth of cortical explants compared to GFP (Fig. 2), similar to previous data showing Sema6A forward signalling to decrease outgrowth of cerebellar granule cells [7]. Together, these results show that protein processing, localization and forward signalling of Sema6A are independent of its intracellular domain.

To identify potential novel Sema6A-interacting proteins involved in reverse signalling, the Sema6A constructs were expressed in N2A cells followed by immunoprecipitation. Protein lysates were analysed by western blot and sent for mass spectrometry analysis. 925 proteins were identified of which 21 were significantly enriched for Sema6A intracellular signalling. Several previously reported interactors for Sema6A (Abl, Mena, Flns and Mpp6)

were not identified in our study [7,26,32]. Abl and Mena are found downstream of Sema6A after PlexinA2 activation [7,26]. Interestingly, when Sema6A is not activated by PlexinA2, Abl does not interact with Sema6A [7]. In our study, Sema6A was not stimulated prior to the IP, which may explain our inability to detect this interactor. Co-transfected Flns and Mpp6 co-IP with Sema6A from Sema6A-transfected HEK293T cells [32]. Perhaps we did not identify Flns and Mpp6 due to experimental differences. In our study, we use an unbiased approach where Sema6A acts as bait in a neuronal cell line while other cell lines were used to identify Flns and Mpp6.

The 925 identified proteins were used for GO-analysis and revealed biological processes involved in general protein production, localization and processing pathways such as protein synthesis, folding and ubiquitination (Table 1). GO-analysis showed a strong enrichment for actin remodelling pathways (Fig. 3, Table 1 and 2), in line with previously reported functions of Sema6A [7,43–45]. Using the GO-analysis data, ten of the 21 significant enriched proteins in Sema6A-GFP complexes were prioritized due to their involvement in actin remodelling and Arp2/3 complex pathways (in italics, Table 2). Finally, a selection of four proteins was based on their actin remodelling capabilities and novelty in Sema6A signalling (in bold, Table 2). The other six identified proteins were Arp2/3 complex proteins. These proteins hits need to be validated in future research by (*in vivo*) co-IP experiments. In addition, their involvement in Sema6A reverse signalling needs to be validated. The downstream signalling cascade can be activated upon chemically induced multimerisation (CIM) of Sema6A complexes, resulting in decreased axonal length in cultured neurons [7]. Using this tool we can determine phosphorylation in the novel identified Sema6A-interacting proteins changes via western blot analysis to validate their role in Sema6A-induced reverse signalling. This will additionally provide valuable information regarding their function in Sema6A signalling.

In conclusion, these results identify the Arp2/3 complex as a possible, novel actin-modulating pathway downstream of Sema6A. Moreover, Cortactin, Coronin1C, CapZb and Twinfilin are strongly implicated in Arp2/3 complex-mediated actin remodelling and may fulfil a regulatory role downstream of Sema6A.

Sema6A-interacting proteins are involved in Arp2/3 complex actin remodelling

Reverse signalling of Sema6A influences actin dynamics [7,26,43]. This study identified the actin modulating Arp2/3 complex and associated proteins: Cortactin, Coronin1C, CapZb and Twinfilin in the interactome of Sema6A via mass spectrometry analysis (Table 2). Actin remodelling requires coordination of numerous complex mechanisms (reviewed e.g. by 46 & 47) where the Arp2/3 complex is a well known actin nucleating mechanism that promotes the formation of branched filaments necessary for lamellipodia [46,48–50]. The identified Sema6A-interacting proteins are also involved in the formation of lamellipodia. Cortactin and Coronin have been implicated in Arp2/3-complex-mediated lamellipodia formation by either promoting or inhibiting its activity, respectively [51–55]. In addition, recent findings reveal that binding of Twinfilin to CapZ resulted in increased stability of barbed ends of actin filaments, thereby limiting actin polymerization [56,57]. Future studies should determine whether actin nucleation is altered upon Sema6A reverse signalling and whether Cortactin, Coronin1C, Twinfilin or CapZb are involved in this process. Although the precise mechanism-of-action is undetermined in Sema6A reverse signalling, this is the first study identifying proteins that are implicated in Arp2/3 complex-mediated actin remodelling in the interactome of class 6 Semaphorins.

In conclusion, we identified novel Sema6A-interacting proteins Cortactin, Coronin1C, CapZb and Twinfilin, which are associated with Arp2/3 complex-mediated lamellipodia formation. Previously identified Sema6A-interacting proteins Mena en Abl are involved in EVL/VASP-pathway-mediated actin remodelling [7,26]. Together this implies that reverse signalling of Sema6A can act through Arp2/3 complex or EVL/VASP-pathway to modulate actin (Fig. 4). A competition theory has been described between EVL/VASP-pathway and Arp2/3 complex for actin to promote filopodia or lamellipodia, respectively [58,59]. Interestingly, cross-talk is observed between EVL/VASP-pathway and Arp2/3 complex by Abl, Mena and Cortactin [60–62]. Perhaps reverse signalling of Sema6A is involved in the balance to form either Arp2/3 complex-mediated lamellipodia or EVL/VASP-pathway-mediated filopodia.

Contributions of novel Sema6A-interacting proteins in reverse signalling

Reverse signalling of Sema6A is important for proper cortical laminar organisation (Box 1). The identified Sema6A-interacting proteins link Sema6A to the actin skeleton (Fig. 3) [7,26,32]. The novel identified Sema6A-interacting proteins may be involved in the balance between lamellipodia and filopodia formation, possibly via Arp2/3 complex and EVL/VASP-pathway, respectively (Fig. 4). The formation and functions of lamellipodia and filopodia in neurons are excellent reviewed [46,63,64]. In short, lamellipodia are characterized by branched actin networks that form major protrusions to promote migration. Filopodia can steer growth cones and cells by dynamic, thin protrusions characterized by dense bundles of actin. Coordinated action of lamellipodia and filopodia is important for axon guidance and cell migration. How Sema6A can influence cortical laminar organisation and whether this involves lamellipodia or filopodia formation is unclear. Interestingly, triple KO of *Mena, VASP* and *EVL* resulted in a cobblestone cortex [65]. This can indicate that downstream signalling of Sema6A via EVL/VASP-pathway could influence cortical laminar organisation. Manipulation of the Sema6A-interacting proteins via overexpression, constitutively active [66] and knockdown/out approaches will help to identify the roles of EVL/VASP-pathway- and Arp2/3 complex-mediated actin remodelling in reverse signalling. In conclusion, investigating the downstream signalling pathway of Sema6A will help to better understand reverse signalling mechanisms and how it can contribute to correct cortical laminar organisation.

Conclusion

In this study, we generated a full-length Sema6A construct and a truncated form of Sema6A lacking the intracellular domain (Sema6AΔcyto-GFP) to study the reverse signalling by identifying novel Sema6A-interacting proteins. Full-length Sema6a-GFP and Sema6AΔcyto-GFP were processed and expressed in similar manners and both acted as a ligand. Immunoprecipitation of Sema6A followed by mass spectrometry resulted in the identification of novel interactors of Sema6A. Our study is the first to identify Arp2/3 complex proteins in the interactome of class 6 Semaphorins. In addition, the novel Sema6A-interacting proteins are key regulators in Arp2/3 complex-mediated actin branching. Following validation, the functions of these interactors in Sema6A reverse signalling need to be established in future experiments. Together this study strongly implies the Arp2/3 complex as a novel actin-remodelling pathway in Sema6A signalling.

Acknowledgements

We are grateful to the members of the Pasterkamp laboratory and the Department of Translational Neuroscience for assistance and helpful discussions throughout this project. An ALW-Vici Grant from NWO, Stichting ParkinsonFonds and Dynamics of Youth Seed Money grant from Utrecht University financially supported this work.

Author Contributions

S.L., M.G.V. and R.J.P designed all experiments. S.L. and K.R. generated Sema6A constructs. S.L. performed *in vitro* validation experiments, immunoprecipitation experiments and GO-analysis. A.K. contributed to cortical explant experiments. E.R. and J.A.A.D. conducted mass spectrometry analysis. S.L., G.M.J.R. and R.J.P. wrote the manuscript with input from all authors.

References

1. Pasterkamp, R. J. Getting neural circuits into shape with semaphorins. *Nat Rev Neurosci* 13, 605–18 (2012).
2. Alto, L. T. & Terman, J. R. Semaphorins and their Signaling Mechanisms. *Methods Mol Biol* 1493, 1–25 (2017).
3. van Battum, E. Y., Brignani, S. & Pasterkamp, R. J. Axon guidance proteins in neurological disease. *Lancet Neurol* 14, 532–546 (2015).
4. Worzfeld, T. & Offermanns, S. Semaphorins and plexins as therapeutic targets. *Nat Rev Drug Discov* 13, 603–21 (2014).
5. Morrie, R. D. & Feller, M. B. A Dense Starburst Plexus Is Critical for Generating Direction Selectivity. *Curr Biol* 1–9 (2018).
6. Belle, M., Parray, A., Belle, M., Chédotal, A. & Nguyen-Ba-Charvet, K. T. PlexinA2 and Sema6A are required for retinal progenitor cell migration. *Dev Growth Differ* 58, 492–502 (2016).
7. Perez-Branguli, F. *et al.* Reverse Signaling by Semaphorin-6A Regulates Cellular Aggregation and *Neuron*al Morphology. *PLoS One* 11, e0158686 (2016).
8. Lakhina, V., Falnikar, A., Bhatnagar, L. & Tole, S. Early thalamocortical tract guidance and topographic sorting of thalamic projections requires LIM-homeodomain gene Lhx2. *Dev Biol* 306, 703–713 (2007).
9. Jongbloets, B. C. & Pasterkamp, R. J. Semaphorin signalling during development. *Development* 141, 3292–3297 (2014).
10. Nogi, T. *et al.* Structural basis for semaphorin signalling through the plexin receptor. *Nature* 467, 1123–1127 (2010).
11. Liu, H. *et al.* Structural basis of semaphorin-plexin recognition and viral mimicry from sema7A and A39R complexes with PlexinC1. *Cell* 142, 749–761 (2010).
12. Kong, Y. *et al.* Structural Basis for Plexin Activation and Regulation. *Neuron* 91, 548–560 (2016).
13. Wang, Y. *et al.* Plexins Are GTPase-Activating Proteins for Rap and Are Activated by Induced Dimerization. *Sci Signal* 5, ra6 (2012).
14. Wang, Y., Pascoe, H. G., Brautigam, C. A., He, H. & Zhang, X. Structural basis for activation and non-canonical catalysis of the Rap GTPase activating protein domain of plexin. *Elife* 2, e01279 (2013).
15. Battistini, C. & Tamagnone, L. Transmembrane semaphorins, forward and reverse signaling: have a look both ways. *Cell Mol Life Sci* 73, 1609–22 (2016).
16. Eckhardt, F., Behar, O. & Calautti, E. A Novel Transmembrane Semaphorin Can Bind c-src. *Mol Cell Neurosci* 419, 409–419 (1997).
17. Granziero, L. *et al.* CD100/plexin-B1 interactions sustain proliferation and survival of normal and leukemic CD5+ B lymphocytes. *Blood* 101, 1962–1969 (2003).
18. Toyofuku, T. *et al.* Guidance of myocardial patterning in cardiac development by Sema6D reverse signalling. *Nat Cell Biol* 6, 1204–1211 (2004).
19. Andermatt, I. *et al.* Semaphorin 6B acts as a receptor in post-crossing commissural axon guidance. *Development* 141, 3709–20 (2014).
20. Sun, T. *et al.* A reverse signaling pathway downstream of Sema4A controls cell migration via Scrib. *J Cell Biol* 216, 199–215 (2017).
21. Kang, S. *et al.* Semaphorin 6D reverse signaling controls macrophage Lipid Metabolism and Anti-Inflammatory Polarization. *Nat Immunol* 19, 561–570 (2018).
22. Yukawa, K. *et al.* Sema4A induces cell morphological changes through B-type plexin-mediated signaling. *Int J Mol Med* 25, 225–230 (2010).
23. Yukawa, K. *et al.* Semaphorin 4A induces growth cone collapse of hippocampal neurons in a Rho / Rho-kinase-dependent manner. *Int J Mol Med* 16, 115–118 (2005).
24. Mauti, O., Domanitskaya, E., Andermatt, I., Sadhu, R. & Stoeckli, E. T. Semaphorin6A acts as a gate keeper between the central and the peripheral nervous system. *Neural Dev* 2, 28 (2007).
25. Bernard, F. *et al.* Role of transmembrane semaphorin Sema6A in oligodendrocyte differentiation and myelination. *Glia* 60, 1590–1604 (2012).
26. Klostermann, A., Lutz, B., Gertler, F. & Behl, C. The orthologous human and murine semaphorin 6A-1 proteins (SEMA6A-1/Sema6A-1) bind to the enabled/vasodilator-stimulated phosphoprotein-like protein (EVL) via a novel carboxyl-terminal zyxin-like domain. *J Biol Chem* 275, 39647–39653 (2000).
27. Michael, M., Vehlow, A. & Navarro, C. c-Abl , Lamellipodin , and Ena / VASP Proteins Cooperate in Dorsal Ruffling of Fibroblasts and Axonal Morphogenesis. *Curr Biol* 20, 783–791 (2010).
28. Drees, F. & Gertler, F. B. Ena / VASP : Proteins at the tip of the nervous system. *Curr Opin Neurobiol* 18,

53–59 (2008).
29. Woodring, P. J., Hunter, T. & Wang, J. Y. J. Regulation of F-actin-dependent processes by the Abl family of tyrosine kinases. *J Cell Sci* 116, 2613–2626 (2003).
30. Colicelli, J. ABL Tyrosine Kinases: Evolution of Function, Regulation, and Specificity. *Sci Signal* 3, re6 (2010).
31. Lambrechts, A. *et al.* cAMP-dependent Protein Kinase Phosphorylation of EVL , a Mena / VASP Relative , Regulates Its Interaction with Actin and SH3 Domains. *J Biol Chem* 275, 36143–36151 (2001).
32. Jeong, S. *et al.* Varicose and cheerio collaborate with pebble to mediate semaphorin-1a reverse signaling in Drosophila. *Proc Natl Acad Sci* 114, E8254–E8263 (2017).
33. Gardel, M. L. *et al.* Prestressed F-actin networks cross-linked by hinged filamins replicate mechanical properties of cells. *PNAS* 103, (2006).
34. Pritchard, R. H., Huangb, Y. Y. S. & Terentjev, E. M. Mechanics of biological networks : from the cell cytoskeleton to connective tissue. *Soft Matter, R Soc Chem* 10, 1864–1884 (2014).
35. Saitoh, Y., Kamijo, A., Yamauchi, J., Sakamoto, T. & Terada, N. The membrane palmitoylated protein , MPP6 , is involved in myelin formation in the mouse peripheral nervous system. *Histochem Cell Biol* 151, 385-394 (2018).
36. Groen, E. J. N. *et al.* ALS-associated mutations in FUS disrupt the axonal distribution and function of SMN. *Hum Mol Genet* 22, 3690–3704 (2013).
37. Van Erp, S. *et al.* Lrig2 Negatively Regulates Ectodomain Shedding of Axon Guidance Receptors by ADAM Proteases Article Lrig2 Negatively Regulates Ectodomain Shedding of Axon Guidance Receptors by ADAM Proteases. *Dev Cell* 35, 537–552 (2015).
38. Cox, J. & Mann, M. MaxQuant enables high peptide identification rates, individualized p.p.b.-range mass accuracies and proteome-wide protein quantificatio. *Nat Biotechnol* 26, 1367–1372 (2008).
39. Kenter, A. T. *et al.* Identifying cystogenic paracrine signaling molecules in cyst fluid of patients with polycystic kidney disease. *Am J Physiol Ren Physiol* 316, (2019).
40. Sap, K. A. *et al.* Global Proteome and Ubiquitinome Changes in the Soluble and Insoluble Fractions of Q175 Huntington Mice brains. *Mol Cell Proteomics* 31, (2019).
41. Mi, H., Muruganujan, A., Huang, X., Guo, X. & Thomas, P. D. Protocol Update for large-scale genome and gene function analysis with the PANTHER. *Nat Protoc* 8, 1551–1566 (2016).
42. Rünker, A. E. *et al.* Mutation of Semaphorin-6A disrupts limbic and cortical connectivity and models neurodevelopmental psychopathology. *PLoS One* 6, e26488 (2011).
43. Prislei, S. *et al.* From plasma membrane to cytoskeleton: a novel function for semaphorin 6A. *Mol Cancer Ther* 7, 233–41 (2008).
44. Ebert, A. M., Childs, S. J., Hehr, C. L., Cechmanek, P. B. & McFarlane, S. Sema6a and Plxna2 mediate spatially regulated repulsion within the developing eye to promote eye vesicle cohesion. *Development* 141, 2473–82 (2014).
45. Emerson, S. E. *et al.* Identification of target genes downstream of Semaphorin6A/PlexinA2 signaling in zebrafish. *Dev Dyn* 1–47 (2017).
46. Rottner, K., Faix, J., Bogdan, S., Linder, S. & Kerkhoff, E. Actin assembly mechanisms at a glance. *J Cell Sci* 130, 3427–3435 (2017).
47. Bilimoria, P. M. & Bonni, A. Molecular control of axon branching. *Neuroscientist* 19, 16–24 (2013).
48. Weaver, A. M., Young, M. E., Lee, W. L. & Cooper, J. A. Integration of signals to the Arp2/3 complex. *Curr Opin Cell Biol* 15, 23–30 (2002).
49. Campellone, K. G. & Welch, M. D. A nucleator arms race: cellular control of actin assembly. *Nat Rev Microbiol* 11, 237–251 (2010).
50. Xavier, C.-P. *et al.* Phosphorylation of CRN2 by CK2 regulates F-actin and Arp2/3 interaction and inhibits cell migration. *Sci Rep* 2, 1–14 (2012).
51. Uruno, T. *et al.* Activation of Arp2/3 complex-mediated actin polymerization by cortactin. *Nat Cell Biol* 3, 259–266 (2001).
52. Selbach, M. & Backert, S. Cortactin: An Achilles' heel of the actin cytoskeleton targeted by pathogens. *Trends Microbiol* 13, 181–189 (2005).
53. Pant, K., Chereau, D., Hatch, V., Dominguez, R. & Lehman, W. Cortactin Binding to F-actin Revealed by Electron Microscopy and 3D Reconstruction. *J Mol Biol* 359, 840–847 (2006).
54. Humphries, C. L. *et al.* Direct regulation of Arp2/3 complex activity and function by the actin binding protein coronin. *J Cell Biol* 159, 993–1004 (2002).
55. Rosentreter, A. *et al.* Coronin 3 involvement in F-actin-dependent processes at the cell cortex. *Exp Cell Res* 313, 878–895 (2007).

56. Johnston, A. B. *et al.* A novel mode of capping protein- regulation by twinfilin. *Elife* 7, (2018).
57. Falck, S. *et al.* Biological role and structural mechanism of twinfilin – capping protein interaction. *EMBO journal* 23, 3010–3019 (2004).
58. Davidson, A. J. & Wood, W. Unravelling the Actin Cytoskeleton : A New Competitive Edge ? *Trends Cell Biol* 26, 569–576 (2016).
59. Rotty, J. D. & Bear, J. E. Competition and collaboration between different actin assembly pathways allows for homeostatic control of the actin cytoskeleton. *BioArchitecture 5*, 27–34 (2015).
60. Hughes, S. K., Oudin, M. J., Tadros, J., Neil, J. & Del, A. PTP1B-dependent regulation of receptor tyrosine kinase signaling by the actin-binding protein Mena. *Mol Biol Cell* 26, 3867–3878 (2015).
61. He, Y. *et al.* Src and cortactin promote lamellipodia protrusion and filopodia formation and stability in growth cones. *Mol Biol Cell* 26, (2015).
62. Courtemanche, N., Gifford, S. M., Simpson, M. A., Pollard, T. D. & Koleske, A. J. Abl2/Abl-related gene stabilizes actin filaments, stimulates actin branching by actin-related protein 2/3 complex, and promotes actin filament severing by cofilin. *J Biol Chem* 290, 4038–4046 (2015).
63. Konietzny, A., Bär, J. & Mikhaylova, M. Dendritic Actin Cytoskeleton : Structure , Functions , and Regulations. *Front Cell Neurosci* 11, (2017).
64. Pacheco, A. & Gallo, G. Actin filament-microtubule interactions in axon initiation and branching. *Brain Res Bull* (2016).
65. Kwiatkowski, A. V. *et al.* Ena/VASP Is Required for Neuritogenesis in the Developing Cortex. *Neuron* 56, 441–455 (2007).
66. Zambrano, N. *et al.* The β-Amyloid Precursor Protein APP Is Tyrosine-phosphorylated in Cells Expressing a Constitutively Active Form of the Abl Protoncogene. *J Biol Chem* 276, 19787–19792 (2001).
67. Greig, L. C., Woodworth, M., Galazo, M., Padmanabhan, H. & Macklis, J. Molecular logic of neocortical projection neuron specification, development and diversity. *Nat Rev Neurosci* 14, 755–69 (2013).
68. Hirota, Y. & Nakajima, K. Control of *Neurona*l Migration and Aggregation by Reelin Signaling in the Developing Cerebral Cortex. *Front cell Dev Biol* 5, 40 (2017).

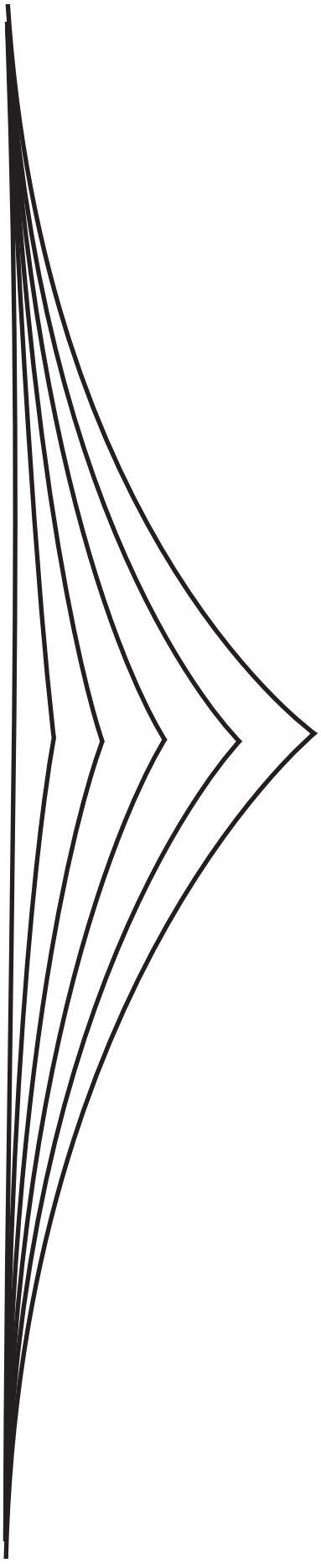

Chapter 6

Functional characterization of PLXNB3 rare variants associated with neurodevelopmental disorders in patients

Suzanne Lemstra[1], Gergely N. Nagy[2], Melissa E. Zwaan[1], Geert M. Ramakers[1], E. Yvonne Jones [2*], Peter M. van Hasselt[3*], R. Jeroen Pasterkamp[1]

[1.] Department of Translational Neuroscience, UMC Utrecht Brain Center, University Medical Center Utrecht, Utrecht University, Utrecht 3584 CG, the Netherlands [2.] Wellcome Trust Centre for Human Genetics, Oxford University, Oxford OX3 7BN, United Kingdom [3.] Department of Genetics and Center for Molecular Medicine, University Medical Center Utrecht, 3584 CX Utrecht, the Netherlands

* These authors contributed equally

In preparation

Abstract

Semaphorin-Plexin signalling is crucial for brain development and genetic alterations in Semaphorins or Plexins can result in neurodevelopmental disorders. DNA of patients with developmental delay, Autism Spectrum Disorder, epilepsy and hypotonia were analysed by diagnostic whole exome sequencing, revealing 19 rare variants in *PLXNB3*. The possible functional consequences of these variants were assessed in this study. First, variants were mapped to a homology structure of PLEXINB3 to predict structural changes. 12 of the 19 variants were predicted to alter the structure of PLEXINB3, ranging from protein misfolding, ligand binding to intracellular signalling. Protein production, localization and autoinhibition capabilities of the variants were determined by transient expression of the variants in cellular models. For 6 of the 19 variants, alterations in protein production, localization or autoinhibition were found, which may suggest defective PLEXINB3 signalling. Conclusive, this study is a first step to examine the genetic contribution of PLEXINB3 variants to brain disorders.

Introduction

Guidance cue families concert several different roles ranging far beyond axon guidance [1,2]. The guidance cue receptor family Plexins (for abbreviations see ref. 3), and their ligands Semaphorins, are largely involved in developmental processes and brain maintenance to ensure proper brain circuit formation and functioning [4,5]. Pathological changes in neural development and maturation are a unifying hallmark of neurodevelopmental disorders. Neurodevelopmental disorders can manifest early in childhood [6,7] and are characterized as multifactorial disorders where both genetic and environmental factors are considered as potential risk factors for their onset [7–10]. Genetic perturbed PLXNs and SEMAs are associated with neurodevelopmental disorders such as Autism Spectrum Disorder (ASD) and epilepsy [11]. Determining the genetic contribution of Semaphorins and Plexins can give valuable information regarding potential risk factors in multifactorial neurodevelopmental disorders.

Whole exome sequencing (WES) is a valuable tool to determine a genetic basis of human disease [12–15]. In this study, whole exome sequencing revealed rare variants of the X-chromosome *PLXNB3* gene in a patient cohort displaying broad clinical characteristics including developmental delay, ASD and epilepsy. PlexinB3 is the receptor for Sema4A and Sema5A [16,17]. The *PLXNB3*, *SEMA4A* and *SEMA5A* genes are associated with cognitive development in humans. *PLXNB3* associates with increased volumes of white matter that correlates with higher performances in vocabulary tests [18]. *SEMA5A* is associated with ASD [19–21] and epilepsy [22]. In one individual with intellectual disability a microdeletion was found that contained the *SEMA4A* gene [23]. Together, this suggests that perturbed PLEXINB3-Semaphorin signalling can be considered as a risk factor underlying multifactorial neurodevelopmental disorders.

PLXNB3 translates into the transmembrane guidance cue receptor PLEXINB3 containing SEMA, PSI (Plexin, Sema, Integrin) and IPT (Ig-like, Plexins, Transcription factor) domains. The intracellular domain consists of binding motifs for end-binding proteins (EB-motifs), a Rho binding domain (RBD), RasGAP domains and lastly a PDZ binding motif [24–27]. To prevent premature activation of downstream signalling, the ectodomain of PlexinA forms a ring-like structure and bind in *cis* with other PlexinAs in a head-to-stalk manner (dom. 1 to dom. 4-5). In this ring-like state, dimerization of the cytoplasmic domain can not occur leading to autoinhibition of PlexinA [28]. Upon ligand binding in *trans* (dom. 1-4 for PlexinA, Dom. 1-2 for PlexinB1), subtle reorientation of Plexin couples from ectodomain dimerization to cytoplasmic dimerization [28,29], which opens the intracellular GTPase activating protein (GAP) active site to allow inactivation of Rap through GTP hydrolysis [30,31]. Inactivation of Rap induces cytoskeleton dynamics and promotes growth cone collapse [30,31]. Rac1 or Rho GTPases are not influenced by Plexins GAP activity, but are involved in downstream actin remodelling signalling cascades of Plexins [32–34]. Although it is undetermined whether autoinhibition of PlexinB3 prevents premature activation, downstream signalling cascades of PlexinB result in actin remodelling by activation of its GAP domain and recruitment of other GTPases.

PlexinB3 is expressed in murine oligodendrocytes, hippocampal neurons and cerebellum neurons [16,35–38]. In human, *PLXNB3* is expressed in the cerebellum ([38], Allen human brain atlas), hippocampus and other brain regions in neuronal and glial cells (Allen human brain atlas). PlexinB3 signalling is involved in cerebellar neurite outgrowth and hippocampal synapse formation [25,35,38,39]. Similar roles are described for Sema4A and Sema5A [40,41]. For instance, Sema4A and Sema5A mediate inhibitory and excitatory synapse

development in hippocampal neurons [41,42]. Semaphorin-Plexin signalling is complex and often is not restricted to one binding partner within one system [43–46]. Therefore, although the changes mediated by Sema4A and Sema5A are related to PlexinB2 and PlexinA2, respectively [41,42], there may be involvement of PlexinB3 as well [38]. In support of this, Sema4A or Sema5A-PlexinB3-mediated effects are known to induce actin remodelling *in vitro* [16,17,47]. Together, this indicates that PlexinB3-signalling is important for proper brain development and wiring.

In this study, in a cohort of patients with a broad phenotypic spectrum are associated with rare variants in the *PLXNB3* gene that were identified via WES and gathered via Genematcher initiative. We studied the potential biological consequences of these rare PLEXINB3 variants. 19 variants were examined *in silico* to predict structural consequences. Next, we determined protein production, localization and autoinhibitory mechanisms in 17 of the PLEXINB3 variants using *in vitro* assays. Together, these data are a first step to provide insight into the potential contribution of perturbed PLEXINB3 signalling in multifactorial neurodevelopmental disorders

Methods

Patient cohort. Patients were gathered via Genematcher initiative [48]. Informed consent for all patients was collected prior to diagnostic evaluation and testing in agreement with institutional and national legislation for the different Centers. The inclusion criterion was the detection of a de novo rare variant (minor allele frequency <1%) in *PLXNB3* (Genbank: NM_005393.3 and NM_001163257.1) confirmed by diagnostic WES using in-house analysis pipelines. Physicians provided a phenotypic description of affected individuals to define clinical overlap.

***In silico* structural modelling.** To study the functional effects of the *PLXNB3* rare variants, the location of the variants was mapped onto structural homology PLEXINB3 models. Homology models for PLEXINB3 1 and 2 isoforms (Uniprot IDs Q9ULL4-1 and Q9ULL4-2, respectively) were generated using the Phyre2 web server [49] with Plexin structural templates derived from PlexinAs, PlexinBs and plxnC1 from the protein data bank (PDB) database. For structure-based assessments in this study, templates for protein variants were chosen based on high sequence identity in the alignment region, optimal resolution and visualization of the analogous residues in the PDB template along with its interaction partners. No energy minimization was performed on the acquired PLEXINB3 models. A sequence alignment of human Plexin Bs, mouse Plexin A and D forms and zebrafish Plexin C was generated using M-COFFEE web server (Moretti et al., 2007, http://tcoffee.crg.cat/apps/tcoffee/do:mcoffee) with default settings and visualized by ESPript 3.0 server (Robert and Gouet, 2014, http://espript.ibcp.fr).

Plasmid generation. PLEXINB3 variants were introduced into a pMT2-PLEXINB3-VSV (PLEXINB3 WT) plasmid, kindly provided by Luca Tamagnone [52]. Via one-site directed mutagenesis specific nucleotide changes were introduced. In short, flanking primers containing the desired single nucleotide polymorphism (SNP) were generated. Pfu PCR generated newly synthesized plasmids containing the correct SNP that were isolated after DpnI incubation (1 hour, 37°C). The PLEXINB3 variants were sent for sequencing to validate the mutations.

Protein expression via western blot. For protein synthesis assessment, HEK293 cells were transiently transfected with PLEXINB3 WT and variants using polyethylenimine (PEI) concentrated 3:1 to DNA. Cells were always kept at 37°C and 5% CO_2. To create protein lysates, cells were quickly washed with PBS and lysed with RIPA buffer (10mM Tris-buffer pH 7.5, 150 mM NaCl, 0.1% SDS, 1% Triton X-100, 1% Deoxycholate, 0.5 mM EDTA, 1 mM PMSF and complete protease inhibitor (Roche)) followed by centrifugation for 30 min at 12.3000 RPM at 4°C. Supernatant was isolated and supplemented with sample buffer (NuPage, 1:4) containing DTT (5 mMol). Samples were stored at -20°C before use. Samples were heated for 10 min at 70°C prior to loading on 4-12% bis-tris gels (Thermo fisher scientific, NP0323BOX) for SDS-polyacrylamide gel electrophoresis. Nitrocellulose membranes (Bio-Rad) were used for the transfer. Samples were labelled with mouse-anti-beta-actin (Sigma, A2228, 1:500) and mouse-anti-VSV (Sigma, V5507, 1:250) antibodies. Immunoblots were exposed to Pierce ECL substrate (Thermo Fisher Scientific, 32106) and digitized on an Epson flatbed scanner (Perfection 4990, Epson America). Intensities were measured using FIJI software via measuring mean grey value of VSV normalized to beta-actin. A ratio was calculated from all corrected WT to variant samples within each experiment ($n = 3$) to assess protein production. Normalized values from each experiment were used to calculate an average followed by statistical testing via a student's *t*-test.

Protein localization via surface immunocytochemistry. For protein localization, HEK293 cells were grown (37°C and 5% CO_2 in incubator) on poly-L-lysine (500 ug/mL)-coated coverslips prior to transfections of PlexinB3 WT and variants. 48 hours after transfection, cells were stained and analysed for surface and cytosolic expression, as described previously [53]. In short, cells were incubated with sheep-anti-PlexinB3 antibody (R&D, AF4958, 1:500) for 10 min in the incubator directly followed by fixation with 4% paraformaldehyde (PFA) for 1 hour at 37°C. Coverslips were washed, blocked (3% BSA) and incubated with donkey-anti-sheep 555 antibody (Life Technologies, A21436, 1:750) for 1 hour at RT. After several washing steps, the coverslips were fixated with PFA (4%) to ensure stabilization of cell surface labelling. Subsequently, for the cytosolic pool of PLEXINB3 WT and variants, cells were blocked (3% BSA, 0,1% triton in PBS) and incubated with mouse-anti-VSV antibody (Sigma, V5507, 1:250) for 1 hour at RT followed by washing steps. Coverslips were incubated with donkey-anti-mouse 488 antibody (Life Technologies, A21202, 1:750) and Hoechst (Thermo fisher scientific, H3569, 1:1000) for 1 hour, followed by washing steps and embedded in Fluorsave. Coverslips were imaged with an Axioskop epifluorescent microscope (Zeiss) with identical settings for each image. Surface expression was quantified using FIJI software by determining the mean grey value of the surface versus cytosolic labelling for each transfected cell (Fig. 3a). Percentage of surface expression of total expression was calculated [53]. To determine the number of cells expressing PLEXINB3 on the surface, cells with surface expression were counted versus total count of PLEXINB3 expressing cells. A ratio was created between total count and surface count to represent the percentage of cells that express PLEXINB3 on the surface. A student's *t*-test was used to assess protein surface localization over independent experiments ($n = 3$, nine HEK293 coated coverslips).

Autoinhibition cell collapse with COS-7 cells. COS-7 cells were cultured in DMEM (high glucose) supplemented with 10% fetal calf serum, 1% L-glutamine and 1% penicillin-streptomycin in an incubator at 37ºC with 5% CO_2. Cells were plated on glass coverslips at a density of 8 x 103 cells/cm^2. After one day, cells were transfected with 0.5 µg of

Table 1 | Rare variants of *PLXNB3* identified in cohort via WES.

Peptide NP_005384.2 (i1) NP_00156729.1 (i2)	Position in genome ChrX (GRCh37/ hg19)	Nucleotide change	Mutation	Truncated protein	GnomAD_exome_NFE (%) / # hemizygotes / # homozygotes	Patient phenotype short description	Sex of patient
Trp 35 * (i2)	153031770	105 G>A	Nonsense	no protein	-	Developmental delay, Short stature	Male
						Developmental delay	Male
						Developmental delay	Male
Gly 337 Arg (i1)	153033291	1009 G>C	Missense	No	1.248E-2 / 0 / 0	Autism spectrum disorder	Male
Val 376 Ile (i2)	153033339	1126 G>A	Missense	No	2.727E-4 / 3 / 0	Autism spectrum disorder, Developmental delay	Male
Val 423 Met (i2)	153033815	1267 G>A	Missense	No	5.544E-2 / 4 / 0	Complex behavior problems	Male
Gln 476 Glu (i1)	153033291	1426 C>G	Missense	No	-	Autism spectrum disorder, Developmental delay, Hyptonia	Male
Pro 489 Leu (i1)	153034687	1466 C>T	Missense	No	2.897E-2 / 2 / 0	Developmental delay	Male
Val 647 Leu (i2)	153034647	1939 G>A	Missense	No	-	Autoimmune hepatitis, coumpound heterozygote Glu693Lys (i2)	Female
Glu 708 Lys (i2)	153036255	2122 G>A	Missense	No	1.81E-4 / 13 / 0	N.D.	Male
Trp 721 Arg (i1)	153035876	2161 T>C	Missense	No	5.624E-3 / 0 / 0	Seizure disorder, Developmental delay, Hypotonia	Male
						Autism spectrum disorder, Developmental delay, Hypotonia	
Gly 814 Asp (i2)	153036965	2441 G>A	Missense	No	9.282E-2 / 1 / 0	Developmental delay, Autism spectrum disorder	Male
						Short stature	Male
						Short stature	Male
Gly 845 Ser (i1)	153037334	2533 G>A	Missense	No	-	Autoimmune hepatitis, Hypotonia, Fevers	Male
						Hypotonia, Fevers	Male
Ala 875 fs* (i2)	153037356	2624 Deletion C	Deletion	Yes	-	Developmental delay, Epilepsy, Autism spectrum disorder	N.D.
Phe 922 Leu (i1)	153037731	2764 T>C	Missense	No	-	Developmental delay, Mild autism spectrum disorder, Hypotonia	Female

Arg 1002 His (i1)	153037731	3005 G>A	Missense	No	-	Autism spectrum disorder, Developmental delay, Hypotonia, Seizures	Male
Val 1678 fs* (i2)	153042698	5032 dup "T"	Insertion	Yes	-	Stroke, Autism spectrum disorder, Developmental delay, Seizures	Male
						Stroke	Male
Pro 1829 Ser (i2)	153043722	5485 C>T	Missense	No	-	Developmental delay, Short stature, Hypotonia	Male
Arg 1837 Gln (i2)	153043747	5510G>A	Missense	No	2.086E-2 / 3 / 0	Developmental delay	Male
Glu 1847 Lys (i1)	153043915	5539 G>A	Missense	No	5.65E-6 / 0 / 0	Developmental delay, Autism spectrum disorder, Seizures	Male
IVS 25	153040559-153040679	IVS 25 +1,G>A	Nonsense	predicted null mutation	within this region, multiple SNPs were found	Development delay, Possible autism spectrum disorder	Male

Overview of rare *PLXNB3* variants found in patient cohort. Nucleotide change detected via WES and the corresponding peptide change is presented in the table. Per *PLXNB3* variant the patient phenotype is described. The allele frequency (NFE, %) and the occurrence in homozygote or hemizygote are described per variant, if present in the Genome Aggregation Database (20181210, GnomAD v2.1.1). N.D. = not determined.

PLEXINB3 WT and variants together with 0.05 µg CAG-GFP plasmid using X-tremeGENE™ HP DNA Transfection Reagent (Merck) following the manufacturer's instructions. One day after transfection, cells were fixated with an equal volume of warm 8% PFA in PBS with 20% sucrose. Cells were blocked and permeabilized (5% BSA, 0.1% Triton X-100) for 30 min. For immunostaining, coverslips were incubated overnight at 4°C with chicken-anti-GFP antibody (Abcam, ab13970, 1:1000), followed by a 2 hour incubation with goat-anti-mouse 488 antibody (Life Technologies, A11039, 1:1000) and Hoechst (Thermo fisher scientific, H3569, 1:1000). Antibodies and Hoechst were diluted in PBS with 2.5% BSA and 0.1% Triton X-100 and washing with PBS was performed between incubation steps. Images were acquired using a 20x objective with an Axioskop epifluorescent microscope (Zeiss). Cell surface area of transfected cells was determined using FIJI software. Cells with a surface area less than 1600 µm^2 were classified as collapsed [28,54]. For each PLEXINB3 variant, the relative collapse was determined by normalizing to the corresponding WT condition. Normalized values were used to calculate the average relative cellular collapse for each variant. One sample *t*-tests were performed using GraphPad Prism version 7.04 for Windows (GraphPad Software, Inc.). Data was acquired from three replicate experiments and for each variant 150-200 randomly sampled cells were analyzed in total.

Results

Identification of rare variants in PLXNB3 in patient cohort

Semaphorin and Plexin signalling is important for brain development and changes in their expression or function can contribute to neurodevelopmental disorders [11]. In this study, 26 patients are reported with 19 rare *PLXNB3* variants of unknown significance via diagnostic WES. The clinical presentation of the patient cohort includes a broad range of phenotypes, as depicted in Table 1. As an example, a patient's

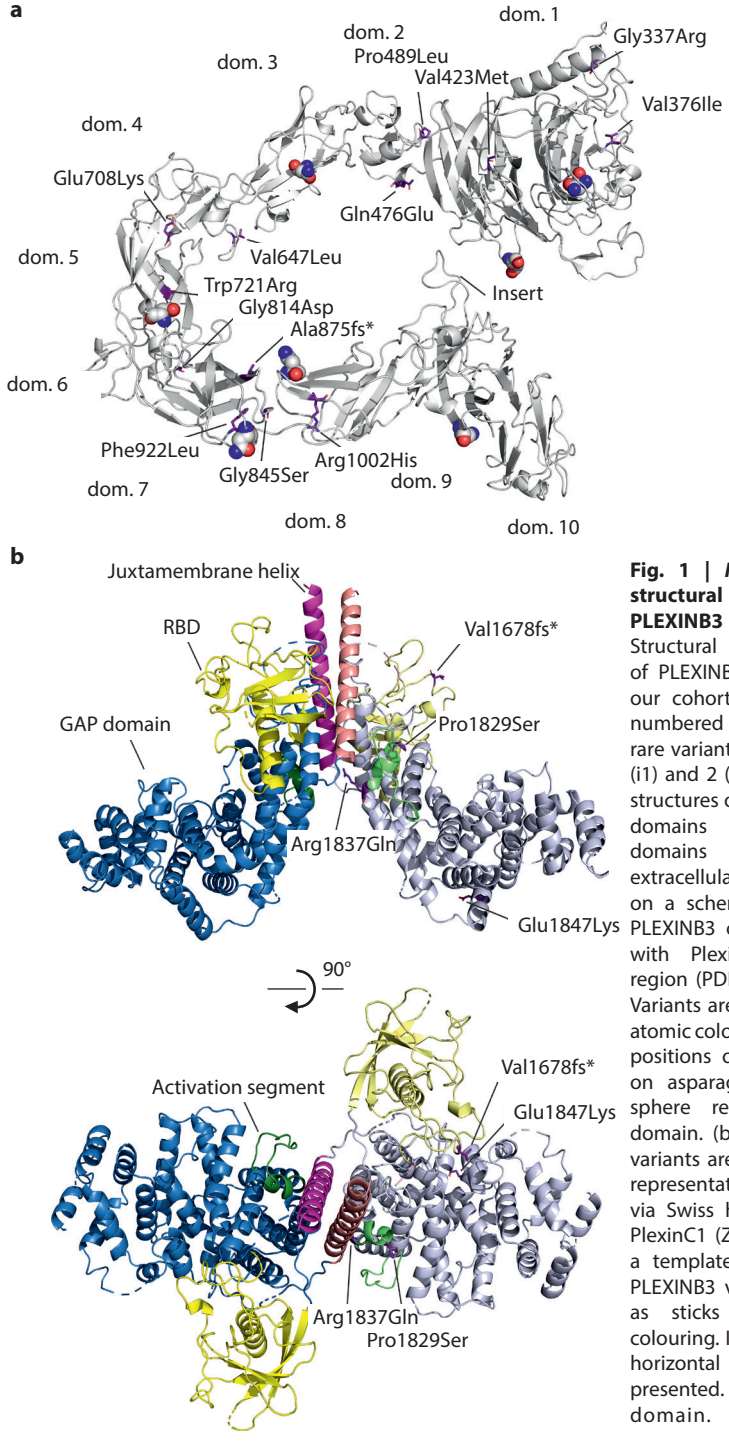

Fig. 1 | *In silico* modelling of structural consequences of PLEXINB3 variants. Structural homology modelling of PLEXINB3 variants identified in our cohort. Affected residues are numbered according to human rare variants of PLEXINB3 isoform 1 (i1) and 2 (i2). Predicted homology structures of extracellular PLEXINB3 domains (a) and intracellular domains (b). (a) PLEXINB3 extracellular variants are shown on a schematic representation of PLEXINB3 created by Swiss-model with PlexinA1 full extracellular region (PDB : 5L5C) as a template. Variants are indicated by stick with atomic colouring (purple). Predicted positions of N-glycosylations sites on asparagines are indicated by sphere representation. dom. = domain. (b) PLEXINB3 intracellular variants are shown on a schematic representation of PLEXINB3 created via Swiss homology modelling of PlexinC1 (Zebrafish, PDB:4M8M) as a template. Residues affected by PLEXINB3 variants are represented as sticks with purple atomic colouring. In addition, a 90 degrees horizontal rotated schematic is presented. RBD = Rho binding domain.

phenotype can range between behavioural problems, short stature and intellectual disability. A form of developmental delay was observed in 17 out of the 26 patients. In 12 of the 26 individuals a form of ASD or other behaviour problems were found. Five of the patients had a history of epileptic seizures. Also, a different subset of individuals (5/26) exhibited hypotonia (decreased muscle tone). Short stature was present in 4 individuals. A variety of dysmorphic features were described in 7 patients displaying microcephaly (in 2 individuals), macrocephaly (in 2 individuals), craniosynostosis, inner ear malformation or a congenital condition (blepharophimosis). In addition, 4 individuals presented stroke (in 2 individuals), autoimmune hepatitis (in 2 individuals) or fevers. Together, these results show a wide phenotypic range within the patient cohort where *PLXNB3* variants of unknown significance were identified.

PLXNB3 is transcribed into two transcripts (Genbank: NM_005393.3 and NM_001163257.1) resulting in isoform 1 (i1) and 2 (i2). Transcript 2 has an additional exon in the 5' region compared to transcript 1 resulting in a longer isoform 2 with a distinct N-terminus compared to isoform 1. Consequently, the signalling peptides differ between the two isoforms with a more extended sequence for isoform 2. Variant Trp35* could only be detected in isoform 2 due to the shorter signalling peptide in isoform 1. Although transcript 1 is considered the canonical transcript (by RefSeq, NCBI, Ensembl and HAVANA), the biological activity or expression levels of both transcripts have not been determined in humans or mice. Therefore, the potential risk of Trp35* is unclear. Patients with this mutation could show no phenotype do to a healthy dominant transcript 1 of PLEXINB3 or would not have a functional protein due to a premature stopcodon preventing a mature isoform 2 PLEXINB3 protein. Apart from the Trp35* variant, all variants can be found in isoform 1 or 2. In conclusion, the PLEXINB3 variants can be located in both isoforms, apart for Trp35* which is only located in isoform 2.

PLXNB3 locates on the X-chromosome, leading to higher chance of pathogenicity of mutations in males [55]. Mutations in a single allele carrying *PLXNB3* are less likely to exhibit symptoms in females [56]. However, two females carrying a Val647Leu (i2) or Phe922Leu (i1) mutation in *PLXNB3* are reported in this study (Table 1). The patient with the Val647Leu mutation carries additionally a Glu693Lys (i2) mutation making her a compound heterozygote. The female subject with Phe922Leu mutation could be a carrier, although it is undetermined whether the patient is homozygote or whether other deleterious mutations in *PLXNB3* are present. In addition, the *PLXNB3* variants found in our cohort were partly found in the GnomAD database (Table 1). The allele frequency (NFE) and reported homozygotes (females) and hemizygotes (males) are reported. Together this indicates that mutations in the X-chromosome bound *PLXNB3* increase their risk factor prevalence in men compared to females, as is observed in our patient cohort.

Structural consequences of PLXNB3 rare variants

The 19 rare variants found for *PLXNB3* were studied *in silico* for structural consequences. Currently, the crystal structure for PLEXINB3 is not available. Therefore, homology models derived from PlexinAs, PlexinBs and plxnC1 were used to map the variants (Fig. 1). Eight of the 19 variants were predicted to not influence the structural integrity to a degree that could affect protein stabilisation or function (see limitations). Eleven out of the 19 rare variants were predicted to perturb PLEXINB3's signalling mechanism due to structural consequences, which are discussed in the following paragraphs.

Two variants could lead to a loss of all protein function. The Trp35* variant results in a stopcodon localized within the signal sequence of transcript 2 and is not expected to

produce a mature protein. As mentioned, whether the Trp35* could be pathogenic depends on the expression of transcript 2 which is currently not known. For the IVS25 (intervening sequence 25) variant a null mutation is predicted since it involves a splicing site. Patients with these variants could lead to a null mutation of *PLXNB3*.

Seven variants are located in the extracellular domain of PLEXINB3 and may interfere with ligand binding or autoinhibitory mechanisms [28,29,57] (Fig. 1a). The Val423Met variant changes a strictly conserved residue that can influence the stability of domain 1 in Plexins. This adverse effect on structural integrity could result in misfolding of the SEMA domain (amino acids 47-472, located in dom. 1-2) and attenuate extracellular Sema4A or Sema5A ligand binding. The Pro489Leu variant may affect local structural integrity at the interaction surface between domains 1 and 2. This can influence the relative orientation of the complete extracellular domain and thereby perturb ligand binding and autoinhibition conformation. Val647Leu variant is localized in a PLEXINB-specific insertion within domain 4. The Leu present in this variant is bulkier than Val, which can accommodate local structural perturbations by preventing conserved disulphide bridge formation that dictate overall domain folding. Misfolding of domain 4 may lead to decreased ligand binding and autoinhibition capabilities. The Gly845Ser variant disrupts a conserved Gly that stabilizes a turn and allows optimal positioning of the adjacent conserved Pro in the interface of domain 7 and 8. Introduction of a Ser could destabilize local inter-domain interactions

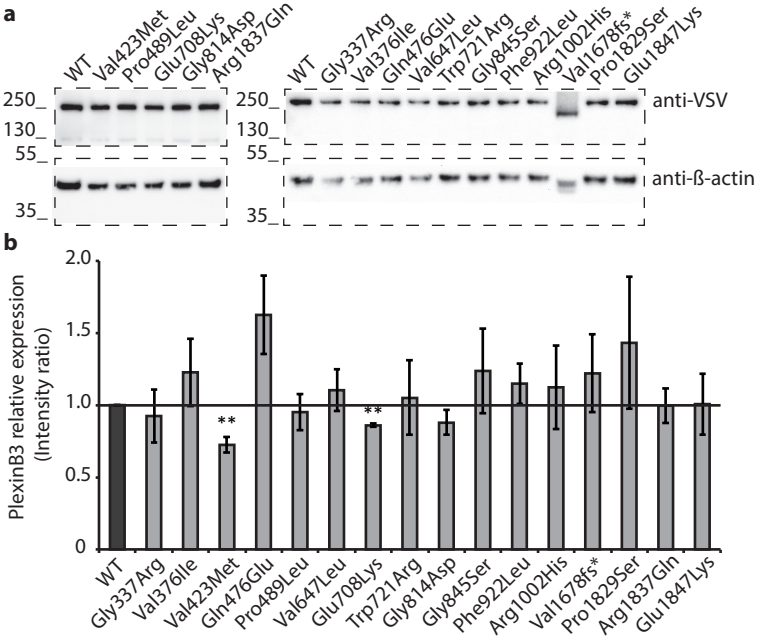

Fig. 2 | Expression of PLEXINB3 variants in HEK293 cells.
Western blot analysis of PLEXINB3 variants expression profiles in HEK 293 cells. (a) Lysates of transient expressed HEK293 cells with PLEXINB3 variants. Representative images are shown for all variants where a VSV antibody is used to visualize PLEXINB3 variants and β-actin as loading control. PLEXINB3 WT shows an average weight of ±260kDa. Note that Val1678fs* shows an average weight of 200kDa due to the frameshift and early stopcodon. (b) Quantification of protein synthesis of WT and variant PLEXINB3s via relative expression intensity to beta-actin and PLEXINB3 WT. Val423Met and Glu708Lys show reduced protein expression compared to PLEXINB3 WT (Student's *t*-test, $p_{(Val423Met)} = 0.006$, $p_{(Glu708Lys)} = 0.004$). $n = 3$ experiments. Data are presented as means ± s.e.m.

that affect overall conformation of the complete ectodomain. The Ala875fs* mutation is found within domain 7 and the Cys nucleotide is deleted resulting in a frameshift followed by a stopcodon 18 residues upstream. Domain 1-6 will have an intact structure followed by 20 correct residues of domain 7 and 18 out-of-frame residues. It is unlikely that this segment adopts a tertiary structure. Ala875fs* may be recognised as misfolded and will, subsequently, be degraded through the ubiquitin-proteasome system 58. Otherwise, the variant could be secreted into the extracellular space since it lacks a transmembrane and intracellular domain. Carriers of this mutation are likely to lack PLEXINB3-signalling. The Phe922Leu variant may cause fold instability for domain 7. The conserved sidechain where Phe922 is located in a tight space that is not ideal for Leu. The different geometry and more flexible conformation of Leu can disturb the structural integrity. In the next variant, the exchange of Arg1002 for His eliminates the salt bridge with D926 which is necessary for a strong interaction between the two beta-sheets in domain 8, leading to fold instability and perhaps altered domain-domain torsion angle. Together, these PLEXINB3 variants are likely to effect domain stability, possibly resulting in altered ligand binding or autoinhibitory interactions.

Finally, three of the four variants in the intracellular domain of PLEXINB3 could affect the downstream signalling mechanisms [28,29,57] (Fig. 1b). In the Val1678fs* variant a duplication of thymine at nucleotide 5032 results in a frameshift followed by a stopcodon resulting in a deletion of a large portion of the cytoplasmic part of PLEXINB3. The mutation could accommodate misfolding of the intracellular domain. The deleted region includes the PDZ binding sequence motif 'VTDL' [59] and also the Arg finger of Plexins that mediates critical interactions with Rap GTPases [31]. Furthermore, the mutation could accommodate misfolding of the intracellular domain. Consequently, Val1678fs* is predicted to abolish downstream signalling. The Pro1829Ser variant is found in the activation loop of the GAP domain of Plexins. The activation segment is a mobile structural element that provides hindrance to Rap GTPase binding in the inactive state of Plexins by employing its proline lid, featuring Pro1829 residue, to have a critical Asn1831 from interacting with Rap GTPase. Upon dimerization-dependent activation of Plexins it is displaced, allowing binding of Rap to its binding site. The Pro1829Ser mutation is predicted to perturb the GAP activation capacity of the enzyme leading to an altered downstream signalling of PLEXINB3. The Arg1837Gln variant the Arg forms a salt bridge with the conserved Glu1321 from the juxtamembrane helix, stabilizing it in a bent conformation. Upon extracellular ligand binding, the juxtamembrane helix undergoes structural rearrangements. In the dimer form, Arg1837 contributes to dimer stability. The Arg1837Gln mutation could lead to improper regulation of downstream signalling abilities. Together, these PLEXINB3 variants are likely to show altered downstream signalling capabilities.

In summary, *in silico* modelling of the PLEXINB3 variants predict functional consequences for 12 of the 19 variants due to protein misfolding or instability, which could eventually affect ligand binding, autoinhibition mechanisms and/or downstream signalling.

Protein expression is partly affected in PLEXINB3 rare variants

Structural modelling suggested perturbed PLEXINB3 signalling mechanisms for 12 variants. The homology modelling was necessarily biased towards PlexinAs, which were used as templates. Therefore, we did not constrict the functional analysis solely to these twelve variants. Functional protein was not expected for Trp35* and IVS25 variants due to a stop codon in the signalling peptide or to splicing site disturbances, respectively [60,61]. Therefore, these variants were not included. The remaining 17 PLEXINB3 variants were

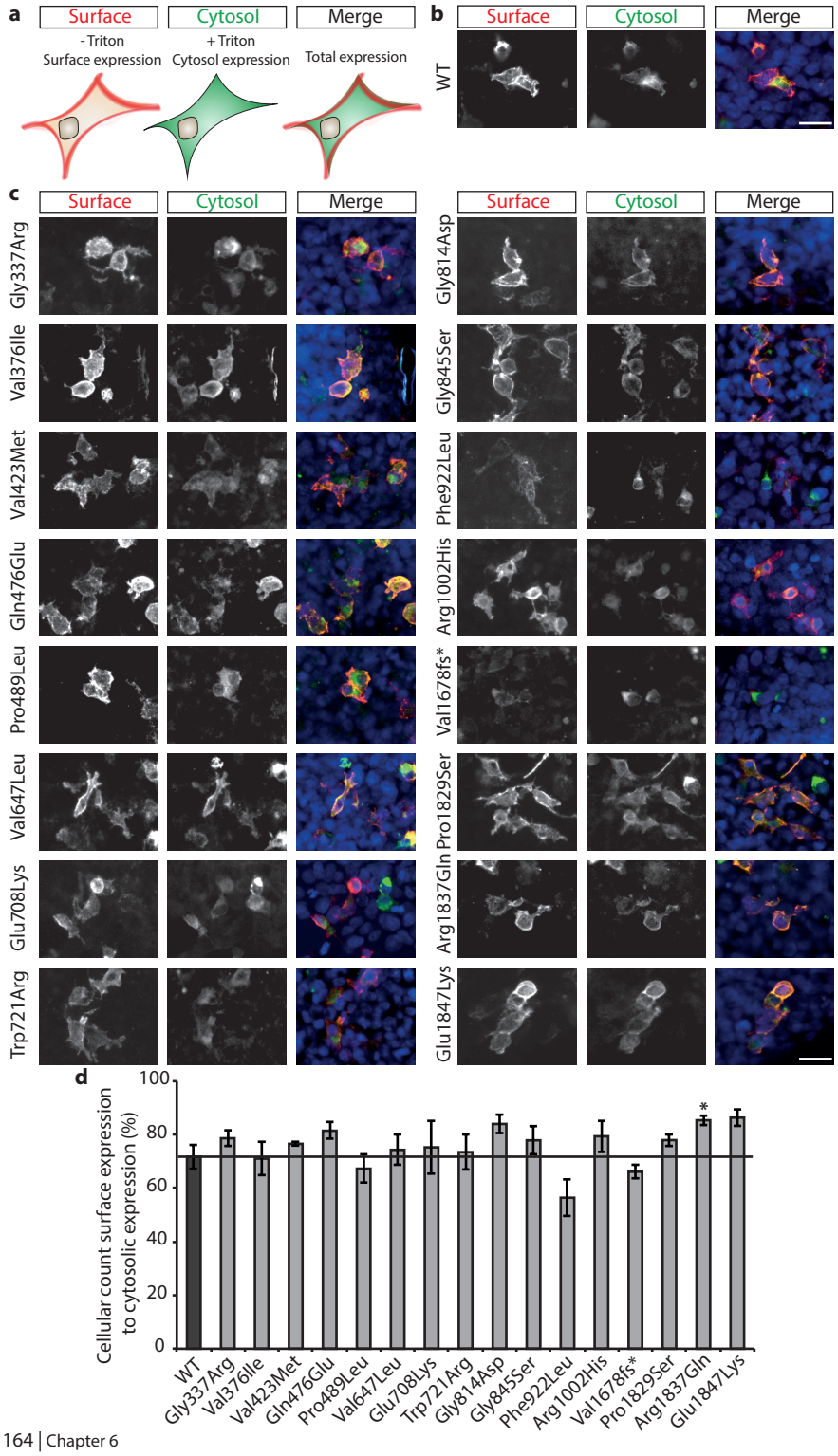
a
Surface
Cytosol
Merge
- Triton
Surface expression
+ Triton
Cytosol expression
Total expression
b
WT
c
Gly337Arg
Val376Ile
Val423Met
Gln476Glu
Pro489Leu
Val647Leu
Glu708Lys
Trp721Arg
Gly814Asp
Gly845Ser
Phe922Leu
Arg1002His
Val1678fs*
Pro1829Ser
Arg1837Gln
Glu1847Lys
d
Cellular count surface expression to cytosolic expression (%)
100
80
60
40
20
0
*
WT
Gly337Arg
Val376Ile
Val423Met
Gln476Glu
Pro489Leu
Val647Leu
Glu708Lys
Trp721Arg
Gly814Asp
Gly845Ser
Phe922Leu
Arg1002His
Val1678fs*
Pro1829Ser
Arg1837Gln
Glu1847Lys

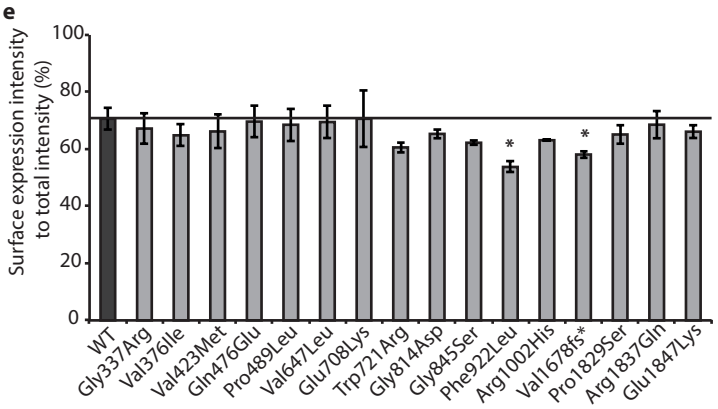

Fig. 3 | Surface localization of PLEXINB3 variants in HEK293 cells.
Protein localization of rare WT and PLEXINB3 variants in HEK293 cells visualized using surface immunocytochemistry. (a) PLEXINB3 WT and variants were transiently expressed in HEK293 cells and visualized via a two-step immunocytochemistry protocol to separate surface from cytosolic expression. (b) PLEXINB3 WT cytosolic and surface expression in HEK293 cells. (c) PLEXINB3 variant expression of the surface and cytosol of HEK293 cells. (d) Quantification of cell number that expressed PLEXINB3 WT or variant on the surface compared to solely cytosol expression. Arg1837Gln variant showed an increased number of HEK293s with surface expression compared to WT control (student's *t*-test, $p_{(Arg1837Gln)} = 0.048$). (e) Quantification of surface expression in relation to cytosolic expression for PLEXINB3 variants compared to WT based on intensity measurements. Phe922Leu and Val1678fs* variants showed significantly decreased surface expression compared to PLEXINB3 WT (Student's *t*-test, $p_{(Phe922Leu)} = 0.018$, $p_{(Val1678fs*)} = 0.038$). $n = 3$ experiments. Data are presented as means ± s.e.m. Scale bars = 25 µm.

tested for functional consequences to provide a complete characterization of the rare PLEXINB3 variants.

To dissect whether PLEXINB3 variants could influence the expression and function of PLEXINB3, *in vitro* protein production was examined. The PLEXINB3 variants were introduced into a pMT2-PLEXINB3-VSV plasmid and transiently expressed in HEK 293 cells (Fig. 2). Lysates of cells were examined with chemiluminescence through western blot via their VSV tag (Fig. 2a). Expression of all variants was detected around ±260 kDa. The PLEXINB3 variant Val1678fs* is a smaller protein of ±200 kDa due to the duplicate thymine leading to a frameshift and early stopcodon. Beta-actin (±42 kDa) was used as loading control. Protein production was quantified by normalizing VSV expression first to actin followed by PLEXINB3 WT protein normalization (Fig. 2b). The Val423Met and Glu708Lys variants were expressed at significantly lower levels (±30% expression reduction) compared to PLEXINB3 WT ($n = 3$ experiments, Student's *t*-test, $p_{(Val423Met)} = 0.006$, $p_{(Glu708Lys)} = 0.004$). Other PLEXINB3 variants were expressed at WT levels in HEK 293 cells.

Altered surface localization of PLEXINB3 variants Phe922Leu, Val1678fs and Arg1837Gln*

PLEXINB3 is a transmembrane protein that is localized at the cellular membrane. To assess whether PLEXINB3 variants affected protein localization, the localization of the variants was visualized and quantified. PLEXINB3 variants were expressed in HEK 293 cells followed by cell surface immunocytochemistry where first PLEXINB3 membrane expression is visualized via a PlexinB3-specific antibody, followed by permeabilization of the cells allowing staining of the intracellular PLEXINB3 domain with a VSV antibody (Fig. 3a). PLEXINB3 WT shows prominent cell surface expression in HEK 293 cells (Fig. 3b). Next, all PLEXINB3 variants were examined for cell membrane expression (Fig. 3c). First, the number of cells expressing PLEXINB3 on its surface, normalized to the total number of transfected

cells was quantified (Fig. 3d). 70% of the transfected cells showed PLEXINB3 membrane localization. The PLEXINB3 variant Arg1837Gln showed an increased percentage of cells that expressed PLEXINB3 on its surface ($n = 3$ experiments, student's *t*-test, $p_{(Arg1837Gln)} = 0.048$) compared to WT. Also, this trend was visible for Glu1847Lys, yet not significant ($n = 3$, student's *t*-test, $p_{(Arg1837Gln)} = 0.055$). The other PLEXINB3 variants showed a percentage of cells expressing PLEXINB3 at the membrane similar to WT. Next, we assessed whether the PLEXINB3 localization within one cell differed between PLEXINB3 variants. Membrane localization of PLEXINB3 variants was quantified via grey value intensity measurements of surface expression normalized to the total grey value intensity per cell (Fig. 3e). Approximately 70% of PLEXINB3 WT protein is localized at the cellular membrane within a cell. For Phe922Leu and Val1678fs* membrane localization was significantly reduced to 55% ($n = 3$ experiments, Student's *t*-test, $p_{(Phe922Leu)} = 0.018$, $p_{(Val1678fs*)} = 0.038$). Other PLEXINB3 variants displayed a cellular localization similar to the PLEXINB3 WT protein.

In conclusion, the Arg1837Gln PLEXINB3 variant showed an increase number of cells that show membrane localization. However, within a cell, the percentage of protein that is localized in the membrane was not affected by this mutation. The variants Phe922Leu and Val1678fs showed decrease surface localization within a cell. Although the total number of cells expressing these variants at the surface seemed to be decreased, this was not significant. Together, these results suggest that PLEXINB3 rare variants have limited influence on the surface localization of the proteins in HEK 293 cells.

Increased COS-7 collapse following transfection of a Gly337Arg PLEXINB3 variant

Cis-interactions between the Plexin ectodomain mediate autoinhibitory interactions. Some of the identified PLEXINB3 mutations may affect the head-to-stalk conformation necessary to adapt autoinhibition (Fig. 1). To probe whether PLEXINB3 variants could mediate autoinhibition, COS-7 cells expressing the variants were examined for cell collapse. PLEXINB3 WT transfected cells displayed a normal, spread-out morphology. In contrast, COS-7 cells transfected with Gly337Arg were smaller, which indicates cell contraction (Fig. 4a). Quantification of the cell area, a measure for cell contraction [28] showed an increased number of collapsed cells in Gly337Arg compared to PLEXINB3 WT (one sample *t*-test, $p_{(Gly337Arg)} = 0.0039$) (Fig. 4b). This indicates that Gly337Arg PLEXINB3 may reduce autoinhibitory interactions. Other PLEXINB3 variants showed cell contraction similar to WT control, suggesting that the head-to-stalk conformation is not affected. Together, these data suggest that genetic alterations in the ectodomain of PLEXINB3 can influence autoinhibitory mechanisms *in vitro*, thereby potentially deregulating PLEXINB3 signalling.

Discussion

In this study, rare *PLXNB3* variants were identified in a cohort of individuals with a wide phenotypic spectrum. Homology models for PLEXINB3 predicted structural alterations for 12 of the 19 variants ranging from protein misfolding, effects on ligand binding and intracellular signalling. Overall protein production, localization or autoinhibition was mildly affected in 6 of the 17 rare PLEXINB3 variants. Together these results begin to provide insight into how rare variants could contribute to defects in PLEXINB3 signalling. Whether the identified PLEXINB3 variants contribute to the phenotypes presented in the patient cohort remains to be established through experiments focussed on ligand binding, intracellular signalling and function of PLEXINB3.

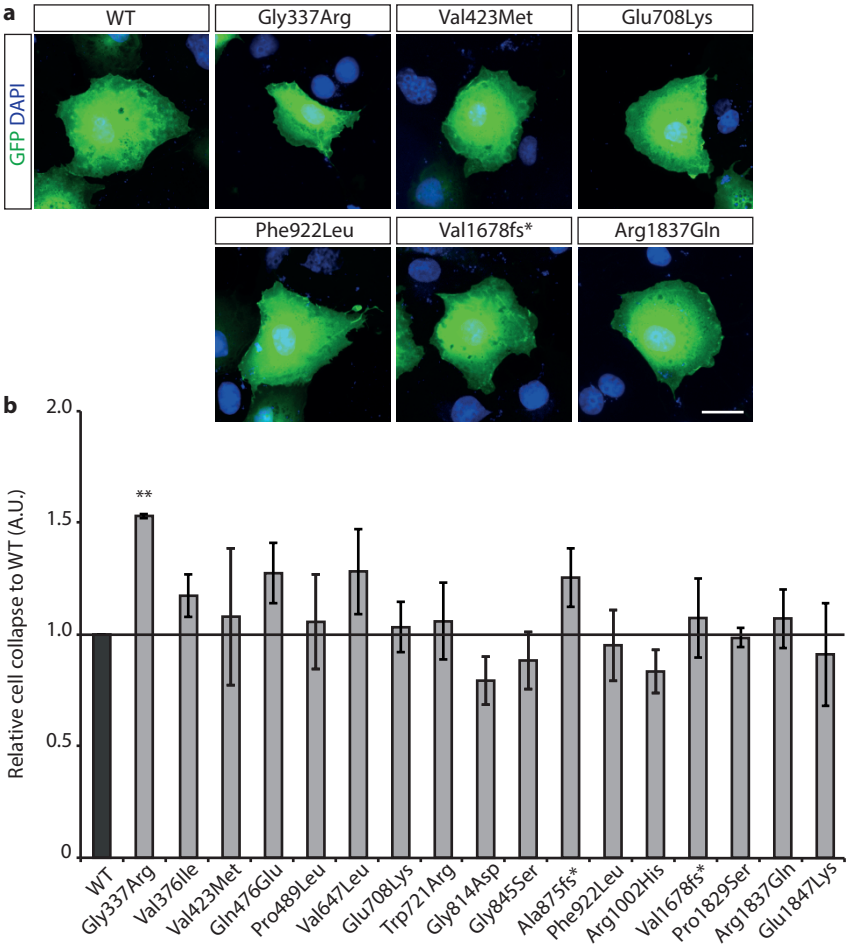

Fig. 4 | Autoinhibition of PLEXINB3 variants in COS-7 cells.
COS-7 collapse assay for PLEXINB3 variants to determine their autoinhibtion capability. (a) Representative images of COS-7 cells transiently transfected with PLEXINB3 WT and variants. Variants were co-transfected with CAG-GFP plasmid. (b) Cell surface area of transfected cells was determined and cells with an area less than 1600 μm² were categorized as collapsed. For each variant, the relative collapse was determined by normalizing to the corresponding WT. Gly337Arg showed an increase in relative COS-7 cell collapse compared to WT control (one sample *t*-test, $p_{(Gly337Arg)} = 0.0039$). Data are presented as means ± s.e.m. $n = 3$ experiments, with 150-200 cells per condition. Scale bar = 10 μm.

Consequences of PLEXINB3 variants located in the extracellular domain

Of the 19 identified *PLXNB3* variants, 14 variants were located in the extracellular domain (Trp35*, Gly337Arg, Val376Ile, Val423Met. Gln476Glu, Pro489Leu, Val647Leu, Glu708Lys, Trp721Arg, Gly814Asp, Gly845Ser, Ala875fs* and Phe922Leu). Misfolding or destabilization of the PLEXINB3 protein structure was expected for six variants (Val423Met, Val647Leu, Gly845Ser, Phe922Leu, Arg1002His and Arg1837Gln) possibly leading to deficits in protein production, localization, autoinhibition mechanisms or ligand binding. We performed *in vitro* experiments to determine the functional consequences of the PLEXINB3 variants.

Only three extracellular PLEXINB3 variants showed altered protein expression levels

(Val423Met and Glu708Lys) and localization (Phe922Leu). The expected misfolding of domain 1 in Val423Met may have lead to reduced protein production. Noteworthy, the Val423Met PLEXINB3 protein is correctly inserted into the membrane. Glu708Lys, unexpectedly, showed reduced protein production as well, although this mutation was not expected to induce misfolding or destabilization based on the homology structure. The sequence similarity for this specific region was low for the homology template PlexinA2, complicating precise structure-based predictions (see limitations). The Glu708Lys variant is located near a conserved loop. The mutation may introduce misfolding of the interface between domain 4 and 5. The Phe922Leu variant showed significantly reduced surface expression compared to the PLEXINB3 WT. This indicates that this variant was less effectively inserted in the membrane although protein production was not altered. Interestingly, mislocalization, e.g. in the endoplasmic reticulum, of Phe922Leu was not observed compared to WT. Surface expression of transmembrane proteins relies on correct control of many pathways including sorting, trafficking, docking or internalization, e.g. surface expression of PlexinD1 requires correct sorting via its PDZ-domain-binding motif [62]. The predicted fold instability of domain 7 may interfere with pathways necessary for sufficient membrane expression. Overall, changes in protein production and localization suggest significant structural changes that may perturb PLEXINB3 signalling. Val423Met and Glu708Lys proteins may be degraded through the ubiquitin-proteasome system [58]. Ubiquitin labelling could assess whether this system is activated in these variants. Furthermore, co-stainings for cellular organelles with Phe922Leu variant could provide more insight into the observed decrease in surface expression. Together, this indicates that the PLEXINB3 variants lead to minor changes in expression levels or membrane localization.

The ring-like head-to-stalk conformation, necessary for autoinhibition of PlexinAs, localizes in domain 1 to domain 4-5 [28]. Changes in autoinhibitory mechanisms may result in deregulation of Semaphorin-Plexin signalling [28,63] as autoinhibition of PlexinAs limit premature signalling by preventing cytoplasmic domain dimerization [28]. Altered protein profiles and changes in protein structure could affect autoinhibition capability of PLEXINB3. The COS-7 collapse cell assay was used to study the cis-interaction of all PLEXINB3 variants to determine cellular contraction [28,38]. The *in silico* homology data predicted changes in autoinhibition for Pro489Leu, Gly814Asp and Gly845Ser, however, none of these variants showed altered cell contraction (see limitations). Strikingly, only the Gly337Arg PLEXINB3 variant showed increased cellular contraction compared to WT indicating that this mutation affects an autoinhibitory mechanism. Gly337Arg is located in a loop of domain one, which could be involved in a head-to-stalk conformation necessary for autoinhibition for PlexinBs [28,29]. However, we did not predict this variant to cause significant changes due to variations of length and sequence within this loop among Plexins, even PlexinB1-3 proteins. Therefore, it was not straightforward to assess conformation and potential interactions of this loop region. Especially since this region is in the proximity of, but not directly in, the protein-protein-interaction surface. How decreased autoinhibition in the Gly337Arg mutation affects PLEXINB3 signalling remains to be determined. In future experiments, cultured dentate gyrus neurons transfected with Gly337Arg PLEXINB3 can be examined for growth cone collapse. Together, although the precise function of PLEXINB3 is obscure, decreased autoinhibition can result in over-activated PLEXINB3 signalling that may contribute to developmental disorders [11].

Ligand binding domains are located in domain 1 of the SEMA domain in PLEXINB3 and alterations in or misfolding of sequences surrounding this region may result in ligand binding failure [29,57,64] as predicted for PLEXINB3 variants Pro489Leu, Val647Leu, Gly845Ser,

Phe922Leu and Arg1002His. For example, the Gly945Ser mutation could destabilize local inter-domain interactions that could affect the overall conformation of the protein and indirectly its ligand binding capacity. To determine whether PLEXINB3 variants affect ligand binding, cell-binding experiments where transiently expressed PLEXINB3 variants are exposed to Sema5A and Sema4A should be performed. In addition, biophysical binding between PlexinB3 and Sema4A/5A could be determined using surface plasmon resonance [29]. Sema5A and Sema4A are involved in synaptogenesis, cell migration, neurite outgrowth [16,17,41,42,65,66], possible via PlexinB3. Alterations in ligand binding between PLEXINB3 and Sema4A or Sema5A could influence these functions and eventually lead to changes in brain developmental.

Consequences of PLXNB3 variants affecting intracellular domains

Based on homology modelling, four of the 19 *PLXNB3* variants were predicted to affect the intracellular domain (Ala875fs*, Val1678fs*, Pro1829Ser and Arg1837Gln). These variants could lead to changes in protein production, localization and intracellular signalling.

Protein production levels determined from transfected HEK293 lysates did not reveal changes for Val1678fs*, Pro1829Ser and Arg1837Gln compared to PLEXINB3 WT. Surface expression was quantified via surface immunocytochemistry and showed altered localization for Val1678fs* and Arg1837Gln. Surface expression within a cell was increased in Val1678fs* variant compared to WT. A frameshift and deletion of a large part of the intracellular domain, including the GAP domain and PDZ binding motif, was expected to result in structural changes. Immunocytochemistry did not reveal retention of Val1678fs* in cellular organelles. Paradoxically, surface expression across all cells was increased for Arg1837Gln, while, within a cell, similar percentage of produced protein was loaded into the membrane compared to WT. If higher levels could result in a gain-of-function of PLEXINB3 signalling remains undetermined. Whether changes in PLEXINB3 expression can alter its function needs to be determined. More in-depth analysis of the Val1678fs* and Arg1837Gln variants, using co-stainings for organelles, will allow more precise determination of protein localization. In conclusion, structural changes in the intracellular domain can affect protein localization of PLEXINB3 variants.

The intracellular domain of PLEXINB3 is crucial for inducing downstream signalling events. PlexinB3-signalling can induce actin remodelling *in vitro* upon homophillic interactions [38] or ligand binding [16,17,40]. Mutations in the intracellular domain may hinder Rap GTPase binding or activation leading to a decrease in signalling capacity thereby perturbing downstream signalling of PLEXINB3. In support, findings in recent studies showed that a PLEXINB3 mutation at residue 1829 (Pro1829Gly) decreased GAP activity [30]. Also, a PLEXINB1 mutation (Pro1829Leu) at this highly conserved residue was identified as an oncogenic SNP [67]. Future experiments should determine the activity of downstream interactors for the PLEXINB3 variants, for instance by phosphorylation and GAP activity assays. Together, these data imply that intracellular structural changes in PLEXINB3 may affect protein localization and downstream signalling cascades, possibly contributing to developmental disorders.

Assessing phenotype – genotype correlation

We identified 19 rare *PLXNB3* variants in a cohort characterized by a broad phenotypic spectrum via diagnostic WES. The structure, stability, production, localization and autoinhibitory mechanisms of PLEXINB3 variants were examined for alterations, which are summarized in Table 2. ASD and epilepsy are multifactorial neurodevelopmental disorders

Table 2 | Net effects of structural and functional consequences of *PLXNB3* rare variants.

Peptide NP_005384.2 (i1) NP_00156729.1 (i2)	Short description of patients phenotype	Predicted structural element effected	GnomAD_exome_ NFE (%) / # hemizygotes / # homozygotes	Predicted structural perturbed mechanism	expression / localization	Auto-inhibition	Potential risk factor score
Trp 35 * (i2)	Developmental delay, short stature	No protein	-	obvious	N.D.	N.D.	2
	Developmental delay						
	Developmental delay						
Gly 337 Arg (i1)	Autism spectrum disorder	Plexin-sema interface, indirectly	1.248E-2 / 0 / 0	not obvious	Normal / Normal	Decreased	2
Val 376 Ile (i2)	Autism spectrum disorder, developmental delay	Plexin-sema interface, indirectly	2.727E-4 / 3 / 0	not obvious	Normal / Normal	Normal	0
Val 423 Met (i2)	Complex behavior problems	misfolding of domain 1	5.544E-2 / 4 / 0	probable	Decreased / Normal	Normal	2
Gln 476 Glu (i1)	Autism spectrum disorder, developmental delay, hyptonia	Domain 1-2 interface	-	not obvious	Normal / Normal	Normal	1
Pro 489 Leu (i1)	Developmental delay	Domain 1-2 interface	2.897E-2 / 2 / 0	probable	Normal / Normal	Normal	1
Val 647 Leu (i2)	Autoimmune hepatitis	Misfolding of domain 4	-	probable	Normal / Normal	Normal	2
Glu 708 Lys (i2)	N/A	Domain 5, Domain 4-5 interface	1.81E-4 / 13 / 0	not obvious	Decreased / Normal	Normal	1
Trp 721 Arg (i1)	Seizure disorder, developmental delay, hyptonia	Misfolding of domain 5	5.624E-3 / 0 / 0	not obvious	Normal / Normal	Normal	1
	Autism spectrum disorder, developmental delay, hyptonia						
Gly 814 Asp (i2)	Developmental delay, autism spectrum disorder	Domain 6 (loop)	9.282E-2 / 1 / 0	not obvious	Normal / Normal	Normal	0
	Short stature						
	Short stature						

Gly 845 Ser (i1)	Autoimmune hepatitis?, Hypotonia, Fevers Hypotonia, Fevers	Interface of domain 7-8	-	probable	Normal / Normal	Normal	2
Ala 875 fs* (i2)	Developmental delay, epilepsy, Autism spectrum disorder	Deletion domain 7 onwards including transmembrane and cytoplasmic domains	-	probable	N.D.	N.D.	2
Phe 922 Leu (i1)	Developmental delay, mild autism spectrum disorder, hypotonia	Misfolding of domain 7	-	probable	Normal / Decreased	Normal	3
Arg 1002 His (i1)	Autism spectrum disorder, developmental delay, hypotonia, seizures	Misfolding of domain 8, Interface of domain 7-8	-	probable	Normal / Normal	Normal	2
Val 1678 fs* (i2)	Stroke, autism spectrum disorder, developmental delay, seizures stroke	Deletion of GAP domain and PDZ segment	-	probable	Normal / Decreased	Normal	3
Pro 1829 Ser (i2)	developmental delay, short stature, hypotonia	GAP activation segment	-	probable	Normal / Normal	Normal	2
Arg 1837 Gln (i2)	developmental delay	Dimerization, GAP activation segment	2.086E-2 / 3 / 0	probable	Normal / Normal	Normal	1
Glu 1847 Lys (i1)	developmental delay, autism spectrum disorder, seizures	Misfolding of GAP domain	5.65E-6 / 0 / 0	not obvious	Normal / Normal	Normal	1
IVS 25	Development delay, possible autism spectrum disorder	null mutation	within this region, multiple SNPs were found	obvious	N.D.	Normal	2

The results of presence in GnomAD, *in silico* structural modelling, protein synthesis and localization and autoinhibition of PLEXINB3 variants are summarised. Green indicates potential changes that could affect PLEXINB3 signalling and are based on exclusion of homozygotes in GnomAD, predictive structural changes, altered protein expression or localization and changed autoinhibition capacity. Together we present a potential risk factor score to assess phenotype-genotype correlation (0 = low potential risk factor). N.D. = not determined.

characterized by a disbalance between excitatory and inhibitory synapses. Interestingly, PLEXINB3-Semaphorin signalling has been implicated in synapse regulation and neurite outgrowth [25,35,38,42]. In particular, PLEXINB3 supresses excitatory and promotes inhibitory synapse formation in cultured hippocampal neurons via distinct intracellular mechanisms [25]. Whether the *PLXNB3* variants in our cohort contribute to the described phenotypes such as ASD or epilepsy is undetermined and should be studied in the future. As a first step in assessing phenotype-genotype correlation, the *PLXNB3* variants were evaluated as a potential risk factor [68] and were scored based upon the occurrence in GnomAD (hemizygote = 0), probable structural changes, altered protein expression and autoinhibitory failure. Together this score can be indicative for the mutation to potentially contribute to disease outcome. As an example, Val1678fs* mutation has a high potential risk factor score due to its predicted structural changes, its exclusion in GnomAD and its decreased surface expression in COS-7 cells. Contrary, Val376Ile has a low risk factor score as it is observed in hemizygotes in GnomAD, structural changes were not predicted and protein levels and autoinhibition were normal. This potential risk factor score can be expanded upon further characterization of the *PLXNB3* variants. In addition to the proposed experiments for ligand binding and signalling cascades, future studies should determine the role of PLEXINB3 variants in synapse plasticity. Eventually the *PLXNB3* variants with high potential risk factor scores are more likely to contribute to multifactorial neurodevelopmental disorders, such as developmental delay, ASD and epilepsy.

Conclusively, the *PLXNB3* variants found in patients with neurodevelopmental disorders may have a subtle effect on PLEXINB3 signalling due to structural changes that may affect protein synthesis, localization and autoinhibition mechanisms. Next experiments should continue to expand the potential risk factor score by determining ligand binding, synapse development and intracellular signalling of *PLXNB3* variants. Eventually, mild changes in PLEXINB3-Semaphorin signalling may affect brain development. This study provides a first step into identifying *PLXNB3* variants that may worsen disease outcome or enhance risk in multifactorial neurodevelopmental disorders.

Limitations

Diagnostic WES is a powerful tool to establish a genetic association with a phenotype. However, it is important to note the limitations of WES technology. Due to an incomplete annotation of the humane genome, some parts of protein-coding regions may not be covered. Also, the non-coding elements, such as long-noncoding RNAs, are not covered. Further, the ability of WES to detect structural variation such as duplication, translocation and inversion are very limited [69]. Despite all this, many gene variants have been causally linked to clinical phenotypes using WES technology [13–15,70], making it a suitable tool to establish *PLXNB3* variants. The *PLXNB3* variants found in our population were partly found in the reference Genome Aggregation Database (GnomAD) of undiagnosed individuals (Table 1). In addition, ExAC data examination did not reveal *PLXNB3* localization in so-called desert areas. The multifactorial aetiology of developmental delay, ASD and epilepsy include many genetic and environmental risk elements [19,20,71–76], including other axon guidance molecules [11,77]. Together, this suggests that apart from the identified *PLXNB3* variants, other genetic, protein or environmental factors are likely to contribute to the observed phenotypes in our cohort.

The *in silico* structural homology model of PLEXINB3 was derived from PlexinAs, PlexinBs and plxnC1 to the best of our capabilities. However, for many variants (e.g. Gly337Arg) large structural differences existed between different Plexins. The nucleotide sequence between

PlexinB3 and the templates were conserved for 12 of the 19 variants. This complicates precise structural predictions. This is observed in Table 2 where the predicted structural changes did not always reflect the *in vitro* findings and vice versa. This underlines the importance of (1) determining the crystal structure of PlexinB3 and (2) to validate the predicted consequences thoroughly.

Conclusion

In this study rare variants of *PLXNB3* were identified in a patient cohort characterized by a broad phenotypic spectrum including developmental delay, ASD, hypotonia and epilepsy (See Table 1). Alterations in protein structure, production, localization and autoinhibitory mechanisms were found for various variants (Table 2). Further characterization of the variants should focus on signalling mechanisms of PLEXINB3. Ligand binding and downstream signalling studies will reveal whether the variants could alter PLEXINB3 function. Combined with the data from this study, we can elucidate the signalling and functions of PLEXINB3 in more detail and assess the impact of perturbed PLEXINB3 signalling on human brain development and multifactorial disorders such as developmental delay, ASD and epilepsy.

Acknowledgements

We are grateful to the patients for participation in this study. We would like to thank the members of the Pasterkamp laboratory and the Department of Translational Neuroscience for assistance and helpful discussions throughout this project. This work was financially supported by an ALW-Vici Grant from NWO, Stichting ParkingsonFonds and Dynamics of Youth Seed Money grant from Utrecht University. The authors would like to thank the Genome Aggregation Database (GnomAD) and the groups that provided exome and genome variant data to this resource. A full list of contributing groups can be found at https://gnomad.broadinstitute.org/about.

Author Contributions

S.L., G.N.N., E.Y.J., and R.J.P designed all experiments. S.L. generated the PLEXINB3 plasmid and performed protein production and localization experiments. G.N.N. and E.Y.J. performed PLEXINB3 homology modelling. M.E.Z. performed the cell collapse assay. P.M.vH. coordinated patient care and the whole exome sequencing data. S.L., G.M.J.R. and R.J.P. wrote manuscript with input from all authors.

References

1. Rubina, K. A. & Tkachuk, V. A. Guidance Receptors in the Nervous and Cardiovascular Systems. *Biochemistry* 80, 1235-1253 (2015).
2. Pasterkamp, R. J. Getting neural circuits into shape with semaphorins. *Nat Rev Neurosci* 13, 605–18 (2012).
3. Unified nomenclature, U. Unified Nomenclature for the Semaphorins/Collapsins. *Cell* 97, 551–552 (1999).
4. Jongbloets, B. C. & Pasterkamp, R. J. Semaphorin signalling during development. *Development* 141, 3292–3297 (2014).
5. Battistini, C. & Tamagnone, L. Transmembrane semaphorins, forward and reverse signaling: have a look both ways. *Cell Mol Life Sci* 73, 1609–22 (2016).
6. Moeschler, J. B. & Shevell, M. Clinical Genetic Evaluation of the Child With Mental Retardation or developmental delays. *Pediatrics* 117, 2304-16 (2006).
7. Shevell, M. Global *Development* al Delay and Mental Retardation or Intellectual Disability : Conceptualization, evaluation and etiology. *Pediatr Clin Neurosci am* 55, 1071–1084 (2008).
8. Keller, R., Basta, R., Salerno, L. & Elia, M. Autism, epilepsy, and synaptopathies: a not rare association. *Neurol Sci* 38, 1353–1361 (2017).
9. Vasa, R. A., Mostofsky, S. H., Ewen, J. B., The disrupted connectivity hypothesis of Autism Spectrum Disorders : Time for the Next Phase in Research. *Biol Psychiatry Cogn Neurosci Neuroimaging* 1, 245-252 (2017).
10. Scharfman, H. E. The Neurobiology of Epilepsy Helen. *Curr Neurol Neurosci* Reports 7, 348–354 (2007).
11. van Battum, E. Y., Brignani, S. & Pasterkamp, R. J. Axon guidance proteins in neurological disease. *Lancet Neurol* 14, 532–546 (2015).
12. Neveling, K. *et al.* A Post-Hoc Comparison of the Utility of Sanger Sequencing and Exome Sequencing for the Diagnosis of Heterogeneous Diseases. *Hum Mutat* 34, 1721–1726 (2013).
13. Gueneau, L. *et al.* KIAA1109 Variants Are Associated with a Severe Disorder of *Brain Development* and Arthrogryposis. *Am J Hum Genet* 102, 116–132 (2018).
14. Lipstein, N. *et al.* Synaptic UNC13A protein variant causes increased neurotransmission and dyskinetic movement disorder. *J Clin Invest* 127, 1005–1018 (2017).
15. Van Haaften-Visser, D. Y. *et al.* Ankyrin repeat and zinc-finger domain-containing 1 mutations are associated with infantile-onset inflammatory bowel disease. *J Biol Chem* 292, 7904–7920 (2017).
16. Artigiani, S. *et al.* Plexin-B3 is a functional receptor for semaphorin 5A. *EMBO Rep* 5, 3–7 (2004).
17. Yukawa, K. *et al.* Sema4A induces cell morphological changes through B-type plexin-mediated signaling. *Int J Mol Med* 25, 225–230 (2010).
18. Rujescu, D. *et al.* Plexin B3 is genetically associated with verbal performance and white matter volume in human brain. *Mol Psych*iatry 12, 190–194 (2007).
19. Weiss, L. A. *et al.* A genome-wide linkage and association scan reveals novel loci for autism. *Nature* 461, 802–808 (2009).
20. Kim, S. A. *et al.* Polymorphism in the promoter region of SEMA5A is associated with sociality traits in Korean subjects with autism spectrum disorders. *Psychiatry Investig* 14, 876–878 (2017).
21. Mosca-Boidron, A. L. *et al.* A de novo microdeletion of SEMA5A in a boy with autism spectrum disorder and intellectual disability. *Eur J Hum Genet* 24, 838–843 (2016).
22. Depienne, C. *et al.* Familial cortical myoclonic tremor with epilepsy and the cerebellum. *Neurology* 74, 5–8 (2010).
23. Aleksiuniene, B., Preiksaitiene, E., Morkuniene, A., Ambrozaityte, L. & Utkus, A. A de novo 1q22q23.1 Interstitial Microdeletion in a Girl with Intellectual Disability and Multiple Congenital Anomalies Including Congenital Heart Defect. *Cytogenet Genome Res* 154, 6–11 (2018).
24. Laht, P., Pill, K., Haller, E. & Veske, A. Plexin-B3 interacts with EB-family proteins through a conserved motif. *Biochim Biophys Acta* 1820, 888–893 (2012).
25. Laht, P. *et al.* Plexin-B3 suppresses excitatory and promotes inhibitory synapse formation in rat hippocampal neurons. *Exp Cell Res* (2015).
26. Driessens, H. E. *et al.* Plexin-B semaphorin receptors interact directly with active Rac and regulate the actin cytoskeleton by activating Rho. *Curr Biol* 11, 339–344 (2001).
27. Driessens, M. H. E., Olivo, C., Nagata, K. ichi, Inagaki, M. & Collard, J. G. B plexins activate Rho through PDZ-RhoGEF. *FEBS Lett* 529, 168–172 (2002).
28. Kong, Y. *et al.* Structural Basis for Plexin Activation and Regulation. *Neuron* 91, 548–560 (2016).

29. Janssen, B. J. C. *et al.* Structural basis of semaphorin–plexin signalling. *Nature* 467, 1118–1122 (2010).
30. Wang, Y., Pascoe, H. G., Brautigam, C. A., He, H. & Zhang, X. Structural basis for activation and non-canonical catalysis of the Rap GTPase activating protein domain of plexin. *Elife* 2, e01279 (2013).
31. Wang, Y. *et al.* Plexins Are GTPase-Activating Proteins for Rap and Are Activated by Induced Dimerization. *Sci Signal* 5, ra6 (2012).
32. Wang, H. *et al.* Structural basis of Rnd1 binding to plexin Rho GTPase binding domains (RBDs). *J Biol Chem* 286, 26093–26106 (2011).
33. Tong, Y. *et al.* Structure and function of the intracellular region of the plexin-B1 transmembrane receptor. *J Biol Chem* 284, 35962–35972 (2009).
34. Tong, Y. *et al.* Binding of Rac1 , Rnd1 , and RhoD to a Novel Rho GTPase Interaction Motif Destabilizes Dimerization of the Plexin-B1 Effector Domain. *J Biol Chem* 282, 37215–37224 (2007).
35. Laht, P., Otsus, M., Remm, J. & Veske, A. B-plexins control microtubule dynamics and dendrite morphology of hippocampal neurons. *Exp Cell Res* 326, 174–184 (2014).
36. Worzfeld, T. *et al.* Mice lacking Plexin-B3 display normal CNS morphology and behaviour. *Mol Cell Neurosci* 42, 372–81 (2009).
37. Worzfeld, T., Puschel, A. W., Offermanns, S. & Kuner, R. Plexin-B family members demonstrate non-redundant expression patterns in the developing mouse nervous system : an anatomical basis for morphogenetic effects of Sema4D during development. *Eur J Neurosci* 19, 2622–2632 (2004).
38. Hartwig, C., Veske, A., Krejcova, S., Rosenberger, G. & Finckh, U. Plexin B3 promotes neurite outgrowth, interacts homophilically, and interacts with Rin. BMC *Neurosci* 6, 53 (2005).
39. Hartwig, C., Gal, A., Santer, R., Ullrich, K. & Finckh, U. Elevated phenylalanine levels interfere with neurite outgrowth stimulated by the neuronal cell adhesion molecule L1 in vitro. *FEBS Lett* 580, 3489–3492 (2006).
40. Yukawa, K. *et al.* Semaphorin 4A induces growth cone collapse of hippocampal neurons in a Rho / Rho-kinase-dependent manner. *Int J Mol Med* 16, 115–118 (2005).
41. McDermott, J. E., Goldblatt, D. & Paradis, S. Class 4 Semaphorins and Plexin-B receptors regulate GABAergic and glutamatergic synapse development in the mammalian hippocampus. *Mol Cell Neurosci* 93, 5–66 (2018).
42. Duan, Y. *et al.* Semaphorin 5A inhibits synaptogenesis in early postnatal- and adult-born hippocampal dentate granule cells. *Elife* 3, e04390 (2014).
43. Jongbloets, B. C. *et al.* Stage-specific functions of Semaphorin7A during adult hippocampal neurogenesis rely on distinct receptors. *Nat Commun* 8, 14666 (2017).
44. Tawarayama, H., Yoshida, Y., Suto, F., Mitchell, K. J. & Fujisawa, H. Roles of Semaphorin-6B and Plexin-A2 in Lamina-Restricted Projection of Hippocampal Mossy Fibers. *J Neurosci* 30, 7049–7060 (2010).
45. Suto, F. *et al.* Interactions between Plexin-A2, Plexin-A4, and Semaphorin 6A Control Lamina-Restricted Projection of Hippocampal Mossy Fibers. *Neuron* 53, 535–547 (2007).
46. Haklai-Topper, L., Mlechkovich, G., Savariego, D., Gokhman, I. & Yaron, A. Cis interaction between Semaphorin6A and Plexin-A4 modulates the repulsive response to Sema6A. *EMBO J* 29, 2635–2645 (2010).
47. Li, X., Law, J. W. S. & Lee, A. Y. W. Semaphorin 5A and plexin-B3 regulate human glioma cell motility and morphology through Rac1 and the actin cytoskeleton. *Oncogene* 31, 595–610 (2012).
48. Sobreira, N., Schiettecatte, F., Valle, D. & Hamosh, A. GeneMatcher: A Matching Tool for Connecting Investigators with an Interest in the Same Gene. *Hum Mutat* 36, 928–930 (2015).
49. Kelley, L. A., Mezulis, S., Yates, C. M., Wass, M. N. & Sternberg, M. J. E. The Phyre2 web portal for protein modeling, prediction and analysis. *Nat Protoc* 10, 845–858 (2015).
50. Moretti, S. *et al.* The M-Coffee web server: A meta-method for computing multiple sequence alignments by combining alternative alignment methods. *Nucleic Acids Res* 35, 645–648 (2007).
51. Robert, X. & Gouet, P. Deciphering key features in protein structures with the new ENDscript server. *Nucleic Acids Res* 42, 320–324 (2014).
52. Balakrishnan, A. *et al.* Molecular profiling of the 'plexinome' in melanoma and pancreatic cancer. *Hum Mutat* 30, 1167–1174 (2009).
53. Van Battum, E. Y. *et al.* The intracellular redox protein MICAL-1 regulates the development of hippocampal mossy fibre connections. *Nat Commun* 5, 4317 (2014).
54. Takahashi, T., Strittmatter, S. M. & Haven, N. PlexinA1 Autoinhibition by the Plexin Sema Domain. *Neuron* 29, 429–439 (2001).
55. Schurz, H. *et al.* The X chromosome and sex-specific effects in infectious disease susceptibility. *Hum Genomics* 13, 1–12 (2019).

56. Shvetsova, E. *et al.* Skewed X-inactivation is common in the general female population. *Eur J Hum Genet* 27, 455–465 (2019).
57. Nogi, T. *et al.* Structural basis for semaphorin signalling through the plexin receptor. *Nature* 467, 1123–1127 (2010).
58. Houck, S. A., Singh, S. & Cyr, D. M. Cellular Responses to Misfolded Proteins and Protein Aggregates. *Methods Mol Biol* 832, 455–461 (2012).
59. Pascoe, H. G., Wang, Y. & Zhang, X. Structural mechanisms of plexin signaling. *Prog Biophys Mol Biol* 1–8 (2015).
60. Ward, A. J. & Cooper, T. a. The Pathobiology of Splicing. *J Pathol* 220, 152–163 (2010).
61. Cuajungco, M. P. *et al.* Tissue-Specific Reduction in Splicing Efficiency of IKBKAP Due to the Major Mutation Associated with Familial Dysautonomia. *Am J Hum Genet* 72, 749–758 (2003).
62. Burk, K. *et al.* Post-endocytic sorting of Plexin-D1 controls signal transduction and development of axonal and cascular circuits. *Nat Commun* 8, (2017).
63. Marita, M. *et al.* Class A Plexins Are Organized as Preformed Inactive Dimers on the Cell Surface. *Biophys J* 109, 1937–1945 (2015).
64. Liu, H. *et al.* Structural basis of semaphorin-plexin recognition and viral mimicry from sema7A and A39R complexes with PlexinC1. *Cell* 142, 749–761 (2010).
65. Nkyimbeng-Takwi, E. & Chapoval, S. P. Biology and function of neuroimmune semaphorins 4A and 4D. *Immunol Res* 50, 10–21 (2011).
66. Masuda, T., Sakuma, C., Yaginuma, H. & Taniguchi, M. Attractive and permissive activities of semaphorin 5A toward dorsal root ganglion axons in higher vertebrate embryos. *Cell Adhes Migr* 8, 603–606 (2014).
67. Seshagiri, S. *et al.* Recurrent R-spondin fusions in colon cancer. *Nature* 488, 660–664 (2012).
68. Haijes, H. A. *et al.* De Novo Heterozygous POLR2A Variants Cause a Neurodevelopmental Syndrome with Profound Infantile-Onset Hypotonia. *Am J Hum Genet* 105, 1–19 (2019).
69. Goh, G. & Choi, M. Application of Whole Exome Sequencing to Identify Disease-Causing Variants in Inherited Human Diseases. *Genomics and Informatics* 10, 214–219 (2012).
70. Machol, K. *et al.* Expanding the Spectrum of BAF-Related Disorders: De Novo Variants in SMARCC2 Cause a Syndrome with Intellectual Disability and developmental Delay. *Am J Hum Genet* 1–15 (2018).
71. Torrico, B. *et al.* Lack of replication of previous autism spectrum disorder GWAS hits in European populations. *Autism Res* 10, 202–211 (2017).
72. Cheng, Y., Quinn, J. F. & Weiss, L. A. An eQTL mapping approach reveals that rare variants in the SEMA5A regulatory network impact autism risk. *Hum Mol Genet* 22, 2960–2972 (2013).
73. The International League Against Epilepsy Consortium on Complex Epilepsies. Genome-wide mega-analysis identifies 16 loci and highlights diverse biological mechanisms in the common epilepsies. *Nat Commun* 9, 5269 (2018).
74. Froukh, T. J. Next Generation Sequencing and Genome-Wide Genotyping Identify the Genetic Causes of Intellectual Disability in Ten Consanguineous Families from Jordan. *Tohoku J Exp Med* 243, 297–309 (2017).
75. Poduri, A. Meta-analysis revives genome-wide association studies in epilepsy. *Epilepsy Curr* 15, 122–123 (2015).
76. Smit, D. J. A. *et al.* Genome-wide association analysis links multiple psychiatric liability genes to oscillatory brain activity. *Hum Brain Mapp* 39, 4183–4195 (2018).
77. Evans, T. L., Blice-baum, A. C. & Mihailescu, M. Molecular BioSystems Analysis of the Fragile X mental retardation protein isoforms 1 , 2 and 3 interactions with the G-quadruplex forming semaphorin 3F mRNA. *Mol Biosyst* 8, 642–649 (2012).

6

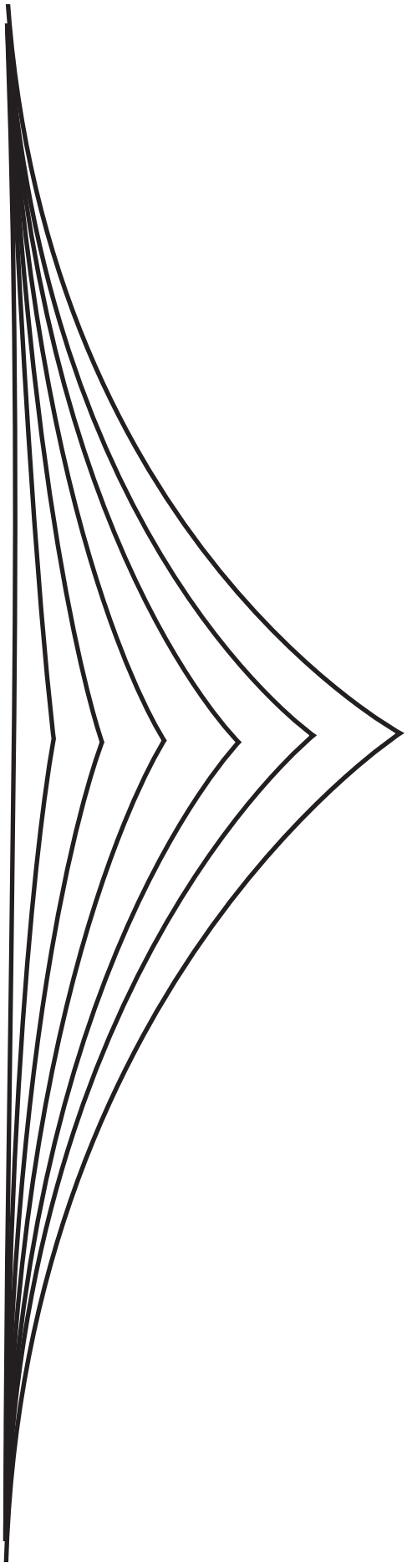

Chapter 7

General discussion

Semaphorins and Plexins instruct cells to proliferate, migrate and extend their axons to connect with multiple cell types and integrate into the brain. Their signalling is tightly controlled and uses complex mechanisms-of-action. This thesis aims to deepen our understanding of Semaphorin-Plexin interactions by studying their extensive signalling mechanisms, diversification strategies, regulation and role in health and disease (Figure 1). In the next sections, I will summarize and discuss the main findings concerning temporal and spatial control, diversified signalling mechanisms and functional implications of Semaphorin and Plexin signalling in health and disease. Finally, I will propose future directions of research to increase the understanding of the role of these axon guidance molecules in brain development and maturation.

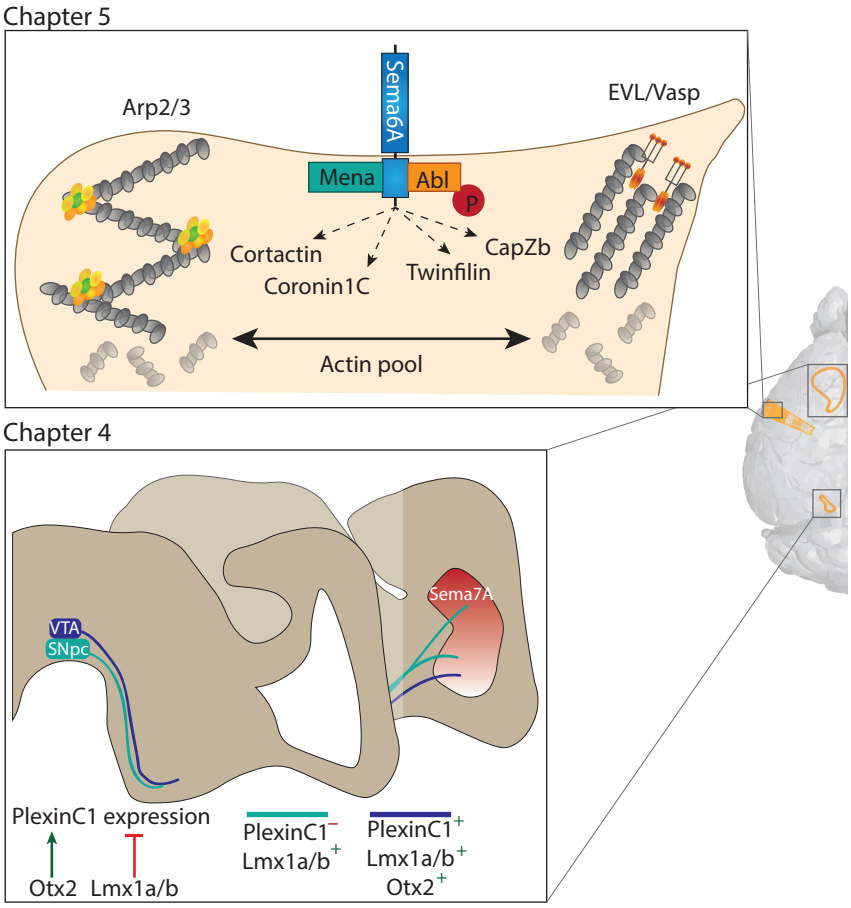

Figure 1 | Graphical outline of thesis.
This thesis examines multiple aspects of Semaphorin (Sema) and Plexin signalling during brain development, maturation and disease. Chapter 2 studies *Sema4F* expression patterns and examines the first *Sema4F* knockout mouse to understand its *in vivo* functions. Chapter 3 identifies pleiotropic effects of Sema7A via PlexinC1 or β1-integrin during hippocampal adult neurogenesis. Chapter 4 shows how PlexinC1 expression in the midbrain is controlled by specific expression of Lmx1a/b and Otx2 to ensure correct Sema7A-dependent striatal integration. Chapter 5 examines reverse signalling of Sema6A by identifying novel

1. Spatiotemporal expression of Semaphorins and Plexins is a balance between restricted and overlapping patterns.

The distinct spatial and temporal distribution of Semaphorins (Sema) and Plexins results in unique interactions necessary to control specific developmental processes [1–3]. **Chapters 2, 3 and 4** show specific spatiotemporal expression patterns of Semaphorins and Plexins and illustrate how they are important for proper brain wiring. In short, in **Chapter 2** I provide an extensive study of Sema4F expression patterns from development until adulthood showing selective expression in the hippocampus, cerebellum, olfactory bulb and cortex. In the dopamine system (**Chapter 4**), graded expression of Sema7A in the striatum ensures specific ventral targeting of PlexinC1 expressing Ventral Tegmental Area (VTA) axons.

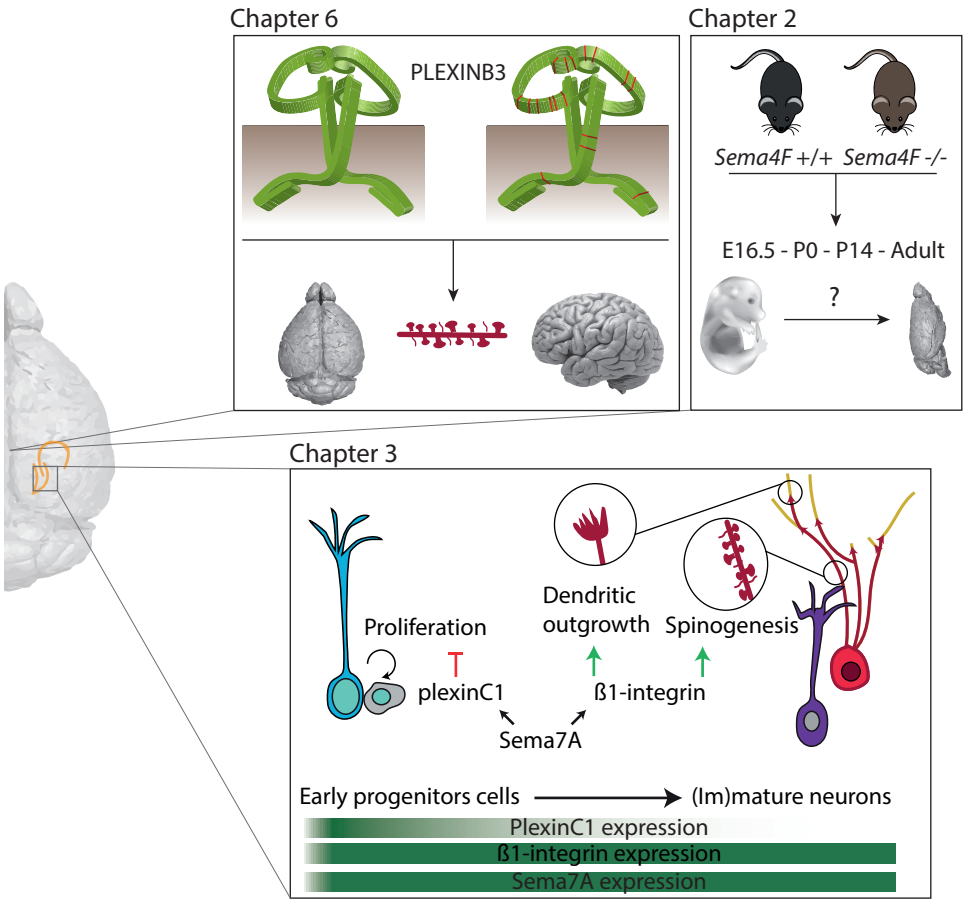

interacting proteins with promising roles in actin remodelling. Finally, in Chapter 6 we explore, through a translational approach, whether genetic alterations in PlexinB3 signalling may contribute to disease outcome and whether *PLXNB3* can be considered as a risk factor in neurodevelopmental disorders. Overall, this thesis underlines the significance of Semaphorin-Plexin signalling for proper brain development and function.

Substantia Nigra pars compacta (SNpc) axons that lack PlexinC1, target the dorsal and ventral striatum. In the subgranular zone of the adult dentate gyrus (**Chapter 3**), Sema7A and β1-integrin are expressed ubiquitously. In contrast, restricted PlexinC1 expression in adult-born neural progenitor cells enables Sema7A-mediated inhibition of their proliferation. Sema7A promote dendritic integration of β1-integrin, not PlexinC1, expressing mature adult-born granule cells into the dentate gyrus. Similar events have been described for other Semaphorin-Plexin interactions. In the hippocampus, PlexinA4 expressing mossy fibers of the dentate gyrus target the Cornu Ammonis (CA), which expresses the repellent Sema6A. Selective Stratum Lucidum targeting is achieved by spatially restricted expression of PlexinA2 that attenuates Sema6A's repulsive activity [4]. Moreover, loss of restricted expression patterns can result in malfunctioning or miswiring of brain regions. This is clearly observed in the dopamine system where ectopic expression of PlexinC1 in the SNpc abnormally targets axons to the ventral striatal (**Chapter 4**). Together, these data illustrate that the spatiotemporal expression of Semaphorin and Plexin members results in selective patterns necessary for correct brain development and maturation.

Transcriptional control of Semaphorin and Plexin expression

Various regulatory mechanisms control the spatiotemporal expression of Semaphorins and Plexins ranging from global to local mechanisms (**Chapter 1**, [5-9]). Transcription factors play leading roles in regulating expression of Semaphorin and Plexin families (**Chapter 1**), however the precise regulatory steps to ensure spatiotemporal expression of specific family members remain mostly unknown [5–7,10]. In **Chapter 4**, we identify novel transcription factors in the spatiotemporal regulation of Semaphorin-Plexin expression: 1) LIM Homeobox Transcription Factor 1 Alpha and Beta (Lmx1a/b). Lmx1a/b negatively controls PlexinC1 expression in mesodiencephalic dopamine neurons in the SNpc. As a result, SNpc neurons target their axons to the dorsal striatum. 2) Orthodenticle homeobox 2 (Otx2) enhances PlexinC1 expression in VTA neurons resulting in ventral axonal innervation of the striatum (**Chapter 4**). This indicates that PlexinC1 expression is tightly controlled by the coordinated action of, at least, three transcription factors in the midbrain.

Similar regulatory axes have been observed in transcriptional control of Semaphorins and Plexins signalling [5,7,11,12]. To exemplify, expression of Sema3C in a human oncology cell line is promoted by androgen receptor-induced GATA2 and negatively regulated by FOXA1 [11]. In addition, a luciferase promoter activity assay in HeLa cells showed upregulation of Sema3C expression due to Sox4 [5]. A regulatory axe is also described *in vivo* in mouse contralateral retinal cells where expression of SoxC transcription factors (Sox4, Sox11 and Sox12) together with Notch-Hes5 signalling control the expression of PlexinA2. Contralateral retinal cells project ipsilateral when SoxC transcription factors are absent [6]. Kuwajima and colleagues show that individual SoxC transcription factors are not functionally equivalent; Sox4 and Sox11 activate PlexinA1 more strongly than Sox12. However, **Chapter 4** is one of the first examples to observe opposing effects of transcription factors on Plexin activation in the brain [7,13].

The RNA sequencing data showing differential expressed genes in the midbrain of WT or *Lmx1a/b c*KO in **Chapter 4** indicates multiple targets for Lmx1a/b, however, none of the family members PlexinC1 or its ligand Semaphorins were observed. This is striking since other transcription factors often regulate multiple Semaphorin and Plexin family members. Sox4 upregulates Sema3A, 3B, 3C and 3E and PlexinA2 and D1 in luciferase assays in HeLa cells [5]. This indicates that transcription factors that control expression of specific Semaphorin and Plexin can control family members as well. Semaphorin and

Plexin family members are expressed in the dopamine midbrain [14,15]. Together this can indicate that transcription factors are more selective *in vivo* or that Lmx1a/b transcriptional effect is restricted to PlexinC1. If the latter would be true, PlexinC1 expression in adult-born neural progenitor cells in the adult dentate gyrus (**Chapter 3**) may be regulated as well through coordinated action of Lmx1a/b and Otx2. Expression of Lmx1a/b and Otx2 in the adult dentate gyrus is unexplored but would be of interest for future research since the coordinated action of suppression and activation, respectively, may underlie the restricted expression of PlexinC1 in adult-born neural progenitor cells. Taken together, transcription factors have a coordinating role to balance the spatiotemporal expression of (multiple) Semaphorin and Plexin family members.

Redundancy in Semaphorin and Plexin signalling

The previous section discussed that the expression of Semaphorin and Plexin members is under tight spatiotemporal control to ensure proper brain development. These distinct expression patterns suggest defined roles for Semaphorins and Plexins. However, redundancy occurs due to the flexible and permissive nature of Semaphorin and Plexin interactions [16–18]. Preliminary characterization of a first *Sema4F* knockout (KO) mouse did not reveal obvious brain deficits (**Chapter 2**). The lack of neuronal defects in single Semaphorin KOs is more often observed, e.g. single KO of *PlexinB3* or *Sema4G* did not affect brain development [16,19]. Perhaps a more extensive characterization will uncover brain deficits for these Semaphorins or Plexins. An alternative theory can explain the redundant expression patterns as well. Overlapping expression of Semaphorin and Plexin members may act as a safeguard to enable accurate brain development, indicating that the redundant nature of Semaphorins and Plexins may be functional. An example of this phenomenon is observed during cortical expansion where *PlexinB1/B2* double KO mice show a reduced neural progenitor pool, while this defect was not detected in *PlexinB1* or *PlexinB2* single KO mice [18]. Similar events are observed in multiple systems [16,17,20–22]. In conclusion, expression of Semaphorins and Plexins is restricted to a degree that allows unique interactions of Semaphorins and Plexins to enable specific wiring events, but also to permit redundancy that prevents wiring errors.

Concluding remarks

This thesis provides data to corroborate that restricted expression of Semaphorins and Plexins is necessary for accurate dopaminergic wiring and proliferation and integration during adult hippocampal neurogenesis. In addition, it suggests that expression of certain Semaphorins and Plexins may serve as a safeguard for miswiring. Together it seems that Semaphorin and Plexin display restricted but overlapping expression patterns resulting in a controlled balance that enables distinct wiring events and prevent miswiring through functional redundancy. The regulation of the spatiotemporal expression of Semaphorins and Plexins is controlled in part by transcription factors. Future studies should elucidate the redundant or safeguarding functions between Semaphorin and Plexin family members. Furthermore, transcriptional control of Semaphorin and Plexins is a relative neglected field where major steps can be taken to identify more transcription factors, how they activate (local) transcription and how they work in concert to allow spatiotemporal restricted expression patterns.

2. Diversification strategies in Semaphorin and Plexin signalling.

It has become increasingly clear that Semaphorin-Plexin signalling relies on specialised mechanisms-of-actions to exert distinct roles in the brain [23]. This thesis examines several aspects of these so-called diversification strategies in **Chapter 3 and 5**. The regulation and functional implication of these mechanisms will be further discussed in the following sections. Furthermore, the biological relevance of diversification in Semaphorin and Plexin signalling is considered.

Regulation of downstream signalling in Semaphorins and Plexins

Chapter 1 describes well-established interactors downstream of Semaphorins and Plexins and illustrate the use of distinct signalling pathways. The known functions and signalling routes in reverse signalling of transmembrane Semaphorins have been excellent reviewed [23]. However, the regulation of this multifaceted signalling system requires a better understanding. Activation of either signalling routes depend on the availability of ligands and receptors, which are subjected to transcriptional control, endocytosis and cleavage. Apart from these more obvious regulatory mechanisms, a model emerged that could regulate forward and reverse signalling. *Cis*-interactions between Semaphorins and Plexins can regulate the activation of forward and reverse signalling [23,24]. It has been shown that *cis*-interaction between Sema6 and PlexinA can attenuate ligand-induced effects of Sema6 on PlexinA (forward signalling), as observed in the hippocampus [25,26], starbust amacrine cells (SAC) [27] and myocardial cells [28]. However, similar *cis*-interactions can not prevent ligand-induced effects of PlexinA on Sema6 in cultured cells (reverse signalling) [24]. This suggests that *cis*-interactions between Semaphorins and Plexins can regulate the signal direction by inhibiting forward signalling and allowing reverse signalling. Interestingly, expression of a single Sema6A and PlexinA2 dimer in *trans* can potentially activate forward and reverse signalling, perhaps simultaneously. However, *cis*-interactions of Semaphorin-Plexin on opposing cells is likely to only induce reverse signalling [24]. How forward and reverse signalling is precisely regulated by *trans* and *cis*-interactions *in vivo* is obscure but could rely on similar mechanisms seen for Ephrins and integrins, including: clustering to stabilize signalling, cleavage of ectodomain to discard forward signalling perhaps leading to endocytosis of the cytoplasmic domain to attenuate reverse signalling as well [29–32]. The described *CAG-Sema6AΔcyto-GFP* construct and *Sema6AΔcyto* mouse in **Chapter 5** are valuable tools to investigate the regulation of forward and reverse signalling further. To conclude, these data suggest that Sema6A forward and reverse signalling depend on the availability of *cis* or *trans* interactions with Plexin.

Sema6A can mediate the switch between lamellipodia and filopodia

Reverse signalling of Sema6A is involved in cellular and neurite migration *in vitro* by modulating actin. In **Chapter 5**, reverse signalling was studied by examining the interactome of Sema6A via mass spectrometry analysis. As hypothesized in **Chapter 5**, Sema6A may influence the formation of actin filaments by modulating the competition between Arp2/3 complex and EVL/VASP-pathway for actin [33,34]. The Arp2/3 complex is a widely used actin modulating system to establish actin meshworks resulting in lamellipodia. Modulation of the Arp2/3 complex to allow growth cone collapse is used by many proteins [34–37], including Semaphorin-Plexin forward signalling. This was observed during bath

application of Sema3A in dorsal root ganglion neurons. Sema3A-mediated growth cone collapse activated RhoA GTPases resulting in decreased lamellipodia and lower levels of Cortactin and Arp2 [38,39]. Plexin-induced GTPases modulate actin via the Arp2/3 complex [40,41], but Plexin does not interact directly with the Arp2/3 complex proteins or modulators. Whether the direct interaction between Sema6A and Arp2/3 complex proteins, as indicated by our mass spectrometry, is used to modulate actin during reverse signalling has to be deciphered in future experiments. All together our data is the first observation of a direct interaction between Sema6A and the Arp2/3 complex. Taken together Sema6A-interacting proteins are involved in the Arp2/3 complex and EVL/VASP-pathway that both compete for actin to establish stable actin meshwork or F-actin bundles, respectively [33,34]. Reverse signalling of Sema6A may steer this competition by promoting or inhibiting either of these pathways.

How reverse signalling of Sema6A would regulate the switch between Arp2/3 complex-mediated or EVL/VASP-pathway-mediated actin modulation remains an open question. Several mechanisms can be proposed to regulate the signalling route downstream of Sema6A. Several observations hint that the mode of Sema6A-activation may specify the signalling pathway: (1) Sema6A downstream signalling can be activated upon ligand interaction or multimerisation of Sema6A itself (as observed for other guidance cues [29,42–44]). (2) Abl and Mena have distinct binding sites on the cytoplasmic domain of Sema6 24,28 enabling distinct regulation of downstream signalling routes. Moreover, (3) ligand-induced activation of Sema6A resulted in Abl phosphorylation while this was not observed upon activation of Sema6A through multimerisation. In contrast, recruitment of Mena was independent of mode of Sema6A-activation [24]. Together these data suggest that activation of Sema6A via PlexinA2 or multimerisation resulted in distinct signalling routes. Whether a similar mechanism can result in distinct activation patterns of the Arp2/3 complex modulation proteins identified in **Chapter 5** or whether PlexinA4 activation can result in a third distinct signalling route is undetermined. In conclusion, the switch between Arp2/3 complex and EVL/VASP-pathway actin remodelling may depend on activation of Sema6A, either via PlexinA2, PlexinA4 or multimerisation of Sema6A itself.

Diversification of Sema7A signalling allows pleiotropic effects

In **Chapter 3** we present data showing novel pleiotropic effects of Sema7A in adult hippocampal neurogenesis. Sema7A inhibits proliferation via PlexinC1 in adult-born neural progenitor cells while, through β1-integrin, it promotes dendritic integration at more mature neuronal stages. This work shows that diversification strategies for Semaphorin and Plexins persist in the adult brain and that stage-specific expression of receptors drives distinct outcomes in the same neuron. The following section discusses how PlexinC1 downstream signalling cascades are selectively activated and could inhibit cell proliferation.

Although both PlexinC1 and β1-integrin are both expressed in adult-born neural progenitor cells, only signalling downstream of PlexinC1 is activated following Sema7A exposure. This suggests that PlexinC1, but not β1-integrin, regulates the stage-specific effect of Sema7A on proliferation in adult-born neural progenitor cells (**Chapter 3**). Several possible explanations for the selective nature of this Sema7A-mediated effect exist. Competition could arise between PlexinC1 and β1-integrin for Sema7A interaction, although this has not been observed before. Inhibition of integrin-mediated adhesive effects has been described for several Plexins [45,46]. PlexinC1 may activate mechanisms to inhibit β1-integrin signalling [47,48] as observed in cultured dendritic cells where viral-Sema7A-induced PlexinC1 activation inhibited integrin-mediated adhesion via Cofilin

phosphorylation [49]. Similarly, overexpression of PlexinC1 completely abolishes Sema7A-induced β1-integrin-mediated migration in cultured gonadotropic-releasing hormone 1 neurons and melanocytes [50,51]. Another explanation for the lack of β1-integrin activation might be that additional interactors or molecules are present in adult-born neural progenitors that inhibit integrin signalling. Integrins are capable of bidirectional signalling depending on their conformation. During integrin-mediated adhesion signalling (inside-out signalling) additional binding of Talin is necessary to mediate integrin activation [44]. It is proposed that removal of Talin is necessary to enable ligand-induced functions (outside-in activation) such as differentiation and proliferation but this mechanism is less well understood [52–54]. Investigation of these hypotheses may reveal how PlexinC1 downstream signalling cascades are selectively activated during early stages of adult hippocampal neurogenesis.

Chapter 3 as well explores the PlexinC1-induced signalling mechanism resulting in decreased proliferation of adult-born neural progenitor cells. Cofilin is a central signal transducer downstream of PlexinC1 in these cells. Cofilin is phosphorylated via LIM kinases downstream of PlexinC1. Inactivated phosphorylated Cofilin in its turn, can attenuate actin remodelling [55,56]. In *Drosophila*, mutants of Cofilin were examined for proliferation properties in neuroblasts. The constitutively active Cofilin could increase proliferation while the inactive Cofilin could not, suggesting that phosphorylation affects cell division negatively [57]. During embryogenesis the role of Cofilin in proliferation has become apparent. Cofilin depletion lead to increased mechanical tension and actin stress fibers, promoting the nuclear localization of transcription factors YAP1 and TAZ that are crucial for cell proliferation [58,59]. Whether similar mechanisms are activated upon PlexinC1-induced inhibition of proliferation in adult-born neural progenitor cells is unknown. Future experiments should examine whether actin stress fibers are formed upon PlexinC1 activation and if transcription factors that control proliferation (e.g. reviewed by [60]) are translocated to the nucleus of adult-born neural progenitor cells.

Together, these data demonstrate a bifunctional role for Sema7A in adult-born granule cells and highlights the beneficial impact of diversification mechanisms in brain development and maturation. This diversification mechanism of Sema7A results in two distinct cellular outcomes: (1) inhibition of proliferation via PlexinC1 and (2) promotion of dendritic growth and integration via β1-integrin. Ablating either Sema7A, PlexinC1 or β1-integrin resulted in malformation and dysfunction of adult-born granule neurons (**Chapter 3**).

Biological relevance of diversification strategies

Spatiotemporal control of Semaphorins and Plexins expression allows a limited number of ligand-receptor complexes to orchestrate complex developmental and maturation processes. In order to achieve accurate brain development, diversification strategies are crucial in Semaphorin and Plexin signalling as is observed in **Chapter 3 and 5** where loss of the bifunctional or bidirectional effects of Sema7A or Sema6A, respectively, results in brain malformations. Although it is unclear how diversification strategies emerged, diversification of Semaphorin and Plexin signalling enhances flexibility (1), accelerates signalling (2) or acts as a Semaphorin-Plexin regulatory mechanism (3). In more detail, (1) flexibility is enhanced by the ability of Semaphorins and Plexins to signal through heterocomplexes, multiple binding partners, activate reverse signalling pathways and engaging in *cis*-interactions. This strategy is widely used in Semaphorin and Plexin signalling and is critical for brain development (**Chapter 3 and 5**) [23,24,61]. In addition, (2) diversification mechanisms can

accelerate the speed of biological processes by achieving distinct cellular outcomes from a single Semaphorin protein (**Chapter 3**). As an example, bidirectional signalling allows for a single protein to induce multiple distinct signalling cascades and cellular outcomes. Sema6A forward signalling reduces cultured cerebellar migration from explants while this is promoted in Sema6A reverse signalling [24]. Alternatively, if bidirectional signalling did not exist, a cell would have to express two distinct proteins for these cellular events. Expressing distinct Semaphorins and Plexins for each cellular outcome would be a massive, time-consuming burden for a cell. Lastly, (3) diversification may function as a feedback loop by regulating the induced signal, e.g. by inhibitory *cis*-interactions 7,24. As an example, Sema6A in *cis* blocks the receptor function of PlexinA2 to control Sema6A repulsive response in trans, this is observed in cellular assays, hippocampal laminar projection integration and SAC (inhibitory neurons in the retina) [25,27,62]. In conclusion, diversification strategies are crucial for efficient Semaphorin-Plexin signalling throughout the development and plasticity of the brain [7,23,63].

Concluding remarks

This thesis provides evidence for diversification of signalling and function of Sema6A and Sema7A that were not previously observed. It shows a first example of the pleiotropic effects of Sema7A depending on stage-distinct receptors in the adult brain within a single cell population. Further, a novel signalling route in reverse signalling of Sema6A is proposed. These data provided more insights into the regulatory roles and functional impact of diversification strategies utilized in Semaphorin-Plexin signalling.

3. Is PlexinB3 a potential risk factor in neurodevelopmental disorders?

Neurodevelopmental disorders, such as Autism Spectrum Disorder (ASD) are characterized by disturbances in spine dynamics, synaptic transmission, excitation/inhibition balance and neuronal number [64,65]. The number of candidate genes implicated in ASD are increasing while the most penetrant mutations occur in genes that regulate synaptic function (e.g. *FMR1, SHANK3* and *PTEN*) [65,66]. Semaphorin-Plexin signalling is implicated with ASD via genome-wide copy number variations or expression studies in patients [67–69]. In **Chapter 6**, a patient cohort with a broad phenotypic spectrum were diagnosed via Whole Exome Sequencing (WES) and revealed rare *PLXNB3* variants. The *PLXNB3* variants were mapped onto an *in silico* structural homology model, due to the unavailability of a crystal structure for PLEXINB3. The majority of the *PLXNB3* variants were predicted to alter the structure of the protein and potentially perturb its signalling and function. Although the functions of PLEXINB3 are poorly understood, its involvement in neurite outgrowth [42,70] and synapse regulation [71,72] indicate that PLEXINB3 can be an interesting candidate in ASD or other neurodevelopmental disorders. However, to assess any potential of *PLXNB3* as a risk factor for neurodevelopmental disorders, such as ASD, many aspects regarding its (synaptic) signalling mechanism and function have to be closely examined, as is discussed below.

PlexinB3 signalling and functions are too obscure to allow assessment as a potential risk factor

To examine *PLXNB3* as a potential risk factor, the function of the *PLXNB3* variants have to be examined. The expression and localization of the proteins carrying the *PLXNB3* variants were examined using cellular models. Transfections of the variants into HEK293 cells followed by western blot analysis for expression levels revealed decreased expression for Val423Met and Glu708Lys variants. In addition, surface localization was examined in HEK293 cells expressing *PLXNB3* variants showing decreased intensity levels on the surface for two other variants, Phe922Leu and Val1678fs*. Together this indicates that the structural changes in *PLXNB3* variants may result in skewed expression patterns of PLEXINB3. The concentration of proteins can be important for their function. This has been shown in chick dorsal root ganglion neurons, where a dose-dependent response to Sema3A leads to growth cone collapse either via local protein synthesis or via GSK-3β signalling pathways [73]. Whether dose-dependent effects are important for PLEXINB3 signalling or function remain unresolved. As mentioned previously, spatiotemporal expression of Semaphorin and Plexins are crucial for their function. Restricted expression of PLEXINB3 is found postnatally in the hippocampus and in oligodendrocytes in humans while murine PlexinB3 is additionally located in the cerebellum [42,72]. Whether the restricted expression of PlexinB3 is important for brain development is not obvious [19], however, subtle alterations may lead to miswiring, as was observed in **Chapters 3 and 4**. Taken together this indicates that *PLXNB3* variants may lead to altered expression patterns that can disrupt PLEXINB3 signalling and function.

PlexinB3 is a regulator of synaptic function by suppressing excitatory and promoting inhibitory synapse formation in rat hippocampal neurons. In particular, overexpression of the cytoplasmic domain of PlexinB3 (mimicking a ligand-induced Plexin [45]) in cultured rat hippocampal dendrites reduced the volume of excitatory synapses while the volume of inhibitory synaptic inputs on neuronal soma was increased [72]. Interestingly, transfections

with truncated PlexinB3 proteins revealed that the N-terminal segment containing microtubule end protein (EB3) binding motifs was crucial to reduce excitatory synapses while RasGAP and Rho GTPases domains were important to promote inhibitory synapses [71,72]. As many proteins contribute to the balance of synapse formation, the *in vivo* role of PlexinB3 should be established. The current *PlexinB3* KO mouse is not characterized for synapse discrepancies or neurodevelopmental phenotypes and showed normal brain development and behavior [19]. ASD mouse models showed alterations in spine density, maturation and activity [65]. It would be interesting to examine the *PlexinB3* KO model to assess synapse formation and maturation in the hippocampus. In addition, this model can be used to examine synapse formation in *PLXNB3* variants. Interestingly, a SNP in the N-terminal segment attenuated PlexinB3s capability of reducing excitatory synapses but held no effect on the formation of inhibitory synapses [72]. The *PLXNB3* variants identified in our patient cohort in **Chapter 6** report 5 mutations that affect the cytoplasmic domain. It is intriguing to test whether these mutations could intervene with EB3 or RasGAP/Rho GTPase pathways important for PlexinB3-dependent synapse formation. Together this indicates that minor changes in the cytoplasmic domain may influence only one of the two signalling pathways leading to altered synapse development downstream of PlexinB3 activation.

The majority of the *PLXNB3* variants are located in the extracellular domain indicating potential disturbances in synapse formation via two aspects of PLEXINB3 signalling: (1) ligand binding and (2) autoinhibition. As described in **Chapter 6**, PLEXINB3 is a receptor for Sema4A and Sema5A and their interaction should be tested in *PLXNB3* variants via ligand-binding assays. Sema4A and Sema5A are both involved in synapse development, without an established role for PlexinB3. Sema4A-PlexinB2 and Sema4D-PlexinB1 signalling mediate inhibitory and excitatory synapse development in hippocampal rat neurons [20,21]. Interestingly, Sema4A promotes inhibitory synapse development via PlexinB1 indicating promiscuity between class 4 Semaphorins and class B Plexins during hippocampal synapse development [20]. The other receptor, Sema5A negatively controls synaptogenesis in the hippocampus via PlexinA2. Knockout of *Sema5A* resulted in increased spine density and PSD-95 puncta on hippocampal neurons [74]. Together this indicates that hippocampal synapse formation is a balanced process controlled by several members of the Semaphorin-Plexin family. Due to the promiscuous nature of Semaphorin-Plexin signalling, it is tempting to speculate that PlexinB3 may be induced as well via Sema4A or Sema5A to influence hippocampal synapse formation. To examine this, elaborate cellular assays using multiple KOs or RNA interfering strategies have to be used in synaptic development assays to circumvent the expression and redundancy of other family members. Together, although the precise mechanism-of-action is unclear, Sema4A and/or Sema5A both have the potential to induce PlexinB3-mediated synapse development.

Secondly, extracellular *PLXNB3* variants may alter autoinhibition mechanisms that are necessary to prevent premature downstream signalling of PLEXINB3 [75,76]. The *PLXNB3* variants were assessed for autoinhibitory mechanisms by a COS-7 collapse assay where only Glu337Arg showed increased cell contraction compared to WT (**Chapter 6**). It is difficult to appreciate the significance of this data since autoinhibitory mechanisms have not been elucidated in PlexinB crystal structures. Autoinhibitory head-to-stalk formation is observed in other PlexinAs, which have a different ectodomain compared to PlexinB therefore making it unclear whether similar, or any, mechanisms are present in PlexinB proteins [75–77]. The truncated PlexinB3 constructs used by Laht et al., 2015, hint towards the existence of

an autoinhibitory mechanism since the deletion of the ectodomain mimicked an active PlexinB3 protein. This is similar as observed for other Plexins [45,78]. Together this suggests that the Glu337Arg may act as a constitutional active protein, which, as shown by Lath et al., may decrease excitatory and increase inhibitory hippocampal synapse development. These data combined with our collapse data indicate that PlexinB3 has an autoinhibition mechanism and that loss of this function may result in an overactivated protein.

Concluding remarks

This thesis proposes *PLXNB3* as a potential risk factor in neurodevelopmental disorders, possibly by influencing the balanced synapse development in the brain. However, to enable such an assessment, future research is needed to decipher the role of PlexinB3 and variants in synapse development by elucidating the existence and impact of autoinhibitory mechanisms, the *in vivo* role of *PLXNB3* and which ligands induce PlexinB3-signalling.

Final words

This thesis provides novel insights into the regulation of expression, diversification strategies and functional implications of Semaphorin-Plexin signalling. In addition, it shows how defects in Semaphorin-Plexin signalling may contribute to neurodevelopmental disorders (Figure. 1). The *in vivo* function of Sema4F was studied in the central and peripheral nervous systems by creating a first *Sema4F* KO mouse. In another chapter, a novel pleiotropic role for Sema7A and its receptors was determined within the same cell during adult hippocampal neurogenesis. We demonstrate that stage-dependent expression of PlexinC1 controls adult-born granule cell proliferation, while their integration is promoted via β1-integrin at later stages. Next, the importance of spatiotemporal control of PlexinC1 expression in the dopaminergic midbrain was high lighted by modulation of transcription factors. Expression of Lmx1a/b and Otx2 influences PlexinC1 expression and ensures correct axonal targeting of the striatum. Further, reverse signalling of Sema6A was studied by identifying novel downstream interacting proteins through mass spectrometry. These data showed the first example of the involvement of the Arp2/3 complex in class 6 Semaphorin reverse signalling. Finally, a patient cohort revealed *PLXNB3* variants, which were characterized to assess whether *PLXNB3* could be a potential risk factor in neurodevelopmental disorders.

The findings presented in this thesis contribute to the current understanding of the complex nature of Semaphorin and Plexin signalling in health and disease on three levels. First, the described restricted spatiotemporal expression patterns of *Sema4F, PlexinC1* and *Sema7A* provide a starting point to investigate their transcriptional control, possibly by further expanding the roles of Lmx1a/b and Otx2 on PlexinC1 in the adult hippocampus. The data showing that ablating restricted spatiotemporal expression of *Sema4F* did not lead to brain deficits will be a valuable tool to decipher whether overlapping expression patterns of Semaphorins and Plexins may result in functional redundancy. Second, the pleiotropic effects of Sema7A and reverse signalling of Sema6A emphasize the need for in-depth investigation of diversification strategies of Semaphorin-Plexin signalling in the developing and mature brain. Future experiments should focus on understanding how diversification is regulated by determining (1) how specific signalling routes are selected and (2) cross-talk or competition between signalling routes. In addition the functional implications of diversification strategies should be investigated further by (1) examining novel pathways in reverse signalling of Sema6A e.g. during cortical laminar organisation and (2) deciphering the benefits of diversification strategies for Semaphorin-Plexin signalling in the brain. Finally, this thesis provided a potential new risk factor for neurodevelopmental disorders. Future research should decipher the functional implications of PlexinB3 in synapses and elucidate its up- and downstream signalling routes. Together, the tools and findings presented in this thesis contribute to an increased understanding of the crucial role and mechanism-of-action of Semaphorin-Plexin signalling in health and disease.

References

1. Nawabi, H. *et al.* A midline switch of receptor processing regulates commissural axon guidance in vertebrates. *Genes Dev* 24, 396–410 (2010).
2. Andermatt, I. *et al.* Semaphorin 6B acts as a receptor in post-crossing commissural axon guidance. *Development* 141, 3709–20 (2014).
3. Perälä, N. M., Immonen, T. & Sariola, H. The expression of plexins during mouse embryogenesis. *Gene Expr Patterns* 5, 355–362 (2005).
4. Suto, F. *et al.* Interactions between Plexin-A2, Plexin-A4, and Semaphorin 6A Control Lamina-Restricted Projection of Hippocampal Mossy Fibers. *Neuron* 53, 535–547 (2007).
5. Huang, H. Y. *et al.* SOX4 Transcriptionally Regulates Multiple SEMA3/Plexin Family Members and Promotes Tumor Growth in Pancreatic Cancer. *PLoS One* 7, e48637 (2012).
6. Kuwajima, T., Soares, C. A., Sitko, A. A., Lefebvre, V. & Mason, C. SoxC Transcription Factors Promote Contralateral Retinal Ganglion Cell Differentiation and Axon Guidance in the Mouse Visual System. *Neuron* 93, 1110–1125 (2017).
7. Jongbloets, B. C. & Pasterkamp, R. J. Semaphorin signalling during development. *Development* 141, 3292–3297 (2014).
8. Alto, L. T. & Terman, J. R. Semaphorins and their Signaling Mechanisms. *Methods Mol Biol* 1493, 1–25 (2017).
9. Russell, S. A. & Bashaw, G. J. Axon guidance pathways and the control of gene expression. *Dev Dyn* 247, 571–580 (2018).
10. Rehman, M., Gurrapu, S. & Cagnoni, G. PlexinD1 Is a Novel Transcriptional Target and Effector of Notch Signaling in Cancer. *PLoS One* 1–21 (2016).
11. Tam, K. J. *et al.* Androgen receptor transcriptionally regulates semaphorin 3C in a GATA2-dependent manner. *Oncotarget* 8, 9617–9633 (2016).
12. Lee, H. *et al.* Slit and Semaphorin signaling governed by Islet transcription factors positions motor neuron somata within the neural tube. *Exp Neurol* 269, 17–27 (2015).
13. Nobrega-Pereira, S. *et al.* Postmitotic Nkx2-1 Controls the Migration of Telencephalic Interneurons by Direct Repression of Guidance Receptors. *Neuron* 59, 733–745 (2008).
14. Prasad, A. a & Pasterkamp, R. J. Axon guidance in the dopamine system. *Adv Exp Med Biol* 651, 91–100 (2009).
15. Brignani, S. & Pasterkamp, R. J. *Neuron*al Subset-Specific Migration and Axonal Wiring Mechanisms in the Developing Midbrain Dopamine System. *Front Neuroanat* 11, 55 (2017).
16. Maier, V. *et al.* Semaphorin 4C and 4G are ligands of Plexin-B2 required in cerebellar development. *Mol Cell Neurosci* 46, 419–431 (2011).
17. Waimey, K. E., Huang, P. H., Chen, M. & Cheng, H. J. Plexin-A3 and plexin-A4 restrict the migration of sympathetic neurons but not their neural crest precursors. *Dev Biol* 315, 448–458 (2008).
18. Daviaud, N., Chen, K., Huang, Y., Friedel, R. H. & Zou, H. Impaired cortical neurogenesis in Plexin-B1 and -B2 double deletion mutant. *Dev Neurobiol* 76, 882–99 (2015).
19. Worzfeld, T. *et al.* Mice lacking Plexin-B3 display normal CNS morphology and behaviour. *Mol Cell Neurosci* 42, 372–81 (2009).
20. McDermott, J. E., Goldblatt, D. & Paradis, S. Class 4 Semaphorins and Plexin-B receptors regulate GABAergic and glutamatergic synapse development in the mammalian hippocampus. *Mol Cell Neurosci* 93, 5–66 (2018).
21. Vodrazka, P. *et al.* The semaphorin 4D-plexin-B signalling complex regulates dendritic and axonal complexity in developing neurons via diverse pathways. *Eur J Neurosci* 30, 1193–1208 (2009).
22. Fazzari, P. *et al.* Plexin-B1 plays a redundant role during mouse development and in tumour angiogenesis. *BMC Dev Biol* 7, 55 (2007).
23. Battistini, C. & Tamagnone, L. Transmembrane semaphorins, forward and reverse signaling: have a look both ways. *Cell Mol Life Sci* 73, 1609–22 (2016).
24. Perez-Branguli, F. *et al.* Reverse Signaling by Semaphorin-6A Regulates Cellular Aggregation and *Neuron*al Morphology. *PLoS One* 11, e0158686 (2016).
25. Haklai-Topper, L., Mlechkovich, G., Savariego, D., Gokhman, I. & Yaron, A. Cis interaction between Semaphorin6A and Plexin-A4 modulates the repulsive response to Sema6A. *EMBO J* 29, 2635–2645 (2010).
26. Tawarayama, H., Yoshida, Y., Suto, F., Mitchell, K. J. & Fujisawa, H. Roles of Semaphorin-6B and Plexin-A2 in Lamina-Restricted Projection of Hippocampal Mossy Fibers. *J Neurosci* 30, 7049–7060 (2010).

27. Sun, L. O. *et al.* On and off retinal circuit assembly by divergent molecular mechanisms. *Science* 342, 1241974 (2013).
28. Toyofuku, T. *et al.* Guidance of myocardial patterning in cardiac development by Sema6D reverse signalling. *Nat Cell Biol* 6, 1204–1211 (2004).
29. Klein, R. Eph / ephrin signalling during development. *Development* 139, (2012).
30. Zhao, X. & Guan, J.-L. Focal adhesion kinase and its signaling pathways in cell migration and angiogenesis. *Adv Drug Deliv Rev* 63, 610–5 (2011).
31. Hynes, R. O. Integrins: Bidirectional, allosteric signaling machines. *Cell* 110, 673–687 (2002).
32. Davy, A. & Soriano, P. Ephrin signaling in vivo: Look both ways. *Dev Dyn* 232, 1–10 (2005).
33. Davidson, A. J. & Wood, W. Unravelling the Actin Cytoskeleton : A New Competitive Edge ? *Trends Cell Biol* 26, 569–576 (2016).
34. Rotty, J. D. & Bear, J. E. Competition and collaboration between different actin assembly pathways allows for homeostatic control of the actin cytoskeleton. *Bioarchitecture* 5, 27–34 (2015).
35. Konietzny, A., Bär, J. & Mikhaylova, M. Dendritic Actin Cytoskeleton : Structure , Functions , and Regulations. *Front Cell Neurosci* 11, (2017).
36. Courtemanche, N., Gifford, S. M., Simpson, M. A., Pollard, T. D. & Koleske, A. J. Abl2/Abl-related gene stabilizes actin filaments, stimulates actin branching by actin-related protein 2/3 complex, and promotes actin filament severing by cofilin. *J Biol Chem* 290, 4038–4046 (2015).
37. Rottner, K., Faix, J., Bogdan, S., Linder, S. & Kerkhoff, E. Actin assembly mechanisms at a glance. *J Cell Sci* 130, 3427–3435 (2017).
38. Brown, J. A. & Bridgman, P. C. Disruption of the Cytoskeleton During Semaphorin 3A Induced Growth Cone Collapse Correlates with Differences in Actin Organization and Associated Binding Proteins. *Dev Neurobiol* 69, 633-46 (2009).
39. Gallo, G. RhoA-kinase coordinates F-actin organization and myosin II activity during semaphorin-3A-induced axon retraction. *J Cell Sci* 119, 3413 (2010).
40. Chen, B. *et al.* Rac1 GTPase activates the WAVE regulatory complex through two distinct binding sites. *Elife* 1–22 (2017).
41. Sumida, G. M. & Yamada, S. Rho GTPases and the Downstream Effectors Actin-related Protein 2 / 3 (Arp2 / 3) Complex and Myosin II Induce Membrane Fusion at Self-contacts. *J Biol Chem* 290, 3238–3247 (2015).
42. Hartwig, C., Veske, A., Krejcova, S., Rosenberger, G. & Finckh, U. Plexin B3 promotes neurite outgrowth, interacts homophilically, and interacts with Rin. *BMC Neurosci* 6, 53 (2005).
43. Seiradake, E., Jones, E. Y. & Klein, R. Structural Perspectives on Axon Guidance. Annual Review of Cell and *Developmen*tal *Biology* 32, (2016).
44. Ginsberg, M. H. Integrin activation. *BMB Rep* 47, 655–659 (2014).
45. Oinuma, I., Ishikawa, Y., Katoh, H. & Negishi, M. The Semaphorin 4D receptor Plexin-B1 is a GTPase activating protein for R-Ras. *Science* 305, 862–865 (2004).
46. Mcclelland, L., Chen, Y., Soong, J., Kuo, I. & Scott, G. Plexin B1 inhibits integrin-dependent pp125 FAK and Rho activity in melanoma. *Pigment Cell Melanoma Res* 24, (2010).
47. Rantala, J. K. *et al.* SHARPIN is an endogenous inhibitor of beta1-integrin activation. *Nat Cell Biol* 13, 1315–1324 (2012).
48. Shattil, S. J., Kim, C. & Ginsberg, M. H. The final steps of integrin activation: the end game. *Nat Rev Mol Cell Biol* 11, 288–300 (2010).
49. Walzer, T. *et al.* Plexin C1 Engagement on Mouse Dendritic Cells by Viral Semaphorin A39R Induces Actin Cytoskeleton Rearrangement and Inhibits Integrin-Mediated Adhesion and Chemokine-Induced Migration. *J Immunol* 174, (2005).
50. Messina, A. *et al.* Dysregulation of semaphorin7A/??1-integrin signaling leads to defective GnRH-1 cell migration, abnormal gonadal development and altered fertility. *Hum Mol Genet* 20, 4759–4774 (2011).
51. Scott, G. a, McClelland, L. a, Fricke, A. F. & Fender, A. Plexin C1, a receptor for semaphorin 7a, inactivates cofilin and is a potential tumor suppressor for melanoma progression. *J Invest Dermatol* 129, 954–963 (2009).
52. Das, M., Ithychanda, S. S., Qin, J. & Plow, E. F. Mechanisms of talin-dependent integrin signaling and crosstalk. *Biochimica et Biophysica Acta* 1838, 579–588 (2014).
53. Anthis, N. J. *et al.* beta Integrin Tyrosine Phosphorylation Is a Conserved Mechanism for Regulating Talin-induced Integrin Activation. *J fo Biol Chem* 284, 36700–36710 (2009).
54. Saltel, F. *et al.* New PI(4,5)P 2 - and membrane proximal integrin–binding motifs in the talin head control beta 3-integrin clustering. *J Cell Biol* 187, 715–731 (2009).

55. Parkash, J. *et al.* Semaphorin7A regulates neuroglial plasticity in the adult hypothalamic median eminence. *Nat Commun* 6, 6385 (2015).
56. Jongbloets, B. C., Ramakers, G. M. J. & Pasterkamp, R. J. Semaphorin7A and its receptors: pleiotropic regulators of immune cell function, bone homeostasis, and neural development. *Semin Cell Dev Biol* 24, 129–38 (2013).
57. Ng, J. & Luo, L. Rho GTPases regulate axon growth through convergent and divergent signaling pathways. *Neuron* 44, 779–793 (2004).
58. Aragona, M. *et al.* A Mechanical Checkpoint Controls Multicellular Growth through YAP / TAZ Regulation by Actin-Processing Factors. *Cell* 154, 1047–1059 (2013).
59. Kanellos, G. & Frame, M. C. Cellular functions of the ADF / cofilin family at a glance. *J Cell Sci* 129, 3211–3218 (2016).
60. Hsieh, J. Orchestrating transcriptional control of adult neurogenesis. *Genes Dev* 26, 1010–1021 (2012).
61. Jeong, S., Juhaszova, K. & Kolodkin, A. L. The Control of Semaphorin-1a–mediated Reverse Signaling by Opposing Pebble and RhoGAPp190 Functions in Drosophila. *Neuron* 76, 721–734 (2012).
62. Armendáriz, B. G. *et al.* Expression of Semaphorin 4F in neurons and brain oligodendrocytes and the regulation of oligodendrocyte precursor migration in the optic nerve. *Mol Cell Neurosci* 49, 54–67 (2012).
63. O'Donnell, M., Chance, R. K. & Bashaw, G. J. Axon growth and guidance: receptor regulation and signal transduction. *Annu Rev Neurosci* 32, 383–412 (2009).
64. Keller, R., Basta, R., Salerno, L. & Elia, M. Autism, epilepsy, and synaptopathies: a not rare association. *Neurol Sci* 38, 1353–1361 (2017).
65. Patel, J., Lukkes, J. L. & Shekhar, A. Overview of genetic models of autism spectrum disorders. Genetic Models and Molecular Pathways Underlying Autism Spectrum Disorders 241, (Elsevier B.V., 2018).
66. Zoghbi, H. Y. & Bear, M. F. Synaptic Dysfunction in Neurodevelopmental Disorders Associated with Autism and Intellectual Disabilities. *Cold Spring Harb Perspect Biol* 4, (2012).
67. van Battum, E. Y., Brignani, S. & Pasterkamp, R. J. Axon guidance proteins in neurological disease. *Lancet Neurol* 14, 532–546 (2015).
68. Mosca-Boidron, A. L. *et al.* A de novo microdeletion of SEMA5A in a boy with autism spectrum disorder and intellectual disability. *Eur J Hum Genet* 24, 838–843 (2016).
69. Kim, S. A. *et al.* Polymorphism in the promoter region of SEMA5A is associated with sociality traits in Korean subjects with autism spectrum disorders. *Psychiatry Investig* 14, 876–878 (2017).
70. Artigiani, S. *et al.* Plexin-B3 is a functional receptor for semaphorin 5A. *EMBO Rep* 5, 3–7 (2004).
71. Laht, P., Otsus, M., Remm, J. & Veske, A. B-plexins control microtubule dynamics and dendrite morphology of hippocampal neurons. *Exp Cell Res* 326, 174–184 (2014).
72. Laht, P. *et al.* Plexin-B3 suppresses excitatory and promotes inhibitory synapse formation in rat hippocampal neurons. *Exp Cell Res* (2015).
73. Manns, R. P. C., Cook, G. M. W., Holt, C. E. & Keynes, R. J. Differing Semaphorin 3A Concentrations Trigger Distinct Signaling Mechanisms in Growth Cone Collapse. *J Neurosci* 32, 8554–8559 (2012).
74. Duan, Y. *et al.* Semaphorin 5A inhibits synaptogenesis in early postnatal- and adult-born hippocampal dentate granule cells. *Elife* 3, e04390 (2014).
75. Kong, Y. *et al.* Structural Basis for Plexin Activation and Regulation. *Neuron* 91, 548–560 (2016).
76. Janssen, B. J. C. *et al.* Structural basis of semaphorin–plexin signalling. *Nature* 467, 1118–1122 (2010).
77. Nogi, T. *et al.* Structural basis for semaphorin signalling through the plexin receptor. *Nature* 467, 1123–1127 (2010).
78. Takahashi, T., Strittmatter, S. M. & Haven, N. PlexinA1 Autoinhibition by the Plexin Sema Domain. *Neuron* 29, 429–439 (2001).

7

Addendum

Samenvatting in het Nederlands
De Complexiteit van Semaphorine en Plexine Signalering in de Gezonde en Zieke Hersenen

Curriculum Vitae

List of Publications

Dankwoord

De Complexiteit van Semaphorine en Plexine Signalering in de Gezonde en Zieke Hersenen

Samenvatting in het Nederlands

Het brein is het orgaan waarvan we de minste kennis hebben. Het bestaat uit ±170 miljard cellen die, door middel van communicatie, zorg dragen voor alle prikkels die wij elke dag ervaren, behandelen en weer distribueren. Ongeveer de helft van de cellen in de hersenen zijn zenuwcellen, zogenoemde "neuronen". Tijdens de embryonale ontwikkeling, van de mens als wel de muis, groeien de hersenen van een aantal cellen uit tot een complex orgaan bestaande uit zenuwcellen en steuncellen. In deze periode worden veel nieuwe cellen gegenereerd. Deze moeten zich verplaatsen naar nieuwe regio's en verbinding maken met andere zenuwcellen zodat er neuronale netwerken ontstaan die ons in staat stellen tot complexe handelingen zoals logisch redeneren. Zenuwcellen zijn gespecialiseerde cellen die bestaan uit een cellichaam en uitlopers. Met de uitlopers kunnen zenuwcellen verbindingen maken met andere (zenuw)cellen om informatie uit te wisselen. Deze zogenaamde zenuwbanen fungeren als communicatieroutes in de hersenen en moeten zeer nauwkeurig aangelegd worden tijdens de ontwikkeling.

Er zijn specifieke eiwitfamilies die een correcte aanleg van de zenuwbanen verzekeren zogenoemde neuriet-sturende eiwitten. Eén van deze eiwitfamilies, de Semaphorines, is van groot belang bij dit proces. Uit vele studies is gebleken dat zenuwbanen aangetrokken of juist afgestoten worden wanneer zij in contact komen met deze eiwitten. In detail: Semaphorines worden tot uiting gebracht op het celoppervlak (membraan) van de zenuwcellen of worden uitgescheiden in de directe omgeving. Op deze manier hebben zij de mogelijkheid om in contact te komen met omliggende cellen, welke andere eiwitten tot uiting hebben gebracht. Bijvoorbeeld de eiwitfamilie Plexines die fungeren als een ontvanger (receptor) voor Semaphorines. Vaak zijn de receptoren van neuriet-sturende eiwitten gelokaliseerd op een specifiek deel van de zenuwcel, namelijk de groeikoon. Dit handvormige deel van de neuriet is erg flexibel en tast zijn omgeving af naar signalen die attenderen op de locatie van zijn eindpunt. Wanneer Semaphorines en Plexines met elkaar reageren zullen er processen binnenin de zenuwcel gestart worden die het skelet van de cel beïnvloeden. Afhankelijk van de cel, locatie en ontwikkelingsstadium zal een Semaphorine- Plexine interactie zorgen voor het afstoten, dan wel het aantrekken, van een zenuwbaan. Op deze wijze kunnen niet alleen neurieten zich verplaatsen door de hersenen maar ook de zenuwcellen zelf. Zodra een neuriet is aangekomen in het bestemde hersengebied, zal er een zenuwcontact (synaps) aangelegd worden met neurieten van andere cellen. Op deze manier worden tijdens de ontwikkeling belangrijke zenuwbanen en hersengebieden gevormd en worden er cruciale netwerken gecreëerd. De hersenen zijn nooit uit ontwikkeld, ook wanneer de volwassenheid is bereikt blijven er veranderingen optreden in de hersenen. Zo kunnen nieuwe cellen gegenereerd worden welke moeten integreren in al bestaande netwerken (volwassen neurogenesis) of kunnen al bestaande zenuwbanen versterkt of verzwakt worden door het aantal synapsen te veranderen. Ook bij deze processen is de Semaphorines-Plexine signalering erg belangrijk. Meerdere studies laten zien dat (genetische) fouten in Semaphorine-Plexine signalering kunnen leiden tot ontwikkelingsziekten zoals Autisme spectrum disorder, epilepsie of ontwikkelingsachterstanden. Hierdoor is de neurowetenschap geïnteresseerd in de

signaleringen die ten grondslag liggen aan de aanleg van zenuwbanen en synapsen. Belangrijke vragen omtrent de regulatie, functie en bijbehorende actie-mechanismes van Semaphorine-Plexine signalering dienen bestudeerd te worden. Om dit nader te onderzoeken stelt deze thesis de hypothese dat membraan-gebonden Semaphorine-Plexine signaleringen zorgen voor een juiste aanleg van zenuwbanen en synaptische connecties via verschillende, complexe signaleringsroutes welke essentieel zijn voor een juiste hersenenontwikkeling.

Om een beter beeld te verkrijgen van de regulatie, signalering en functie van Semaphorins en Plexins wordt in Hoofdstuk 1 een overzicht gegeven van de huidige kennis. Dit literatuuroverzicht laat zien dat Semaphorine-Plexine signalering streng gereguleerd wordt en betrokken is bij vele stappen tijdens de hersenontwikkeling. Een beperkt aantal Semaphorines of Plexines worden tot uiting gebracht tijdens ontwikkelingsstadia in hersengebieden. Het beperkte aantal Semaphorines of Plexines kan toch substantieel bijdragen aan de hersenontwikkeling doordat de signaleringsroutes verschillende uitwerkingen op een cel kunnen hebben. Er worden 4 van deze zogenoemde diversiteitsstrategieën besproken waaronder: (1) wijze van binding tussen Semaphorine en Plexin, (2) tweeledige signalering die resulteren in tegenovergestelde effecten door een enkel eiwit, (3) tweerichtings-signalering waarbij een eiwit kan fungeren als een receptor dan wel een ligand en (4) het vormen van eiwitcomplexen van meerdere specifieke Semaphorins of Plexins. Vervolgens worden de mechanismes na Semaphorine of Plexine activatie bestudeerd en blijken er typerende eiwitten een rol te spelen per familie (lid). Uiteindelijk wordt de rol van Semaphorine-Plexine signalering besproken tijdens de ontwikkeling van de hersenschors en hippocampus. Hieruit wordt geconcludeerd dat tijdens de ontwikkeling verschillende Semaphorines en Plexines tot uiting komen en typerende verbindingen aan gaan met elkaar. Zij gebruiken diversiteitsstrategieën om tot nauwkeurige regulatie van hersenontwikkeling te komen.

In deze thesis worden stapsgewijs specifieke Semaphorines en Plexines interacties ontleed. Er wordt gekeken waar in de hersenen deze eiwitten tot uiting komen en welk doel zij vervullen in die gebieden. Ook worden de signaleringsroutes bestudeerd die zorgen voor de effecten van Semaphorine-Plexine signalering in verschillende hersengebieden en ontwikkelingsstadia. Als laatste wordt er gekeken hoe genetische mutaties (in het erfelijke materiaal) in Plexine B3 (PlexineB3) kunnen bijdragen aan ontwikkelingsachterstanden. Samen benadrukken deze hoofdstukken de relevantie van Semaphorine-Plexine signalering tijdens de hersenontwikkeling.

Een grote belangrijke opgave binnen de neurowetenschappen is het in kaart brengen van de functies van Semaphorines en Plexines in de hersenen. Verscheidene Semaphorines en Plexines zijn erg beperkt gekarakteriseerd. Zo wordt er in Hoofdstuk 2 naar Semaphorine 4F (Sema4F) gekeken waarover weinig kennis bestaat. Het is bekend dat Sema4F tot uiting komt in de hersenen en een repulsief effect kan hebben op zenuwcellen. Om de functie van dit eiwit in de hersenen beter te begrijpen is er in Hoofdstuk 2, voor het eerst, een zogenoemde knock-out (KO) muis voor Sema4F gecreëerd. Dit resulteert in een muis die vanaf de embryonale ontwikkeling geen Sema4F in zijn cellen heeft. Vervolgens is deze muis gekarakteriseerd op neuronale defecten om vast te stellen wat de functie is van dit eiwit. Alhoewel er uit deze eerste karakterisering geen duidelijk defect is gebleken, blijft de Sema4F KO muis een nuttig hulpmiddel om meer inzichten te geven in de functie van

Sema4F. Bijvoorbeeld door de steuncellen te karakteriseren in plaats van de neuronen zoals besproken in Hoofdstuk 2.

Naast Sema4F is er ook gekeken naar de functie van Semaphorine7A (Sema7A). Dit eiwit heeft een duidelijke rol in het immuunsysteem en de ontwikkeling van de hersenen. Sema7A komt ook sterk tot uiting in volwassen hersenen, maar de functie is onbekend. In Hoofdstuk 3 blijkt dat Sema7A via zijn receptoren PlexineC1 en β1-integrine kan fungeren als een bi-functioneel eiwit. Hier worden de effecten van Sema7A-PlexineC1/β1-integrine signalering bestudeerd door middel van cel en dier modellen. Hieruit wordt geconcludeerd dat Sema7A de groei remt van stamcellen in de volwassen hippocampus via interactie met PlexinC1, en niet β1-integrine. In een later ontwikkelingsstadia stimuleert Sema7A de integratie van dezelfde cellen enkel via β1-integrine. Concluderend, de bi-functionele functie van Sema7A is afhankelijk van de receptor welke tot uiting komt in verschillende ontwikkelingsstadia. Bij elkaar is dit een eerste voorbeeld dat laat zien hoe Sema7A een diversiteitsstrategie gebruikt in de volwassen hersenen binnen eenzelfde cel. Het is nog onduidelijk hoe Sema7A enkel interacteert met PlexineC1 zonder activatie van β1-integrine en welke signaleringscascades in de cel daarbij betrokken zijn. Daarnaast is het onbekend wat voor impact Sema7A-PlexinC1/β1-integrine signalering kan hebben op functionerende hersenen (Hoofdstuk 3). Modulaties van Sema7A-PlexinC1/β1-integrine signalering kunnen meer inzichten geven op betrokken intracellulaire signaleringscascades (Hoofdstuk 7) en hoe deze uiteindelijk kunnen leiden tot veranderingen in zenuwbanen en circuits.

Uit Hoofdstuk 3 is gebleken dat het moment èn de locatie waarop een eiwit tot uiting komt, cruciaal is voor zijn functie. In Hoofdstuk 4 worden om die reden bepaalde eiwitten, zogenoemde transcriptie factoren, bestudeerd die ten grondslag kunnen liggen aan eiwit expressie. De transcriptie factoren Lmx1a en b waren nog niet eerder geassocieerd met het tot uiting brengen van PlexinC1. In Hoofdstuk 4 laat een Lmx1a/b KO muis zien dat het wegvallen van hun regulatie zorgt voor afwijkende zenuwbanen. Het blijkt dat Lmx1a/b de uiting van PlexinC1 onderdrukt terwijl Otx2 (een andere transcriptiefactor) deze juist stimuleert. Samen is dit systeem erg belangrijk tijdens de ontwikkeling van het dopaminerge systeem waar specifieke PlexinC1 uiting van belang is voor een complete integratie van zenuwuitlopers van de middenhersenen in het corpus striatum. Of deze transcriptiefactoren ook een functie vervullen in het tot uiting komen van PlexinC1 in het systeem (besproken in Hoofdstuk 3) is onduidelijk. In Hoofdstukken 4 en 7 wordt geconcludeerd dat de Semaphorines en Plexines streng gereguleerd worden via meerdere mechanismes en door verschillende eiwitten waarvan nog maar beperkte kennis is.

Uit de literatuurstudie en Hoofdstuk 3 is gebleken dat Semaphorines en Plexines op grote schaal gebruik maken van diversiteitsstrategieën om de ontwikkeling van de hersenen nauwkeurig te sturen met een beperkt aantal eiwitten. In Hoofdstuk 5 wordt één van deze mechanismes verder bestudeert in de signalering van Semaphorine 6A (Sema6A). Dit eiwit kan fungeren als ligand dan wel als receptor waardoor het een tweerichtings-signalering route heeft. De signaleringsroute waarin Sema6A als ligand en PlexinA2 of PlexinA4 activeert is al bekend. Daarentegen is de signaleringsroute waarin Sema6A zelf wordt geactiveerd nog sterk onderbelicht. In Hoofdstuk 5 worden Sema6A eiwitten gegenereerd waarvan het intracellulaire deel intact of verwijderd is waardoor er nieuwe eiwitten geïdentificeerd kunnen worden die specifiek binden met een volledige Sema6A

eiwit. Dit is de eerste studie die de aanwezigheid van een eiwitcomplex laat zien die een belangrijke rol speelt in cel en neuriet migratie, mogelijk in de hersenschors. Daarnaast worden er specifieke, nieuwe eiwitten geïdentificeerd die nog niet eerder geassocieerd waren met type 6 Semaphorines. Zoals besproken in Hoofdstuk 5 en 7, dienen deze bevindingen gevalideerd te worden. Daarnaast kan de rol van deze nieuwe interacterende eiwitten bestudeerd worden tijdens Sema6A activatie.

De vorige hoofdstukken benadrukken het belang van Semaphorine-Plexine signalering in de hersenen. Wanneer signalering van Semaphorines of Plexines niet-succesvol verlopen kan dit leiden tot ontwikkelingsziektes. In Hoofdstuk 6 is het DNA van patiënten met een ontwikkelingsstoornis bestudeerd. Door middel van een techniek waarbij de nucleotide volgorde in het DNA geïdentificeerd worden zijn verscheidene enkelvoudige nucleotide polymorfiën (single nucleotide polymorphism, SNPs) vastgesteld in het gen voor PlexinB3. Vervolgens is gemodelleerd hoe deze SNPs kunnen leiden tot structurele veranderingen en hoe de functie van PlexinB3 beïnvloedt kan worden. Hierna is een start gemaakt met het valideren van deze verwachtingen door de SNPs na te bootsen in PlexinB3 (hierna PlexinB3 varianten genoemd) en deze vervolgens in cellen tot uiting te brengen. Er werden kleine verschillen geobserveerd in PlexinB3 varianten tijdens eiwit productie of lokalisatie in de cel. Daarnaast was er één variant die een verminderde capaciteit had om premature signalering te stoppen. Verdere studies moeten uitwijzen welke andere functies van PlexinB3 zijn beïnvloedt door de veranderingen in het gen. Uit de voorlopige data wordt geconcludeerd dat de structuur van PlexinB3 varianten enigszins is gewijzigd wat kan leiden tot beperkte veranderingen in de signalering en functie van PlexinB3 (Hoofdstuk 6 en 7). Nader onderzoek zou aan moeten aantonen welke genetische variaties, in PlexinB3, zouden kunnen bijdragen aan ontwikkelingsstoornissen zoals ontwikkelingsachterstand, autisme of epilepsie. Daarnaast biedt dit onderzoek mogelijkheden om beter te begrijpen hoe PlexinB3 signaleert en welke effecten het teweeg kan brengen.

Deze thesis geeft nieuwe inzichten in de complexe signalering van Semaphorines en Plexines die ten grondslag liggen aan een gezonde ontwikkeling van de hersenen. De bevindingen in Hoofdstukken 2, 3 en 4 geven weer dat Semaphorines en Plexines onder strenge regulatie staan en dat deze cruciaal zijn voor hun rol in de hersenen, zowel tijdens de ontwikkeling als in volwassen stadia. Het gebruik van diversiteitsstrategieën in Semaphorine-Plexine signalering wordt duidelijk in Hoofdstukken 3 en 5. Een nieuwe tweeledige functie voor Sema7A in de volwassen hippocampus door specifieke binding met PlexinC1 of β1-integrine wordt beschreven in Hoofdstuk 3. In Hoofdstuk 5 wordt de signaleringsroute tijdens de tweerichtings-diversiteit strategie van Sema6A bestudeert, waar nieuwe eiwitten zijn geïdentificeerd die een rol kunnen spelen tijdens de ontwikkeling van de hersenschors. De studies beschreven in Hoofdstukken 2, 3, 4 en 5 verhoogden het begrip van de functie van Semaphorines, met name Sema4F, Sema7A en Sema6A in de hersenen. De studie beschreven in Hoofdstuk 6 legt de basis voor verder onderzoek naar de betrokkenheid van PlexineB3 in ontwikkelingsziektes.

Tot slot draagt deze thesis bij aan een beter begrip van de complexe signalering van membraan-gebonden Semaphorines en Plexines tijdens de aanleg van zenuwbanen en neuriet-integratie welke ten grondslag liggen aan een gezonde hersenontwikkeling.

Curriculum Vitae

Suzanne Lemstra was born on 08 November 1989 in Hoogeveen, The Netherlands. In 2007 she graduated high school and received her HAVO diploma (Scholengemeenschap Lelystad, Lelystad). Later that year she started the bachelor program "Life Sciences – Zoology" at the Applied University of Utrecht. In her third year she fulfilled an internship in the group of Dr. Ronald S. Oosting at Psychofarmacology, University Utrecht where she studied the effects of Celecoxib and Memantine on behavioural and cognitive deficits in a neurodegeneration animal model. In her final year she worked with Prof. Louk J.M.J. Vanderschuren at the Rudolf Magnus Institute, UMC Utrecht to study the involvement of the infralimbic cortex in rodent choice behaviour. In 2011 she obtained her bachelor degree and enrolled in a 2-years research Master Neuroscience and Cognition, track Experimental and Clinical Neuroscience at the University Utrecht. During her Master, Suzanne performed an internship in the group of Prof. R. Jeroen Pasterkamp at the Brain Center Rudolf Magnus UMC Utrecht, where she investigated the role of MICAL in the development of hippocampal mossy fibers. Hereafter, she continued with an internship at the Experimental psychology Department of the University of Cambridge in the group of Prof. Jeffrey W. Dalley. Here she studied the neurometabolite content in the prefrontal cortex and ventral striatum in rats exhibiting low- versus high-impulsive behaviour. In 2013 she completed her Master's degree (cum laude). She continued her scientific career in 2014 as a PhD in the group of Prof. R. Jeroen Pasterkamp in the department Translational Neuroscience, UMC Utrecht where she focussed on the roles of Semaphorins and Plexins during brain development. The results of this research are presented in this thesis.

Suzanne Lemstra is geboren op 08 november te Hoogeveen, Nederland. In 2007 behaalde zij haar HAVO diploma (Scholengemeenschap Lelystad, te Lelystad). In dat zelfde jaar begon ze aan haar studie Biologie en Medisch Laboratorium onderzoek aan de Hogeschool Utrecht, Utrecht met een specialisatie in zoölogie. Tijdens deze studie heeft ze twee stages afgerond. De eerste was in de groep van Dr. Ronald S. Oosting (psychofarmacologie, Universiteit Utrecht), waar ze de effecten van Celecoxib en Memantine op gedrag en cognitie in een diermodel voor neurodegeneratie bestudeerde. In haar laatste jaar heeft ze de kans gehad om in de groep van Prof. Louk J.M.J Vanderschuren (Rudolf Magnus Instituut, UMC Utrecht) te werken aan de rol van de infralimbische cortex op keuzegedrag in ratten. Na het behalen van haar diploma in 2011, startte ze de 2-jarige onderzoeks-master Neurowetenschappen en Cognitie, experimentele en klinische neurowetenschappen, aan de Universiteit Utrecht. Tijdens haar master heeft Suzanne twee stages afgerond. De eerste in de groep van Prof. R. Jeroen Pasterkamp, Brain Center Rudolf Magnus UMC Utrecht, waar ze de rol van MICAL op de ontwikkeling van hippocampale neuronen bekeek. Hierna vervolgde ze haar studie aan de Universiteit van Cambridge waar ze stage liep bij Prof. Jeffrey W. Dalley, Experimental Psychology. Hier bestudeerde ze neurometabolieten in the prefrontale cortex en ventrale striatum in ratten met lage of hoge impuls-controle. In 2013 behaalde zij haar mastertitel (cum laude). Ze begon haar PhD in 2014 in de groep van Prof. R. Jeroen Pasterkamp met een focus op de rollen van Semaphorins en Plexins in de ontwikkeling van de hersenen. Dit proefschrift is daarvan het resultaat.

List of Publications

Jongbloets BC*, Lemstra S*, Schellino R, Broekhoven MH, Parkash J, Hellemons AJCGM, Mao T, Giacobini P, van Praag H, De Marchis S, Ramakers GMJ, Pasterkamp RJ. Stage-specific functions of Semaphorin7A during adult hippocampal neurogenesis rely on distinct receptors. *Nat Commun* 8, 14666 (2017)

Chabrat A, Brisson G, Doucet-beaupré H, Salesse C, Profes MS, Dovonou A, Akitegetse C, Charest J, Lemstra S, Côté D, Pasterkamp RJ, Abrudan MI, Metzakopian E, Ang S, Lévesque M. Transcriptional repression of Plxnc1 by Lmx1a and Lmx1b directs topographic dopaminergic circuit formation. *Nat Commun* 8, 933 (2017)

Pronker MF, Lemstra S, Snijder J, Heck AJR, Thies-weesie DME, Pasterkamp RJ, Janssen BJC. Structural basis of myelin-associated glycoprotein adhesion and signalling. *Nat Commun* 7, 13584 (2016).

Van Battum EY*, Gunput R-AF*, Lemstra S, Groen EJN, Yu K Lou, Adolfs Y, Zhou Y, Hoogenraad CC, Yoshida Y, Schachner M, Akhmanova A, Pasterkamp RJ. The intracellular redox protein MICAL-1 regulates the development of hippocampal mossy fibre connections. *Nat Commun* 5, 4317 (2014)

Schmidt ERE, Brignani S, Adolfs Y, Lemstra S, Demmers J, Vidaki M, Donahoo A-LS, Lilleväli K, Vasar E, Richards LJ, Karagogeos D, Kolk SM, Pasterkamp RJ. Subdomain-mediated axon-axon signaling and chemoattraction cooperate to regulate afferent innervation of the lateral habenula. *Neuron* 83, 372–87 (2014)

Heesch F Van, Prins J, Korte-bouws GAH, Westphal KGC, Lemstra S, Olivier B, Kraneveld AD, Korte SM. Systemic tumor necrosis factor-alpha decreases brain stimulation reward and increases metabolites of serotonin and dopamine in the nucleus accumbens of mice. *Behav Brain Res* 253, 191–195 (2013)

Borre Y, Lemstra S, Westphal KGC, Morgan ME, Olivier B, Oosting RS. Celecoxib delays cognitive decline in an animal model of neurodegeneration. *Behav Brain Res* 234:285–91 (2012)

Borre Y, Bosman E, Lemstra S, Westphal KG, Olivier B, Oosting RS Memantine partly rescues behavioral and cognitive deficits in an animal model of neurodegeneration. *Neuropharmacology* 62, 2010–7 (2012a)

* These authors contributed equally tot his work

Dankwoord

Dat ik in mijn carrière me wilde focussen op de hersenen had ik al besloten in het laatste jaar van de HAVO. De vraag was voornamelijk, kies ik meer de psychologie (zoals mijn moeder en zus) of de biologie kant (zoals mijn vader). Uiteindelijk ben ik heel blij met de richting die ik gekozen heb. Dit boekje was nooit tot stand gekomen zonder alle mensen om mij heen. Graag zou ik een aantal in het bijzonder willen bedanken.

Beste Prof. R. J. Pasterkamp, beste **Jeroen**, tijdens mijn Master kwam ik in aanraking met je werk in axon guidance. Ook al was ik eigenlijk vooral geïnteresseerd in gedragsonderzoek, liep ik toch na een presentatie naar je toe om te kijken of er een mogelijkheid was om stage te lopen in jouw lab. Ik was van mening dat de moleculaire kant nodig was om gedragsonderzoek naar een hogere niveau te tillen. Ik had dan ook niet verwacht zo te genieten van het moleculaire onderzoek! Aan het einde van mijn stage bood je mij een PhD aan, die ik in eerste instantie niet aannam omdat het vooral zou gaan om moleculair werk. Gelukkig heb ik mijn keuze veranderd en heb ik je aanbod geaccepteerd. Jeroen, bedankt dat je mijn gedachte hebt veranderd en voor het aanbieden van deze unieke kans. Je gedrevenheid, ambitie en kennis zijn erg inspirerend. Ga zo door!

Dr. G. M. J. Ramakers, beste **Geert**, in de laatste stappen van mijn PhD ben jij mijn co-promoter geworden. Je houdt je nu voor namelijk bezig met de educatie, en dat was te merken in je stijl van begeleiden. Ik heb veel aan je gehad tijdens het schrijven van mijn thesis, erg bedankt hiervoor.

Beste **Louk**, ik vind het heel bijzonder dat je aanwezig zult zijn tijdens mijn verdediging. Tijdens de HBO-stage die ik liep bij Petra Baarendse in jouw groep wist ik dat ik een Master wilde doen in Neuroscience. Dankzij jouw steun, vertrouwen en hulp is het me gelukt om de Master binnen te komen. Sindsdien zien we elkaar met enige regelmaat om elkaar op de hoogte te houden. Ik geniet van onze koffie-momenten en de discussies over (non-)wetenschap en alles daar om heen. Jouw enthousiasme, kennis en openheid is noemenswaardig. Je bent het voorbeeld van een carrière en gezin. Ik wil je heel graag bedanken voor het delen van je wijsheid en levenslessen.

De leden van de beoordelingscommissie, **Prof. L. J. M. J. Vanderschuren, Prof. F. E. Hoebeek, Prof. J. P. H. Burbach, Prof. C. C. Hoogenraad** en **Prof. J. Verhaagen** wil ik graag bedanken voor de beoordeling van mijn thesis en het plaats nemen tijdens de ceremonie.

I would like to express my grattitude to all the collaborations of the past years. Dr. **Peter van Hasselt**, thank you for your work, ideas and input for the PlexinB3 project. Prof. **E. Yvonne Jones** and **Dr. G. Nagy**, thank you for your work and insights in the PlexinB3 project.

Het lab-leven bevalt uit vallen en op staan. Je zou denken dat het urenlang doen van experimenten of het tellen van cellen leuk genoeg is op zichzelf, maar eigenlijk zijn het vooral de mensen er om heen die het tot een hele bijzondere tijd hebben gemaakt.

Ten eerste mijn paranimfen, Anna en Marieke. **Anna**, je begon op het lab als stagiaire bij Sara en ik kan me nog goed de gezellige Italiaanse gesprekken herinneren. Ik ben heel blij dat je voor een plek bij Jeroen hebt gekozen. Je bent een van de liefste personen op de

wereld. Je staat altijd klaar voor anderen, no matter what. Ik kan genieten van jou brede interesses, laten we in de toekomst nog vaak naar musea en (licht)voorstellingen gaan. **Marieke**, stiekem gaan wij al heel ver terug. Beiden zijn we begonnen op het HBO en we kwamen elkaar hier weer tegen. De laatste jaren hebben we samen kunnen werken aan het Sema6A project. Na een miserabele start weet ik zeker dat hier een hele mooie paper van komt. Je gedrevenheid en empathie zijn indrukwekkend en daar heb ik ontzettend veel steun aan gehad. Ik genoot van onze brainstorm sessies en stiekem hoop ik dat we in de toekomst weer kunnen samenwerken. Kortom, zonder jullie had ik hier niet gestaan, het is dan ook meer dan logisch dat jullie naast mij staan op 19 december.

Bart, met jou heb ik aan het begin van mijn PhD veel samen gewerkt. Wat hebben wij toen een werk verricht zeg! Het verveelde nooit met jou. Ik vind het heel tof dat je de VENI gekregen hebt en ik kijk uit om je werk te blijven volgen. Als er iemand is die een goede professor kan worden, dan ben jij het!

It's beginning to look a lot like Christmas... Wat begon als een flauwe grap om mij te irriteren, hebben we kunnen omvormen tot een ware sensatie die al in de zomer begint. Allemaal dankzij jou, **Danielle**. Met een frisse wind kwam je het lab binnen. Je energie en vrolijkheid gecombineerd met je drive zijn een enorme meerwaarde geweest voor het lab. Ik heb altijd genoten van onze reizen, hardloopsessies en geouwehoer. Het liefst had ik jouw als derde paranifm erbij gehad.

Ketharini, you are the most bubbly person of the lab. I enjoyed our times in the cell culture, movies and opera. You are a hard worker with a lot of love for science, but even more for people. I have so much respect for you and how you deal with life. Keep your open spirit, its such a good quality to have.

Divya, you have all the qualities in place to become a professor. I know that once you open your own lab, you will have no trouble with finding excellent PhD and Postdocs. Discussing science and life with you have been all my pleasure. I've learned many things regarding oligodendrocytes, babies and politics because of you. I would also like to extend my thanks to your husband Anuj and your son Advik. The dinners we had were amazing and fun.

Ten slot, **Youri**. Ik weet niet wat het lab moet wanneer jij ooit besluit je talenten ergens anders in te zetten. Je staat altijd klaar voor iedereen. Jouw imaging kwaliteiten hebben al vele hopeloze images gered. Je bent een leuke en betrokken vader, ooit gaat het je lukken om te winnen met schaken. Het is altijd gezellig met jouw, zeker toen in Parijs. En onthoud, NIET DRUKKEN!

Melissa, je bent een van de nieuwste aanwinsten in het lab. Na een mooie stage bij Marieke ga je nu verder aan het PlexinB3 project. Je doet het super en ik weet zeker dat je het project tot een mooi geheel gaat maken. **Renata** and **Emma**, although we haven't worked together directly it was always good to talk you guys about anything and everything. Emma, I love your humour and secretly I'm hoping you will stay in the Netherlands. Renata, luckily you will stay in the Netherlands. Our boys can teach each other so many things! **Lieke**, je bent de enige in het lab die bezig was met RNAseq, maar dat weerhield jou niet. Je ambitie is niet alleen inspirerend in het lab, maar ook tijdens de hardloopsessies! **Andreia**, I still remember the first time we swam together, you were the only one that could keep up. I love your spirit, keep it up. **Mark**, eigenlijk was jij geboren als PI, ik ken weinig mensen die zo gedreven zijn als jij. Heel veel succes met je Postdoc. Also I would like to

thank **Katerina, Wouter** and **Inge** for their hard work and (scientific) contribution to my PhD, I wish you all the best for your own scientific careers. Further I would like to thank all the current members of the team, **Mateja, Vamshi, Pavol, Svetlana, Marina, Lill Eva, Özge, Danielle** and **all other members**. There were also many people before me. **Ewoud, Sara, Kati, Dianne** and **Oliver**, I have learned a lot from each of you. **Eljo**, jij bent zowel een alumni als een huidig lid van het lab. Je hebt me veel geleerd tijdens mijn stage bij jou en het is leuk om te zien dat je nu terug bent om verder te gaan met je wetenschappelijke carrière. Ik wens je veel geluk.

Verder wil ik graag alle mensen bedanken zonder wie het lab niet draaiende gehouden kan of kon worden. **Mark B**, jij opereert als de beste. Het Sema7A hoofdstuk had zonder jou niet kunnen bestaan. **Anita**, jij hebt mij in mijn eerste jaar veel geleerd, bedankt hiervoor. **Leo** en **Henk**, jullie worden elke dag gemist! **Christiaan**, ik kan me niet eens meer herinneren hoe het muizen werk was voordat jij er was, wat een impact heb jij gemaakt.

Ook mensen buiten het Pasterlab hebben bijgedragen aan mijn tijd hier. **Jiska**, we waren tegelijk in Cambridge en kwamen elkaar spontaan hier weer op de gang tegen. Als er iemand hart heeft voor dier onderzoek dan ben jij het. **Janna**, vooral het laatste jaar hebben wij veel aan elkaar gehad, wat een bijzondere tijd om samen mee te maken. **Emma, Jessy, Amber, Bart, Marjolein, Sophietje, Roland, Tamar en Jelle,** en **alle anderen,** bedankt voor alle gezellige lunches en borrels. Ik heb enorm genoten van de competities tussen de onderzoeksgroepen en ik hoop dan ook dat deze traditie blijft bestaan. Graag wil ik de **hele afdeling Translational Neuroscience** bedanken voor deze indrukwekkende tijd met nog speciale aandacht voor **Ria, Krista, Vicki, Roger, Sandra** en **Joke** zonder wie er geen BCRM zou zijn.

Ook al heb ik 80% van mijn tijd op het lab gestaan, hebben mijn kantoor buddies die tijd 1000x ingehaald door hun gezelligheid en steun. **Guus**, wij kenden elkaar van de master en het was leuk om het eerste jaar met jou de kamer te delen. Ik vind het altijd gezellig wanneer we elkaar tegen komen, bijvoorbeeld tijdens het schaatsen op de singel. **Annelot**, hoe jij de kliniek combineert met onderzoek is ongelofelijk. Ik heb altijd veel gehad aan je adviezen en ik heb zin om samen een wijntje te drinken op 19 december. **Ramona**, jij beleeft zo ontzettend veel, het is altijd feest om te horen wat je hebt meegemaakt. Eigenlijk ben je te lief voor deze kamer, maar gelukkig kan je ook goed van je af bijten. Je bent altijd behulpzaam en staat altijd klaar voor iedereen, een erg bijzondere eigenschap! **Kristel**, jij bent de zittenblijver van de kamer, al lang je PhD afgerond, maar je vind het niet erg om naar ons geklaag te luisteren. Je bent rete-slim en je weet alles van programmeren, daarom wordt de deur ook plat gelopen door mensen die jouw hulp nodig hebben. **Paul**, je stond je mannetje (letterlijk en figuurlijk) in de kamer vol met vrouwen. Je kan ouwehoeren als de beste en als het over microglia gaat dan stop je nooit meer met praten. De wetenschap heeft een goede scientist verloren. Jullie hebben mij zo vaak geholpen met meer dan alleen PhD-kwesties. Wij hadden leukste kamer van heel BCRM. Ik had geen betere kamergenoten kunnen wensen.

Naast mijn leven op het lab had ik ook nog een leven in de echte wereld. **Atze & Maaike, Feike & Inneke, Bastijn & Kirsten, Paul & Laura, TimB, Rienko, Geert, Maarten, Tom, Nol, Tim O** en **alle andere Uranymussers**, bedankt voor de leuke borrels, 3e kerstdag, ouwe lullen weekenden en koningsdagen.

Zonder koffie is er geen **koffieleute**. Door jullie ben ik nu afhankelijk van koffie, en

wat is het lekker! Vele uurtjes heb ik doorgebracht in het Brauhaus, om te puzzelen, te discussiëren over films of om te schrijven.

Ook de borrel momenten met **Michel & Eva, Stefan & Anne, Vincent** en **alle andere uit Ruurlo** waardeer ik enorm en hebben altijd voor veel gelach en afleiding gezorgd. Bedankt!

Ik begon mijn studententijd ooit aan de WS60 en ik ben heel blij dat wij elkaar nog steeds zien. Ik denk dat onze discussies altijd open, eerlijk en onbevooroordeeld zijn. Ook al zijn de onderwerpen in de loop van de jaren veranderd, zijn deze avonden altijd 1 van mijn favoriet. **Spit**, ik herinner me nog de eerste dag in WS60 dat ik met mijn ouders de woonkamer binnen liep en jou voor het eerst ontmoette. Tijdens discussies staan wij vaak tegenover elkaar, maar dat maakt het juist leuk. Ook **Stephan** doet altijd mee met deze discussies en zo hebben we vaak avonden lang gekletst onder het genot van vele flessen wijn. Stephan, jouw vragen geven altijd stof tot nadenken. Toen **Nico** het huis binnen kwam werden deze flessen wijn veranderd in flessen tequila tijdens een epische avond. Nico, de positiviteit die jij meebrengt is inspirerend. Ik voel me altijd gelukkiger naar een kop koffie met jou.

Lieve Leuke Meiden van Uranymus, zonder jullie was niet alleen mijn studenten tijd een stuk saaier geweest maar ook het leven daarna. Ook al zien we elkaar niet zo vaak meer, het is altijd feest. Onze weekendjes weg en vakanties zijn altijd geslaagd. Ik heb nu al zin in het voorjaar voor ons nieuwe avontuur. **Iris B, Iris H, Anne, Kim, Maaike, Marlies** en **Ronne**, bedankt voor alle leuke momenten. **Sanne**, nog eventjes en je bent weer lekker hier in NL. Ik kan niet wachten op jou en Philo. **Saskia**, we zijn gegaan van feestende vrijgezellen naar burgerlijke miepen, heerlijk zeg! **Marlot**, ik vind het zo cool dat jij staat voor wie je bent. **Claudia**, wat ben jij een doorzetter. **Dina**, jij kan koken en feesten als de beste en daarnaast ook nog eens je PhD afgerond op super jonge leeftijd. Zo knap! **Malou**, wij hebben altijd goede gesprekken onder het genot van thee of wijn. En je bent de beste scheidsrechter in discussies. **Melis**, ik discussieer het liefst met jou over de zin en onzin van het leven. Je loopt op me voor in alles, dat werkt enorm motiverend. Ik geniet van onze gezinnen samen, grote knuffel aan **Roob & Elai**. **Rianne**, jij bent mijn grootste steunbaken geweest tijdens mijn PhD. Samen wekelijks naar de bios en een Macje om de gedachten te verzetten of gewoon gezellig een theetje drinken, het kan allemaal. Aan alle meiden, met jullie kan ik alles delen en ik ben heel blij dat jullie in mijn leven zijn.

Lieve **Jaap & Meea**, de eerste keer bij jullie thuis in Ruurlo vond ik heel mooi om te zien. Met z'n allen eten aan tafel als een gezin, en ik hoorde daar ook direct bij. Ik kan altijd bij jullie terecht en jullie staan altijd klaar om bij te springen. Bedankt voor jullie steun en vertrouwen.

Ivo & Stefanie, ik zie zelden twee personen zo verschillend, die toch zo goed bij elkaar passen. Het is heerlijk om **Elise** te zien en ik vind het mooi dat onze kinderen samen kunnen opgroeien.

Ilse, Marc, Chris & Tobias, ik ben dankbaar dat ik ook jullie heb leren kennen. Bedankt voor de gezellige avonden en boeiende gesprekken.

Dayana, jij bent een van de sterkste vrouwen die ik ken. Samen met je twee schatten van kinderen, **Bo & Izzy**, kan jij de hele wereld aan. Ik ben blij dat je weer in Nederland woont

en dat we elkaar vaker zien. Bedankt dat je altijd klaar staat voor ons en voor Camilo.

Yoko & Obede, I still remember the time before we started our families. Long talks with bottles of wine, eating Bacalhau com natas in London. Now that you moved back to London I hope we can do it soon again. It's always great to talk to you and learn about **Tallulah & Kye**. I can't wait to see you all again.

A minha primeira vez em Angola foi muito emocionante para mim e graças a vossa hospidalidade e carinho senti-me muito bem-vinda. Muito obrigado por receber-me com braços abertos **Helena, Antonio & Gueth**. Estou ansiosa para voltar para Angola e visitar-vos. **Hélio**, a proxima vez que estarei aí vamos numa boa festa.

Lieve **Oma**, de 90 al gepasseerd en nog steeds erg fit! Ik vind het heel bijzonder dat je er bij kan zijn. Bedankt voor al je tijd en liefde. **Jan**, bedankt dat je er altijd bij wilt zijn.

Lieve **Elly & Henk**, het is altijd feest met jullie. Jullie verjaardagen zijn het minst Nederlandse van allemaal en daar geniet ik enorm van. Jullie aanwezigheid zorgt altijd voor mooie gesprekken over vakanties, de perikelen van de camper en de perikelen van Hoogeveen. Bedankt voor jullie interesse en steun. **Kevin & Jerry**, bedankt voor de leuke gesprekken, het gamen toen we jong waren, en de liefde voor dino's.

Lieve **Kim & Maarten,** en **Fiona & Mina**, ook jullie bedankt voor de nodige afleiding tijdens mijn PhD. Ook al was het soms moeilijk te plannen, ik vond de dagjes uit altijd erg gezellig. En sinds de kinderen er zijn geniet ik ook van de oppas momenten en de gezamenlijke speeldates.

Lieve **Anneloes**, onder andere dankzij deze PhD, hebben wij een ontzettende mooie reis kunnen maken in de USA. Jij zit vol levenslust en begint altijd enthousiast aan nieuwe uitdagingen. Je hebt me altijd gesteund en geluisterd wanneer ik er door zat of gewoon een klaagmuur nodig had. Je bent een voorbeeld grote-zus en ook al zit je momenteel wat verder weg, voelt dat niet zo. Ik ben ontzettend trots op de stappen die je nu zet. Samen met **Jonathan** leer jij ons hoe je echt zou moeten genieten van het leven.

Lieve **Rita & Arjen**, ik kan moeilijk in woorden onder brengen hoeveel ik jullie steun, adviezen en liefde waardeer. Jullie staan altijd voor Anneloes en mij klaar. Jullie fascinatie voor de natuur is aanstekelijk en ik weet zeker dat daar mijn biologie interesse vandaan komt. Ook mijn doorzettingsvermogen heb ik aan jullie beiden te danken (Nee Rita, niet alleen de Lemstra's zijn koppig). Jullie bieden altijd een luisterend oor en geven gewogen adviezen. Jullie zijn de beste ouders. Bedankt voor jullie onvoorwaardelijke steun en betrokkenheid. Thuis blijft altijd bij jullie.

Tot slot, **Fábio**, ik kan me geen leven voorstellen zonder jou. Ik wil je bedanken voor al je geduld en onvoorwaardelijke steun. Wanneer ik weer eens chagrijnig thuis kwam probeerde je me aan het lachen te krijgen met flauwe grappen. Stiekem waardeer ik die enorm, maar dat zou je me nooit horen toegeven. Bij jou vind ik altijd rust door je positieve blik en motiverende woorden. 2019 is een bijzonder jaar om meerdere redenen, met als ultiem hoogtepunt de geboorte van onze zoon, **Camilo**. Ik geniet van ons leven samen en kijk uit naar de toekomst. Ik ben het liefst bij jullie. Alleen maar liefde.